SAHC

Master's Thesis

Beatrice Di Napoli

**Modelling and safety
assessment of the Santa
Maria Maddalena Church,
Ischia, Italy**

University of Minho

Portugal | 2019

Modelling and safety assessment of the Santa Maria Maddalena Church, Ischia, Italy

Beatrice Di Napoli

Portugal | 2019

Master's Thesis

Beatrice Di Napoli

Modelling and safety assessment of the Santa Maria Maddalena Church, Ischia, Italy

ADVANCED MASTERS IN STRUCTURAL ANALYSIS OF MONUMENTS AND HISTORICAL CONSTRUCTIONS

DECLARATION

Name: Beatrice Di Napoli

Email: beatrice.dinapoli1992@gmail.com

Title of the   Modelling and safety assessment of the Santa Maria Maddalena Church, Ischia, Italy

Msc Dissertation:

Supervisor(s):   Professor Paulo B. Lourenço, professor Claudia Casapulla

Year: 2018-2019

I hereby declare that all information in this document has been obtained and presented in accordance with academic rules and ethical conduct. I also declare that, as required by these rules and conduct, I have fully cited and referenced all material and results that are not original to this work.

I hereby declare that the MSc Consortium responsible for the Advanced Masters in Structural Analysis of Monuments and Historical Constructions is allowed to store and make available electronically the present MSc Dissertation.

University: Universidade do Minho

Date: July 17th 2019

Signature:

_____

ACKNOWLEDGEMENTS

This page is left blank on purpose.

ABSTRACT

The church of Santa Maria Maddalena in Casamicciola Terme, Ischia Island, Italy, represents one of the very rare examples of the particular building technique of the Borbonic *Baraccato* system, one of the earliest engineered earthquake resisting systems developed in Southern Italy between the 18th and 19th Centuries. Its unicity lies on the materials adopted. It presents Neapolitan yellow tuff-masonry walls embraced in iron frames, while the traditional *Baraccato* system utilizes embedded timber frames in the masonry texture. The church was stroke by the recent earthquake of 21st August, 2017 with epicenter in Casamicciola Terme. Though the moderately high seismic intensity of the event, the post-seismic surveys carried out in the frame of the emergency protocols did not evidence relevant structural damage thanks to the constructive system.

The present work aimed at developing a better understanding of the structural behavior of the church. The scope was addressed by developing a three-dimensional numerical Finite Element Model (FEM) in order to assess the structural safety of the building under gravitational and seismic loads performing advanced numerical analyses.

The modelling workflow has been guided by the following preliminary tasks which are considered mandatory to rely on the outcomes of the numerical analyses: historic review and definition of the territorial framework in terms of geology and seismicity proneness; geometrical overview of the church and description of the structural elements main features, understanding also the level of knowledge reached for the structural details; description of the observed pre- and post-seismic damage; definition of the modelling strategies to adopt in the numerical model and the material characteristics to use; modal identification of the structure through the post-processing of ambient vibration tests performed under operational conditions; calibration of the numerical model.

The execution of preliminary safety assessment of the structure was carried out through the application of non-linear static analyses to different model versions, capable of describing a possible range of responses of the building under horizontal loads. The numerical models considered for the analyses namely involved the response of the structure under the assumption of a behavior mainly governed by the non-linear response of the masonry walls, discarding the contribution of the *Baraccato* frames (lower-bound response), conversely a second model was analyzed by taking the response of the frames as infinitely elastic (upper-bound response).

The work accomplished the full implementation of the numerical model and the performance of sensitivity analyses based on its response with regards to the uncertainties and the modelling strategies adopted. However, the refinement of the knowledge of structural details, deeper investigation of the influence of different modelling strategies for the *Baracccato* system, more experimental tests, and the improvement of ambient vibration tests are recommended in the scope of executing non-linear dynamic analyses that could comply with the effective observed post-seismic damage and better define the seismic safety assessment of the church.

ADVANCED MASTERS IN STRUCTURAL ANALYSIS OF MONUMENTS AND HISTORICAL CONSTRUCTIONS

This page is left blank on purpose.

RESUMO

Modelação e avaliação da segurança da igreja da Santa Maria Maddalena em Ischia, Italia

A igreja de Santa Maria Madalena em Casamicciola Terme, Ilha de Ischia, Itália, representa um dos exemplos mais raros da singular técnica construtiva do sistema Baraccato de época Borbonica, um dos primeiros sistemas resistentes aos terramotos existentes, desenvolvidos no sul da Itália entre os séculos XVIII e XIX. A sua unicidade está nos materiais adotados. Apresenta paredes de alvenaria napolitanas de tufo amarelo envolvidas por armações de ferro, enquanto o sistema Baraccato tradicional utiliza molduras de madeira embebidas na textura de alvenaria. A igreja foi atingida pelo recente terremoto que aconteceu no dia 21 de agosto 2017 com epicentro em Casamicciola Terme. Apesar da intensidade sísmica moderadamente alta do evento, as inspeções pós-sísmicas realizadas no âmbito dos protocolos de emergência não evidenciaram danos estruturais relevantes devido ao bom funcionamento do sistema construtivo.

O presente trabalho teve como objetivo obter uma melhor compreensão do comportamento estrutural da igreja. O tema foi abordado com o desenvolvimento de um modelo numérico aos elementos finitos (FEM) tridimensional para avaliar a segurança estrutural do edifício sob cargas gravitacionais e sísmicas realizando análises numéricas avançadas.

O fluxo de trabalho de modelação foi guiado pelos seguintes passos preliminares que são considerados obrigatórios para validar os resultados das análises numéricas: revisão histórica e definição do quadro territorial em termos de geologia e propensão à sismicidade; visão geral geométrica da igreja e descrição das características dos elementos estruturais principais, analisando também o nível de conhecimento alcançado nos detalhes estruturais; descrição dos danos pré e pós-sísmicos observados; definição das estratégias de modelação que tem de ser adotadas no modelo numérico e as características do material utilizadas; identificação modal da estrutura através do pós-processamento de ensaios de vibrações ambientais realizados em condições operacionais; calibração do modelo numérico.

A execução da avaliação preliminar de segurança da estrutura foi realizada através da aplicação das análises estáticas não lineares considerando diferentes versões de modelos capazes de descrever uma possível gama de respostas do edifício sob cargas horizontais. Os modelos numéricos considerados para as análises envolviam a resposta da estrutura sob o pressuposto de um comportamento principalmente governado pela resposta não linear das paredes de alvenaria, descartando a contribuição do esqueleto (ou armação) de Baraccato (resposta conservadora), por outro lado um segundo modelo foi analisado tomando a resposta da armação como infinitamente elástica (limite superior da resposta).

O trabalho realizou a implementação completa do modelo numérico e o desempenho das análises de sensibilidade baseado na sua resposta em relação às incertezas e às estratégias adotadas durante a fase de modelagem adotadas. No entanto, o refinamento do conhecimento dos detalhes estruturais, a investigação mais profunda da influência de diferentes estratégias de modelação para o sistema Baraccato, mais ensaios

experimentais e a melhoria dos ensaios de vibração ambiental são recomendados para a executar análises dinâmicas não lineares que podem validar os danos pós-sísmicos observados e mais bem definir a avaliação da segurança sísmica da igreja.

SINTESI

Modellazione e verifica della sicurezza sismica della chiesa di Santa Maria Maddalena a Ischia, Italia

La chiesa di Santa Maria Maddalena a Casamicciola Terme nell'isola di Ischia, Italia, è uno dei rari esempi di edificio religioso costruito con il sistema Baraccato. La tecnologia costruttiva, ideata in epoca Borbonica nel Sud Italia tra il XVIII e il XIX secolo, costituisce uno dei primi sistemi strutturali ingegnerizzati per rispondere alle azioni sismiche. La singolarità dell'edificio, inoltre, risiede nei materiali adottati. Le strutture verticali dei muri, infatti, sono realizzate in muratura di tufo giallo napoletano rinforzata da telai metallici sulle facce esterne, mentre il tradizionale sistema Baraccato prevede l'utilizzo di telai lignei inseriti all'interno della muratura stessa. La chiesa è stata interessata dal recente terremoto che ha colpito l'isola di Ischia il 21 agosto 2017 con epicentro in Casamicciola Terme. Nonostante la significativa intensità dell'evento sismico, i successivi controlli di agibilità post-sisma non hanno evidenziato particolari danni strutturali grazie al sistema costruttivo presente nella chiesa.

Il presente lavoro ha lo scopo di sviluppare una migliore comprensione della risposta strutturale della chiesa. Questo obbiettivo è perseguito tramite l'implementazione di un modello tridimensionale agli elementi finiti (FEM) nell'ottica di valutare la sicurezza dell'edificio in relazione ai carichi gravitazionali e sismici, svolgendo analisi numeriche avanzate.

Il processo di modellazione vero e proprio è stato preceduto dalle seguenti fasi preliminari, considerate necessarie alla definizione di un grado di affidabilità accettabile dei risultati delle analisi numeriche: analisi storico-critica e inquadramento territoriale del sito dal punto di vista geologico e sismico; implementazione della geometria della chiesa e descrizione tecnologica degli elementi strutturali, considerando il livello di conoscenza raggiunto in merito ai dettagli costruttivi; descrizione del rilievo del danno pre e post sismico; definizione delle strategie di modellazione e delle proprietà meccaniche dei materiali da adottare nel modello numerico; identificazione modale della struttura attraverso l'analisi dei test di identificazione dinamica della struttura, eseguiti precedentemente in condizioni operative; calibrazione del modello.

La formulazione di un preliminare giudizio di sicurezza della struttura è stata ottenuta mediante l'esecuzione di analisi statiche non lineari applicate a diverse versioni del modello numerico, identificate in modo tale da descrivere un possibile intervallo di definizione della risposta strutturale. I modelli numerici adottati per le analisi hanno permesso di descrivere la risposta della struttura valutando il solo contributo non lineare della muratura nella risposta ai carichi orizzontali, non

considerando il contributo dei telai (limite inferiore), e valutando un comportamento ideale dell'edificio ottenuto considerando i telai del Baraccato come materiali infinitamente elastici (limite superiore).

I risultati del presente lavoro hanno permesso di implementare il modello numerico in tutte le sue parti e di eseguire delle analisi di sensitività nei riguardi delle incertezze del modello e di alcune delle strategie di modellazione adottate. In conclusione, il raggiungimento di un maggiore livello di conoscenza dei dettagli costruttivi, la definizione dell'influenza delle strategie di modellazione adottate nell'a definizione della risposta strutturale, l'esecuzione di campagne sperimentali addizionali e il completamento dei test di identificazione modale sono raccomandati nell'ottica dell'esecuzione di analisi dinamiche non lineari che possano essere confrontate con l'effettivo rilievo del danno post-sismico e che possano contribuire alla definizione di un giudizio finale della sicurezza della chiesa.

TABLE OF CONTENTS

LIST OF FIGURES

ADVANCED MASTERS IN STRUCTURAL ANALYSIS OF MONUMENTS AND HISTORICAL CONSTRUCTIONS

LIST OF TABLES

1 INTRODUCTION

1.1 Motivation

During the earthquake that hit the Ischia Island on August 21st, 2017, a relatively moderate magnitude seismic event (Mw = 4.2) caused a largely widespread damage across the island and the almost total destruction of the Casamicciola Terme town, the municipality closest to the earthquake epicenter. Thus, the post-earthquake damages indicated a high vulnerability of the local building environment, witnessed also by the long seismic history of the area (Rovida et al. 2016).

Among the buildings hit by the recent earthquake, the church of Santa Maria Maddalena in Casamicciola Terme consisted of a rare exception to the widespread destruction of the built environment, presenting a relatively low post-seismic damage to the structural system, with distributed crack patterns were detected mainly in the decorative elements.

The building was constructed at the end of the 19th century, after one of the deadliest earthquakes that stroke Ischia Island in its history, i.e. the Casamicciola Terme earthquake of 1883. The seismic events caused the total collapse of the pre-existing building of the church and demanded the design and construction of a new one in a different location. The construction design was carried out by Eng. Gambara in the light of some of the most advanced techniques for the seismic risk mitigation at the time and in compliance with the post-seismic recommendations of the municipalities, the adoption of the Borbone *Baraccato* system. The building survived until our days and was hit by the strong earthquake of Casamicciola Terme in 2017. It underwent mandatory safety check thanks to the post-seismic emergency protocols, such as the *in-situ* compilation of the A-DC survey form, the pre-compiled form used in Italy to assess the safety of heritage structures after natural calamities (MIBACT 2015).

During the safety inspections in the church, its peculiar constructive system revealed to be particularly suitable to withstand seismic actions and assure the structural safety of the building. It is composed by a mixed iron-masonry constructive technology used for the walls of the church. This way, the masonry results enveloped in two layers of iron frames connected transversally through the walls thickness. Additionally, the use of the traditional *Baraccato* system, i.e. timber frames embedded inside the masonry texture, was also detected. This is a constructive system widespread in Southern Italy as one of the first engineered earthquake resisting systems developed between the 18th and 20th centuries (Ruggieri and Tampone 2015).

The use of the two constructive systems together in a religious building defines the peculiarity of the building itself. Moreover, the mixed iron-masonry constructive system, presenting a frame layout that attends to the typical *Baraccato* layout, allows the identification of one of the rare cases in which the post-earthquake reconstruction recommendations of the municipality were correctly observed. Even if the *Baraccato* system with iron elements was already recognized at the time as one of the most suitable for the public buildings reconstruction, only few cases are found today, of which the church of Santa Maria Maddalena is a truly representative example.

Currently, the overall knowledge of the building by means of historical investigation, design and survey drawings, constructive typology and damage survey have been mostly carried out by the University of Naples Federico II, together with in situ observation and modal testing, committed by the Campania Regional Directorate for Cultural Heritage (MiBACT), in the scope of a finite element model implementation on which perform advanced structural analyses.

1.2 Objectives

One of the main objectives of the present work is the definition of a numerical model of the church of Santa Maria Maddalena in Casamicciola Terme (NA), in the light of the data collected during the damage surveys and further studies conducted in consequence of the recent seismic event that hit the Ischia Island on August 21st, 2017, damaging the great part of the building environment in the Casamicciola Terme town and surroundings.

Seen the earthquake proneness of the area and the response of the structure to the last seismic event, the numerical model is to be utilized to perform a safety assessment of the church. It must be reminded that a complete and reliable seismic assessment of the church would only be possible once implemented a numerical model representing with satisfying approximation the structure real conditions, geometry and materials. For this reason, the implementation of a model sufficiently detailed is the first and mandatory step to proceed with the needed advanced numerical analyses to formulate a safety judgment on the structure.

According to the Italian codes and regulations (MIBACT 2010; NTC 2018), enacted in compliance and extension of the European codes (EC-Standards 1990, 1998), for the existing buildings of historical interest, the appropriate requirements of structural safety and risk mitigation are assured through the adoption of the definition of three limit states (EC-Standards 1990; NTC 2018): the ultimate limit state (ULS, SLU), the damage limit state (DLS, SLD) and the damage limit state for the buildings of artistic interest (SLV). The latter references to a specific limit state defined for the scope

of preserving the protected artistic heritage buildings and was introduced in the corresponding Italian regulation (MIBACT 2010).

The objectives of the present work are pursued through the development of a 3D finite element model of the structure, including all the features of its complexity and the subsequent execution of seismic non-linear analyses, if applicable. These should be capable of justifying the damage observed in consequence to the earthquake, defining a damage limit state and the seismic vulnerability of the church per Italian code demand.

The tasks accomplished for the persecution of the objectives are:

- Historical and literature review of the church;
- Analysis of the geometrical survey of the church and analysis of the present condition of the church in the state of post-seismic damage;
- Preparation of the Finite Element Model;
- Calibration of the numerical model with the results of the already performed *in-situ* ambient vibration tests and performance of sensitivity analyses to validate the adoption the selected modelling strategies;
- Preliminary seismic vulnerability assessment of the church through the execution of non-linear static analyses (pushover analyses) on different model versions and definition of a possible range of seismic response of the church.

1.3 Outline of the thesis

The present thesis is organized in seven chapters, each one describing a different aspect of the studies carried out on the church. The main contents of the chapters can be summarized as follows:

Chapter 1:   consists of the introduction to the present work, declaring the motivations that led to the choice of the church as object of study, the main objectives of the work carried out and the organization of the thesis document.

Chapter 2:   is focused on the understanding of the object of the work at the territorial level by considering a brief territorial description of the location in which the case study is placed, the history of the building as a result of the previously accomplished historical survey and the description of the main geological and seismic features of the area of the case study.

Chapter 3:   regards the description of the church of Santa Maria Maddalena from the architectonical point of view and primarily from the technological point of view as a

product of the understanding of the information obtained from the geometrical and material survey. In this sense also an understanding of the level of knowledge reached is provided. The description of the various structural elements of the church is conducted in the scope of the latter implementation of the knowledge in modeling strategies to apply to the numerical model. Lastly, a description of the present state of conservation of the church as a consequence of the recent earthquake that stroke Ischia Island is included.

Chapter 4: the choices made for the numerical model preparation are the main focus of the chapter where all the basic procedures are briefly illustrated, and all the particular modeling strategies adopted for the simulation of the behavior of the church peculiar structural systems. In particular, the modeling strategies adopted for the *Baraccato* walls are discussed. In addition, an insight of the loads applied to the numerical model, the linear and non-linear parameters of the adopted material models and the defined boundary conditions are provided. Furthermore, it presents the linear gravitational analysis of the model in the scope of the model validation.

Chapter 5: focuses on the dynamic identification of the building which was achieved through the execution of *in-situ* ambient vibration tests. The results post-processing performed in ARTeMis environment is presented and compared with the eigenvalue analyses results of the obtained numerical model. Lastly, the chapter describes the calibration procedures obtained through the comparison of the modal shapes and frequencies of the existing structure and the numerical model, enabling the validation of some of the adopted modeling strategies and the updating of the Young's moduli of the masonry walls. In addition, it presents final remarks regarding the calibration phase and the experimental campaign.

Chapter 6: shows the main results of the non-linear static analysis performed. The seismic response of the church was studied through the application of the non-linear analyses to different model versions, in order to inspect the influence of the iron and timber frames reinforcing the masonry walls. The analyses were performed both on a full model where all the constructive elements were included considering an ideal elastic response of the frames and on an un-reinforced version where all the frames were removed, in the scope of defining a possible range of responses of the structure to the horizontal loads. In this sense, analyses with forces distributions proportional to the

masses were executed in the two main directions (XX and YY) positives and negatives.

Chapter 7:   presents the conclusions of work carried out, the open issues and future developments of the study giving final remarks, in the scope of obtaining a better knowledge of the studied object in terms of its architectural and technological aspects. The knowledge of the structural behavior oriented to the structural analysis of the building and a more comprehensive seismic and safety assessment of all the structural elements defining the church are also discussed.

2 HISTORIC REVIEW

The object of the present work is the parish church of Santa Maria Maddalena, located in the volcanic island of Ischia, in the Municipality of Casamicciola Terme, one of the six districts of the island of Ischia (NA).

The choice of this particular case study is related to the post-earthquake observations carried out after the seismic event of the 21st August 2017, with epicenter in Casamicciola Terme. According to the first report of the University of Naples Federico II, in charge of the post-seismic damage survey, the church suffered low damage, though widespread cracks were evidenced, probably thanks to the mixed structure of the church (Casapulla et al. 2019b). The damage survey lead to an increasing interest on the structural behavior of the church in order to discuss the performance observed and to determine the residual safety of the church. The structural system adopted for the church, dating back to 1896, consists of a mixed iron-masonry and timber-masonry system, widely recognized as the "Baraccato system".

An essential preliminary historic analysis is required in order to understand the structural system, the construction techniques used, the present state of conservation of the structure and so the expected structural behavior of the building pre and post-earthquake.

2.1 Location

The Ischia island is a volcanic island located in the Gulf of Naples in the Tyrrhenian Sea (Figure 2.1), approximatively 30 km from the city of Naples. It is the major of the Phlegraean Islands, since it has a trapezoidal shape measuring approximatively 10 km E-W and 7 km N-S and having about 34 km of coastline and a surface area of 46.3 km². The island is very densely inhabited, and it is composed of six districts: Ischia, main district – *comune* – of the island, Barano d'Ischia, Casamicciola Terme, Forio, Lacco Armeno, and Serrara Fontana.
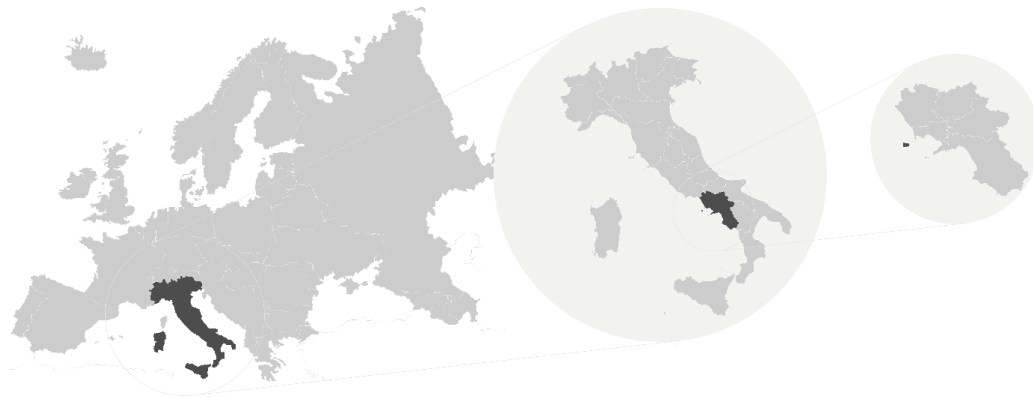
Figure 2.1 Geographical location of the Ischia island in the Tyrrhenian Sea

The church of Santa Maria Maddalena is located on the hill of Casamicciola Terme (Figure 2.2), in the Perrone area between *Majo* and *Bagni* neighborhoods, precisely in Via Roma, 2, 80074 Casamicciola Terme NA, Italia, GMS coordinates: 40°44'38'' N, 13°54'20'' E.

(a)   (b)

Figure 2.2 Map of Ischia island (a) and geographical location of the church (b)

The altitude of the site is approximatively 66 m above sea level, on the top of a hill characterized by a significant slope ~11.4% towards north-east direction, and the church dominates the square Piazzetta Funno at the urban node between via Principessa Margherita, via Roma and via Dottor De Rivaz.

As stated above, after the 1883 earthquake, the choice of the location, decided in 1886 by the municipal authorities of Casamicciola Terme, was not considered as the most suitable because the area had been subjected to serious seismic damage and because of the known bad quality of the soil at the location. The designer of the new church underlined the threats of the location and the post-earthquake town planning map identified the area of the *Marina* district as the one for the reconstruction. Still, the municipality forced the choice of such a location to encourage the development of the higher part of the city and to constitute a natural urban connection between it and the marina area (Arcamone and Argiento 2018).

2.2 Brief history of Santa Maria Maddalena Church

The date of foundation of the parish of Santa Maria Maddalena is unknown, even if the first report about its existence dates back to the first half of the16th century when the bishop of Ischia granted some ecclesial rights to the men of Casamicciola Terme ("Website of the parish of Santa Maria Maddalena" n.d.).

The building standing today is the result of the reconstruction of the main church after the devastating earthquake that stroke Casamicciola Terme in 1883 causing the collapse of most of the buildings in the city. The remaining ruins of the original church (Figure 2.3), which before the earthquake was located in the square piazza Majo, were demolished after the seismic event and the building was relocated in the current position.

Figure 2.3 Interiors of the original church after the 1883 earthquake, private collection G. Fiorentino. Source: (Luongo et al. 2006)

The building object of the present work dates back to March 2nd, 1892, date of the start of the construction works, after a long procedure that started in March 20th, 1886. The building was designed by Eng. Giovanni Gambara, appointed by the Mayor of Casamicciola Terme G. Dombrè. Eng. Gambara produced and sent to the municipality on February 25th, 1890 eight project drawings, an illustrative report, the metric calculation and the estimate of the work. These documents can still be consulted today in the state archives in Naples ("Archivio di Stato di Napoli, Corpo Reale Genio Civile, fascio 342, incart. 3" n.d.). Examples of the documents are an extract of the plan layout (Figure 2.4), the transversal cross-section (Figure 2.5a) and the lateral façade (Figure 2.5b), the full documentation is reported in Annex 1.
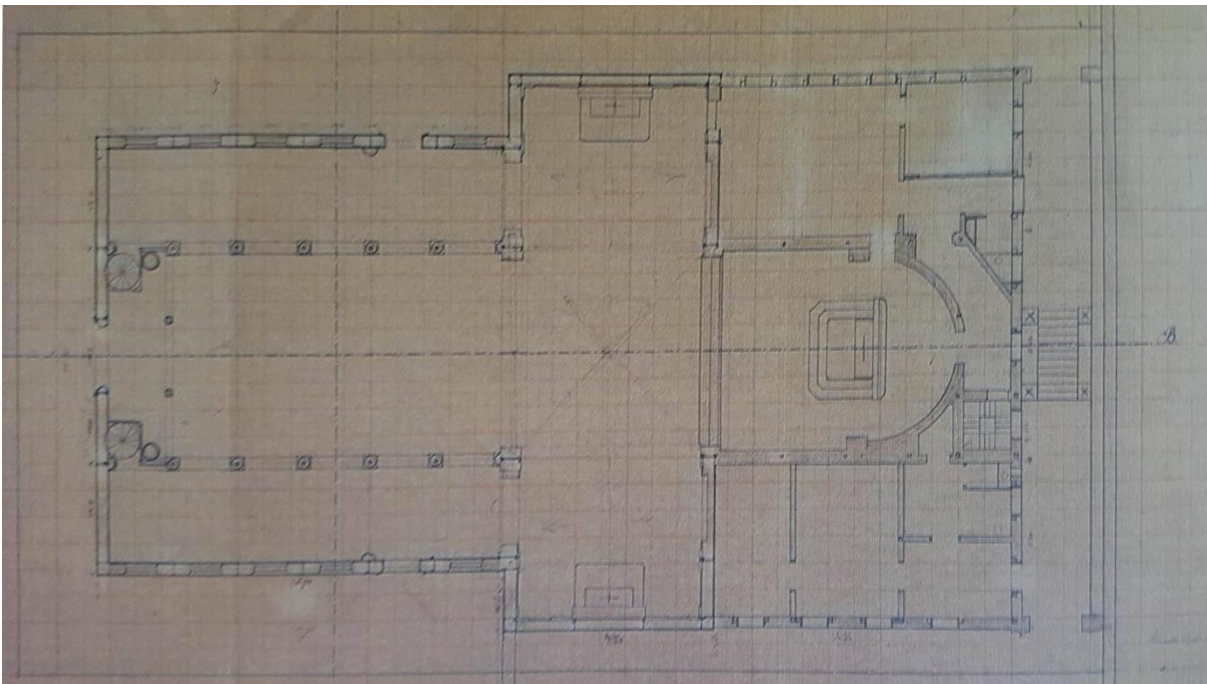
Figure 2.4 Historic plan layout from the original drawings of Eng. G. Gambara. Source: ("Archivio di Stato di Napoli, Corpo Reale Genio Civile, fascio 342, incart. 3" n.d.)

(a)   (b)
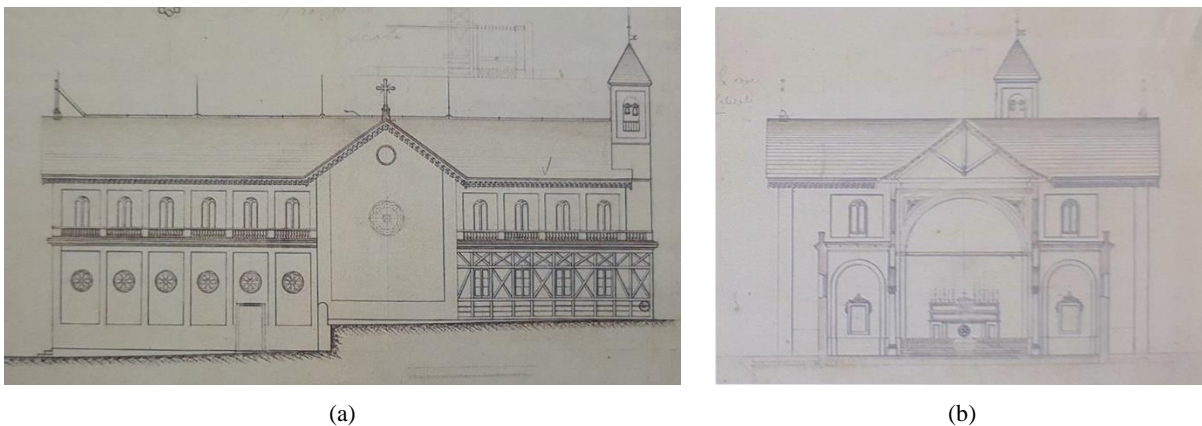
Figure 2.5 Historic drawings of the lateral elevation (a) and the transversal cross-section (b). Source: ("Archivio di Stato di Napoli, Corpo Reale Genio Civile, fascio 342, incart. 3" n.d.)

The building techniques applied for the construction of the current building are, therefore, strongly linked with the innovations and the measures adopted during the post-earthquake reconstruction of the city. These regulations can be considered among the first Italian examples of seismic risk mitigation, along the regulations subsequent the earthquake of Reggio and Messina of 1783 (G. Vivenzio 1788) and the earthquake that stroke Norcia in 1859. The building regulations – *Regolamento Edilizio* – that were published subsequently to the seismic event contained prescriptions in terms of location of the allowed reconstruction areas, identified as those which suffered less damage during the earthquake, and in terms of construction systems and materials to adopt for the new buildings. Indeed, the building

of the church in the identified location was only permitted by waiving the post-earthquake regulations under the condition of a choice of a structural system appropriate to the seismicity of the area (Arcamone and Argiento 2018). That system was identified by Gambara, and from the authorities in charge of the reconstruction, as an encaged system of mixed iron-masonry and timber-masonry structure following the construction techniques already applied in the south of Italy, known as "Baraccato system".

It is worth mentioning that Gambara stated that the aforementioned bad quality of the soil of the construction area of the new church was not known before the design delivery and the approval of the entire project was conditioned by the execution of some soil tests to confirm the location. The tests, up to 14 m depth, evidenced a stratigraphy of the soil consisting of layers, with an average thickness of ~2 m, made of rubble material, organic soil, loose clays, more compact clays and finally a layer of rock, addressed literally as "strong rock" – *sasso forte* (Arcamone and Argiento 2018). The design was subsequently refined deepening the foundation level of about 2 m and on September 2nd, 1892 the construction works began under the direction of Eng. Luigi Parisi.

During the construction, the director carried out some modifications *"in the interest of grater solidity and stability"* (Casapulla et al. 2019b) such as the addition of metal profiles to connect the upper part of the columns and more diagonal bracings in some of the areas with large spacing of the iron mesh. For this reason, even if the original drawings are available in the public archives, their use for the identification of the structural system scheme is not reliable, as shown in Figure 2.6 where a comparison between the original drawing and the building survey is provided.

| (a) | (b) |
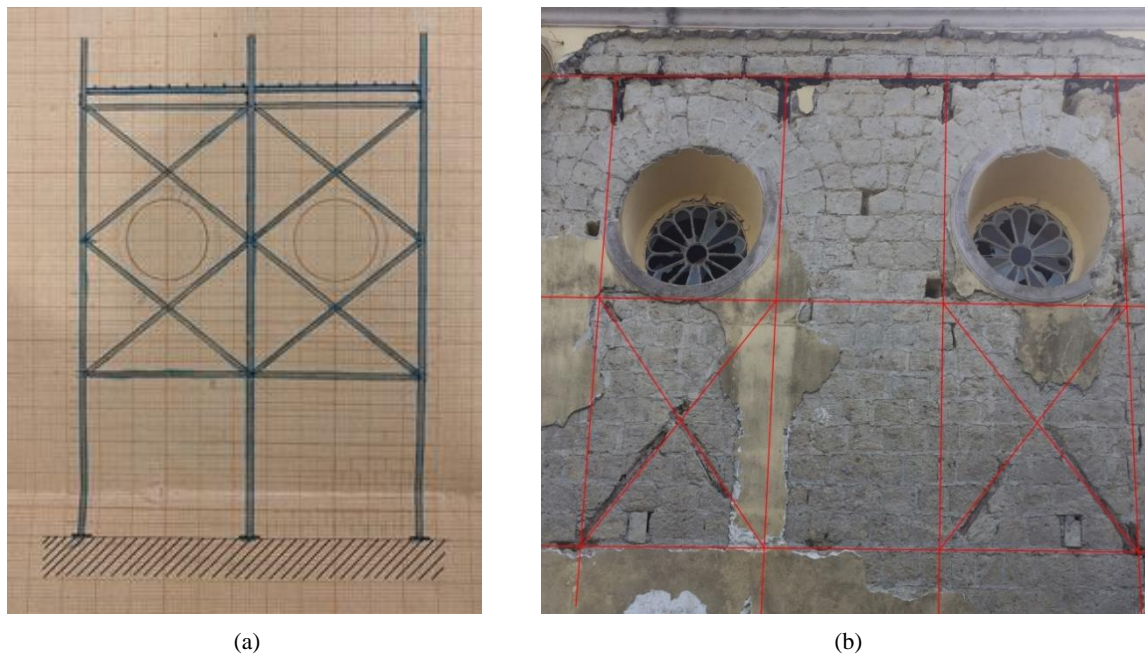
Figure 2.6 Original drawing of the structural organization of the iron frames (a) and _in-situ_ survey result (b) for the lateral wall. Source (a): ("Archivio di Stato di Napoli, Corpo Reale Genio Civile, fascio 342, incart. 3" n.d.)**. Source (b):** (Casapulla et al. 2019b)

During 20th century, the church did not undergo major changes with exception of the reconstruction of the diaphragm in the sacristy (Casapulla et al. 2019b). Nevertheless, it must be pointed out that, even if there are no traces in the documents, the reconstruction of the abovementioned diaphragm might have affected also other structural units like the supporting timber _baraccato_ walls. The substituted diaphragm is located in the north-eastern corner of the canonical house, where the timber _baraccato_ structure is connected with the church structure itself, at the first floor. In this location, the presence of wider openings was detected along with the presence of differences in the level of the floor slabs of the first floor and the northern terrace, to assure a greater clear height of the room of the ground floor. Moreover, while investigating the possible layout of the timber _baraccato_ structural system, and the possible position of its timber columns, posts, and diagonals, it was observed that the actual location ad dimension of the openings is in contrast with the regularity and the continuity of these elements in the adjacent parts. The configuration and layout of the timber _baraccato_ system of this portion of the building will be later discussed in the following sections but, for the reason just mentioned, the possibility of an intervention also in the walls connecting the replaced floor slabs was taken into consideration.

During the recent 2017 Ischia earthquake, the church suffered some damage mainly in the finishing elements. After the seismic event, the University of Napoli Federico II was in charge of the damage survey and the usability check of the church under the coordination of the Ministry of Cultural Heritage (MiBACT). The assessment, carried out by filling the level II survey form (GNDT 2001),

evidenced an "unsafe condition" and the church was closed for provisional safety interventions, committed by the Campania Regional Directorate for Cultural Heritage. These interventions were carried out from September 2018 to January 2019 and comprehended provisional measures to prevent debris from the earthquake damages to cause harm to the devotees, but also, they addressed some of the static deficiencies due to the age of the structure that were worsened by the occurrence of the earthquake itself. In the specific, the adopted measures of protection were: installation of a tube and coupler scaffolding covered by timber planks to protect the main altar (Figure 2.7a) and the secondary altars and tombs of the aisles (Figure 2.7b); application of indoor and outdoor safety-nets (Figure 2.7c); replacement of some disconnected roofing tiles. Moreover, the additional measures that were applied, not dealing directly to the earthquake damage, were the consolidation of the mortar joints and the anti-rust protection of the iron frames in the external walls of the church (Figure 2.8), the consolidation of a timber beam and the trusses of the roof with carbon fibers and steel connection plates, re-plastering of the intervened walls.

| (a) | (b) | (c) |

Figure 2.7 Provisional interventions, installation of tube and coupler scaffolding in the apse (a) and in the isles (b), and application of safety-nets (c)

Figure 2.8 Anti-rust protection of the iron frames of the external walls

2.3 Volcanic and geological history of Ischia island

Ischia is an active volcanic island that represents the emerged part of a volcanic area of about 42 km^2 that extents from Procida island to the off-shore volcanos in east-west direction to Ischia (INGV n.d.).

Its seismic history is long and dates back to the first reported seismic event in 1228. In particular, the Casamicciola Terme town is widely known for being particularly earthquake-prone, due to the number of seismic events with epicenter close to the town that have been recorded in its history. Thus, it seismic history is so deeply-rooted in the Italian popular culture that the word *casamìcciola* is contained in the Italian dictionaries to indicate a great chaos, that was probably associated to the total destruction of the city after the 1883 earthquake ("casamìcciola" n.d.).

Indeed, the area faced a long history of earthquakes and volcanic activity, with the last reported volcanic eruption in the mount Arso in 1301, being affected in the past by local volcanic and volcano-tectonic earthquakes with intensity scale (MCS) up to XI (Rovida et al. 2016).

From the geological point of view, the island can be considered being part of the Flegrei Fields volcanic region (Figure 2.9), located in the facing main land of the Gulf of Naples, dominated by the volcano Vesuvio. The region is delimited by a NW-SE trending fault at the north-east boundary, down-thrusting the Apennine mountains, and by a NW-SR trending fault at the north-west and south-east edge (Briseghella et al. 2019).
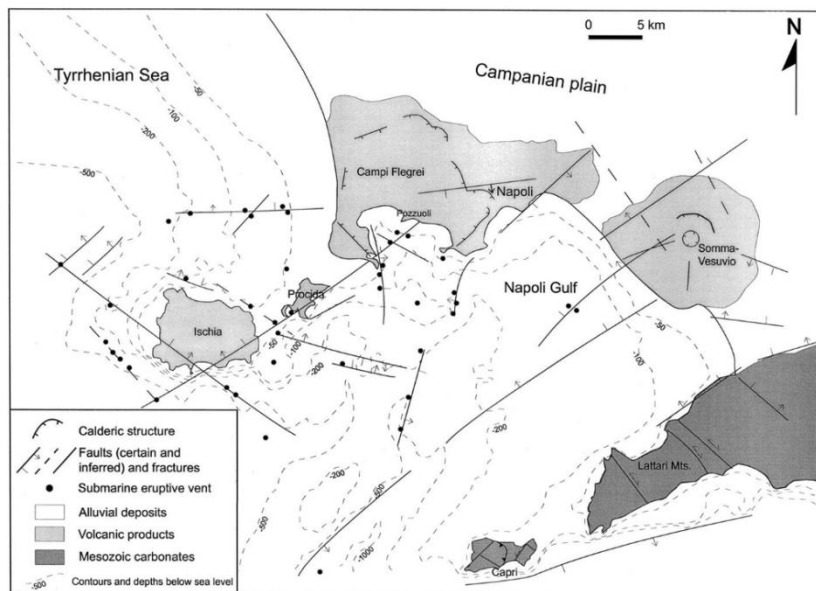
Figure 2.9 Campi Flegrei volcanic region. Source: (Briseghella et al. 2019)

In particular, the island's geological history has developed from 150 ka B.P (kilo annum Before Present). and may be grouped into five main periods of activity (Vezzoli 1988) identifying the formation of the various lava units composing the island and the subsequent deposit and cementation of the other volcanic products into banks of scoriae. The volcanic origin of the island justifies the largely distributed presence of hydro-magmatic tuffs all around the island.

The tectonics of the island is also defined by the presence of a resurgent caldera (Figure 2.10, triangle-dashed ellipse) activated by explosive acme of the volcanic activity around 60-55 ka B.P. and whose movements of uplifting and subsidence are related to the presence of a shallow laccolith. The magmatic body is located around 2 km depth with respect to the actual surface level. Its increasing pressure produces a resultant of the maximum stress applied to the uplifting rocks in vertical direction (Carlino 2012). The resurging-uplifting cycles and the marine origin of the resurgent caldera are geologically evidenced by the presence of marine fossil deposits and the signs of marine erosion in the volcanic lithographic layers above the actual surface level.
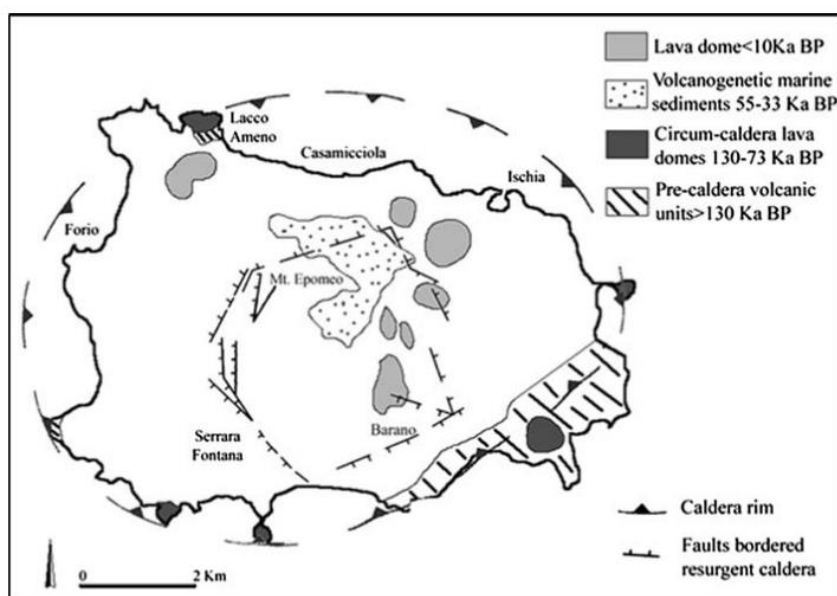
Figure 2.10 Major structural and volcanological features related to resurgence. Source: (Carlino et al. 2010)

Since the volcano-tectonic system is facing a phase of volcanic dormancy subsequent to the last volcanic eruptive activity dating back to the 1302, the general trend of the last 2000 years appears to be the differential uplifting and subsidence of the different sections of the island and of the surrounding offshore. Indeed, since 1913, a slow subsidence was registered, with an average velocity of 1-5 mm/yr, with maximum drops located in the central sector and in correspondence of the recent landslide deposits (Carlino 2012).

ADVANCED MASTERS IN STRUCTURAL ANALYSIS OF MONUMENTS AND HISTORICAL CONSTRUCTIONS

The resurging movements originated the most important tectonic element represented by the resurgent block of Mount Epomeo (787 a.s.l). Its quadrangular structure, about 4x4 km, is delimited by a mainly sub-vertical faulting system with orientation NW-SE, NE-SW, N-S and E-W Figure 2.10. Along the boundaries of the resurgent block are also located the principal hydrothermal eruptive centers. The total average uplifting of Mount Epomeo block is estimated around 800 m, approximatively corresponding to the current maximum height of the relief, and it presents an asymmetric trend with a maximum uplift located in the northern flank, estimated at 920-970 m, and a minimum in the southern section, about 710 m (Carlino 2012; Nappi et al. 2018).

Many authors attributed the activation of the resurgence of Mt. Epomeo block to a simple-shearing (Orsi et al. 1991) to a trapdoor uplift (Acocella et al. 1997; Acocella and Funiciello 1999; Molin et al. 2003)mechanisms resulting in a sub-vertical faulting system (Figure 2.11), which movement, combined with the seismic activity and the presence of the hydrothermal system, results in steep slopes on the flanks of Mt. Epomeo and in slope instability, landslides and debris avalanches due to the geotechnical properties (Nappi et al. 2018).
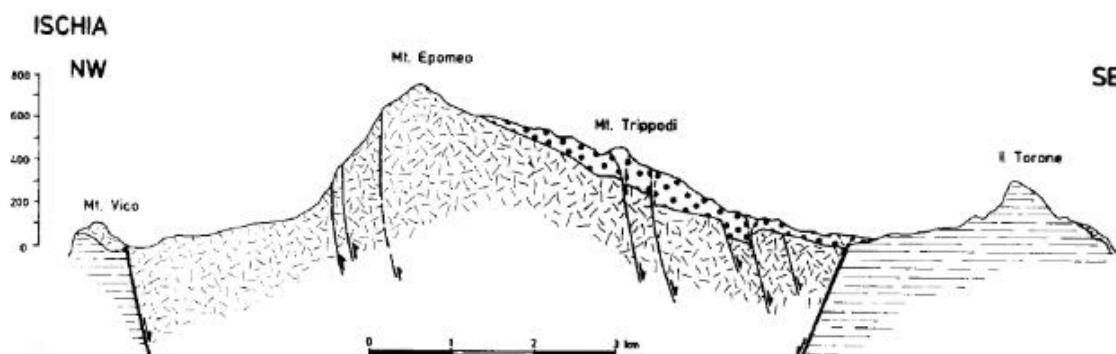
Figure 2.11 Simple-shearing mechanism of the faulting system of the resurgent block of Mt. Epomeo. Source: (Orsi et al. 1991)

2.4 Seismicity

2.4.1 Seismicity and seismic hazard of Italy

The Mediterranean region, to which Italy belongs, is a seismically active region due to the converging movements of the boundaries of the African Plate and the Eurasian Plate. The converging boundary is located along the Italian Appennino, the mountain chain that develops throughout the country longitudinal direction. The boundary characteristics are complex and result in the identification of different zones characterized by extensional, translational or convergence movements. These are defined by the plates boundaries movements that, generally speaking, consist of a motion range from

~4 millimeters per year (mm/yr) (in a northwest-southeast direction) in the western Mediterranean to ~10 mm/yr (north-south) in the eastern Mediterranean (Herman et al. 2015).
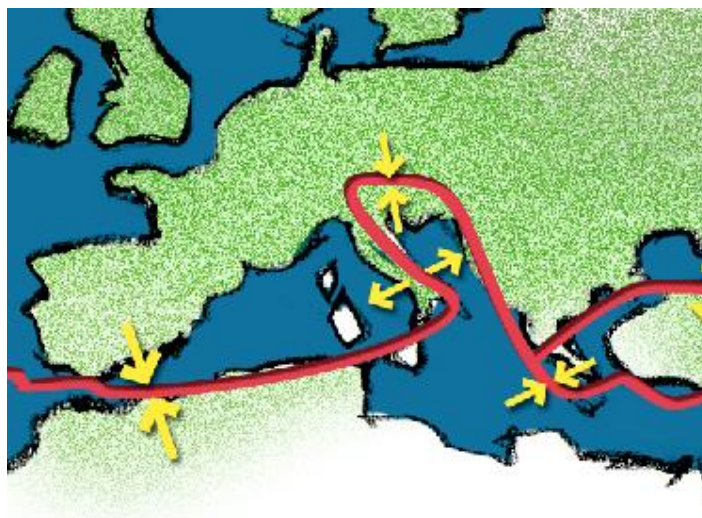
Figure 2.12 Tectonic plates boundaries interferring with the Italian territory. Source: (INGV 2015)

Peninsular Italy is one of the most tectonically and seismically active regions of the central-western Mediterranean area. Almost all the strongest seismic events along the chain (7 > M > 6) are generated by NW-SE normal faults (Fig. 1), which accommodate, on the whole, a NE-SW extension.

The entire Italian territory except for Sardinia has been struck at least once by an earthquake of I-VI degree on the Mercalli scale i.e. producing only minor damage. Quakes of higher intensity have never struck the Piedmont, a portion of Lombardy and Alto Adige, the Tyrrhenian coast from Versilia to the Volturno River the Adriatic coast south of Ancona and Salento.

Different seismic areas of Italy can be distinguished in relevance of the activating movement. They can be summarized as follows:

- Sicily and southern Sicily region, characterized by a subduction movement occurring beneath the Tyrrhennian sea and the Cantabric Arch, which generated some of the deadliest events in the Italian seismic history, e. g. Messina 1908;
- Eastern Appennine Chain, dominantly compressional with associated thrusting earthquakes;
- Western Appennine Chains, resulting on normal faulting seismicity due to the collapse of the mountain belt for gravitational loads.

The seismicity of the Peninsular region impacted not only the constant preparedness of the people to the seismic event, but also the construction typology of the buildings present in the region to ensure minimum damage.

The following Figure 2.13 shows a map of the major earthquakes occurred in the range period between 1900-2016 in relation also the plates boundaries interacting with the Mediterranean region. It is clearly visible, in the case of Italy the concentration of great relevance seismic events in the Cantabric Arc and along the Appennino.
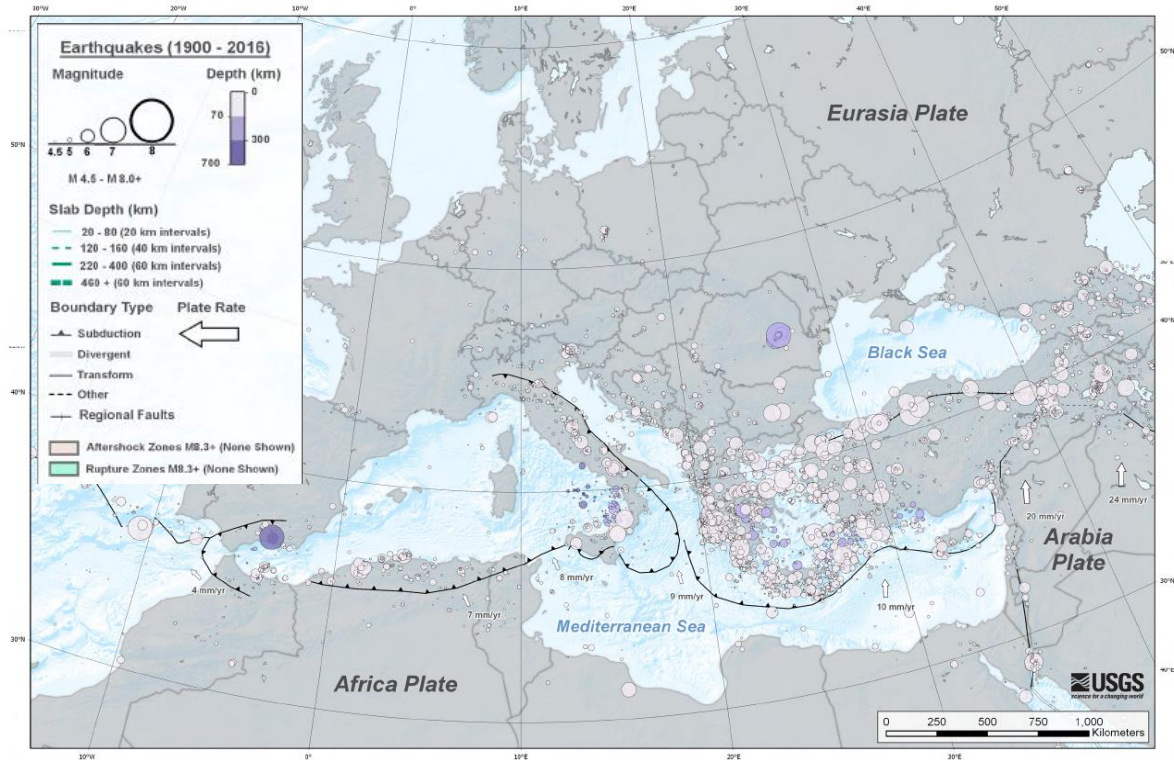
Figure 2.13 Map of the major earthquakes occurred in the Mediterranean Region and its vicinity in the range period between 1900-2016. Source: (USGS n.d.)

From the seismic history of the country, the fundamental parameters for the definition of the seismic action are defined on the basis of the study of the probability of reaching or exceeding in a defined time period, denoted as return period, a certain intensity of the seismic action for the considered location. In the case of Italy, the seismic risk studies are performed by the *National Institute of Geophisics and Vulcanology* (INGV) and are available in different formats. One of the most used is the map of the seismic risk (Figure 2.14) which graphically displays the different expected intensities of the seismic action expressed in terms of Peak Ground Acceleration (PGA) mapped throughout the Italian topographic map. Moreover, quantitative data are provided by the Italian codes (NTC 2018) according to the definition of a reticular mesh of points of assigned seismic characteristics (a_g, F_0 and T_C^*)[1] distributed over the Italian territory.

---

[1] See Section 2.4.3.
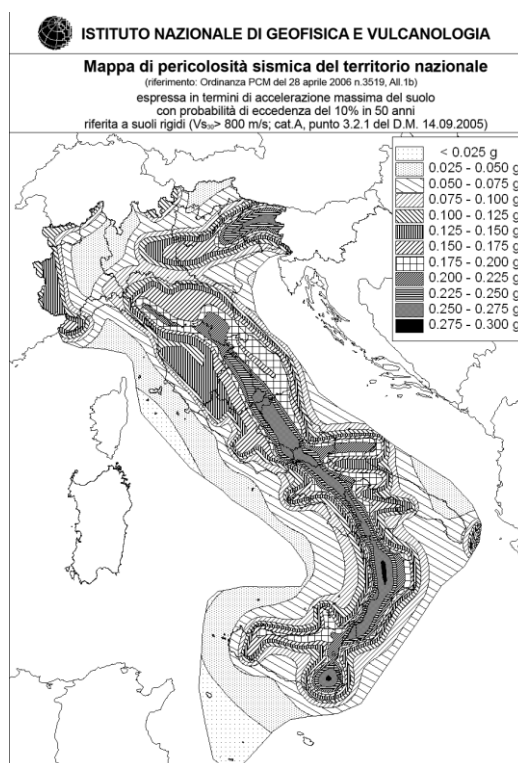
Figure 2.14 Seismic risk map for the Italian territory. Source: INGV

2.4.2 Ischitan seismicity

The seismicity of the island of Ischia has a clear volcano-tectonic origin characterized by shallow hypocenters mostly located along the northern flank of Mt. Epomeo and correlated with its uplifting movements. For active tectonic areas generally, it is reasonable to take into account three superimposing sources of seismic stress accumulation: the regional tectonic-stress source, the stress transferred from the neighboring faults, and the effects of the different viscosity of the lower crust. In the case of the island of Ischia, the regional tectonic-stress accumulation rate is not sufficient to generate enough pressure that justifies such short return period seismic events. Moreover, the recurrence of seismic events in the same resurging area of Mt. Epomeo supports the hypothesis of a seismicity generated by the pressure on the magma acting along the northern flank of the relief (Carlino 2012). The seismogenic volume is thought to be generated in the northern sector at a lower geothermal gradient, while in the southern sector, a high geothermal gradient promotes slow-slip phenomena and absence of earthquakes (Carlino et al. 2010).

The intense seismic activity on Ischia is evident from the historical records of the past earthquakes that date back up to the 1228, as stated before. It consists of at least 12 relevant events (MCS > VII), of which one was followed by an eruption (Arso 1302), (Carlino 2012). The main earthquakes that stroke the island are reported in Table 2.1, showing the approximated location of the epicenter, MCS

intensity, earthquake duration magnitude (M_D) and the earthquake effects. The list illustrates a decreasing return period between the seismic events that may be attributed both to an increasing seismicity of the area and to the limited amount of data available (Carlino 2012).

Table 2.1 List of the principal earthquakes that stroke the Ischia island

YEAR	EPICENTER	INTENSITY (MCS)	M_D	DAMAGES AND CASUALTIES
1228	Casamicciola Terme	IX - X	-	700 deaths, big landslide from mount Epomeo
1302	Eastern part of the island	VIII	-	Many buildings collapsed
1557	Campagnano	VII - VIII	3.5	Collapse of the church
1762	Casamicciola Terme	VII	3.5	Damage of the buildings
1767	Eastern part of the island	VII - VIII	-	Collapse of the Rotaro Church
1796	Casamicciola Terme	VIII	3.88	7 deaths, severe damage in the high part of the city
1828	Casamicciola Terme	VIII - IX	4.01	28 deaths, 50 seriously injured, severe damage in the high part of the city
1841	Casamicciola Terme	VII	3.25	Damage of the buildings
1863	Casamicciola Terme	VII	2.87	Collapse of the dry-stone walls, small landslides from mount Epomeo
1867	Casamicciola Terme	V - VI	2.99	
1881	Casamicciola Terme	IX	4.14	126 deaths, many severely injured, many collapsed buildings in Casamicciola and Lacco Armeno
1883	Casamicciola Terme	XI	5.2	2333 deaths. 762 severely injured, many collapsed buildings in Casamicciola, Lacco Armeno, and Forio
1980	South-western part of the island	V	MW = 4.37	No damages
2008	Mount Epomeo	IV	ML = 2.3	No damages
2017	Casamicciola Terme	VIII	4.0	2 deaths, 42 injured and 1000 people displaced

Note: the earthquake list references can be found mainly at (Rovida et al. 2016) with more information about earthquake's consequences at (Nappi et al. 2018), (Luongo et al. 2006) and (Cubellis and Marturano 2009).

It can be observed that the given large intensities of the seismic events are associated with relatively moderate magnitudes and with a strong intensity attenuation of the seismic energy, i.e. in the 1883 Earthquake very severe damage (IX to XI MCS) was observed in the range of about 1.5 km from the epicenter decreasing to relatively low (VI MCS) between 2.5 and 5.0 km (Carlino et al. 2010). This can be related to the buildings' vulnerability and to the shallowness of the seismogenic source, generally located at 1-2 km depth, along with the correlation of the intensity amplification with the outcropping of the reworked tuffs. For this reason, the evidenced great heterogeneity of the superficial geological conditions are potential sources of differential site effects that can lead to an overestimation of the macroseismic magnitude of historical events. On the other hand, an appropriate characterization of the local geological characteristics is, in Ischia's particular case, even more crucial for the prediction of the potential site effects.

Historically, the most catastrophic events occurred on 4th March 1881 (IX MCS) and on 28th July 1883 (XI MSCS) destroying almost entirely of the villages of the epicentral area, in both cases located in Casamicciola Terme. In addition, the recent earthquake that stroke the village once again on 21st August 2017 (VIII MCS) demonstrate the proneness of the city to seismic events, along the list of historical earthquakes with epicenter located in Casamicciola Terme provided at Table 2.1.

2.4.3 Seismic parameters of the church location

As mentioned, the seismic demand of a determined building site can be calculated according to the seismic parameters defined by the code. According to the Italian codes (NTC 2018-Chap. 3.2.3.2), the seismic characteristics of the seismic input expected of the site in which the studied building is located can be expressed in term of elastic response spectrum in acceleration which can be determined according to the following equations:

$$\text{For} \quad 0 \leq T < T_B \qquad S_e(T) = a_g \cdot S \cdot \eta \cdot F_0 \cdot \left[\frac{T}{T_B} + \frac{1}{\eta \cdot F_0} \left(1 - \frac{T}{T_B} \right) \right] \qquad (2.1)$$

$$\text{For} \quad T_B \leq T < T_C \qquad S_e(T) = a_g \cdot S \cdot \eta \cdot F_0 \qquad (2.2)$$

$$\text{For} \quad T_C \leq T < T_D \qquad S_e(T) = a_g \cdot S \cdot \eta \cdot F_0 \cdot \left(\frac{T_C}{T} \right) \qquad (2.3)$$

$$\text{For} \quad T_D \leq T \qquad S_e(T) = a_g \cdot S \cdot \eta \cdot F_0 \cdot \left(\frac{T_C T_D}{T^2} \right) \qquad (2.4)$$

Where:

- a_g is the peak ground acceleration (PGA) of the site location in the return period T_R;

- F_0 is the the maximum amplification coefficient of the horizontal acceleration spectrum in the return period T_R;

- T_C^* is the reference period of the constant velocity range of the spectrum in the return period T_R;

- S is the topographic coefficient obtained through the formula:

$$S = S_S \cdot S_T \qquad (2.5)$$

where:

- S_S is the stratigraphic amplification coefficient;
- S_T is the topographic amplification coefficient.

- η is the elastic spectrum alteration factor for damping structures with damping ratio less than 5%;

- T_C is the period corresponding to the starting point of the constant velocity section of the spectrum, given by the relation:

ADVANCED MASTERS IN STRUCTURAL ANALYSIS OF MONUMENTS AND HISTORICAL CONSTRUCTIONS

$$T_C = C_C \cdot T_C^* \qquad (2.6)$$

where:

- C_C is a coefficient representing the soil cathegory.

- T_B is the period corresponding to the starting point of the constant acceleration section of the spectrum taken equal to $T_C/3$;

- T_D is the period corresponding to the starting point of the constant acceleration section of the spectrum, expressed by the relation:

$$T_D = 4.0 \cdot \frac{a_g}{g} + 1.6 \qquad (2.7)$$

As observed, the definition of the elastic response spectrum depends on coefficients that take into consideration the soil characteristics and the location topography, out of the PGA parameter referred to the site. The described parameters can be obtained with the aid of the code and the adopted relative values are summarized in Table 2.2 and graphically visualized in **Errore. L'origine riferimento non è stata trovata.** where the characteristics seismic parameters are plotted for the whole Ischia island.

Table 2.2 Adopted parameter for the elastic response spectrum calculation according to the Italian codes for the USL (NTC 2018)

PARAMETER	VALUE	NOTES
a_g	0,152g = 1.4911 [m/s^2]	
F_0	2.29	
T_C^*	0.33	
S_S	1.20	Soil cathegory (B)[2]
S_T	1.2	Topographic cathegory (T2)
C_C	1.37	Cat. B (sottosuolo), Tab. 3.2.V
T_C	0.45	$T_C^* \cdot C_C$
T_B	0.15	$T_C/3$
T_D	8.29	$T_D = 4,0 \cdot \dfrac{a_g}{g} + 1,6$

(a)   (b)

(c)   (d)
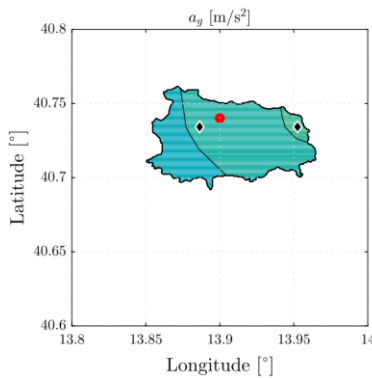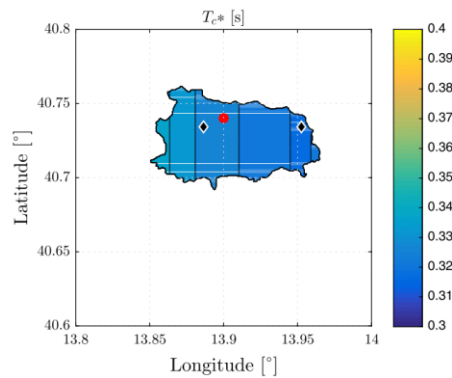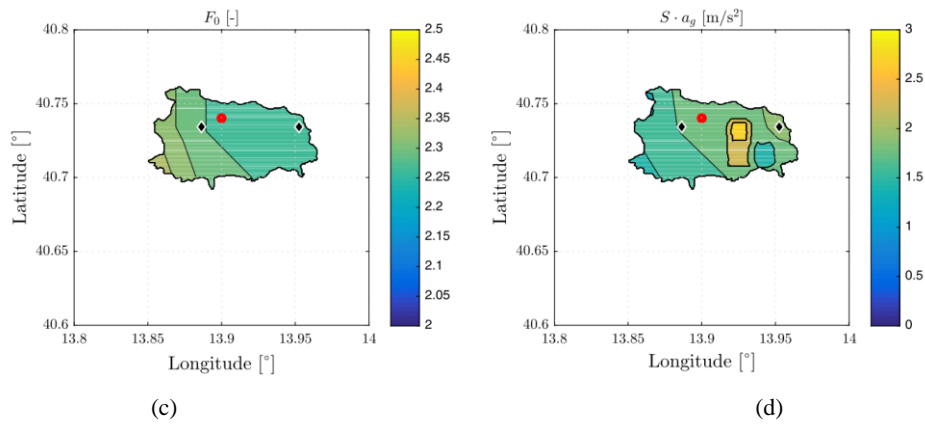
Figure 2.15 a_g (a), T_C^* (b), F_0 (c), $S \cdot a_g$ (d) with 10% probability of exceedance in 50 years (return period 475 years) according to Italian Building Code (NTC 2018) for the Ischia island. The red dot indicates the epicenter of the seismic event of the 21st August 2017. The black squares indicate the location of the nodes of the seismic mesh. Source: (Briseghella et al. 2019)

The described parameters are obtained from the code with respect to the building location, referencing the seismic hazard map of the region (Figure 2.14). Finally, the elastic response spectrum in acceleration is plotted in Figure 2.16.
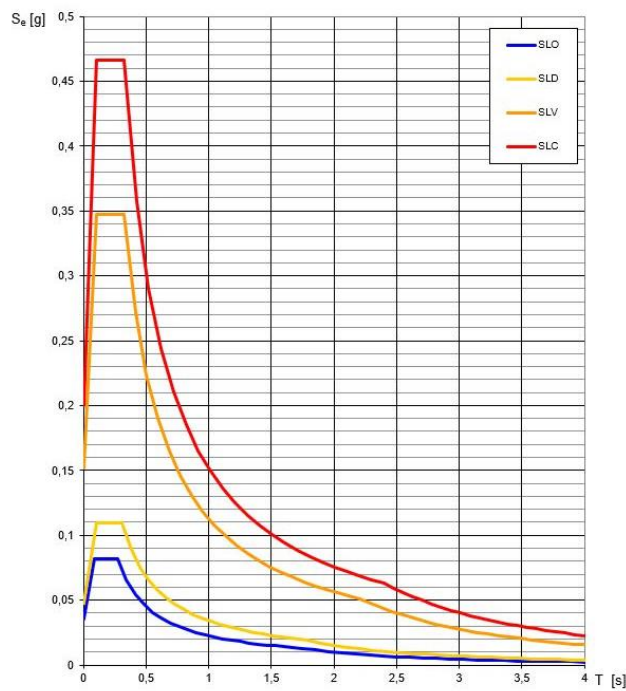
Figure 2.16 Elastic spectrum responses in acceleration for the church site considering the various limit states

The elastic response spectrum in acceleration can be directly compared with an equivalent *s*-DOF system opportunely converted from the pushover curves of a *n*-DOF system. The determination of the safety factor is, then, submitted to a safety judgment that in the case of heritage structures

3 DESCRIPTION OF THE CHURCH

3.1 Architectural description

The Santa Maria Maddalena catholic church is an isolated building. As previously mentioned, it is located on the top of a hill with a NE-SW orientation (Figure 3.1), in a position characterized by a significant slope that justifies the different altimetry of the ground levels of the church from the north-eastern front and the back part. The entrance of the church is located at the top of a staircase covering a height gap of about 1.30 m.

| Church | Canonical house | Belltower |

<div align="center">(a)   (b)</div>
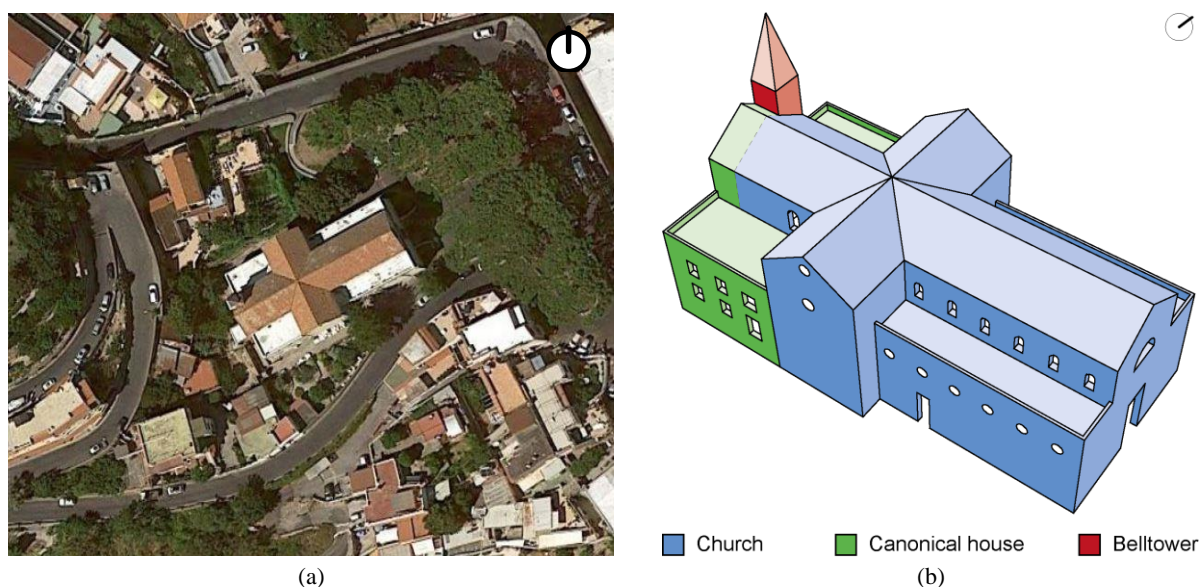
Figure 3.1 Aerial of the location of the church (a) and volumetric representation of the church (b). Source (a): GoogleMaps

From the volumetric point of view the building is composed by the church itself, a two-story back part, which hosts some spaces for the parish's activities and the priest's house, and the bell tower, located in the north-western corner (Figure 3.1a). Moreover, an additional volume hosting a W.C. and the kitchen can be observed alongside the western wall of the canonical house at the first floor. At the ground floor, this volume consists of a small patio in the backyard of the house. For its limited extension and its architectural and structural autonomy, it has been decided not to include this element into the structural analysis.

The church has a typical Latin-cross shaped plan configuration that, along the back portion of the building, consists of an almost rectangular footprint of dimension 39.04 m x 20.72 m. Five different height levels can be identified (Figure 3.2): the first one is identified as the +0.00 m level and

corresponds to the pavement of the church, the parvis[3] level is defined then with the altimetry -1.30 m. Approximatively around +7.30 m the third level is defined, corresponding to the extradoses of the terraces covering the lateral naves and the sides of the canonical house, another level corresponds to the attic floor (approx. +11.80 m) which supports the truss system composing the roof (max. height +16.33 m). The maximum height of the church is defined by the bell tower (+22.30 m). Extracts of the drawings of the church are presented in Figure 3.2 and the full documentation, comprising plans at the various floors, cross-sections and a representation of the main façades, are included in Annex 2.
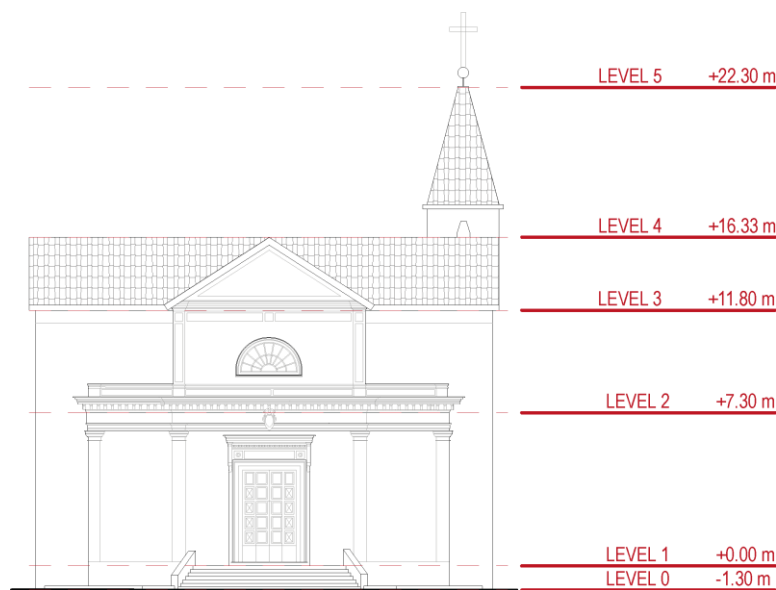
Figure 3.2 Scheme of the levels of the church

The majority of the building spaces is related to the religious functions as the church occupies around 80% (578 m^2) of the total footprint of the building (742 m^2). The remaining 20% of the building area is devoted to the complementary functions related to the parish activities. In particular, the spaces for the common activities of the parish and the sacristy are located at the ground floor, while the rooms of the canonical house are located at the first floor (Figure 3.6). The central section of the back building consists of the connecting spaces and staircase system that put in communication the various levels of the canonical house, the attic and the interiors of the bell tower.

---

[3] The vacant enclosed area in front of the church.

GROUND LEVEL (+0.00 m)

Figure 3.3 Grround floor plan view
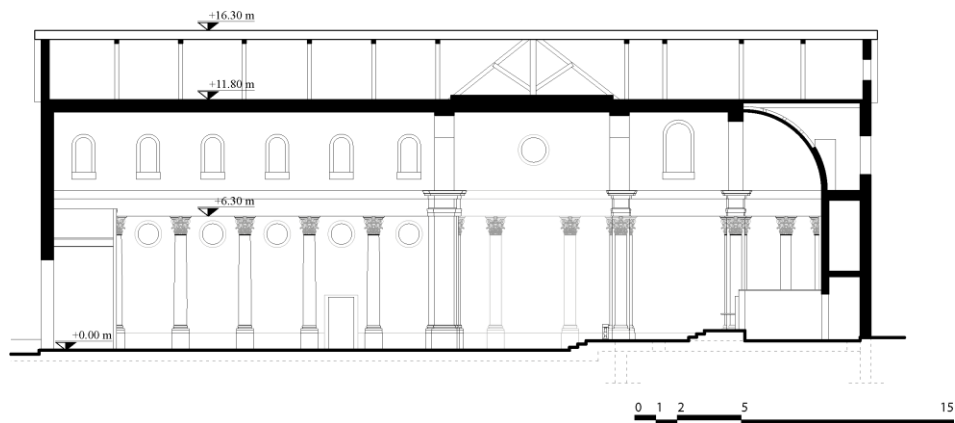
Figure 3.4 Longitudinal section

WEST FAÇADE (FRONT) AND TRANSVERSAL SECTION (BB') - 1:200
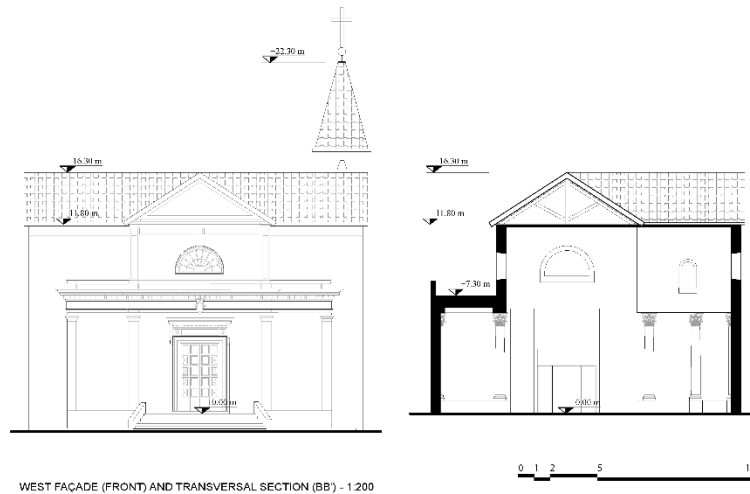
Figure 3.5 Front façade and transversal section

ADVANCED MASTERS IN STRUCTURAL ANALYSIS OF MONUMENTS AND HISTORICAL CONSTRUCTIONS

GROUND LEVEL (+0.00 m)

FIRST FLOOR LEVEL (+3.70 m)

CENTRAL NAVE LEVEL (+7.30 m)

ATTIC LEVEL (+13.08 m)

Central nave	Apse	Hallway/Services
Lateral naves	Deambulatory	Library
Transept		Sacristy/Living spaces

Bedrooms	Resulting space
Repository	Attic floor
	Belltower
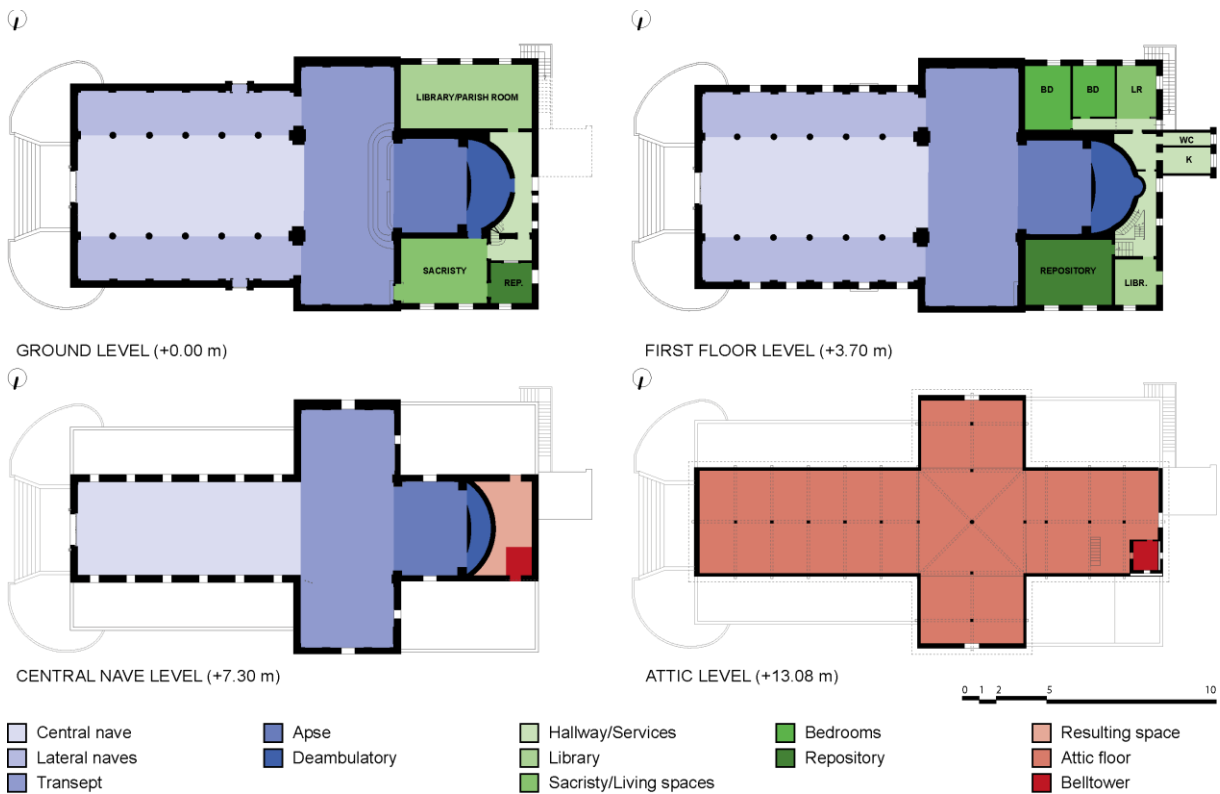
Figure 3.6 Functional scheme of the spaces of the church[4]

3.1.1 Interiors

As can be observed from the plan view, the church is composed by three longitudinal naves, a central one (Figure 3.7a) spanning 8.38 m, and two lateral ones (Figure 3.7b), defined by two rows of five columns and a pier, spanning around 3.70 m. The central nave meets the transept in the cross-shaft and the presbyterial section is composed by the apse, located on the top of a three-stair staircase, with a semicircular wall supporting a half dome.

(a)
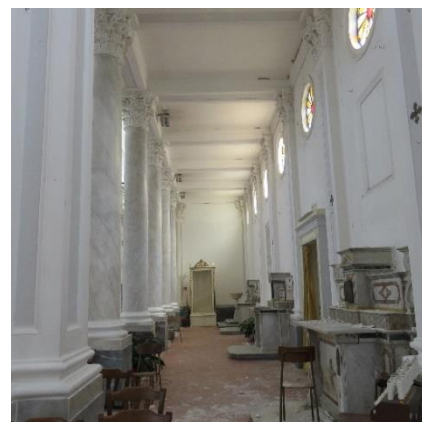
(b)

---

[4] For reasons of space the reported schemes are recalled in a larger scale in Annex 3for better legibility.

Figure 3.7 Internal views of the church: the central nave and the apsidal part (a), the south-eastern lateral nave (b)

The church has its main entrance in the north-eastern façade facing the staircase on the parvis. Two more entrances can be found in the lateral naves in correspondence to the fifth span of the gallery from the main façade. Moreover, the church relates to the sacristy with a door in the western branch of the transept and another one in the deambulatory. The main façade presents a semicircular opening at the second level, while the lateral naves have a circular opening in each span of the columns, corresponding to the arched windows of the higher wall of the central nave (Figure 3.8a). A few more arched and rounded openings can be found in the transept (Figure 3.8b).

| (a) | (b) |

Figure 3.8 Openings layout in the external walls of the lateral and central naves (a) and in the north-western branch of the transept (b)

The floor slabs covering the lateral naves are flat supporting the superimposed terraces, and flat is also the decorated ceiling of the church that hides the attic and supports the *stucco* ceiling decoration. Since the church was rebuilt in the late 19th century with the purpose of retrieving the lost dignity due to the collapse of the former church due to the earthquake, the interiors present notable plaster and *stucco* decorations following the decorative style of the Neoclassic style. In most of the cases, decorations are made with thick layers of plaster to form "fake" half-pilasters (*lesene)* and beams to underline a post-lintel structural scheme of the horizontal and vertical elements, consistently with the decorative style chosen for the church. It is noted that not always the decorative elements hinting structural elements correspond to effective ones. For example, the ceilings of the lateral naves present some decorations representing the floor beams connecting the columns to the lateral walls (Figure 3.9a) while the floor slab consists of a one-way slab with smaller beams closer spaced (Figure 3.9b).

<div align="center">(a)   (b)</div>

Figure 3.9 Post-lintel decorations of the ceilings of the lateral naves (a) and effective underlying structural scheme (b)

3.1.2 Exteriors

While the decorations are quite rich in the interiors, the external appearance of the church remains rather simple. The exterior façades are rendered with a thick layer of yellow-colored plaster that can reach in some cases a relevant thickness, up to 10 cm. A consistency between the style of the internal and the internal decorations is found, relating to a Neoclassic style, with the external decoration also underlying the post-lintel scheme with *lesene* and cornices painted in white color (Figure 3.10).

It must be pointed out that the presence of thick layers of both external and internal renders for the church walls, and their deficient anchorage to the supporting walls, is the most probable cause for the moderate to high damages that the church suffered to the decorative system after the earthquake that stroke Casamicciola Terme in 2017. Indeed, the damages suffered by these non-structural parts required urgent interventions, in terms of consolidation of the plasters and protection from the falling debris, that were applied to the church after the earthquake. Moreover, they played an important role in the definition of the church safety in the post-seismic condition. Thus, as it will be explained in the following sections, while the resisting structural elements of the building presented null to low damages after the seismic event, the bad condition of the non-structural ones caused the interdiction of the church from use in order to assure public safety.

Figure 3.10 Front façade of the church

3.2 Structural system

One of the reasons that makes the Church of Santa Maria Maddalena an interesting example of Italian religious architecture, which should be protected through appropriate studies and the application of measures of risk mitigation, is its unique constructive system for two different perspectives. Firstly, as already mentioned, part of the church was built according to the construction technique of the traditional Campanian *Baraccato* system, that can be enumerated among the engineered earthquake-resisting systems, e. g. *Gaiola Pombalina*, that were developed and spread between the 18th and 20th centuries as consequence of some of the deadliest earthquakes reported in the Europe's seismic history (Sicily 1693, Lisbon 1755, Messina 1908) (Ruggieri and Tampone 2015). The use of this mixed timber-masonry solution – later denoted as *timber-Baraccato* system – was largely spread in the earthquake prone areas of Southern Italy, thanks to the first European seismic regulation enacted by Ferdinando IV of Borbone, King of Naples and Sicily in the 18th century, after the catastrophic seismic events that occurred in Calabria in 1783 (Casapulla et al. 2019a; Serpe et al. 2016), although mostly related to the residential constructions as regular houses and palaces rather than religious or public buildings. Secondly, as it will be explained, the main body of the church was built according to a construction technique that can be identified as a variety of the *Baraccato* system – later addressed as *iron-Baraccato* system – which consists of a mixed iron-masonry solution with tuff masonry load-bearing walls juxtaposed to two layers of iron frames, following the main concepts of the layout schemes of a traditional *timber-Baraccato* solution. As reported in the Municipality indications for the post-seismic reconstruction, the use of iron was mandatory for buildings of public interest (Luongo et al. 2006). To this end, the Church of Santa Maria Maddalena and the Pio Monte della Misericordia,

public hospital and charity house in Casamicciola Terme, consists of unique examples in the island of this technique.

3.2.1 Identification

The uniqueness of the church's structural system is well documented in the information and drawings existing about the church's construction and emerged early during the first surveys and safety checks performed on the building after the seismic event of August 21st, 2017. In fact, from the observed damage it was possible to detect a global box-like response of the structure to the shake, evidenced from the mainly in-plane mechanisms that originated from the seismic input and from the widespread cracks developed in directions that could be only understood knowing the singularity of the vertical structural system.

In addition, a detailed geometrical survey and material identification was conducted in order to identify the existing structural units of the church, their structural schemes and materials. To this end, as a completion of the details already observable thanks to the post-seismic plaster damage, some plaster removals were performed additionally in some of the walls of the main body of the church and the canonical house, along with roof inspections and a thermographic survey that contributed to the validation of the hypotheses made about the *iron-Baraccato* frames' layout.

Summarizing the structural scheme of the building, the church can be divided in three structural blocks that reflect also the functional division of the building along with the hierarchy of the spaces (Figure 3.6):

- *Main body*: consisting of the Latin-cross portion of the church, built with the technique of the *iron-Baraccato* system, required for the construction of the most important part of the building depositary of its religious and social functions;
- *Canonical house*: consisting of the back portion of the church, built according to the traditional *timber-Baraccato* technique consistently with the other residential buildings in timber braced masonry around the island;
- *Bell-tower*: light-weighted structural block built with iron frames and light covering panels that for its lightness and its scarce influence in the determination of the global response of the church was discarded from the present analysis.

Bearing in mind this classification, in the following paragraphs a detailed description of the various structural units divided by their structural role is provided. This is based on the abovementioned surveys and some reasonable assumptions when the data gathered were not sufficient to completely

describe the structural concept, the geometrical measurements and layouts and the materials of the elements.

For the sake of clarity and to have a general overview of the structural scheme of the building, Figure 3.11 presents a structural/material identification of the various elements of the church. These can be classified by structural role as: vertical elements, horizontal elements, roofing system, and foundation system.
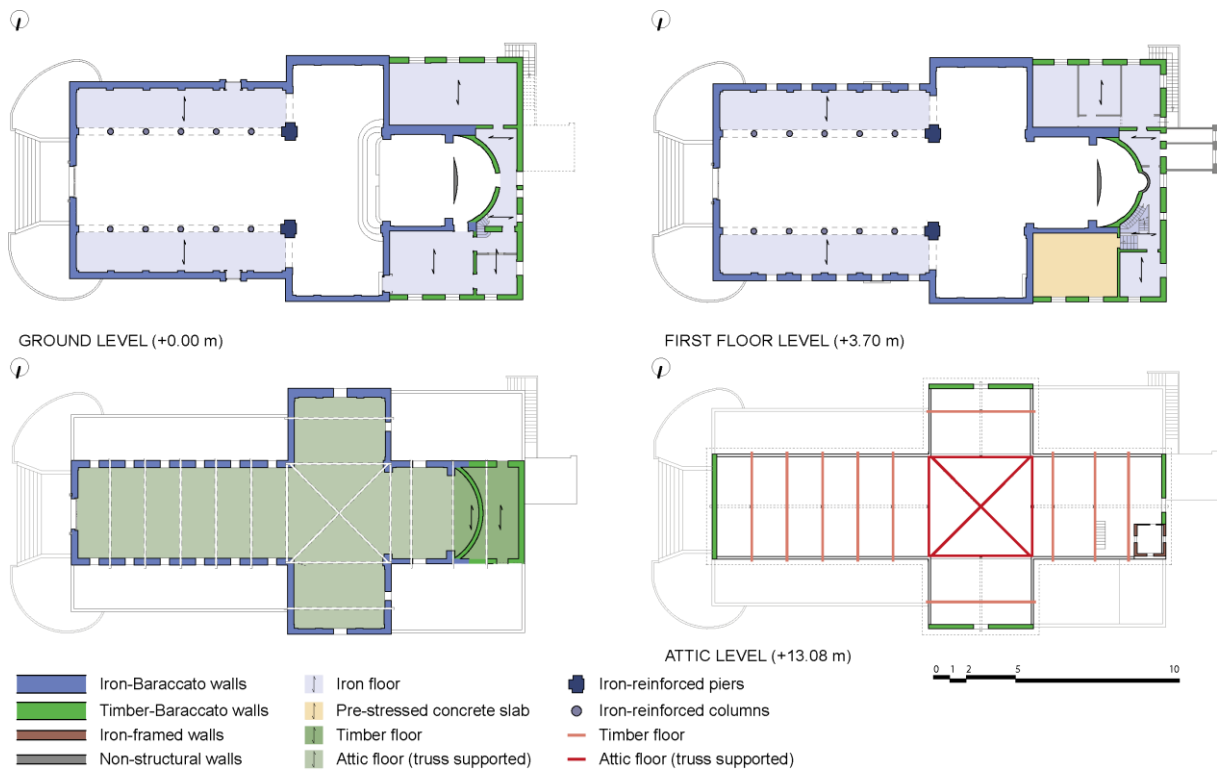
Figure 3.11 Material and structural elements identification[5]

3.2.2 Vertical elements

The vertical elements of the structural system under study are represented by the supporting walls of the church's naves, the front façade, and the transept and apse walls built in *iron-Baraccato* system, the walls of the canonical house in *timber-Baraccato* systems and the columns and the piers supporting the upper walls of the first story of the central nave.

For the purpose of the numerical simulation of the behavior of the church, crucial information that in some cases defines the size of the elements of the mesh is the wall thickness. For this reason, a

---

[5] The material and structural identification of the floor slabs are referred to the ceiling of each level of the represented drawings.
For reasons of space the reported schemes are recalled in a larger scale in Annex 3 for better legibility.

preliminary identification of the various thicknesses of the walls detected during the geometrical survey was performed and is presented in Figure 3.12. As shown also in the drawings at larger scale reported in Annex 3, the maximum thickness for the *iron-Baraccato* walls is about 77.5 cm while the minimum is around 42.0 cm in one of the side walls of the apse, the average thickness weighted on the length is 57.4 cm. Conversely, for the *timber-Baraccato* walls it is clearly visible that the long transversal wall facing south-west direction is the one with the largest thickness of 52.0 cm when the orthogonal supporting walls measure around 45.0 cm, for the external walls, and 20.0 cm, for the internal walls. Additionally, the curved wall of the deambulatory is around 35.0 cm and the other internal partition walls have thicknesses around 13-15 cm.
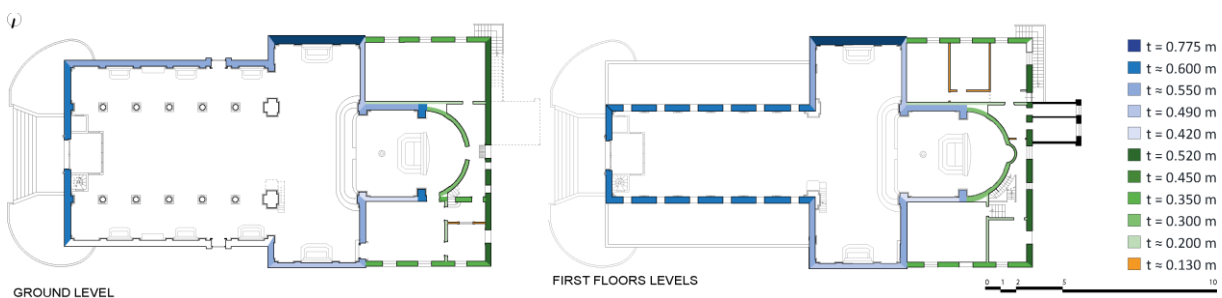
Figure 3.12 Thickness of the walls graphic scheme[6]

3.2.2.1 Iron-Baraccato walls

As mentioned, the so-called *iron-Baraccato* system consist of a complex solution for vertical load-bearing walls which takes advantage of the traditional technique of masonry walls along with the contribution of iron frames that increase the in-plane and out-of-plane response of the walls.

The surveys evidenced that the masonry part of the *iron-Baraccato* walls of the church of Santa Maria Maddalena are built with masonry units in Ischian and Torre Gaveta yellow tuff stones laid on lime-based mortar joints (Casapulla et al. 2019a). The stones are arranged along two faces with an internal core of rubble material, following the traditional technique of *sacco* masonries. Indeed, in the Neapolitan area between the first half 16th century and the first half of the 20th century masonry walls were built mainly with yellow tuff stones and can be divided according to three typologies, clearly identifiable also for the historical period. The typology of *a cantieri* tuff masonry, dating back to the 16th and 17th century, was realized by stacking roughened tuff blocks with thick layer of mortars that can be considered as conglomerates for the presence of big size aggregates and stone scales, where the horizontal alignment was not particularly attended but the transversal connection was assured thanks

---

[6] For reasons of space the reported schemes are recalled in a larger scale in Annex 3for better legibility.

to the presence of thin through stones. A second typology, widespread in the area in the first half of 18th century, is identified in the *bozzette* masonry typology where the horizontal alignment of the masonry units was better taken care of also with the use of better cut stone faces. However, for the construction period and the technology with which the masonry units of the walls of Santa Maria Maddalena church were found to be, they can be identified in the latter *a sacco* typology, used in the 19th century and in the first half of 20th century (Figure 3.14). In this, the walls were constructed with roughly worked stones of about 20-25 cm height, well aligned in rows with mortar joints of variable thicknesses and the external faces of the units presented flat surfaces and squared edges while rough internal finishing was given to the units in order to facilitate the bond with the internal core, constituted of irregular stone pieces and abundant mortar (Calderoni et al. 2006, 2009).

Figure 3.13 Picture of a masonry portion of one of the lateral walls of the apse

(a)

(b)

(c)
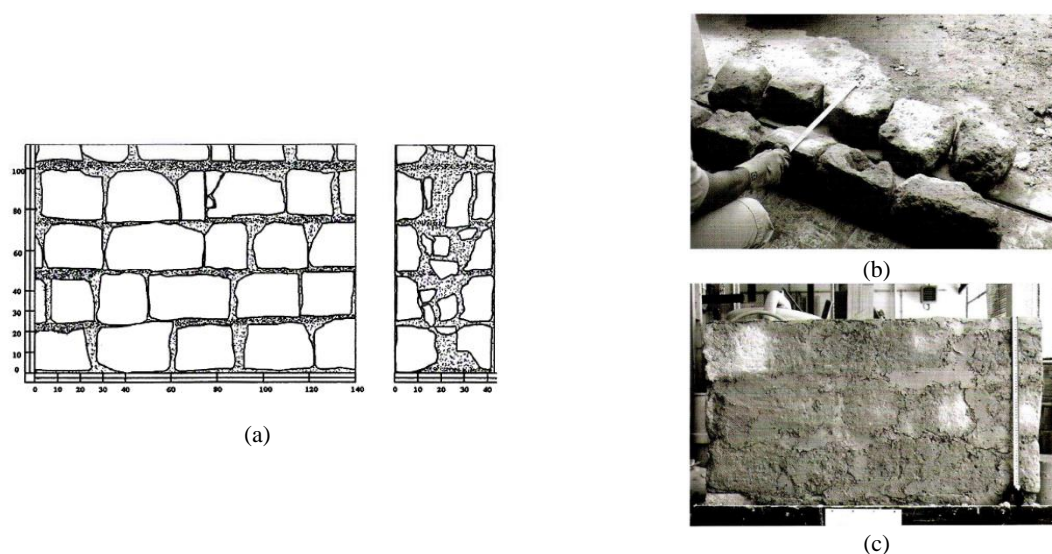
Figure 3.14 Sample of *a sacco* masonry with yellow tuff units realized for and experimental campaign for the definition of the mechanical characteristics. Drawings of the front view and the cross-section (a) and pictures of the building process (b) and front view of the sample (c). Source (a): (Calderoni et al. 2009). Source (b) and (c): (Calderoni

et al. 2006)

Moreover, in the church, the stone elements are suitably shaped against the iron elements and in some cases some small thickness blocks are used to cover the metallic elements in order to regularize the surface of the wall and to protect the iron frames from corrosion (Figure 3.15). The surveys evidenced that the tuff blocks have average dimensions of 270 mm x 230 mm (Casapulla et al. 2019a) consistently with the information about block dimensions found in literature which indicate standard ratios for tuff units of 1:1, 1:1.5 and 1:2 ratios (Calderoni et al. 2009).

(b)

Figure 3.15 Arrangement of the masonry units around the iron frames (a) and use of small thickness stones to cover the vertical iron elements (b)

The damages caused by the 2017 Ischia earthquake and the latter plaster removals performed for the geometrical survey, allowed also to observe clearly the metallic profiles used to build the two layers of metallic frames. While no information was found in the church documentation regarding the iron quality (cast iron, wrought iron, early steel, etc.) used for the profiles, the state of conservation of some profiles located in positions particularly exposed to water damage (Figure 3.16a), like the ones close to the terraces and the drainpipes, allowed to identify the material used for the profiles as wrought iron for the typical layered rust corrosion that they presented (Figure 3.16b). This observation is also supported by the profile shapes used for the iron elements. Indeed, the iron frames of the *iron-Baraccato* walls of the church are constituted with L-shaped and T-shaped profiles for the vertical elements and plate elements for the horizontals and the diagonals, which can be considered as thin profiles, corresponding to a typical characteristic of wrought iron cross-sections. Conversely, the hypothesis of the iron typology of the frames is drawn in disagreement with the types of connections observed between the various iron profiles. Indeed, it is well known that one of the most relevant

indicators of wrought iron structural elements is the riveted connection between the various sections (Bussell 1997). The connections observed between the metallic elements are, in some cases, represented by riveted connections (continuity connections, Figure 3.17a), though, in other cases they are assured with the use of single bolts both between the vertical and the horizontal elements ad between the horizontal and diagonal ones (Figure 3.17b).

<table>
<tr><td>(a)</td><td>(b)</td></tr>
</table>

Figure 3.16 Layered corrosion of an horizontal iron element element of the church (a), typical delaminated corrosion of a wrought iron element

(b)

(a)

Figure 3.17 Example of riveted (a) and bolted (b) connections between the iron elements of the church

As mentioned, the iron profiles constituting the two frames juxtaposed to the internal and external face of each wall are differentiated by the structural role. Indeed, since just the vertical columns are designed to work to resist bending actions, they are the ones presenting the T-shaped section, which is substituted by an L-shaped one when it is used for an element embracing masonry at the corner intersection between two orthogonal walls. The L-shaped section is also used at the top of each wall again to embrace the masonry. All the other elements, such as the horizontals and diagonals, consist of plate profiles that mainly undergo axial forces. The multiple transversal connections that horizontally

connect the two frames of each wall are also built with flat profiles, which the original drawings and some punctual inspections indicated to be spaced around 1 m throughout the height of each wall. A simplified scheme of the arrangement of the different profiles with the masonry is provided in Figure 3.18a, while a comparative picture of an actual section of a wall of the church is reported in Figure 3.18b. From the dimensional point of view, Table 3.1 presents the measured dimensions of the profiles surveyed in the church and their principal geometrical characteristics.

(a)   (b)
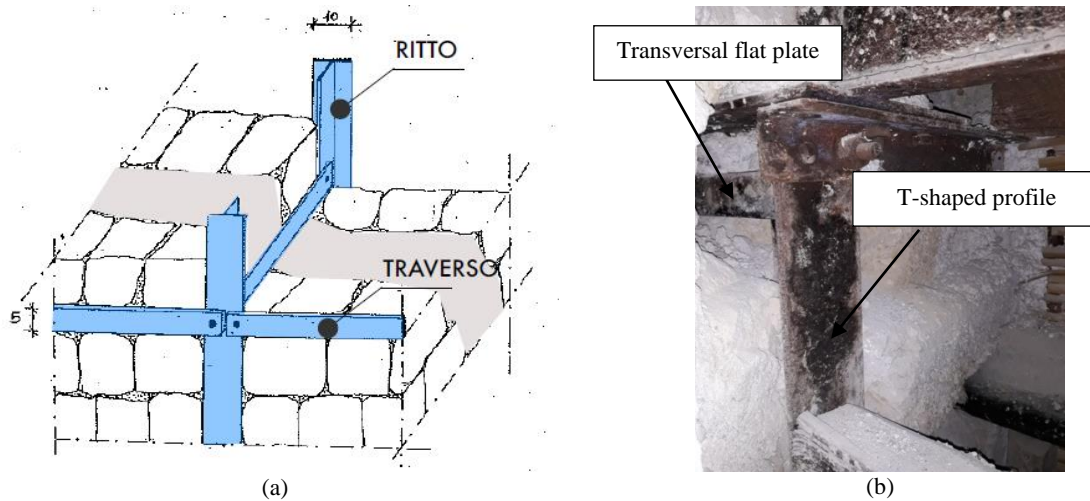
Figure 3.18 Conceptual sketch of the structural scheme of the *iron-Baraccato* walls (a) with a comparative picture (b) of an actual wall of the church. Source (a): (Casapulla et al. 2019b)

Table 3.1 Geometrical measurements of the iron profiles of the *iron-Baraccato walls*

Profile	Geometrical measurements			
	b	70 mm	A	1600 mm^2
	h	100 mm	I_y	6.477 10^4 mm^4
	t_w	10 mm	I_z	8.383 10^4 mm^4
	t_f	10 mm	I_t	5.973 10^3 mm^4
	b	150 mm	A	2900 mm^2
	h	150 mm	I_y	6.372 10^6 mm^4
	t_w	10 mm	I_z	6.372 10^6 mm^4
	t_f	10 mm	I_t	9.570 10^3 mm^4
	b	50 mm	I_y	2.083 10^4 mm^4
	h	20 mm	I_z	3.333 10^3 mm^4
	A	1000 mm^2	I_t	9.840 10^3 mm^4

The *in -situ* investigations, along with a thermographic survey, allowed to clearly identify the layout and the arrangement of the various metallic elements along the masonry walls of the church. Obviously, not the totality of the frames was directly observed during the investigations, but the extent of the elements directly observed assures a high confidence level for this portion of the building and reasonable assumptions were made to complete the structural scheme. Additionally, the iron frames were found to be in most of the cases corresponding between the two faces of the walls and for this reason they are presented in Figure 3.19 and in Annex 2 just once per wall in the various sections provided.

(a)

(b)

(c)
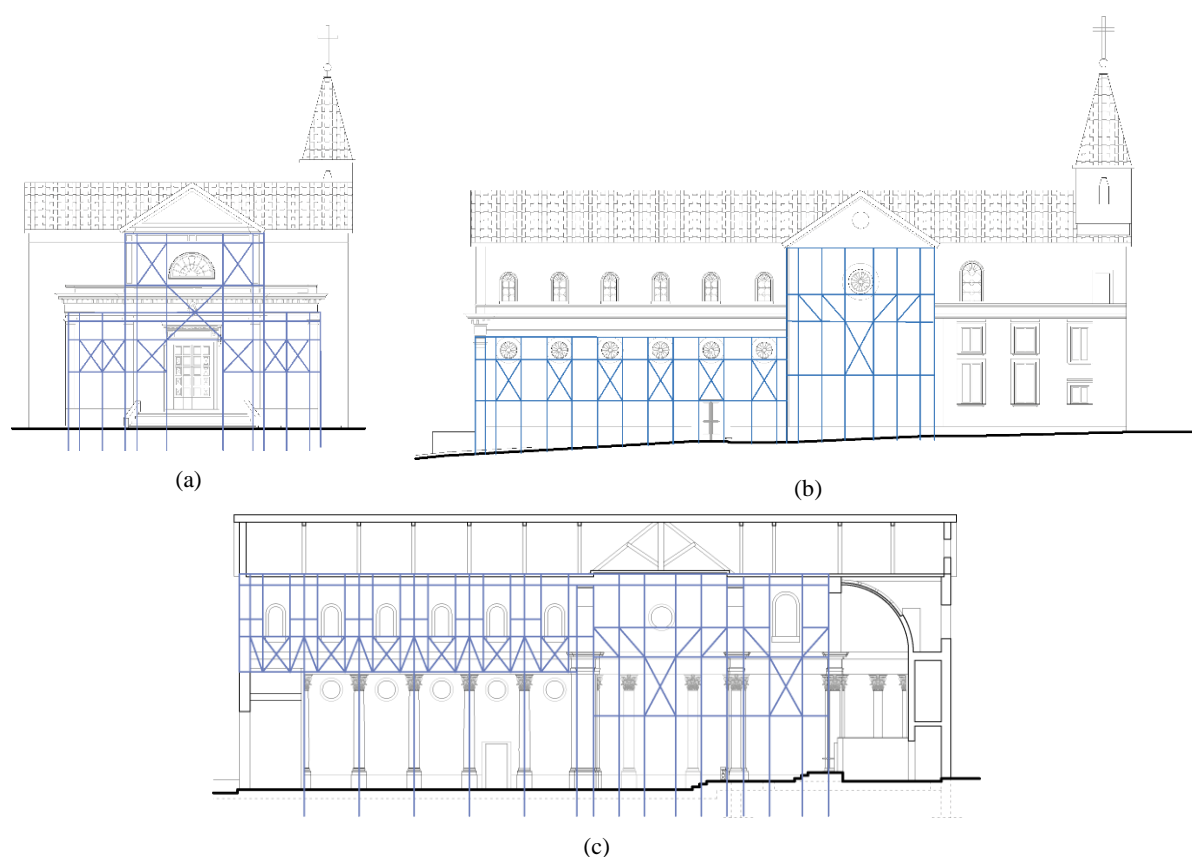
Figure 3.19 Layouts of the iron frames of the system: front façade (a), lateral façade (b), upper wall of the central nave (c)

Figure 3.20 shows a spatial representation of the *iron-Baraccato* system of the church in its totality with a chromatic identification of the elements profiles and location, where the L-shaped profiles are represented in red, the T-shaped ones in blue, the horizontal and diagonal plates in green and the hypothesized positions of the internal ties are represented in pink, inside the grey solid representing the masonry. As observed and also evident from the historic pictures of the construction phases of the building (Figure 3.21), the frames encaging the walls constitute a rigid skeleton whose principal

advantage to the structural behavior is the connection that they provide between the various structural units. In fact, they primarily assure the almost perfect connection between orthogonal walls which is witnessed by the complete absence of development of out-of-plane mechanisms of the walls in consequence to the seismic event of 2017. Moreover, the connection is also assured with the other adjacent structural elements, such as the floors and the columns. The use of the iron also in these structural units, indeed, enables a structural continuity of the iron frames of the walls and their metallic elements which connection is easily and effectively resolved. Lastly, the presence of a double layer of iron frames tied with each other provides to the walls a certain level of confinement which increases the overall strength of each wall section.
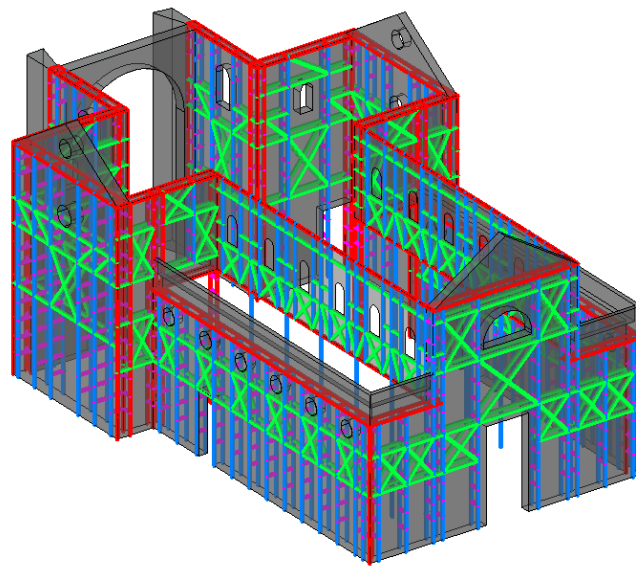
Figure 3.20 Spatial representation of the surveyed iron frames
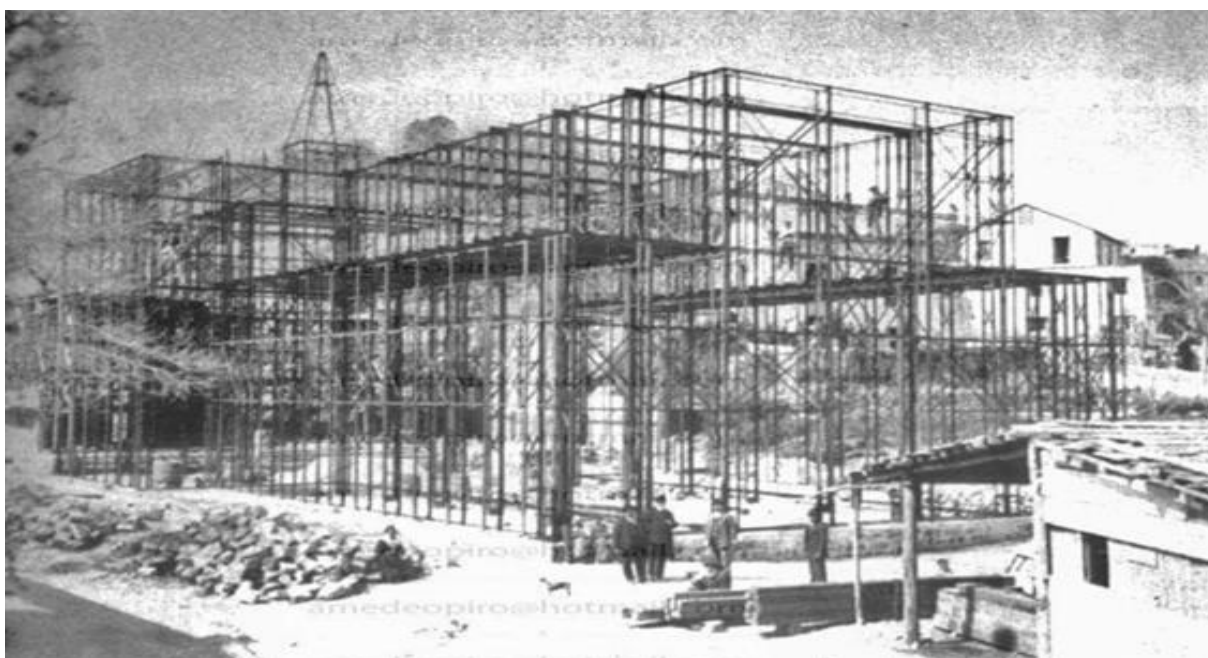
Figure 3.21 Historic picture of a construction phase of the church, taken after the completion of the iron framed skeleton and before the building of the masonry walls. Source: (Casapulla et al. 2019a)

3.2.2.2 Naves' columns

In continuity with the iron frames of the walls, the other vertical elements of the main body of the church are built according to the construction technique used for the church's walls using iron profiles to increase the structural performance of the resisting elements. The two rows of columns that separate the central nave from the two lateral aisles consist of a total of 12 vertical elements, 6 per side, of which 10 have a rounded section (columns) and the last two, located in correspondence of cross-shaft, have rectangular cross-section (piers). For these elements it was not possible a detailed technological survey due to their good state of conservation that did not justify a partial demolition. The information was anyway able to be gathered from the original drawings and some pictures taken during a plaster and decoration renewal of the columns done in the Eighties of the 21st century (Figure 3.22).

As can be seen from Figure 3.22a, the internal iron profiles, that, according to Figure 3.22b, are arranged in two T-shaped profiles with the iron web oriented towards the center of the column and connected with rectangular plates, are embedded in a chaotic material that can be identified as conglomerate covered by a thick layer of decorated plaster. In conclusion, for the purpose of the present analysis the cross section reported in Figure 3.23a was assumed.

As for the piers located in correspondence of the cross-shaft of the church, no other information was found but, consistently with the layout of the metallic elements that emerged from the geometrical

survey and in analogy with the columns of the church, they were assumed to have the cross-section presented in Figure 3.23b where L-shaped vertical elements, connected with rectangular plates, embrace an inner core of chaotic material.

(a)   (b)
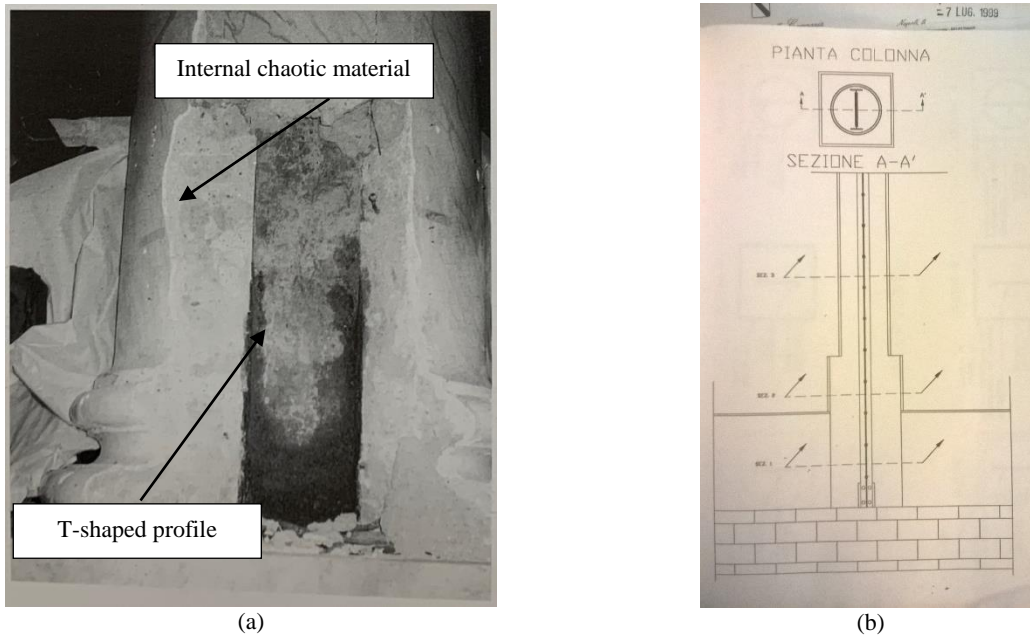
Figure 3.22 Literature information about the internal composition of the columns, historical picture (a) and historical drawing of the cross-section (b). Source (a): (Polverino 1998)**. Source (b):** ("Archivio di Stato di Napoli, Corpo Reale Genio Civile, fascio 342, incart. 3" n.d.)

(a)   (b)
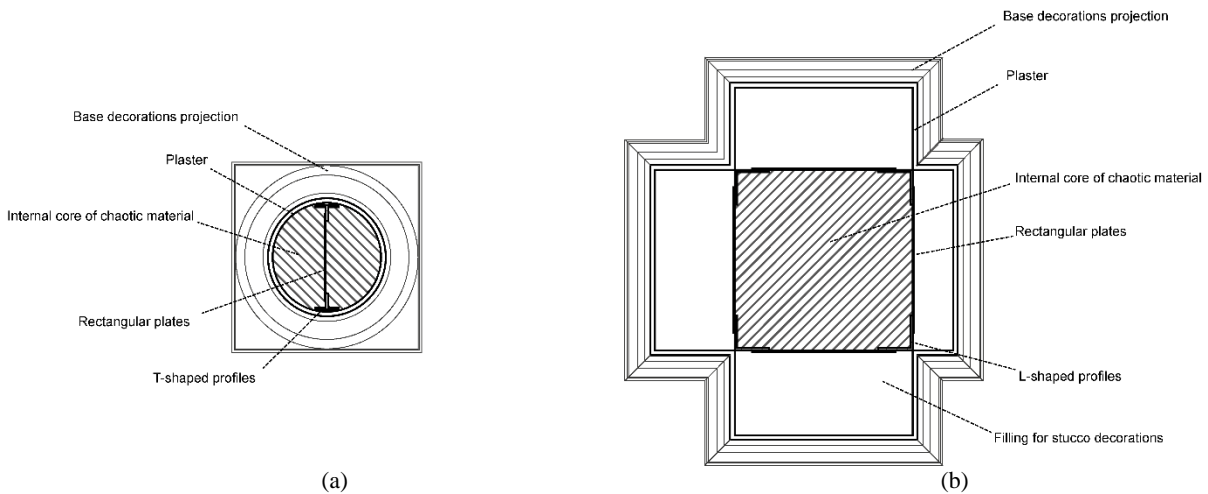
Figure 3.23 Structural section of the columns (a) and the piers (b) of the church

Lastly, the connection between the columns and piers of the church naves and the supported second-story wall of the central nave is worth a mention. Indeed, three different structural elements converge in this node, the vertical columns of the nave, spanning around 3 m along the longitudinal direction, the upper wall of the central nave, and the iron floor covering the side aisle (Figure 3.24). Those elements need to be properly supported to assure the stability of the system.

As it can be observed from the iron frames layouts (Figure 3.19c), the vertical connection between the columns of the gallery and the upper wall is probably assured by the continuity along the height of the vertical iron elements embedded in the columns, to constitute the vertical elements of the frame encaging the wall. The upper wall, then, present the typical configuration of the iron frames similarly as it was detected all around the *iron-Baraccato* structure, but the geometrical and technological survey were not able to find any presence of a horizontal elements connecting longitudinally the columns and supporting the upper walls and the beams of the floor. Different hypotheses can be drawn about the structural concept of this portion of the building. A first hypothesis can be the presence of an horizontal beam supporting the aisle terrace, on which the masonry of the upper wall is laid and on which the iron frames of the wall are anchored, but in this case the continuity of the vertical iron elements would not be assured. More likely, it could be supposed that the structural system takes advantage of the layout of the iron frames of the lower part of the supported wall to form a three-dimensional iron truss filled with masonry which works as a truss beam laid on the columns and supporting the floor. In this case, the masonry physical support in correspondence of the architrave could have been resolved with the positioning of an iron plate supported by the horizontal iron elements of the frame.

In any case, even if the knowledge of the structural functioning of the node is not well known and concerns may arise about the structural safety of the underlying gallery even just for gravitational loads, it must be pointed out that no damage was detected in the columns, in the architrave or in their connection. In fact, if any structural deficiency was included in the node some damage would be detected before the earthquake during the normal use of the church and especially after the seismic event. For this reason, the structural detail should be inspected to reach a higher level of knowledge of the node and to properly model it in the numerical simulation, while, seemingly, not being a threat to the structure integrity.

Figure 3.24 Unresolved node of the connection between the columns, the central nave second floor wall and the iron floor of the side aisle

3.2.2.3 Timber baraccato walls

The remaining walls, that constitute the vertical load-bearing system of the canonical house, are built with the more traditional *timber-Baraccato* system. As mentioned, this solution has been used since the 18th century all across Southern Italy in response to the disastrous earthquakes that hit the region frequently. The technology of the structural technique for such walls is well known to consist of a main timber frame structure, of vertical columns and horizontal lintels of similar dimensions supporting the diaphragm and closing the frame, and a secondary timber structure stiffened by Saint-Andrews timber crosses, fixed to the primary structure by means of simple metal connections (Casapulla et al. 2019a). The timber structure of the walls was then filled with masonry. The typical layout of a *casa Baraccata* is presented in Figure 3.25a.

<table>
<tr><td>(a)</td><td>(b)</td></tr>
</table>
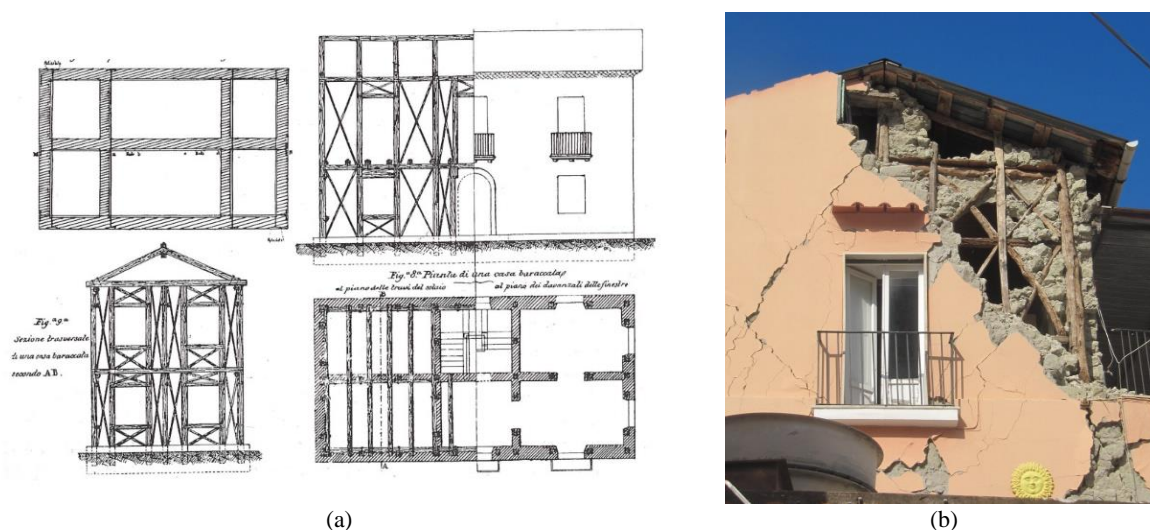
Figure 3.25 Historic drawings of the traditional *timber-Baraccato* system (a) and an example of its use in a building located in Casamicciola Terme (b). Source: (Casapulla et al. 2019a)

The presence of such a system in the back part of the church was evident from the existing documentation of the building (Figure 3.26) and from the plaster removals that also interested this portion of the church, mainly to confirm it. A thermographic survey was also performed on the walls of the canonical house, as done for the *iron-Baraccato* walls, but in this case the internal and external conditions of the day of the survey and the similar specific temperatures of the elements of the *timber-Baraccato* walls did not allow to add any contribution to the knowledge of the technology of these inspected walls.

The surveyed sections allowed to estimate the timber elements' widths measuring around 30 cm for the principal ones and around 15 cm for the diagonals and the horizontals, to identify the position of some of them (Figure 3.27), and to inspect the timber specie that in the bill of quantities was indicated to be chestnut. Other information about the system layout that must be included in the numerical model of the church was deduced from the above mentioned *in-situ* observations, but mostly the layout of the timber frames was assumed from the original drawings of the church (Figure 3.26). As already mentioned, the use of the original documentation on the geometrical aspects of the church, especially from the Eng. Gambara drawings, is not always reliable, because during the construction period many changes were made by Eng. Parisi, responsible for the construction of the building. For example, in the drawings the canonical house is represented as a single-story building while two floors were then built and are still standing today. Nonetheless, since at this level the information about the *timber-Baraccato* walls is not sufficiently detailed and it would require deeper studies and inspections, the drawings were considered the best source of information to make educated assumptions about the layout. Moreover, the layout presented in the original drawings is consistent with the typical layout of a Campanian *casa Baraccata*, as seen from Figure 3.25. The assumed layout taking in consideration

ADVANCED MASTERS IN STRUCTURAL ANALYSIS OF MONUMENTS AND HISTORICAL CONSTRUCTIONS

the position of the wall openings forcing the position of many of the columns and posts of the timber system, and this was considered a satisfying starting point for a preliminary analysis of the behavior of this part of the church. In Figure 3.28 the layout of the *timber-Baraccato* walls is presented where the lines in blue represent the timber elements with a high level of confidence – inspected elements or positioned in obvious locations, e.g. angular columns, above-opening lintels, etc. – and in grey are represented the elements with lower confidence level where the elements were positioned with the aid of the historical drawings (Figure 3.26). A representation of the assumed layout for each wall is also included in Annex 2.

(a)   (b)
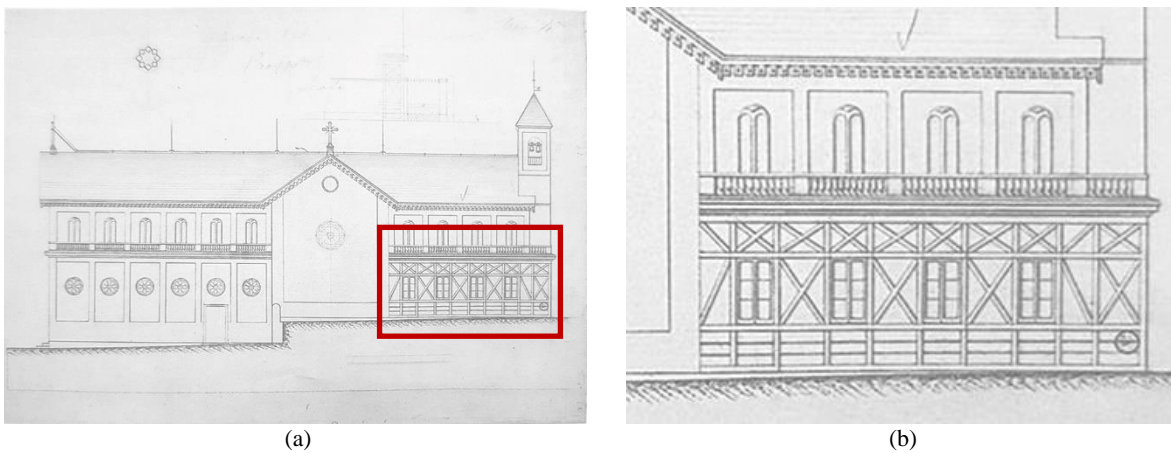
Figure 3.26 Historic drawing of the North façade (a) and relative detail of the timber frame layout (b). Source:
("Archivio di Stato di Napoli, Corpo Reale Genio Civile, fascio 342, incart. 3" n.d.)

(b)   (b)

**Figure 3.27 Inspection spots of the *timber-Baraccato* walls, internal wall of the parish common room (a) and
Northern lateral wall of the apse (b)**
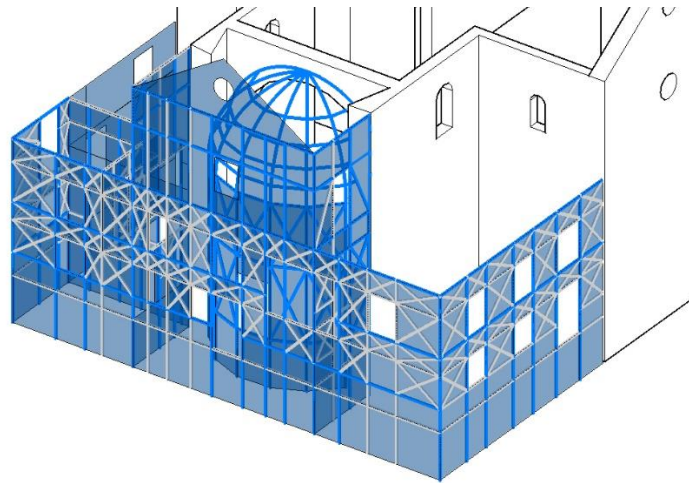
Figure 3.28 Layout scheme of the *timber-Baraccato* walls

It must be pointed out that, in the process of retracing the layout of the timber frame of the Northern external wall of the canonical house, a possible presence of a recent intervention in the wall was noticed, probably influencing the actual layout. As also explained in Section 2.2, in its North-Western portion the building underwent the substitution of the floor slab covering the first floor with a reinforced concrete one and the modification of the underlying spaces. In the related supporting external wall, the presence of non-aligned openings, bigger than the others existing in the canonical house walls, can be noticed (Figure 3.29). Additionally, their position does not match with the guessed layout of the timber sub-structure of the wall. Therefore, the interventions carried out on the floor slab and on the related internal spaces could likely have affected also the side wall of the building with a partial or total reconstruction of the wall and its opening layout. Since the construction technique adopted for the floor used modern materials, a re-proposed application of the *Baraccato* system of the wall is unlikely to be present. These considerations lead to the conclusion of not reporting any timber element in that portion of the lateral wall and analyzing it as an unreinforced masonry panel in the numerical model.

Figure 3.29 Bigger size, non-aligned openings of the external Northern wall of the canonical house

An additional observation can be carried out about the wall thicknesses and the number of the timber frames present along the thickness of each single wall. Indeed, documents about the traditional *Baraccato* systems report the possible presence of single framed solutions for the walls but also wall diaphragms that present a double layer of timber frames encaging an internal core of masonry (G. Vivenzio 1788), as also seen in the *iron-Baraccato* walls (Section 3.2.2.1). As discussed in Section 3.2.2, the various *timber-Baraccato* walls present different thicknesses in relation to their structural role and position that can reach 52 cm in the case of the long external Western wall and 45 cm in the case of the external walls oriented in the orthogonal direction. The thicknesses of these diaphragms are compatible with a double-framed solution which presence is, though, not certain and has to be verified. In any case, to the aim of the structural analysis, the width of the timber elements was assumed equal to the thickness of the wall for each case, but more refined analyses would be possible if a better level of knowledge is reached for these structural elements.

A final mention is needed with respect to the connections between the two structural systems that constitute the vertical load-bearing structure of the church. It is clear, now, that the use of two different constructive systems for the building of the vertical walls in different sections of the building would necessarily include some discontinuities that should be properly investigated in a structural analysis, which is aimed to catch the global behavior of the structure. In the present case, only limited inspections were possible. The contact points of the two structural systems and the locations of the direct observations of the connections that it was possible to carry out are indicated in Figure 3.30. These direct observation points lead to different conclusions. Firstly, at the first floor of the canonical house, it was observed the internal wall of the priest's bedroom presents sections where the two framed systems overlap (Figure 3.31a). In this case, it is believed that the walls in continuity with the

lateral walls of the apse present the two structural solutions along their length and throughout the height of the two floors. On the other hand, the portion of the same walls emerging from the canonical house in continuity with the lateral walls of the apse present a clear discontinuity, as can be observed from Figure 3.31b. As for the connection of the canonical house with the walls of the transept, no direct inspections were possible.
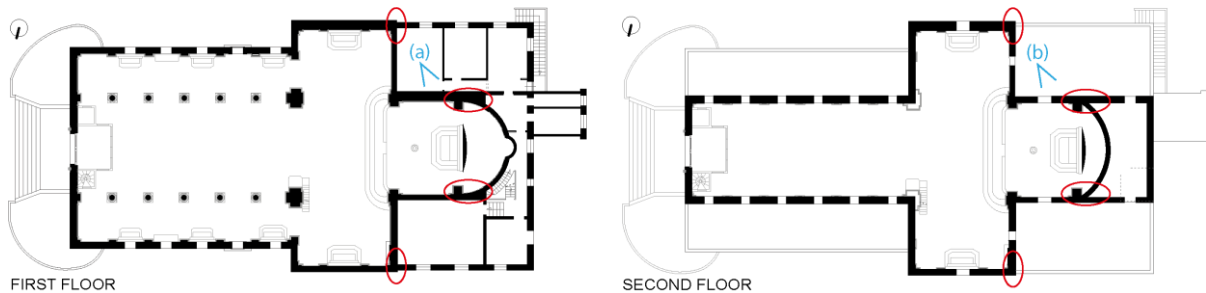
Figure 3.30 Connection points of the Baraccato systems and location of the points of inspections

| (a) | (b) |
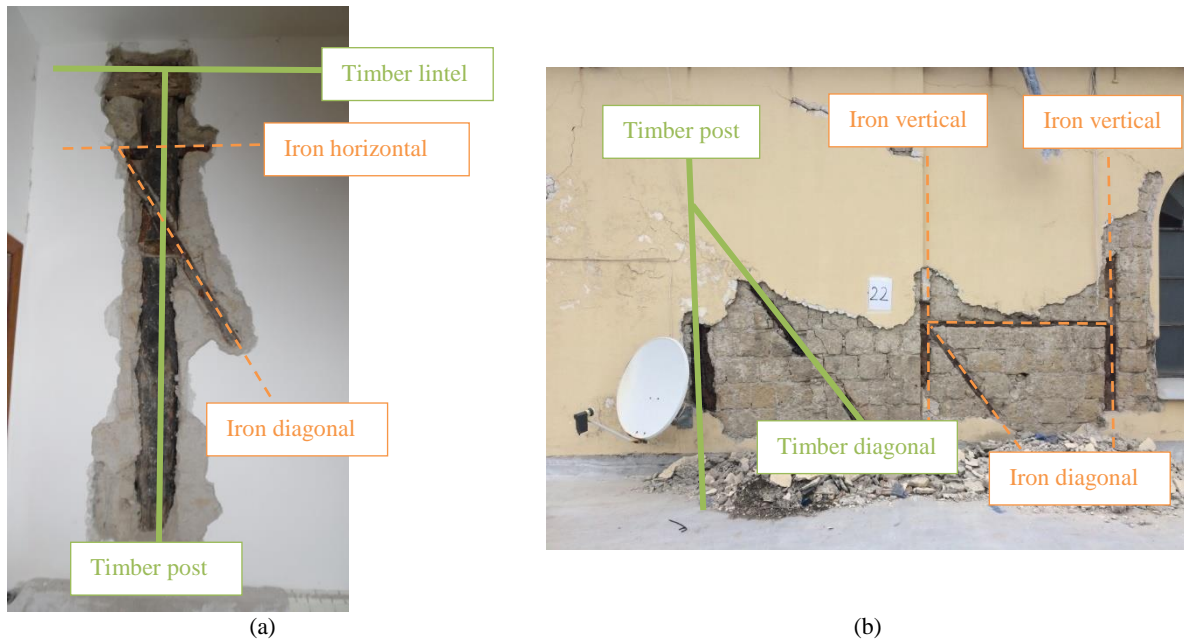
Figure 3.31 Inspected connections between the two Baraccato systems, in the priest's bedroom (a) and on the Northern terrace (b)

3.2.3 Horizontal elements

The horizontal elements of the church of Santa Maria Maddalena are identified as the few plain floor slabs present in the building, which consists mostly of a single order of iron beams floors in the side aisles and in the canonical house, the timber floors covering the resulting spaces between the deambulatory and the back wall of the canonical house and the pre-stressed concrete floor installed in the last decades of the 20th century in the North-Western terrace. Among these elements also the light

ADVANCED MASTERS IN STRUCTURAL ANALYSIS OF MONUMENTS AND HISTORICAL CONSTRUCTIONS

floor supporting the attic could be included but it will be discussed in the next section along with the roofing system. Unfortunately, as will be explained, very few information about the technological composition of the existing floor slabs is available from the collected data, for example most of the thickness dimensions are missing and about the reinforced concrete slab just the material, the construction technique and the orientation are known. For this reason, the following descriptions are affected by a high level of uncertainty and further inspections are recommended in order to perform a safety assessment of these parts of the building.

In the following paragraphs, the data and the assumptions about the technological description of the various floor slabs detected in the building will be presented, along with an approximate estimation of the masses involved in the definition of each of the floor elements, since this information will be later used for the modeling of the floor slabs in the numerical model.

The presence of floor slabs exhibiting an iron supporting structure of single oriented I-shaped beams was observed both in the main body of the church and in the canonical house (Figure 3.11). In the case of the church, hints of the metallic structure of the floors covering the side aisles were found thanks to plaster detachment in the ceiling of the lateral naves (Figure 3.32a) and, also, to external plaster detachments in the lateral walls of the church (Figure 3.32b), where the beams ends can be clearly identified emerging from the tuff masonry. Additionally, the presence of an iron system for the floor slabs of the main body of the church connected with the *iron-Baraccato* walls was already indicated by the original drawings of the building and it is considered the obvious choice for the continuity of the structural concept of the main body of the church, which clearly aims to define a three-dimensional iron skeleton for the building (Figure 3.16).

(a)   (b)

Figure 3.32 Direct observation spots for the metallic structure of the lateral naves floor slabs

Nevertheless, in the lack of more detailed drawings of the composition of these iron floor slabs, the direct observation allowed the definition of some structural details such as the beams orientation in the transversal direction of the church, the spacing between the iron beams, which was measured of around 80 cm, and the cross-section of the beams which has an height of around 16 cm and was

considered to the ends of the structural analysis a standardized INP160. Other geometrical measurements were directly deduced from the results of the geometrical survey of the whole church, which indicated a clear span for the floor slabs of around 3.73 m and in both naves. As for the thicknesses, the measurements provided contrasting results which cannot be considered fully reliable. Indeed, these floor slabs were reported to have a thickness of around 31 cm while, looking at the surveyed transversal cross-section of the church, these slabs have thickness of around 70 cm, which is obviously too large for such an element and the measurement may be attributed to the highest point of the terrace slope that assures the water drainage or measurements inconsistencies and errors.

In terms of stratigraphy, from Figure 3.32a it is clearly visible that some flat elements are supported on the low wing of the I-shaped profile of the iron beams to anchor the plaster and the *stucco* decorations of the naves' ceilings. These elements were assumed to be flooring brick planks (30-35 kg/m^2)[7] that were traditionally used in combination with the iron beams in this floor slab typology. Taking into consideration the reported thickness of 31 cm for the floor slabs of the church, considering a 2 cm thickness for the plaster of the ceiling (12 kN/m^3), and considering an external finishing of the floors with a painted waterproof membrane (0.3 kN/m^2), a thickness of about 13 cm of unknown material layers were considered. These would consist of a certain amount of conglomerate filling laid probably on some flat elements, timber or brick planks. In view of the lack of any further information, to the ends of the mass analysis the resulting thickness was considered to present a mass corresponding to lightweight conglomerate (~10 kN/m^3). The total mass of a unitary element of 1 m^2 of the considered floor was determined to be 2.24 kN/m^2 through simple calculations. A graphical scheme of the considered cross-section for the floor slab is presented in Figure 3.33 with a recall of the principal mass properties and dimensions of the layers considered.
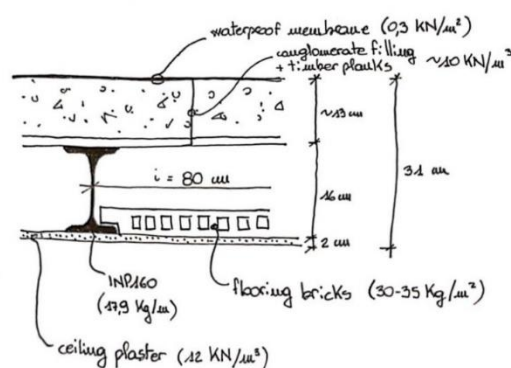
Figure 3.33 Schematized drawing for the iron floor cross-section

---

[7] The values are determined from some technical data sheets and from the indications contained in the most updated Italian code for the structures, (NTC 2018).

As mentioned, the presence of iron floor slabs was also detected to cover some of the spaces in the canonical house. In particular, as seen in Figure 3.34, the floor slab covering the parish room for the common activities located at the ground floor is the only observable example in the canonical house in which the floor structure is evident. To the observer, the technological composition of this floor slab is similar to the ones located in the church having the same transversal orientation and flat elements constituting the ceiling supported by the low wing of the iron beams. The spacing and the clear span of the beams are compatible with the ones of the floor slabs of the aisles measuring about 92 cm for the spacing (dimension obtained with the total length of the covered room divided by the total number of present beams) and about 5.35 m of clear span. As for the thicknesses, unfortunately the geometrical survey did not provide any useful information for the slabs in the canonical house, with the exception of the ones represented in the longitudinal section of the whole church which are, though, much smaller floor slabs, than the one in consideration, oriented in the longitudinal direction, and supported by timber beams. In any case, since only the just presented floor slab of the canonical house was directly inspected and considered the high uncertainty related to the elements, for simplicity and to the purpose of the structural analysis, the same typology of iron floor was used for the floor slabs of the canonical house and a more detailed description should be given in case of further analyses of these elements.

Figure 3.34 Intrados of the iron floor of the parish room in the canonical house

Lastly, some more timber floors were observed to cover the resulting spaces behind the deambulatory in the canonical house in which the timber beams and their orientation are clearly identifiable. Figure 3.35 reports the timber floor located at the attic level (Figure 3.35a), which is oriented in the transversal direction of the apsidal branch of the church, parallel to the roof trusses disposition, and the timber floor covering the space at the ground floor (Figure 3.35b) presenting rounded beams supported by the apse curved wall and oriented in the longitudinal direction.

(a)	(b)

Figure 3.35 Timber floors observed in the resulting space behind the apse at the roof level (a) and at the ground level (b)

3.2.4 Roofing system

The church covering is supported by a simple system of Palladian timber trusses (Figure 3.36a), which are aligned along the longitudinal direction of the church when they constitute the roof of the central nave and the facing apsidal branch of the church, and along the transversal direction when covering the transept. The trusses follow the traditional scheme of a king post truss with inclined rafters and struts connected to a vertical king post and closed by a low horizontal tie. The timber elements connections are made with dowel joints and, additionally, a metallic U-shaped connection is used between the king post and the tie beam to limit their relative vertical displacement. The cross-shaft covering is resolved with a three-dimensional truss (Figure 3.36b) following the structural scheme of the other trusses and presenting a king post in central position, diagonal ties connected with it at the highest point and through the struts and closed through four perimeter timber ties. The roof regular trusses have a total height, with respect to the attic floor extrados, of 2.83 m and a clear span of about 8.18 m in the longitudinal branches and of 7.30 m in the transept, meaning the clear internal distance between the supporting walls. The trusses are positioned with an average spacing of about 3 m.

ADVANCED MASTERS IN STRUCTURAL ANALYSIS OF MONUMENTS AND HISTORICAL CONSTRUCTIONS

(a)   (b)

Figure 3.36 Regular timber truss of the roof (a) and the three-dimensional truss covering the cross-shaft (b)

As it can be understood from Figure 3.36a and b, where the tie beams of the trusses are not visible, the lower ties of the trusses are also used to support the floor planks, conversely with the traditional use of trusses, where the elements are designed to withstand only axial load. A layer of conglomerate filling and the false ceiling of the central nave complete the layers of the attic floor slab arranged according to the sketch presented in Figure 3.37. In this case the wooden tie beams of the trusses would also be subjected to flexural action due to the specific weight of the floor and the accidental loads of the attic level. Nonetheless, it has been noticed that, since the iron skeleton of the church is also connected at the roof level with the use of some iron beams, which are clearly visible when they emerge from the lateral walls, and since in most of the cases the roof trusses are supported by these additional iron beams (Figure 3.38), the flexural actions can be considered as completely absorbed by the above mentioned iron beams while the thrust actions deriving from the roof are laid on the axial strength of the timber ties of the trusses.
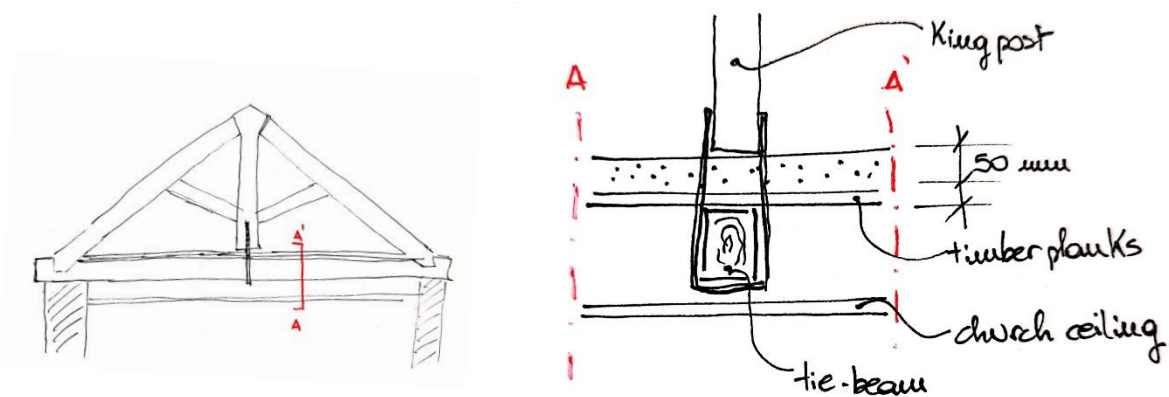
Figure 3.37 Sketch representing a probable layer arrangement for the attic floor slab and its relationship with the elements of the roof trusses

Figure 3.38 Timber ties of the roof trusses supported by the iron beams connecting the iron skeleton of the church at roof level

As done for the other floors, an analysis of the mass involved at the attic floor level and in the roof was performed in order to later include this information in the numerical model. To this end, the layers constituting the attic floor slab were considered as follows: church false ceiling (0.35 kN/m^2), timber planks s $\approx$ 3 cm (0.18 kN/m^2), conglomerate filling s $\approx$ 10 cm (1.4 kN/m^2), for a total weight of the floor per square meter evaluated around 1.93 kN/m^2. The roof overload was evaluated taking into consideration the various elements constituting the covering. The roof trusses support a second order of transversal purlins on which a layer of timber planks is fixed. The stratigraphy of the roof is completed by a waterproof membrane and brick roofing tiles (0.6-0.8 kN/m^2) anchored to timber elements, as shown in Figure 3.39, for a total weight of the roof overloads of about 0.9 kN/m^2.

(a)

(b)

Figure 3.39 Sketch of the roof stratigraphy (a) and a picture of the external layers of the roof (b)

3.2.5 Foundation system

Some information about the foundation elements was collected from the original drawings and documents and from a punctual inspection in the small cryptal space below the apse, but no more ground inspections were performed during the geometrical survey. As reported in the historical documentation about the church, the foundations of the church are constituted by foundational walls

excavated below the church vertical diaphragms, deepened until two different depths relative to the main body of the church (10 m depth) and to the canonical house (8 m depth). The foundation walls were built, consistently with the other walls of the church, in yellow tuff masonry of the indicative thickness of 1 m which is reported in the original bill of quantities of the construction site (Arcamone and Argiento 2018). Moreover, the original documentation contains some information regarding the depth of penetration in the ground of the vertical elements of the *iron-Baraccato* system. In fact, according to the bill of quantities, these elements have an additional length of 3 m with respect to the total height of the free walls, for this reason they should have been stuck in the ground for at least this length. On the other hand, no information regarding the sticking depth of the timber columns of the *timber-Baraccato* walls is available, but the common practices for the constructive system indicate two possible solutions for this node: either the principal timber columns reaching the total height of the construction were embedded in the foundational system and connected by dormant beams lying on the extradoses of the foundations and supporting all the other vertical elements, either the extrados of the foundations was used as lying level for the whole timber structure by positioning horizontal elements throughout the full length of the foundations. (Arcamone and Argiento 2018)
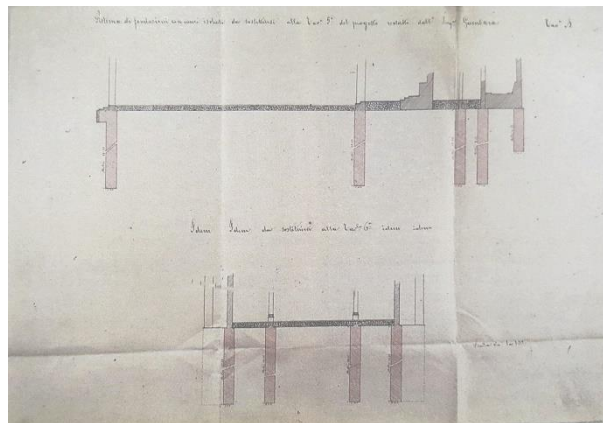
Figure 3.40 historic drawing of the foundation system of the Eng. Gambara ("Archivio di Stato di Napoli, Corpo Reale Genio Civile, fascio 342, incart. 3" n.d.)

Out of the foundation system, the soil-structure interaction is also crucially defined by the quality of the soil quality on which the structure is laid. Without specific investigations that inspect the characteristics of the soil which interacts at the local level with the foundations of the structure, little information is available to this extent, regarding historical reports or other information from literature dealing with the vicinity of the site of the church building.

In particular, the historical research evidenced that at the time of the church construction approval procedures, the site indicated by the Municipality for the church reconstruction was clearly in disagreement with the town planning since it was developed taking into consideration the areas of the

city which suffered major damages during the 1883 earthquake and indicating them as not suitable for reconstruction. The area in which the church was built is one of these, and for the approval of the construction, more geotechnical surveys were requested in order to prove the suitability of the soil. The tests on the soil at the time, which reached the depth of 14 m, evidenced the presence of soil layers of the average thickness of 2 m composed by (from the ground level to the bottom): landfill soil, organic soil, loose clays, compact clays and a layer of rock. The results of the surveys lead to the deepening of the foundation walls of about 2 m with respect to the design originally presented (Arcamone and Argiento 2018).

More information was found in literature thank to a document edited by the Italian Institute of Geophysics and Volcanology (INGV) reporting the results of a study conducted with the purpose to determine the geothermal potential for energy production of the island of Ischia. The study reports some results for the core penetration surveys conducted in the island from 1939 until 1954 in locations indicated in Figure 3.41a. From the available test results, just the one related to the perforation carried out at Mount Tabor can be considered sufficiently close to the location of the church to have relevance to the scope of the present work and help the qualitative understanding of the soil condition in the studied area. The surveyed soil layers for the Pc 42 penetration reached a depth of 100 m and evidenced, after a layer of organic material up to 5.70 m, a layer of tuff rocks up to 8.70 m, vulcanite (10.20 m), pyroclastic deposits (11.80 m) and some deeper layers constituted by green tuffs of Mount Epomeo interposed with some trachyte lavas. A detailed representation of the surveyed soil layers and the corresponding depths are reported at Figure 3.41b (INGV n.d.).

Pozzo **Pc 42 (Monte Tabor)**

Profondità		Litologia
da (m) 0.0	a (m) 5.70	Terreno vegetale
da (m) 5.70	a (m) 8.80	Tufo
da (m) 8.80	a (m) 10.20	Vulcaniti
da (m) 10.20	a (m) 11.80	Piroclastiti
da (m) 11.80	a (m) 25.30	Tufo
da (m) 25.30	a (m) 29.00	Trachite
da (m) 29.00	a (m) 32.80	Vulcaniti con trachite
da (m) 32.80	a (m) 100.00	Trachite (lava)

(a)

(b)
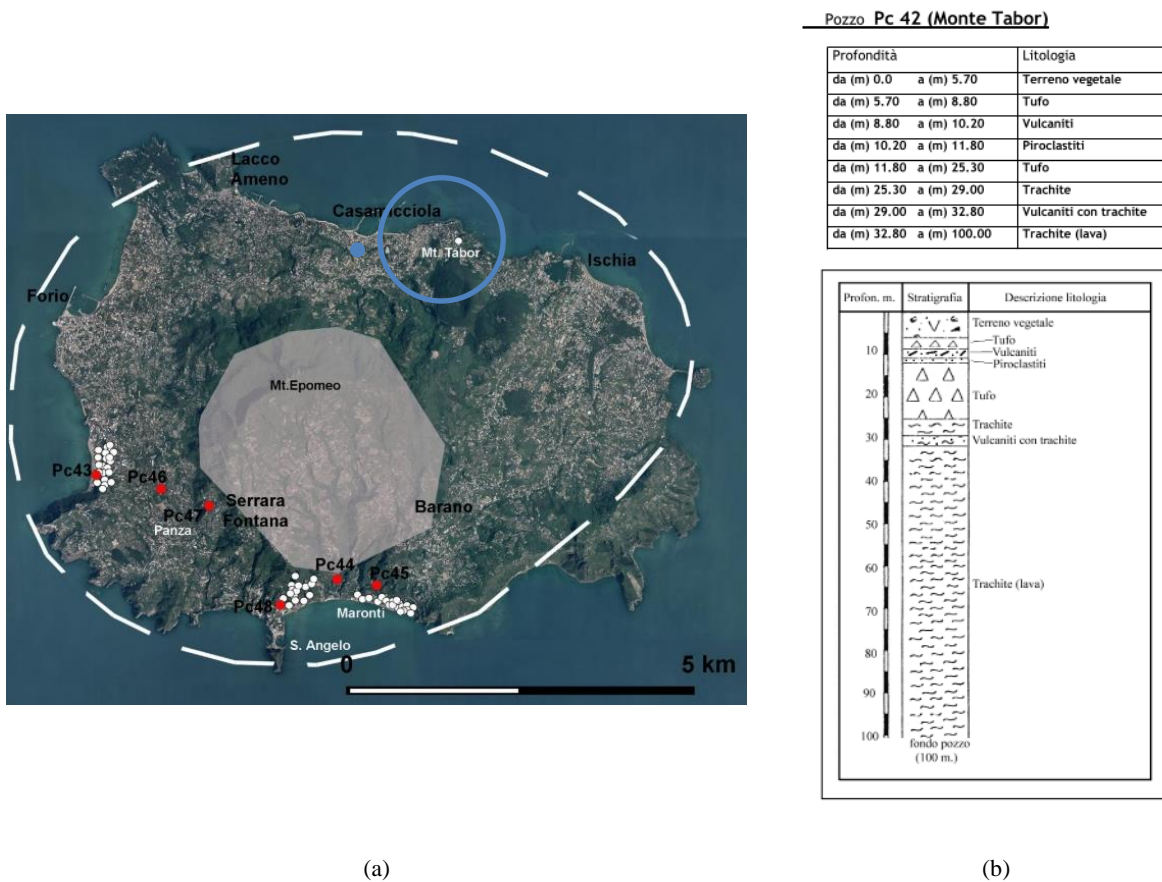
Figure 3.41 Location (a) and results (b) of some perforations performed between 1939 and 1950 from the society SAFEN for INGV. The small blue dot indicates the approximated location of the church and the big blue circle indicates the pit which results are presented in (b). Source: (INGV n.d.)

Obviously, with the historical information and with a stratigraphy obtained from a relatively far site from the church, a classification of the soil according to the last updated Italian Building Code (NTC 2018) and to the Eurocode 8 (EC-Standards 1998) is not possible, neither using the proposed simplified approach (soil classification into typologies defined from A to E), nor with the more rigorous method based on the calculation of the equivalent velocity of the shear waves in the considered soil. However, the shear wave velocities can be estimated using the 1:100,000 geological map of Italy published by the Geological Survey of Italy and a map of the soil classes of the island is reported at Figure 3.42 as elaborated from Briseghella et al. (2019). In the map, the red dot reports the position of the epicenter of the last Casamicciola Terme earthquake that occurred on August 21st, 2017 which is approximately 1 km in the SW direction with respect to the location of the church. Given that, the soil interacting with the studied building is classified as a soil Class B - Deposits of very dense sand, gravel, or very stiff clay, at least several tens of meters in thickness, characterized by a gradual increase of mechanical properties with depth (EC-Standards 1998). Nonetheless, the reported historic information and the stratigraphy observed in the close Mount Tabor suggest the presence in

the site area of soft soils prone to liquefaction and site amplification effects that would lead to a soil class decrease, if confirmed by further analysis of the soil properties.

In conclusion, in view of the lack of further information, the data collected can be considered sufficient to assume the class B typology of the soil in relation to the definition of the characteristic seismic action of the site, but the planning of some more detailed surveys is recommended to reach an higher reliability of the results and mandatory according to the Italian Building code (NTC 2018) for the safety assessment of an existing building.
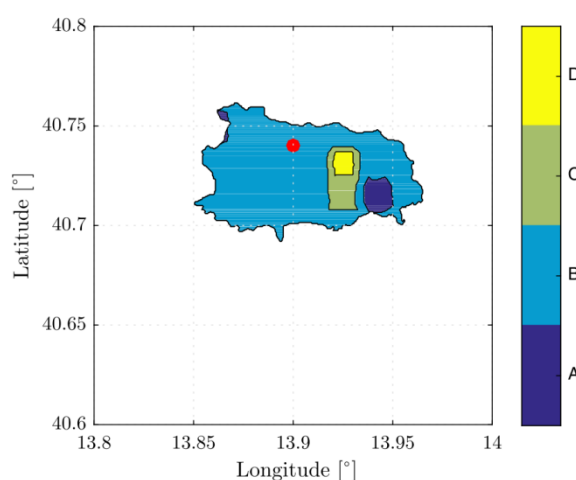
Figure 3.42 Map of the soil classes for Ischia island according to the Italian Building Code (NTC 2018) **or the Eurocode 8** (EC-Standards 1998) **estimated using the shear wave velocity Vs,30 in Italy from Global Vs,30 Map Server of the USGS. Source:** (Briseghella et al. 2019)

3.3 Confidence levels

As extensively discussed in the previous sections, the knowledge of the church is affected by heterogeneous levels of confidence that influence the preparation of a numerical model for the safety assessment of the building with unknown magnitude. Moreover, the intrinsic operations and definitions that a numerical model requires, such as mechanical material properties, boundary conditions, etc. which will be discussed in the next chapters, involve obviously additional sources of uncertainty to the results. So, it is useful to express the level of confidence that the studies performed on the various parts of the church have reached so far. To do so, different sources of uncertainty affecting the geometrical and technological knowledge of the church elements were identified, considering the various data sources that contributed to the description of the church. For the sake of clarity, the data sources that were considered in the previous sections can be resumed as follows:

- Original drawings of the church drafted by Eng. Gambara;
- Original documentation of the construction site (bill of quantities, historic pictures, etc.);

- Geometrical survey;
- Thermographic survey;
- Plaster removals and localized demolitions.

As for the reliability of each data source, it can be concluded that, since during the construction works many changes were made with respect to the original documentation presented to the Municipality, the original drawings drafted by Eng. Gambara can be considered reliable to understand the structural concept of the building but not fully reliable when it comes to the geometrical and spatial definition of the elements. On the other hand, the remaining documentation about the construction site can be used with a satisfactory level of confidence. As for the *in-situ* investigations performed on the church after the 2017 Ischia earthquake, the measurements and the observations made can be considered fully reliable even if they evidenced some lacunas for the technological definition of the various structural elements that would require further investigation.

Given the definition of the various data sources and discussed their specific reliability with respect to the geometrical and technological definition of the church elements, it was possible to define different confidence levels to assign to each structural element of the church based on the following criteria:

- *Confidence Level 0 (CL0)*: the geometry and the technological arrangement of the structural element is based on a rough hypothesis derived from the knowledge of traditional building techniques;
- *Confidence Level 1 (CL1)*: the geometry and the technological arrangement of the structural element is deduced or is based on an educated assumption, which is supported by punctual *in-situ* observations or by the information contained in the original drawings;
- *Confidence Level 2 (CL2)*: the geometry and the technological arrangement of the structural element is determined as a consequence of the observation of partial details and completed with the observation of contiguous or similar elements;
- *Confidence Level 3 (CL3)*: the knowledge of the structural element is originated by the direct observation of the details through plaster removals, localized demolitions, existing damages, etc. and the direct measurement of the details.

The definition of the confidence level relative to each existing structural element of the church enabled the elaboration of the color maps reported in Figure 3.43. As shown by the picture, the main body of the church is on average characterized by a higher level of confidence (darker color) with respect to the portion representing the canonical house. In particular, the scarce confidence related to the floors of the back sub-structure can be noticed as already explained at Section 3.2.3. In conclusion, this section contains an attempt to provide an overall idea of the level of knowledge of the structural

system in terms of geometrical and technological characteristics, similarly to what the Italian Codes (NTC-Circolare 2018) prescribe, meaning the knowledge of the buildings in terms of geometry, material properties and structural details.

GROUND LEVEL (+0.00 m)

FIRST FLOOR LEVEL (+3.70 m)

CENTRAL NAVE LEVEL (+7.30 m)

ATTIC LEVEL (+13.08 m)

CL0 - Vertical el. CL1 - Vertical el. CL2 - Vertical el. CL3 - Vertical el.
CL0 - Horizontal el. CL1 - Horizontal el. CL2 - Horizontal el. CL3 - Horizontal el.
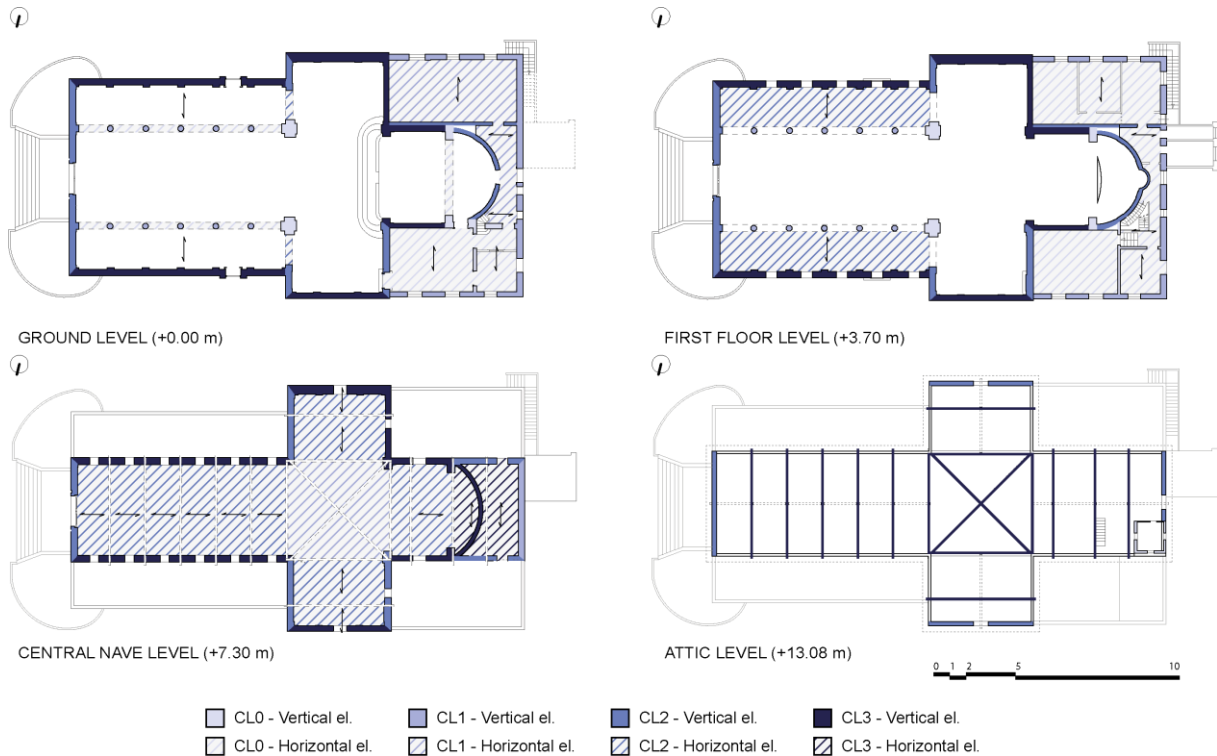
Figure 3.43 Confidence levels maps

3.4 State of conservation

Lastly, the characterization of the actual state of conservation of the church is a crucial point in the assessment of its structural safety. As was mentioned, the present study of the church was undertaken right after the earthquake that stroke the area in 2017, when a safety assessment was required for every building in the damaged area. The author has no knowledge of the pathologies that may have affected the building before the seismic event, since no structural and material damage survey was carried out before that. In any case, the post-seismic intervention documentation reports the application of repairing measures to address some static deficiencies due to ageing of the structure which were actually worsened by the earthquake and were detected during the post-seismic survey (Casapulla et al. 2019a).

3.4.1 Pre-2017 earthquake damage

As reported at Section 2.2, the interventions carried out in the structure not addressing a post-seismic damage are the consolidation of timber trusses of the roof and the anti-rust protection of iron frames of

the *iron-Baraccato* walls. Indeed, the corrosion of the iron elements present in the structure was observed in many locations along the walls (Figure 3.44) and it is one of the most severe damages that affects such a system. Corrosion may lead to the presence of localized stresses inside the masonry walls due to the swelling of the corroded iron elements and to the loss of mechanical strength of the iron sections leading to the ineffectiveness of the structural cage formed by the iron frames. Moreover, even if not surveyed during the inspections on the church, a certain level of decay of the timber elements embedded inside the walls built with the *timber-Baraccato* system may occur and should be properly investigated and addressed to the scopes of a structural retrofitting of the church if needed.

| (a) | (b) |

Figure 3.44 Corroded iron vertical and horizontal elements of an iron frame of the church nave wall (a) and the rusting beam end of a floor beam covering the side aisle (b)

3.4.2 Post-2017 earthquake damage

The safety check of the church of the post-seismic assessment of the town of Casamicciola Terme was performed on September 14th, 2017, resulting in "Unsafe condition" for the presence of a widespread damage pattern associated with the vertical walls. After the safety check, the church was closed to normal use and the safety assessment was made, and a detailed damage survey was performed to identify the presence, the extent and possibly the source of the structural and non-structural cracks originated after the seismic event. It was noticed that the damages were largely widespread and the cracks that opened followed directions that, understanding the underlying constructive system, could be related mostly to damage concentrated in the plaster covering the walls due to the different stiffnesses of the materials constituting the walls (iron-masonry, timber-masonry). It must be pointed out, as already discussed, that the dense distribution of iron and timber frames along the walls of the structure positively affected the overall behavior of the structure and enabled the global response of the building, by restraining the local collapse mechanisms typical of an existing masonry building and, in particular, of a church. Thus, the detected crack patterns mostly indicated the positions of the frames of the *Baraccato* systems and did not consist of concerning structural crack forecasting local failures of the masonry panels.

Figure 3.45 to Figure 3.48 report the crack patterns for the longitudinal section, the North and South façades and the transversal section respectively. As mentioned, they mostly follow the already reported layout schemes of the iron and timber frames, except for the third level walls of the canonical house adjacent to the church apse. In these positions – Figure 3.47 positions 1 and 2 and Figure 3.46 positions 3 and 4 – the *timber-Baraccato* walls present some inclined cracks that may correspond to shear failure of the relative masonry panels since in these positions the timber frames of the walls have relatively spaced elements. In addition, it can be observed that one of the above mentioned diagonal cracks is located in correspondence of the iron bell tower of the church – Figure 3.46 position 4 – and may be an indicator of the interaction between the sub-structure of the tower and may suggest the out of plane rotation of the secondary structure causing a sliding shear failure of the adjacent masonry panels. A picture of the damages is provided at Figure 3.49.

Moreover, it is highlighted that numerous damages localized in the non-structural and decorative elements were observed. These damages such as the detachments of some plaster portions from the ceiling (Figure 3.50a) and the walls of the church and the cracking and the crushing of some *stucco* decorations (Figure 3.50b) required the closing of the church for safety reason. In fact, the debris caused by those damaged decorative elements and the possibility of them to harm in any moment the user of the building required the adoption of safety measures, such as the installation of safety nets to avoid the debris from falling while waiting for more definitive measures to consolidate the plasters.

Figure 3.45 Crack pattern of the longitudinal section

Figure 3.46 Crack pattern of the North façade
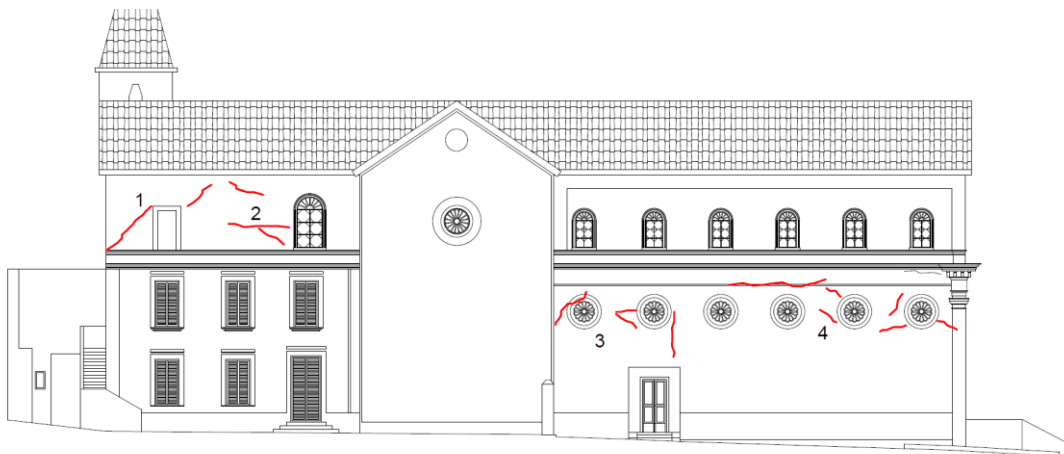
Figure 3.47 Crack pattern of the South façade
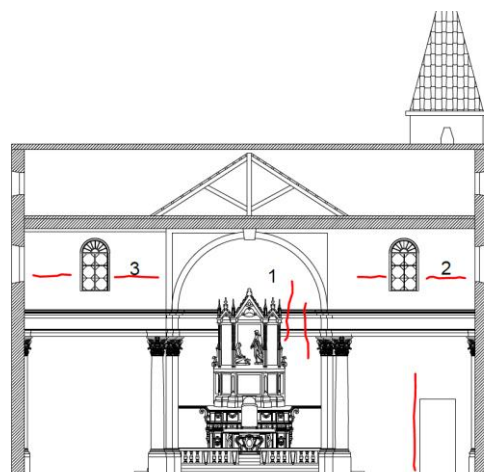
Figure 3.48 Crack pattern of the transversal section

ADVANCED MASTERS IN STRUCTURAL ANALYSIS OF MONUMENTS AND HISTORICAL CONSTRUCTIONS

(a)

(b)

Figure 3.49 Details of the diagonal cracks developed in the South façade at position 1 (a) and in the North façade at position 4 (b)

(a)

(b)

Figure 3.50 Plaster detachment from a ceiling (a) and cracking of a stucco decoration of a capital (b)

4 MODELLING OF THE PRESENT CONDITION

The numerical model of the church was prepared in order to perform structural analyses with the software DIANA 10.3 (Displacement ANAlyser) (DIANA FEA BV 2019). To do so, firstly a three-dimensional model of the building was accomplished with the aid of the 3D-modeler of AutoCAD and then imported to Midas FX+ pre/post processor. After a few more geometrical passages, a Finite Element Mesh was created with the elements and the properties that will be discussed in the following sections. Some of the choices made during the model preparation process, e. g. material properties, modeling strategies, etc., underwent changes in the calibration phase, in which the results of the numerical model in terms of eigenvalue analysis were compared and matched with the results of the ambient vibration tests performed on the church. In this sense, in the following sections the strategies will be presented as the result of the calibration phase and justified with the studies carried out and presented in Chapter 5. Moreover, the relevant changes with respect to the initial assumptions will also be highlighted in the attempt to describe the didactic process of the model composition.

4.1 Model units

The units of the numerical model had to be defined at the beginning of the modeling process and used consistently in the three software packages used for the model preparation, in order to avoid unwanted inconsistencies and errors during the exchange phases. Moreover, a preliminary understanding of the units used for the structural analyses helps a better reading of the latter results presented later as outputs. Table 4.1 presents the system of units adopted in the numerical model both in AutoCAD (length units only), Midas FX+) and DIANA 10.3.

Table 4.1 System of units used in the definition of the model

LENGTH	MASS	TIME	TEMPERATURE	VELOCITY	ACCELERATION	FORCE	PRESSURE
m	T	s	°C	m/s	m/s^2	kN	kN/m^2 (kPa)

4.2 Description of the model geometry

Various types of Finite Element Models could have been prepared with the objective of studying different aspects of the structural response of the church of Santa Maria Maddalena. In the present case, it was decided to build a model capable of catching the global response of the structure, at least in its potentiality if not fully optimized and validated in the present level of progress of the modeling, at least in its potential and ability to implement the needed changes once (or if) the suggested studies to refine the knowledge of some elements of the church are performed. In particular, the interest of the assessment of the church is to study the same subjected to the horizontal loading, given the earthquake

proneness of the area in which the church is built. For these reasons, it was decided to implement a full three-dimensional model including all the church structural parts, even if characterized by different levels of knowledge. Only some parts were excluded, such as: (a) the light bell tower for its lightness and its limited relevance in the definition of the global response of the church; (b) the services block along the back wall of the church for the same reasons and also for the structural autonomy that it evidenced as a consequence of the Ischia earthquake of 2017 (Figure 4.1).

Figure 4.1 Horizontal crack in the WC floor witnessing the autonomous response of the services block

4.2.1 Geometry

According to the previously mentioned scopes of the numerical model, the main body of the church was modeled along with the canonical house, taking in consideration the results of the geometrical survey and the technological observations. In order to optimize the numerical model size and to focus the analyses on the structural elements only, some simplifications were carried in the representation of the church. Among the geometrical simplifications carried out for the model geometry definition, the following operations can be enumerated:

- All the thickness variations smaller than 15 cm (e. g. *lesene*, doors and windows details, etc.) were simplified to planar surfaces or simple corners;
- The apse semi-circumference geometry was corrected and simplified to a single center arch properly connected with the chancel walls;
- The surveyed misalignments of the transept walls between the North and South branches and of the central nave walls with the apse walls were corrected;
- The piers of the cross-shaft were positioned consistently with the wall alignments;

- The church foundation level was set for both the main body of the church and the canonical house to –1.30 m with respect to the church floor, corresponding to the effective level of the facing parvis[8];

- Due to measurement inconsistencies of the geometrical survey and to the modeling strategy adopted for the floor slabs, the lateral naves floor levels were set to a lower height corresponding to the reported highest iron horizontal elements of the iron frames in the lateral walls;

- The modeling strategies adopted for the simulation of the *timber-Baraccato* walls required their thicknesses to be simplified in families (Walls_0.52, Walls_0.45, Walls_0.35 and Walls_0.20) identified among the geometrical measurements of the walls in the back portion;

- Some floor levels and horizontal frames level were matched to an equal level between the main body model portion and the canonical house model portion in order to decrease the numbers of horizontal levels defined in the geometry and to enable the connection between the nodes of the two parts, providing a higher quality mesh.

4.2.2 Modeling strategies

Since the constructive techniques surveyed in the church revealed to be quite complex, the choice of an appropriate modeling strategy for each structural element has a great impact in the definition of the response of the global model, both in terms of accuracy of the results and in terms of expenditure of computational resources. Indeed, these choices should be made with great care and supported by appropriate smaller scale analyses focused on the response of the single structural element and constructive system and then applied to the global model of the church. On the other hand, the complexity of a global model representing all the elements of a church, especially a church with such peculiar constructive systems, would require naturally a simplification in order not to overweight the model size and to imply too long-time consuming analyses.

In the following paragraphs a brief description of the modeling strategies adopted for each structural element included in the numerical model will be discussed. An overview of the adopted strategies is reported schematically in Table 4.2. These, along the choice of the appropriate mesh size defined the total size of the numerical model.

---

[8] Being the foundation depth known from the original drawings, but being also unknown the soil-structure interaction stiffness, it was decided to set the model foundation level to a reference depth that enables to apply perfectly rigid boundary conditions (fixed, see Paragraph 4.3.3) and express the possible rotation of the foundational level through the modelling of a wall section corresponding to the represented depth.

Table 4.2 Overview of the modeling strategies adopted for the various structural elements

STRUCTURAL ELEMENT	MODELING STRATEGY
Iron-Baraccato walls	Solid walls + embedded transverse beams + imprinted beams
	Shell walls + imprinted beams (with doubled geometrical characteristics)
Timber-Baraccato walls	Shell walls + imprinted beams
Columns and piers	Beams with homogenized section
Lateral naves floor slabs (iron beams)	Orthotropic shells
Canonical house floor slabs	Orthotropic shells (iron floors)
	Isotropic shell (RC slab)
Apse dome	Beams
Roofing system	Mass applied to the roof perimeter
Foundations solid walls	Perfectly pinned constraints
Foundations shell walls	Perfectly fixed constraints
Foundations of columns	Perfectly fixed constraints

The identification of an appropriate mesh size is an important parameter in the definition of a numerical model, since it requires an optimal compromise between the results accuracy and the model size. In fact, the adoption of a model of lower accuracy, in the case of the structural assessment of historical buildings, implies a lower reliability of the results and larger investments in terms of cost of strengthening and repair, while higher accuracies of the model require much more computational effort and more costs in the assessment phase. In the present case, the use of a relatively small mesh size was defined by the choice of having at least two finite elements along the thickness of the walls, and so a mesh size of 0.25 m was set for the model.

As discussed later, various versions of the model were investigated during the calibration phase, which included obviously a different number of elements and Degrees Of Freedom (DOFs). In conclusion, the final model including all the various parts and the *Baraccato* systems is displayed in and consists of a total number of 271,208 elements, 80,081 nodes equivalent to 315,353 DOFs.

4.2.2.1 Modeling of the Baraccato walls

The modeling strategies capable of appropriately describing the response of the *Baraccato* walls, representing the great part of the resisting system to investigate, should be properly addressed. In this sense, some previous studies can be found in the literature regarding the technology of the *timber-Baraccato*, where various modeling strategies were adopted to forecast the response of mixed masonry-timber structures, such as this understudied system and the so-called *Pombalino* system. The

proposed modeling techniques range from a highly detailed model-preparation to more simplified ones.

For example, the modeling techniques applied by Galassi et al. (2014, 2015), Salerno et al. (2015) and Poletti (2013) can be enumerated among the more refined ones, where the behavior of the *Baraccato* and *Pombalino* walls is described with the complete inclusion of the non-linearities of the timber elements and their mutual connections, modeled as springs (Salerno et al. 2015) or non-linear contact surfaces (Galassi et al. 2014, 2015; Poletti 2013; Poletti et al. 2015), and of the masonry elements, modeled as rigid blocks and contact surfaces (Galassi et al. 2014, 2015) or as discretized units and mortar joints (Salerno et al. 2015) or as 2D plane-stress elements with isotropic properties (Poletti 2013; Poletti et al. 2015). Images of the numerical models obtained by the cited authors can be found in Figure 4.2. As can be easily understood, such a detailed modeling strategy is not appropriate for the present case, since it would require the implementation of complex finite elements, e. g. interface elements, requiring great computational effort, in a numerical model of an already very relevant size.

(a)

(b)

(c)
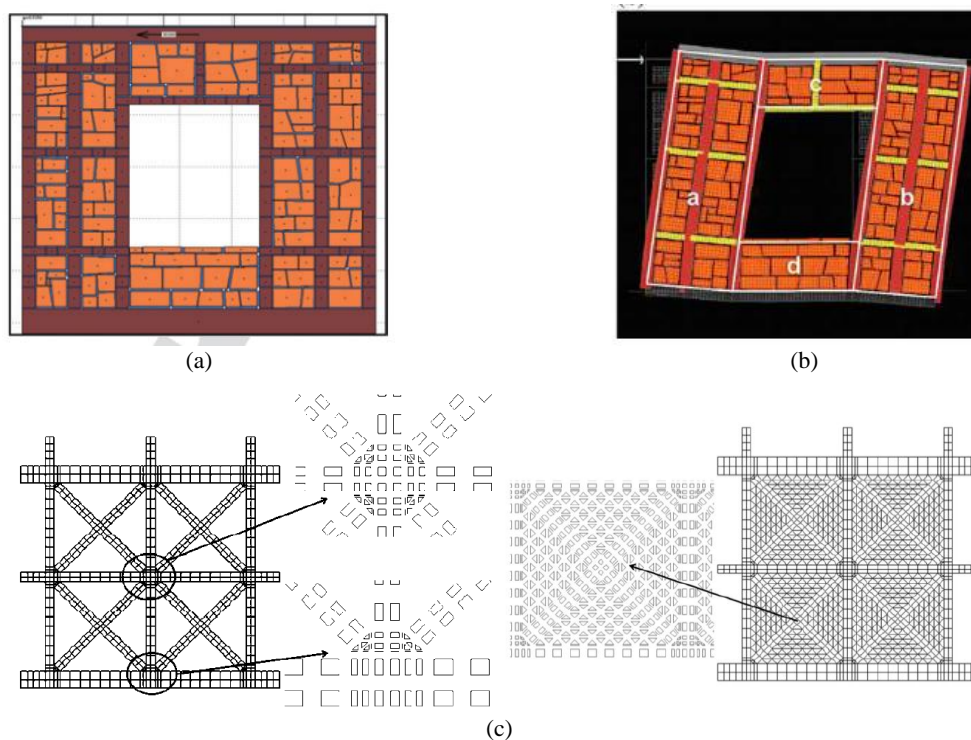
Figure 4.2 Numerical models of Galassi et al. (2014, 2015) **(a), Salerno et al.** (2015) **(b) and Poletti** (2013) **(c)**

A more simplified approach was adopted by Ruggieri et al. (2015), where the shear behavior of a mixed timber-masonry wall panel was idealized through the analysis of a timber framed structure with rotational spring connections (Figure 4.3) including all the possible non-linearity sources of the system. Also in this case, the adopted modelling strategy cannot be considered applicable to the

numerical model of the church due to its excessive simplicity, being only able to capture the single shear behavior of the *Baraccato* walls.
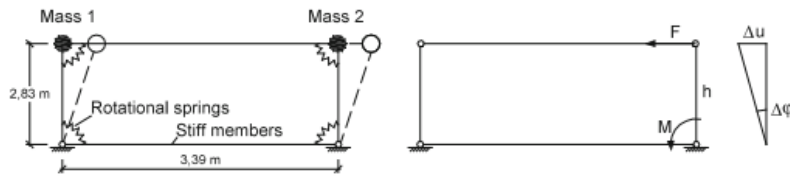
Figure 4.3 Simplified model of the shear behavior of a mixed timber-masonry panel, according to Ruggieri et al. (2015)

In conclusion, in light of the already discussed scarce level of knowledge reached for the construction details of the *timber-Baraccato* walls of the church (dimensions and layout), the most appropriate modelling strategy to represent the response of these walls in the canonical house was found to be a shell modelling of the infill masonry, with *regular curved shell elements*, reinforced with *3D-beam* elements representing the layout of the timber frames of the system (Figure 4.4a), constituting a system with *beam elements embedded in shells*. In this sense, this modelling approach was found suitable for different reasons, namely the approach:

- Is sufficiently simplified to support the reached level of knowledge;
- Enables the possibility of inspecting the influence of the presence of the timber reinforcement in the global response by performing analyses in the reinforced and the unreinforced condition, obtaining a self-supporting structure also in the unreinforced condition by deleting the frames;
- Enables the possibility of analyzing the influence of different timber frame layouts in the walls without major changes to the geometry of the model.

On the other hand, for the *iron-Baraccato* vertical walls, since the construction technique is relatively rare, no reference was found for any possible modelling strategy. For this reason, and thanks to the existing high level of knowledge, a three-dimensional approach was chosen with the use of *solid* elements to represent the masonry and 3D-*beam* elements to represent the iron frames (Figure 4.4b). Following this approach, the two layers of iron frames would be modeled as *beam embedded in solid* as well as the transversal connections between the two frames.

<table>
<tr><td>(a)</td><td>(b)</td></tr>
</table>
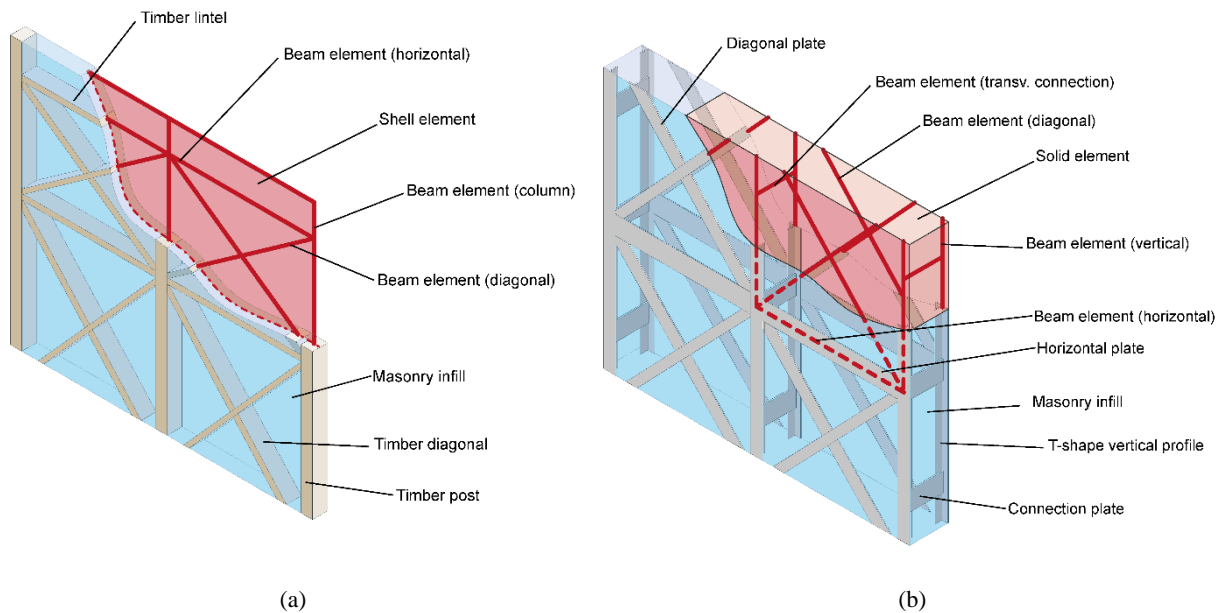
Figure 4.4 Modelling strategy schemes for *timber-Baraccato* (a) and *iron-Baraccato* (b) walls

Given the choices about the modelling strategies, it is important to note that in both approaches the nodal connectivity between the different types of elements belonging to the same walls – beams and shells, and beams and solids – should be assured. This can be reached by implementing correctly the geometry with two different methods: the use of the *imprint* command in Midas FX+ that enables to imprint line shapes on surface and solid shapes, in order to obtain new surface and solid geometry containing already the lines traces to mesh later with beam elements; the preparation of an appropriate geometry in AutoCAD (or another geometrical modeler) in which the same result is obtained by the operation of dividing the surfaces and the solids whenever they are in contact with a line. In the latter way, the geometry can be later fused in the meshing software (*fuse* command) preserving the surfaces divisions. In both methods, the strategy to mesh directly the imprinted shapes forces the meshing software to create coincident nodes while creating the meshes for the solids, the surfaces and the lines, enabling a *merge nodes* operation that can be performed directly during the meshing procedures. In the present case study, since the number of line shapes to imprint on the remaining geometry was relevant, and since the *imprint* command, even if useful, is not as so manageable in the Midas environment as a simple Boolean operation of division in AutoCAD is, the imprint of the elements was reached with the second approach. In any case, in order to obtain a good quality mesh after the meshing procedures, this phase of the definition of the geometry was dealt with great care and additional simplifications to the geometry of the church were added, as already mentioned in Section 4.2.1.

Figure 4.5 shows the imprinted geometry of the solids and the surfaces of the final model before the mesh creation (a), after the solid and shell mesh creation (b) and after the beam mesh creation (c).

ADVANCED MASTERS IN STRUCTURAL ANALYSIS OF MONUMENTS AND HISTORICAL CONSTRUCTIONS

(a)   (b)

(c)
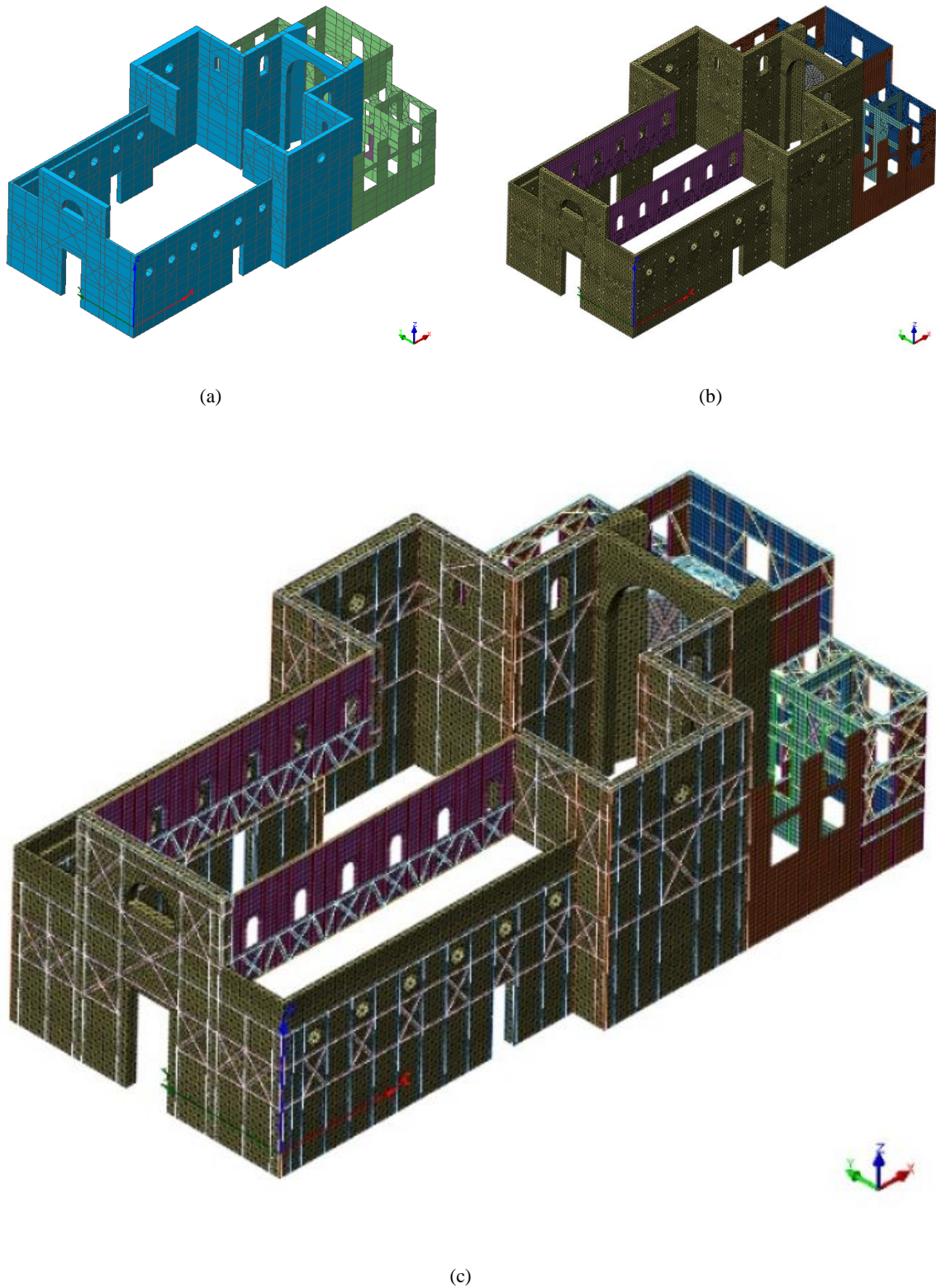
Figure 4.5 Meshing of the walls with the *imprint* technique, geometry before meshing (a), mesh of the walls (b), and complete mesh with the beams of the iron and timber frames (c)

Lastly, it must be pointed out that, since the behavior of the walls of the central nave at the second level of the church is not completely understood due to the lack of knowledge of the construction details (Section 3.2.2.1), the model in these portions was simplified to *regular curved shell* elements reinforced with *3D-beam* elements representing the iron frames of the upper wall. Additionally, this approach revealed itself to be particularly suitable for this case, since it allowed the solution of the node column-wall-floor in an easy way, with the two shells of the wall and the floor (see Section 4.2.2.2) converging in the beam elements representing the columns (Section 4.2.2.4). This approach also allowed the wall and the floor elements to be properly supported above the gallery. On the other hand, the strategy required the reinforcing frame elements of the *iron-Baraccato* shells to feature the same stiffness as in a three-dimensional modelling approach. For this reason, the frame elements reinforcing the upper wall of the central nave were defined as beam elements with doubled area, with respect to the area assigned to the beam elements reinforcing the solid walls, and increased geometrical stiffness properties, in terms of moment of inertia. The increased moments of inertia were calculated with the Huygens-Steiner formula.

4.2.2.2 Floor slabs

For the floor slabs, the level of knowledge did not justify the adoption of complex modelling strategies, as already mentioned in Section 3.2.3. The only floor element identified as a reinforced concrete slab was modelled with *regular curved shell* elements with isotropic properties since no information was collected about the structural details. For the floor slabs in which the support system was identified to consist of iron beams and for the analogous ones in which it was not possible to inspect the constructive system, the simplified approach of the *regular curved shell* elements was adopted as well, but with the definition of an equivalent orthotropic material representing the orientation of the iron beams.

Different homogenization techniques were used to simplify the composite typical section of the floor slabs with iron beams to the equivalent flat section represented. As is usually done for the reinforced concrete sections and the composited sections of mixed steel-concrete structures, firstly the geometrical properties – area and inertia properties – of the considered effective width of the slab can be homogenized through the homogenization coefficient n, calculated as the ratio between the Young's moduli of the two materials. Secondly, the equivalent mass density of the fictious material can be calculated as the average of the mass densities of the two materials of the sections weighted on the homogenized areas. Lastly, the equivalent mechanical properties, equivalent thickness (t_{eq}) and

equivalent modulus of elasticity in the strong direction ($E_{11,eq}$), of the fictious orthotropic material can be calculated as the solutions of the linear system reported in Equation (4.1).

$$\begin{cases} E_r \cdot A_r = E_{11,eq} \cdot t_{eq} \cdot i \\ E_r \cdot I_r = E_{11,eq} \cdot \dfrac{i \cdot t_{eq}^3}{12} \end{cases} \qquad (4.1)$$

where:

- E_r is the Young's modulus of the homogenized material;

- A_r is the calculated homogenized area of the section;

- I_r is the calculated homogenized moment of inertia;

- t_{eq} is the thickness of the equivalent rectangular section;

- i is the spacing between the beams.

4.2.2.3 Roofing system

It was decided not to include the full three-dimensional representation of the roofing system and the four tympani of the church for several reasons: (a) for simplicity and to reduce the number of elements and the size of the model; (b) for the lack of knowledge regarding the structural system and the connection with the supporting walls, and; (c) to avoid the appearance of local modes of vibrations at low frequency while performing eigenvalue analysis; (d) to avoid local failures in the model leading to numerical instability while performing non-linear structural analysis.

The influence of the roofing system, both in terms of mass participation and of stiffness contribution at the floor level of the church, was studied during the dynamic identification phase. That lead to the conclusion to take into consideration the participating mass of the roof and the tympani by adding it in form of distributed mass along the roof perimeter of the structure (Figure 4.6a). ,To include some stiffness contribution, specifically in terms of longitudinal walls connection and redistribution of the stiffness, some *truss* elements were added at the roof level representing the tying action of the roof timber trusses, the roof iron beams connecting the iron frames and the stiffness contribution of the attic floor slab (Figure 4.6b). In this second case, the adoption of *truss* elements enables the possibility to perform also some sensitivity analyses in order to inspect the stiffness contribution of the roofing system to the global behavior of the structure (see Section 5.3.1).

The roof mass to apply to the model was calculated according to the mass estimation described in Section 3.2.3 and was distributed according to the scheme presented in Figure 4.7. The values of the total masses applied to each section of the church perimeter, the distribution lengths and the total distributed mass are presented in Table 4.3.

(a)   (b)
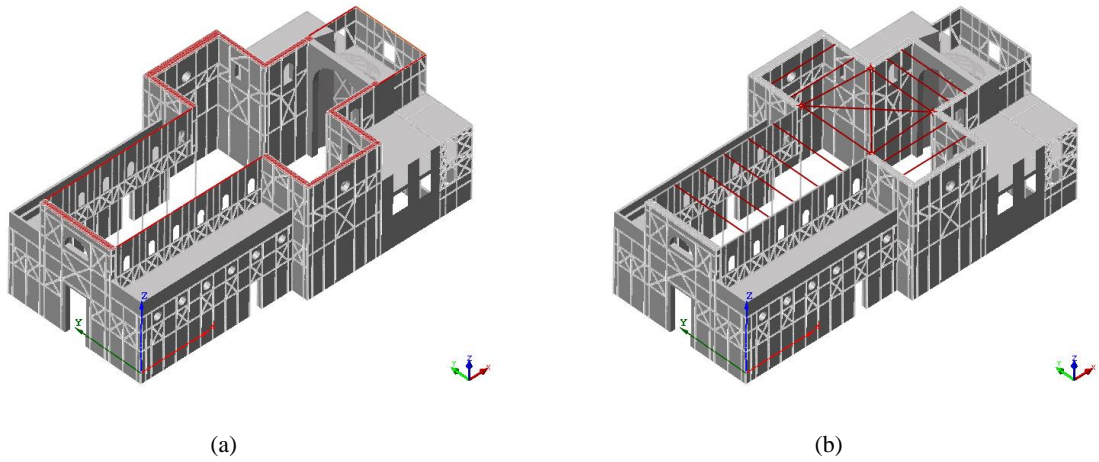
Figure 4.6 Modelling strategies of the roofing system, distributed mass (a) and roof ties (b)
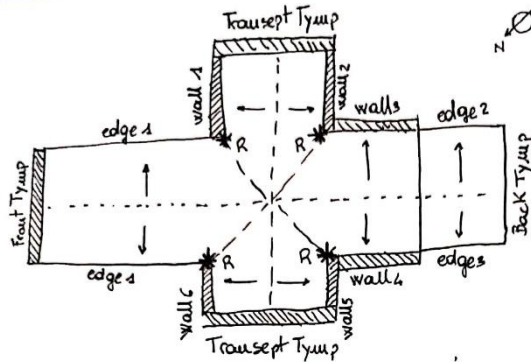
Figure 4.7 Scheme of the mass distribution for the roof

Table 4.3 Summary of the distributed masses applied to simulate the roofing system

NAME	TYPE	DISTRIB.	MASS	DISTRIB. LENGTH	DISTRIB. LOAD	DISTRIB. MASS
FrontTymp	Masonry wall	Area	10.612 T	5.25 m²	19.84 kN/m²	2.022 T/m²
TranseptTymp	Masonry wall	Area	8.864 T	5.66 m²	18.64 kN/m²	1.90 T/m²
BackTymp	Masonry walls	Line	10.758 T	8.97 m	9.69 kN/m	0.99 T/m
Edge1	Roof	Line	33.82 T	18.01 m	18.40 kN/m	1.87 T/m
Edge2	Roof	Line	10.21 T	5.75 m	17.42 kN/m	1.78 T/m
Edge3	Roof	Line	10.21 T	5.75 m	17.42 kN/m	1.78 T/m
Wall1	Roof	Area	13.54 T	2.98 m²	44.57 kN/m²	4.54 T/m²
Wall2	Roof	Area	13.54 T	2.80 m²	47.44 kN/m²	4.84 T/m²
Wall3	Roof	Area	11.98 T	3.04 m²	38.66 kN/m²	3.94 T/m²
Wall4	Roof	Area	11.98 T	2.40 m²	48.96 kN/m²	4.99 T/m²
Wall5	Roof	Area	13.35 T	3.18 m²	41.18 kN/m²	4.20 T/m²
Wall6	Roof	Area	13.35 T	3.00 m²	43.65 kN/m²	4.48 T/m²
CrossTruss	Truss reaction	Point	2.05 T	4 [adim.]	5.02 kN	0.51 T

4.2.2.4 Other

The remaining elements of the columns constituting the gallery were modelled with *3D-beam* elements as well. Since the presence of iron profiles reinforcement was observed during the historical survey embedded in a not very well identified chaotic material there were two possible strategies to adopt:

- Model of the columns as beam elements with iron profiles consistent with the reinforcing frames of the walls;
- Model of the colums as homogenized beam elements using an embedding low quality concrete material.
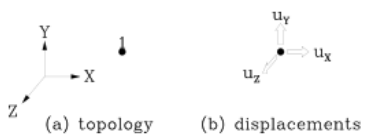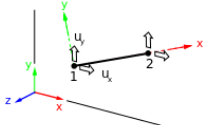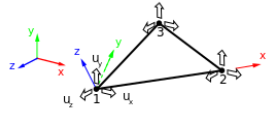
Since the iron profiles to be used consist of very thin sections, the adoption of single iron profiles may present buckling problems already in the application of the self-weight of the structure, which do not have a correspondence in the reality since the profiles are confined by the columns material. Therefore, the second strategy was chosen.

The homogenization was conducted by means of the Young's moduli of the two materials with the same procedure already described in Section 4.2.2.2 for the geometrical homogenization.

4.2.3 Type of elements

The just described modelling strategies required the adoption of the element types (DIANA FEA BV 2019) reported in Table 4.4, which can be visually identified in Figure 4.8.

Table 4.4 Element types of the numerical model (DIANA FEA BV 2019)

ELEMENT	NAME	TYPE	LOCATION
	PT3T	Point mass/damping, Translation, 1 Node	Cross-shaft truss mass
	L4TM	Mass element, Straight line, 2 Nodes	Distributed linear mass of the roof
	T9TM	Mass element, triangular, 3 Nodes	Distributed surface mass of the roof
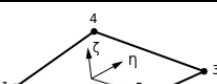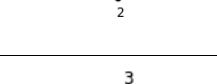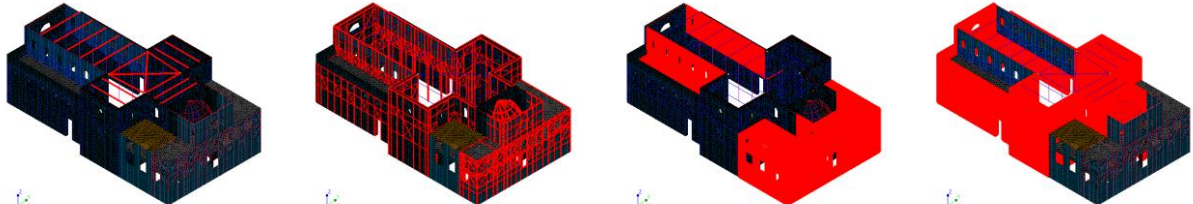
	L2TRU	Regular Truss, 2 Nodes	Roof ties
	L12BE	Class-I Beam, 3D, straight, 2 Nodes	Timber and iron frames
	Q20SH	Regular curved shell, quadrilateral 4 Nodes	Floor slabs, *timber-Baraccato* infill masonry and the 2nd level masonry wall of the central nave
	T15SH	Regular curved shell, triangular, 3 Nodes	Floor slabs, *timber-Baraccato* infill masonry and the 2nd level masonry wall of the central nave
	TE12L	Tetrahedron solid element, 3 Sides, 4 Nodes	*Iron-Baraccato* walls of the church

(a)   (b)   (c)   (d)

Figure 4.8 Location of the truss elements (a), beam elements (b), regular curved shell elements (c) and solid elements (d)

4.3 Description of the model materials, loading and restraints

4.3.1 Material properties

The different materials identified in the description of the church were included in the numerical model. In particular, two different masonry types were initially identified as different materials to constitute the tuff-masonry walls of the church built with the *iron-Baraccato* technology, consisting of a good quality masonry with respect to the infill tuff masonry of the *timber-Baraccato* walls. Since two different masonry materials can be identified in the structure, namely the one constituting the *iron*-Baraccato walls and the one constituting the infill material of the *timber-Baraccato* walls, initially two different masonry material models were applied to the numerical model. Doing so, the

influence of the different mechanical properties of the two materials could have been investigated during the dynamic identification phase. For the influence evidenced to be scarce (see Section 5.3.1), and in lack of any further information coming from tests performed directly on the church walls, in the final model a single type of masonry was assumed.

For the other materials identified in the church, due to the lack of quantitative information regarding the physical and mechanical properties, model typical values are adopted based on literature and codes.

4.3.1.1 Linear and non-linear properties of masonry

As for the masonry materials, since no direct tests were performed on the walls of the church, the adopted values can be referred to the literature and codes indications. In particular, the elastic Young's modulus of the material was estimated from the Italian Codes indications (Figure 4.9) and the results obtained by tests performed on masonry specimens by the University of Naples (Calderoni 1996; Calderoni et al. 2006, 2008, 2009). Identified the church tuff-masonry as an *a sacco* typology according to the period of construction and the observations made on site, a first tentative value of 920 MPa was adopted for the masonry materials of the model (Figure 4.10). The Young's modulus was later calibrated with respect to the results of the dynamic identification tests (see Section 0) and a final value of 890 MPa was adopted.

Tipologia di muratura	f (N/mm²)	τ_0 (N/mm²)	f_{V0} (N/mm²)	E (N/mm²)	G (N/mm²)	w (kN/m³)
	min-max	min-max		min-max	min-max	
Muratura in pietrame disordinata (ciottoli, pietre erratiche e irregolari)	1,0-2,0	0,018-0,032	- -	690-1050	230-350	19
Muratura a conci sbozzati, con paramenti di spessore disomogeneo (*)	2,0	0,035-0,051	- -	1020-1440	340-480	20
Muratura in pietre a spacco con buona tessitura	2,6-3,8	0,056-0,074	- -	1500-1980	500-660	21
Muratura irregolare di pietra tenera (tufo, calcarenite, ecc.,)	1,4-2,2	0,028-0,042	- -	900-1260	300-420	13 ÷ 16(**)
Muratura a conci regolari di pietra tenera (tufo, calcarenite, ecc.,) (**)	2,0-3,2	0,04-0,08	0,10-0,19	1200-1620	400-500	
Muratura a blocchi lapidei squadrati	5,8-8,2	0,09-0,12	0,18-0,28	2400-3300	800-1100	22
Muratura in mattoni pieni e malta di calce (***)	2,6-4,3	0,05-0,13	0,13-0,27	1200-1800	400-600	18
Muratura in mattoni semipieni con malta cementizia (es,: doppio UNI foratura ≤40%)	5,0-8,0	0,08-0,17	0,20-0,36	3500-5600	875-1400	15

Figure 4.9 Reference values for irregular tuff masonries in the Italian Codes (Tab. C8.5.I - NTC-Circolare 2018)

PROVINO	DIMENSIONI (cm)			σ_{max} (N/mm²)	$\varepsilon(\sigma_{max})$	$\varepsilon(\sigma_{max}/2)$	E (N/mm²)
	l	t	H				
C1 A CANTIERI	125	67	90	3,60	0,0088	0,024	746
C2 A CANTIERI	120	65	95	4,34	0,0049	0,016	1183
B1 A BOZZETTE	100	55	82	2,85	0,0049	0,031	1252
B2 A BOZZETTE	100	55	86	3,32	0,0055	0,018	1067
S1 A SACCO	133	42	91	2,55	0,0035	0,013	923
S2 A SACCO	120	42	88	2,74	0,0061	0,017	743

Figure 4.10 Experimental values of some compressive test performed by the University of Naples (Calderoni et al. 2006)

As for the non-linear material properties, since the comparison of the results obtained by Calderoni (Calderoni 1996; Calderoni et al. 2006, 2008, 2009) did not matched exactly with the code proposed range, it was decided to adopt a conservative approach by taking the minimum values of the code.

A *total strain based crack* model with rotating cracks was assumed to describe the non-linear behavior of masonry, with an *exponential (EXPONE)* stress-strain diagram for the tension (Figure 4.11a) and a *parabolic (PARABO)* behavior in compression (Figure 4.11b).

(a)

(b)
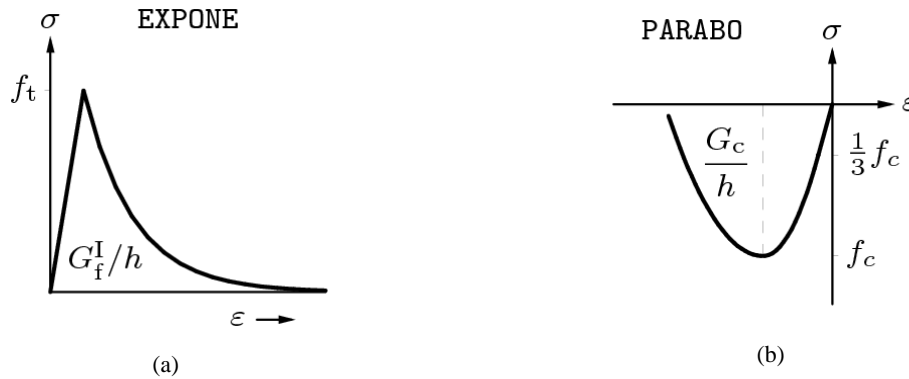
Figure 4.11 Stress-strain diagrams adopted for the behavior of masonry in tension (a) and in compression (b)
(DIANA FEA BV 2019)

In the case of the compressive behavior, the adopted softening model requires the definition of the compressive fracture energy G_c that can be calculated according to Lourenço (2008). In fact, considering the ductility index d expressed by Equation (4.2), this energy can be calculated as Equation (4.3):

$$d = \frac{G_f}{f} \tag{4.2}$$

$$G_c = \begin{cases} d = 2.8\ mm - 0.1 \cdot f_c & if \quad f_c < 12 MPa \\ 15 + 0.43 \cdot f_c - 0.0036 \cdot f_c & if \quad 12\ MPa < f_c < 80 MPa \\ d = 0.33\ mm & if \quad f_c > 80 MPa \end{cases} \tag{4.3}$$

ADVANCED MASTERS IN STRUCTURAL ANALYSIS OF MONUMENTS AND HISTORICAL CONSTRUCTIONS

On the other hand, to define the tensile behavior of masonry, typical literature values can be assumed, such as 100-150 kN/m^2 for the tensile strength and 0.012 N/mm for the Mode-I fracture energy. In conclusion, the mechanical properties assumed for the masonry material are summarized in Table 4.5

Table 4.5 Linear and non-linear properties of the masonry

		TENSILE BEHAVIOR	COMPRESSIVE BEHAVIOR
Linear prop.	Young's modulus	$E = 887$ MPa ($887\ 10^3\ kN/m^2$)[*]	
	Poisson ratio	$\nu = 0.2$	
	Mass density	$M = 14\ kN/m^3$	
Nonlinear prop.	Constitutive law	Exponential	Parabolic
	Strength	$f_t = 140\ kN/m^2$	$f_c = 1400\ kN/m^2$
	Fracture energy	$G_{f}{}^I = 0.012\ kN/m$	$G_c = 3.72\ kN/m$
	Ductility index	$d_f = 8.57\ 10^{-3}$ mm	$d_c = 2.66$ mm

[*] Young's modulus obtained through modal calibration of the model

4.3.1.2 Other materials

As said, all the other material properties used in the numerical model were estimated on the basis of the literature and suggested (Italian) code values. The other materials were modelled as linear-elastic materials with isotropic characteristics and are summarized in Table 4.6.

Table 4.6 Elastic material properties of the other materials in the model

WROUGTH IRON (Bussell 1997)

Material property	Symbol	Value	Units
Density	ρ	7.85	$[T/m^3]$
Young's modulus	E	154	[GPa]
Poisson's ratio	ν	0.3	[-]

TIMBER – CHESTNUT (EC-Standards 2003; Sousa et al. 2014)

Material property	Symbol	Value	Units
Density	ρ	0.64	$[T/m^3]$
Young's modulus	E	8000	[MPa]
Poisson's ratio	ν	0.3	[-]

CONCRETE (NTC 2018)

Material property	Symbol	Value	Units
Density	ρ	2.4	$[T/m^3]$
Young's modulus	E	25.3	[GPa]
Poisson's ratio	ν	0.2	[-]

The only exception to the above is represented by the material used to model the behavior of one-way spanning iron floor slabs. Once the elastic Young's modulus in the strong direction is determined as described in Section 4.2.2.2, according to simple engineering calculations, the other elastic

components of the Young's moduli, E_{22} and E_{33}, can be estimated as follows in Equations (4.4) and (4.5):

$$E_{22} \approx 10 - 20\% \, E_{11} \qquad (4.4)$$

$$E_{33} = \frac{E_{11} + E_{22}}{2} \qquad (4.5)$$

The Poisson's ratios for this orthotropic material can be estimated by checking the requirements of Equations (4.6) and (4.7):

$$v_{ij}^2 < \frac{E_{ii}}{E_{jj}} \qquad (4.6)$$

$$2 \cdot v_{12} \cdot v_{23} \cdot v_{31} < 1 - v_{12}^2 \cdot \frac{E_{22}}{E_{11}} - v_{23}^2 \cdot \frac{E_{33}}{E_{22}} - v_{31}^2 \cdot \frac{E_{33}}{E_{11}} \leq 1 \qquad (4.7)$$

For simplicity, the shear stiffnesses in the three directions were then calculated following the definition of isotropic behavior, Equation (4.8), bearing in mind that this estimation of the shear moduli can lead to errors in the computation of the shear response of the floor slabs. Another approach for the calculation of the shear moduli is proposed by Li and Barbič (2014), Equation (4.9).

$$G_{ij} = \frac{E_{ii}}{2 \cdot (1 + v_{ij})} \qquad (4.8)$$

$$G_{ij} = \frac{\sqrt{E_{ii} \cdot E_{jj}}}{2 \cdot (1 + \sqrt{v_{ij} \cdot v_{ji}})} \qquad (4.9)$$

Finally, the computed properties for the equivalent orthotropic material adopted for the finite shell elements representing the iron floor slabs are summarized in Table 4.7.

Table 4.7 Equivalent material properties adopted for the orthotropic shells of the floor slabs

MATERIAL PROPERTY	SYMBOL	VALUE	UNITS
Young's modulus	E_{11}	18.837	[GPa]
	E_{22}	0.942	
	E_{33}	9.890	
Poisson's ratio	v_{12}		[-]
	v_{23}	0.27	
	v_{31}		
Shear modulus	G_{12}	7.419	[GPa]
	G_{23}	0.371	
	G_{31}	3.894	
Mass density	ρ	2.97	[T/m^3]
Eq. thickness	t_{eq}	0.222	[m]

4.3.2 Loads

No additional vertical loads were applied to the structure out of the self-weight of the building. These are automatically computed by DIANA according to the assigned densities of the various materials and the geometrical features of the mesh. For a check of the vertical reactions of the model when only subjected to gravitational loads, some hand calculations were also performed and reported in Table 4.8.

Table 4.8 Summary of the total masses of the model divided by structural element

STRUCTURAL ELEMENT	MATERIAL	VOLUME [m³]	WEIGHT [kN]	MASS [T]
Solid walls	Masonry	665.08	9311.08	949.14
Shell walls - Iron	Masonry	106.67	1493.35	152.23
Columns	Concrete	15.19	364.56	37.16
Pillars	Concrete	5.12	122.76	12.51
Iron frame T	Iron	2.23	173.57	17.69
Iron frame L	Iron	2.51	195.53	19.93
Iron frame pl	Iron	1.25	97.54	9.94
Embedded elements	Iron	0.25	19.70	2.01
Floors - Iron part	Iron_floor	28.48	853.99	87.05
Roof ties	Iron	0.37	28.60	2.91
Shell walls - Timber (sp. 52)	Masonry	98.20	1374.81	140.14
Shell walls - Timber (sp. 45)	Masonry	87.72	1228.04	125.18
Shell walls - Timber (sp. 35)	Masonry	22.67	317.42	32.36
Shell walls - Timber (sp. 20)	Masonry	14.94	209.18	21.32
Timber 40x30	Timber	105.24	673.53	68.66
Timber 30x30	Timber	20.70	132.47	13.50
Timber 20x30	Timber	11.39	72.89	7.43
Floors - Timber part	Iron_floor	35.67	1069.84	109.06
Concrete slab	Concrete	13.09	314.21	32.03
Roof weight	-	-	1645.98	167.79
Front tympanum	Masonry	7.58	106.12	10.82
Transept tympani	Masonry	15.37	215.16	21.93
Back tympanum	Masonry	6.33	88.64	9.04
TOTAL		1266.03	18053.07	1840.27

As said, even if it was decided not to model the roof to limit the number of nodes of the system, its weight and mass contribution were taken into account by modelling it as distributed mass. For this reason, the load of the roof was not even applied to the structure since the Finite Element Program

already calculates the applied masses to the model as a contribution to the weight under gravitational acceleration.

For the seismic analyses, the model was then loaded with horizontal load patterns proportional to the masses in the *x* and *y* directions of the model to perform pushover analyses, which correspond to the first lateral forces distribution proposed in the second group of distributions of the Italian Code (NTC 2018).

4.3.3 Boundary conditions

As an initial tentative approach to define the boundary conditions of the model, seen the scarce reliability of the data regarding the foundation system and the soil-structure interaction characteristics, and also considering the complexity of the numerical model, perfectly rigid boundary conditions were applied to the base nodes of the structure. With this approach, as already mentioned in Section 4.2.1, the rotational capacity of the foundational system can be modelled by deepening the foundation level. In the present case the foundation level was deepened of about –1.30 m. It is also noted that cracking is allowed in the material, thus allowing a hinge to be formed in case of tensile stresses.

The base nodes of the solid walls of the church were assigned a *pinned* boundary condition, by limiting the three translations, which necessarily also blocks the rotation of the walls as the entire thickness of each single wall would necessarily block also the rotations in the three directions of the same nodes.is supported. The same boundary conditions were applied to the shell elements representing the walls of the canonical house. For the nodes at the base of the columns of the gallery a fully *fixed* boundary condition (three translations and 3 rotations) was applied.

Lastly, it is worth mentioning additional boundary conditions between some different elements of the structure. In fact, as will be explained in Section 5.3.1, the different modelling strategies adopted influenced drastically the response of the church, especially when submitted to horizontal loads applied in its transversal direction. The adoption of shell models and solid models to represent the *iron-Baraccato* walls required the insertion of internal tying between the shells and the connected solid walls orthogonal to them, in order to ensure compatibility of the shell rotation degrees of freedom and obtain a consistent behavior between the wall elements modelled with different strategies. This objective was reached by coupling the translations of the corner nodes between shell and solid and the correspondent nodes belonging to the shell element at a certain distance from the corner (Figure 4.12).
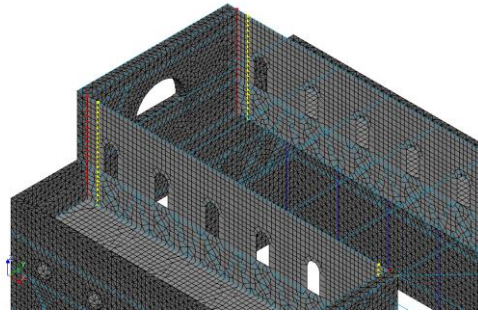
Figure 4.12 Internal tying between the solid and the shell walls of the church, in red the *master node* and in yellow the *slave node*

The appropriate distance between the *master node* and the *slave node* is unknown since it represents the rotational stiffness of the corner of the masonry walls that depends on the quality of the connection between the wall, the adhesion between the units and the bonding mortar, the mortar quality, etc. A sensitivity analyses may be performed to inspect the influence of the tying distance on the global response of the corner, supported by appropriate *in-situ* surveys.

4.4 Preliminary model validation

A first analysis was performed by considering the structure just submitted to gravitational loads and considering elastic response of the materials of the building. The aim of performing this type of analysis is to detect possible inconsistencies and errors committed in the modelling phase, since, for masonry structures mainly characterized by the non-linear response, it has limited relevance.

The linear static analysis was used first to check the external vertical reaction which should correspond to the total weight of the structure as calculated in Section 4.3.2. The total vertical reaction obtained by the linear static analysis is equal to 18,250 kN that, when compared with the total calculated weight of the structure (18,053 kN), corresponds to about 1% of difference.

Additionally, a check of the stresses at the base of the structure and the corresponding vertical reactions can be performed along with the maximum vertical displacements both in terms of values and in terms of locations. Indeed, the maximum vertical displacement of the structure analyzed to the gravitational loads are expected mainly in the central sections of the floor slabs and at the key stone of the arch above the apse. At the base of the masonry walls the vertical reactions are evenly distributed (dark blue vectors in **Errore. L'origine riferimento non è stata trovata.**), with some peaks in c orrespondence of the vertical frames (other color vectors in **Errore. L'origine riferimento non è stata trovata.**). In terms of principal stresses, the results show an average stress state at the base of the masonry walls of about 25-30 kPa with a maximum peak in the south branch wall of the apse. The

normal (i.e. axial forces) are about 98 kN in the canonical house and 52 kN in the main body of the church (Figure 4.14). As for the displacements, the maximum observed displacement occurs, as expected, in the deformable floor slabs of the canonical house (Figure 4.15), where it is about 4 mm. In the church walls very small vertical displacements are observed, with a maximum of about 2 mm at the top the arch above the apse.

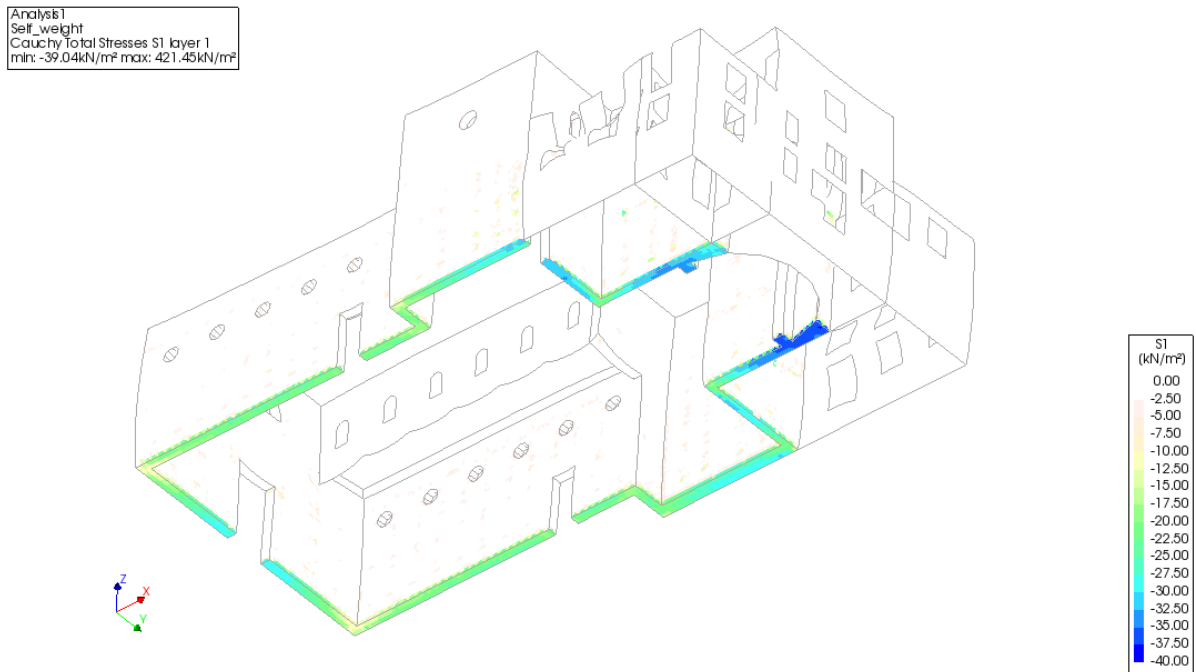**Figure 4.13 Structural linear static: distribution of the maximum compressive principal stresses (S1) at the base of the masonry walls**

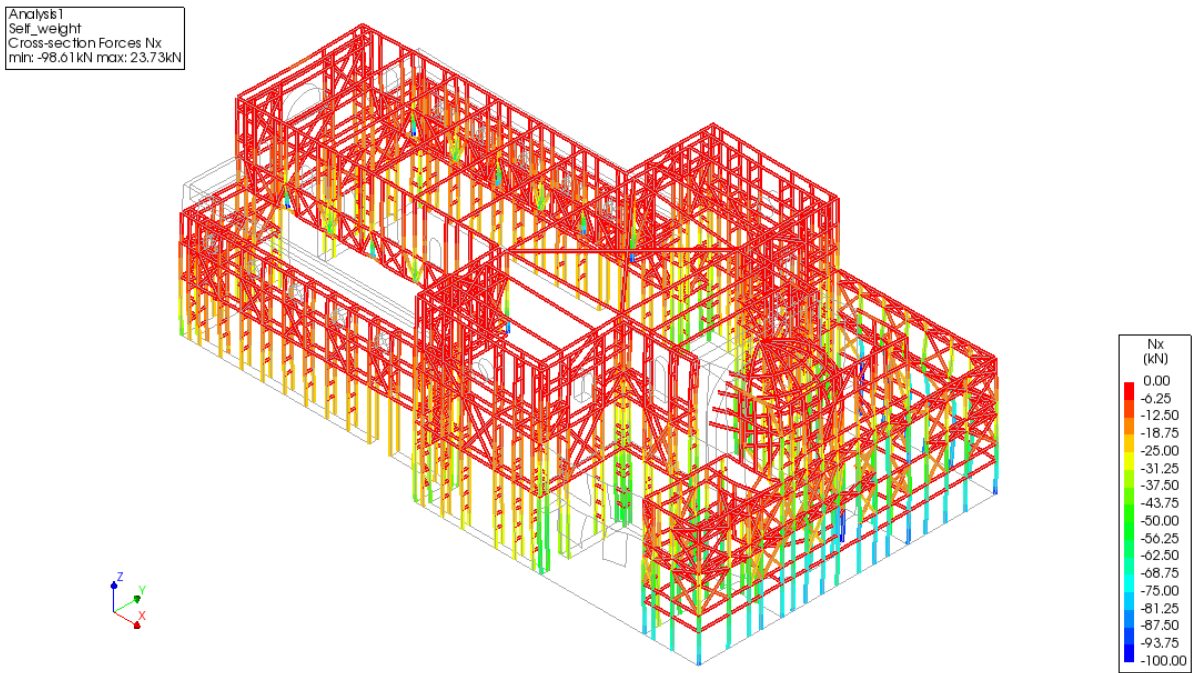ADVANCED MASTERS IN STRUCTURAL ANALYSIS OF MONUMENTS AND HISTORICAL CONSTRUCTIONS

Figure 4.14 Structural linear static: normal forces in the elements of the *Baraccato* frames
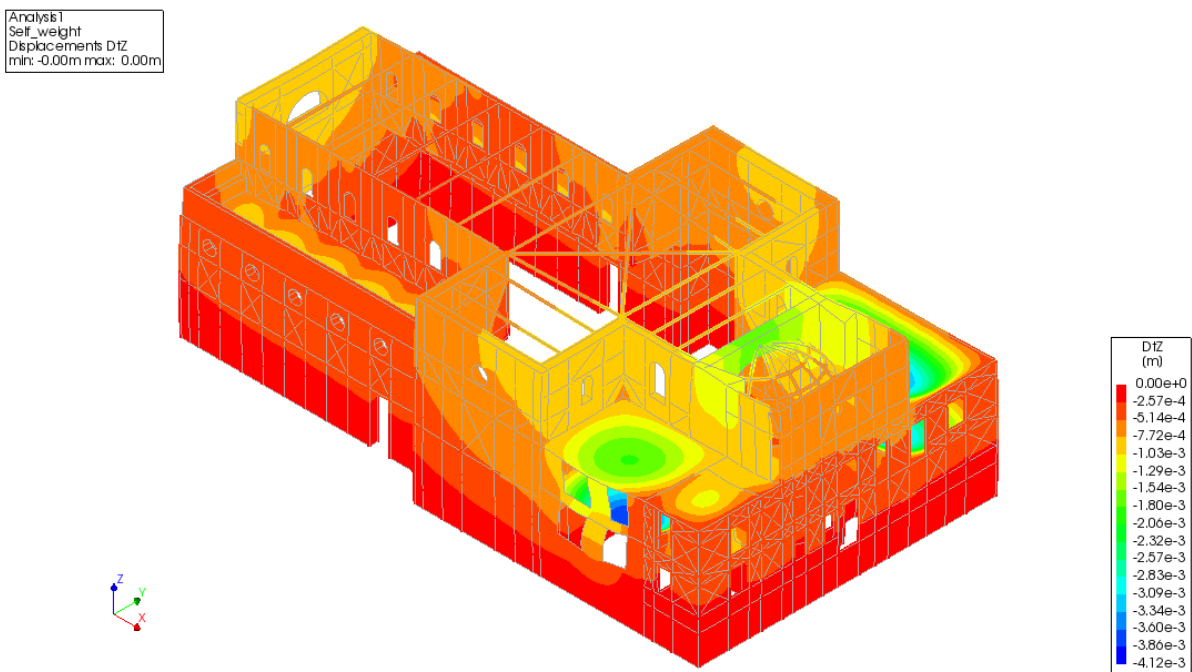
Figure 4.15 Structural linear static: Vertical displacements

5 AMBIENT VIBRATION TEST AND CALIBRATION

One of the key tests performed on the church of Santa Maria Maddalena were the *in-situ* ambient vibration tests. The tests were made under operational conditions in order to deepen the knowledge about the dynamic response of the structure in the post-seismic condition, setting the goal of identifying the natural modes of vibration of the building, in terms of natural frequencies, modal shapes and, possibly, the damping ratios.

The data collected during the ambient vibration tests were validated and processed in this work with the ARTeMIS software (ARTeMIS Modal v3.5.1.1 2018) and compared with the results obtained by the company which performed the test. Once identified the modal frequencies and shapes of the structure, assessed in a post-damage condition, the results of the Operational Modal Analysis (OMA) were used to calibrate the numerical model by tuning the numerical modal frequencies with the experimental ones, modifying to some extent the characteristics of the structure, which included major uncertainties that affect its dynamic response.

In the following paragraphs, the description of the setups of the ambient vibration tests and their main results, the results of the eigenvalue analyses of the numerical model and the process of its calibration and validation will be explained. Since there is still a relevant level of uncertainty about the church structural details, and since the initially adopted modelling strategies did not allow a satisfying matching of the numerical and experimental modal shapes, the present study also focused on the sensitivity of the dynamic behavior of the structure to some of the adopted strategies.

5.1 Dynamic tests

5.1.1 *In-situ* ambient vibration tests

The non-destructive tests were performed on the church by the company S2X S.r.l., under commission of the Campania Regional Directorate for Cultural Heritage (MiBACT), in the days of January 28th, 29th and 30th, 2019.

The data were collected using 25 piezoelectric accelerometers of the type identified by the company with the name IEPE_1, corresponding to ceramic piezoelectric uniaxial accelerometers with high sensitivity (10.0 V/g), low noise (0.13 μg/√Hz), resolution of 10^{-5} g rms and frequency range 0.1-200 Hz. The accelerometers were arranged in two different test setups and connected to two acquisition boards (DAQ_32) with 32 channels and a central notebook.

The two layouts for the test setups consisted of 36 measurement points, which were determined *a priori* by the company that performed the tests and located at three different levels of the church: the terraces level (+7.35 m), +10.00 m level, and the attic level (+11.80 m). Figure 5.1, Figure 5.2 and Figure 5.3 show the location of the measurement points as reported by the report of the company (S2X Srl 2019) with the relative heights with respect to the corresponding level and the sampling orientation[9]. In the drawings, the measurements reported in red color are the ones that were left in the same position for the implementation of the two setups, in green the ones corresponding to the first setup (Setup_01) and in blue to the second setup (Setup_02). The piezoelectric sensors were firmly anchored to the church walls by using metallic plates avoiding damaged zones and plaster detachments, in order to assure good quality readings (Figure 5.4a and b). Aiming at cable arrangement optimization, the accelerometers were connected to two different acquisition boards located at the extremes of the church (at the entrance and in the apse), subsequently connected to the notebook (Figure 5.4c). The presented arrangement of the accelerometers defines the two setups that consist of 25 sensors for the Setup_01 and 23 sensors for the Setup_02. The two setups recorded the ambient vibrations for a total time of 3600s with a sampling frequency of 100 Hz.

It must be pointed out, that an experimental campaign in which ambient vibration measurements are to be taken in order to catch the natural modes of vibration of the structure should be properly planned with preliminary simplified numerical analyses. The use of a preliminary simplified model of the structure to inspect, with a corresponding eigenvalue analysis, can help in the definition of the accelerometer locations. Especially in the case of a church, whose dynamic response and modal shapes are not as intuitive as a simple building, the location of the measurement points plays an important role in the outcomes of the test. For example, in the present case the eigenvalue analyses performed on the numerical model of the church evidenced the appearance of a local mode of the second-story wall of the central nave at low frequencies (see Section 5.3.1.3). However, the experimental results did not evidence such a behavior since no accelerometers were placed in the wall section or level interested by this dynamic phenomenon.

---

[9] It must be pointed out that an inconsistency was detected from the sampling direction of accelerometer nr. 14 declared in the drawing and from some of the pictures taken by the company operators during the tests. For the analysis of the results, the direction of the accelerometer was, then, taken as reversed. In the same way, it was noticed during the data analysis that accelerometer nr. 12 presented measurement directions in contrast with the other accelerometers. In the absence of any picture that could confirm the actual orientation of the accelerometer, its orientation was assumed reversed for the OMA.

Figure 5.1 Locations of the accelerometers at +7.35 m
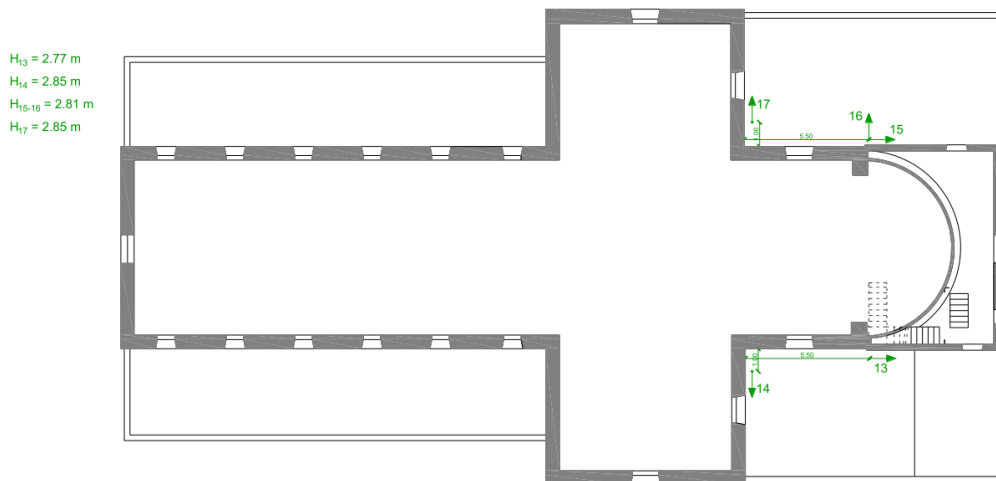
Figure 5.2 Location of the accelerometers at +10.00 m
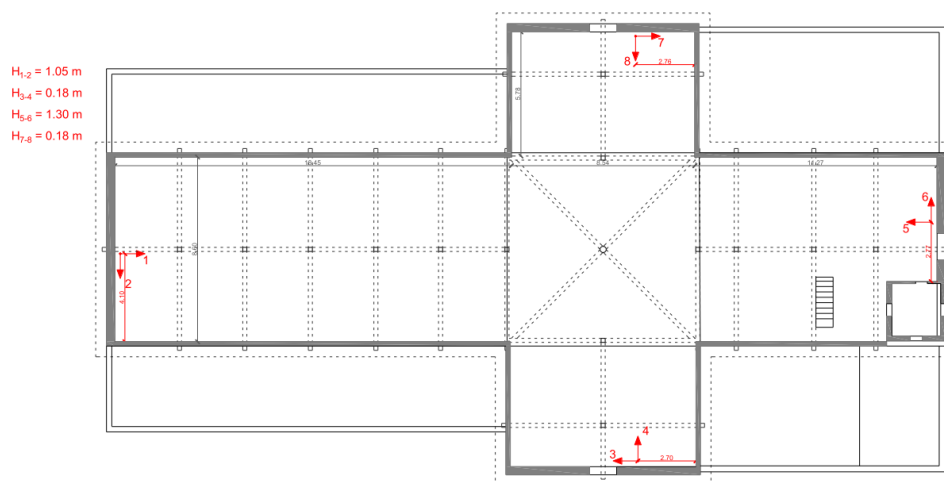
Figure 5.3 Location of the accelerometers at +11.80 m

| (a) | (b) | (c) |
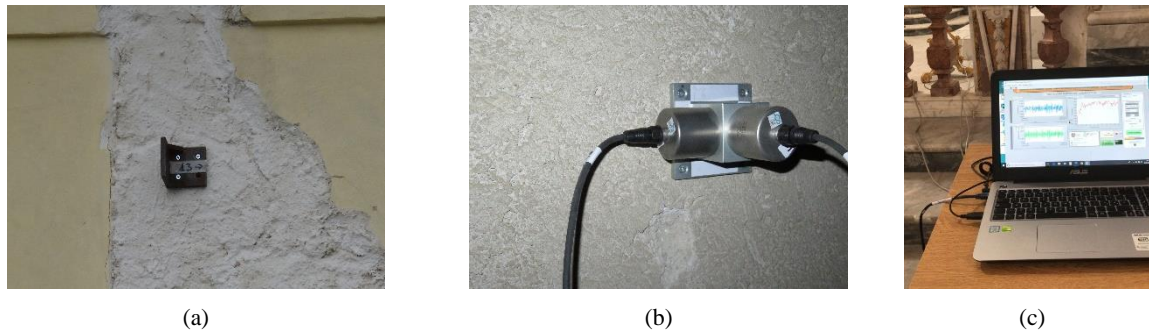
Figure 5.4 Anchor plates for mono-directional measurements (a), double-directional measurements (b) and the notebook used for the tests (c)

5.1.2 Preliminary results

The data obtained from the tests were initially processed by the company which performed the test. Before processing them, the raw data obtained from the *in-situ* measurements were pretreated by proceeding with a preliminary validation and with some filtering actions, e.g. clipping, spikes and drop-out recognition (S2X Srl 2019). Subsequently, the data were analyzed according to the method of the Frequency Domain Decomposition (FDD) and Covariance Driven Stochastic Subspace Identification (CoV-SSI). The analysis and the comparison of the two methods allowed to estimate the first three natural modes of the structure, in terms of natural frequency and damping ratios (Table 5.1), along with a representation of the modal shapes represented by sampling plane (Figure 5.5). The modal shapes were identified as follows:

- *Mode I*: Flexural mode in the transversal direction with major amplitudes in correspondence of the transept (Figure 5.5a);
- *Mode II*: Flexural mode in the longitudinal direction with major amplitudes in correspondence of the central nave (Figure 5.5b);
- *Mode III*: Torsional mode (Figure 5.5c).

Table 5.1 Dynamic identification results obtained from the S2X company (Casapulla et al. 2019a; S2X Srl 2019)

MODE NR.	f [Hz]	ξ [%]
#1	2.54	1.8
#2	3.74	3.0
#3	3.89	2.7
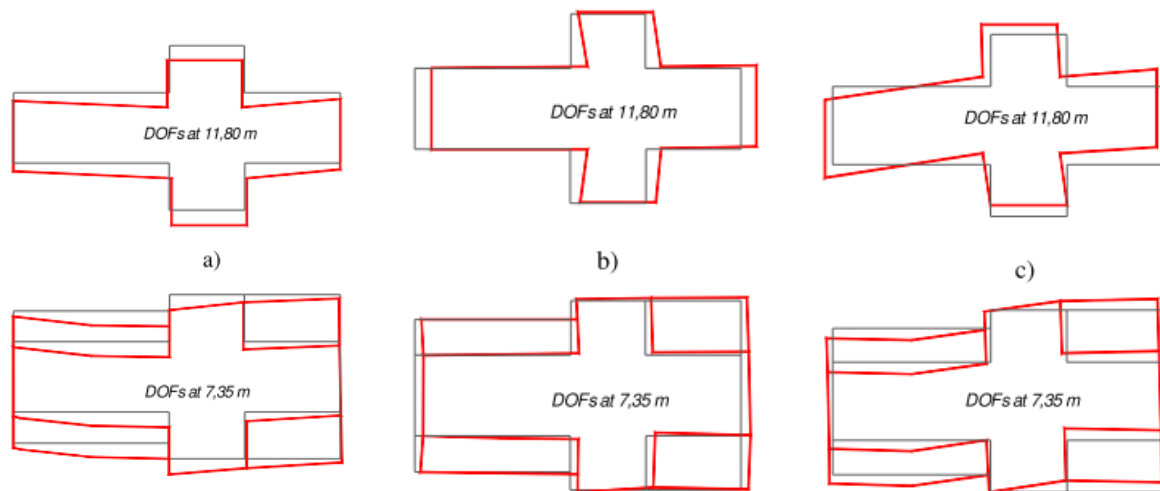
Figure 5.5 Modal shapes of the structure obtained by S2X, Mode I (a), Mode II (b), Mode III (c). Source: (Casapulla et al. 2019a)

5.2 Operational Modal Analysis (OMA)

In order to refine the modal estimation, the results of the ambient vibration tests were post-processed directly with the software ARTeMIS (ARTeMIS Modal v3.5.1.1 2018). In order to analyze the recorded signals of the accelerometers used for the tests and to visualize the modal shapes resulting from the processing of the signals and the recognition of the natural modes of the vibration of the structure, a geometrical model of the church was implemented in the software. It must be pointed out that, since the measured points in which the accelerometers were placed consist of a limited number of points of the effective geometry of the building, the non-measured geometrical points defined in the geometry of the ARTeMIS model, which do not correspond to DOF measurements, do not represent effective responses of the structure. In fact, the geometrical definition of a model in ARTeMIS should compromise between a sufficiently detailed representation of the analyzed building, capable of allowing the user a reliable understanding of the structure modes of vibration, and a sufficiently simplified representation that does not make use of much more geometrical points than the measured ones. In any case, the software used for the OMA can take advantage of some interpolation functions to apply to the non-measured nodes, to represent appropriately the modal shapes that have to be used with care in order not to obtain misleading interpretations.

For these reasons, a few versions of the geometrical model in ARTeMIS were produced and analyzed before reaching a final configuration capable of appropriately describe the modal shapes of the structure and represent the complex geometry of the church (Figure 5.6).

ADVANCED MASTERS IN STRUCTURAL ANALYSIS OF MONUMENTS AND HISTORICAL CONSTRUCTIONS

(a)   (b)

Figure 5.6 ARTeMIS geometry of the initial model (a), final version (b)

After the geometry definition and the management of the measured DOFs that were loaded to the appropriate point locations of the geometry and once the measurements' data was assigned with the corresponding direction, the two setups were analyzed with the 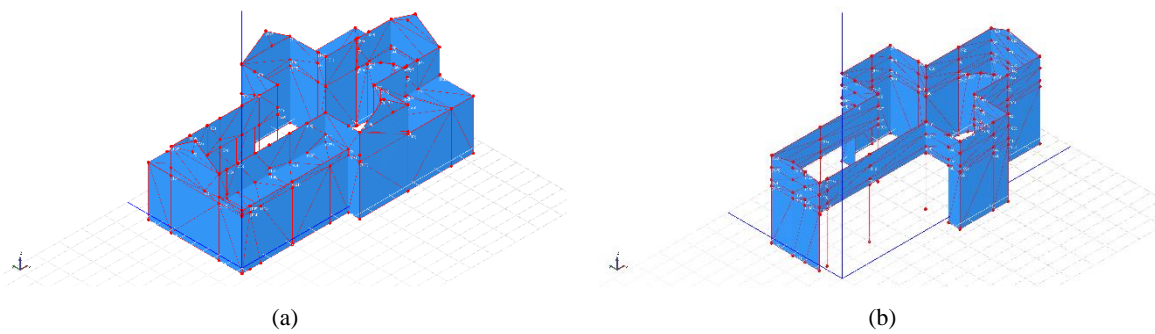Enhanced Frequency Domain Decomposition method (EFDD) and the Stochastic Subspace Identification - Unweighted Principal Components Merged Test Setups method (SSI-UPCX), with the goal of performing the OMA with at least two different methods, one time-domain based and the other frequency-domain based.

The EFDD method is a non-parametric method developed in the frequency domain (FD). It is based on the estimation of the modal parameters from the power spectral densities of all the measurement points after the application of the Fast Fourier Transform (FFT) process to the signals. With this method, it is possible to choose manually the possible principal modes of the structure, selecting on the top of the peaks of the spectral density graph (Figure 5.7).

The Stochastic Subspace Identification (SSI) method, used in this case, was the SSI-UPCX method. The SSI methods are parametric methods developed in the time domain (TD), based on the identification of modal parameters by fitting the response correlation functions for each measurement point to a mathematical model, representative of the dynamic behavior of the structure. The time domain methods are robust and allow an accurate modal parameter estimation. The stabilization diagram presents the natural frequencies of all the estimated eigenvalues (Figure 5.8).

As observed, the spectral density diagram evidences some peaks and spikes that enable the peak-picking procedures required by the EFDD method, even if the graph is characterized by a rather stable development and the peaks do not correspond to much energy variation with respect to the ambient noise. Conversely, the SSI-UPCX stabilization diagrams of the two setups do not allow the automatic identification of any natural mode, being characterized by many noise mode points (Figure 5.8 brown dots) and very few stable mode points (Figure 5.8 red dots). For this reason, the initial goal of estimating the natural modes of the structure in order to have more robust and reliable results coming

from the comparison of multiple, different type methods could not be attended and the dynamic identification was performed with the only EFDD method.
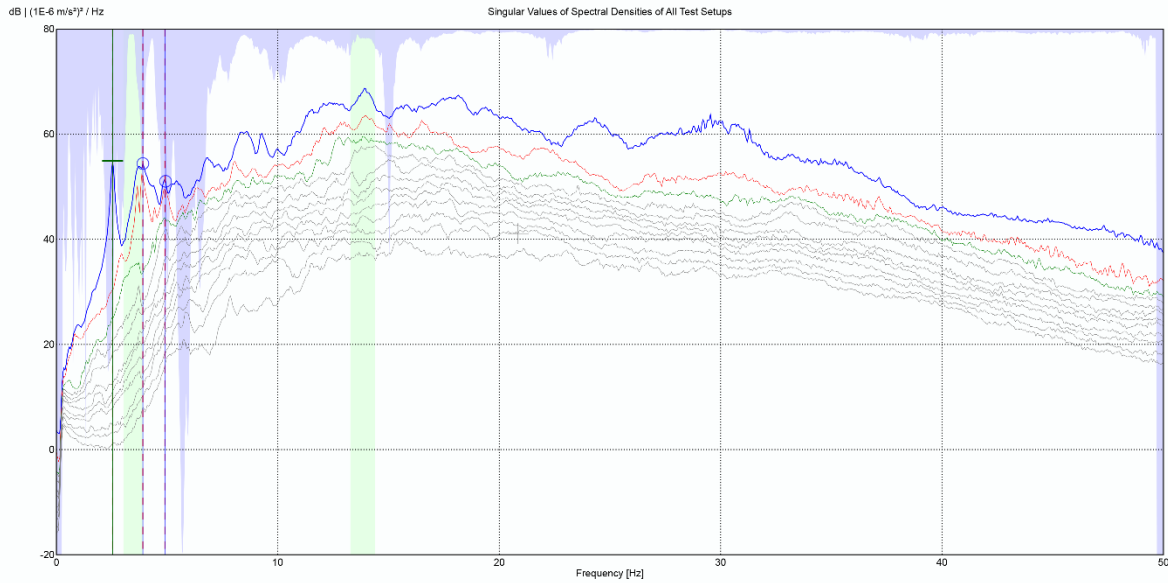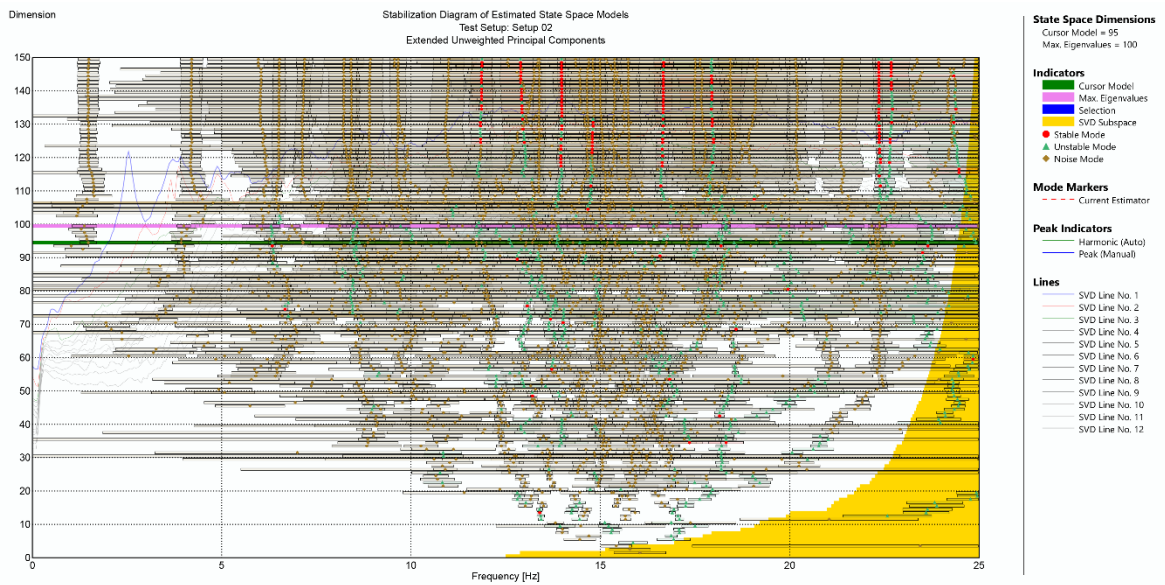

Figure 5.7 Spectral density diagram[10]

Figure 5.8 SSI-UPCX Stabilization diagram (Setup_01)[11]

---

[10] For reasons of space the reported graph is recalled in a larger scale in Annex 4 for better legibility.
[11] For reasons of space the reported graph and the corresponding Setup_02 are recalled in Annex 4 a larger scale in for better legibility.

The identification of the peaks of the spectral density diagram was conducted by reducing the frequency range in which to identify the natural modes of the structure to 0-25 Hz (Figure 5.9) and three first modal frequencies were identified as shown in Figure 5.9 from the vertical lines. It is reminded that the present analysis is aimed at the identification of the global modes of the structure, which involve a significant mass of the building. It can be observed that the graph shows many minor peaks following the ones identified, but in terms of modal shapes they always correspond to local modes of the church chancels. At the same way, an additional frequency range 13-14 Hz at high energy (green highlight) is identified by the analysis, where it is probable the identification of a natural mode of the structure. Also in this case, the picked frequency shown a local mode of the chancel of the front façade and it was discarded from the analysis.
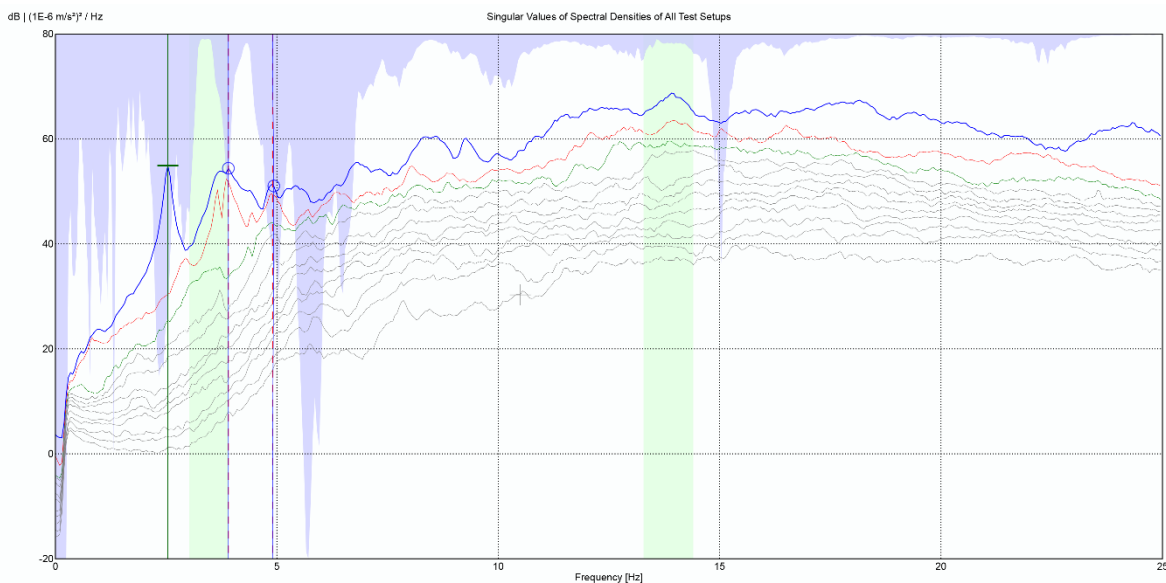
Figure 5.9 Spectral density diagram in the range 0-25 Hz for the peak-picking procedures

The described procedures allowed, finally, to identify three natural modes of the structure whose principal characteristics are reported in Table 5.2. As mentioned, the displayed modal shape of the selected mode is highly influenced from the geometry implemented in the ARTeMIS model. The only representation of the measured nodes for a modal shape is not enough to clearly understand the effective mode of vibration of the structure. Therefore, the interpolation equations available in the software were used to reach the optimum compromise between the accuracy and the graphics. Moreover, with the comparison of the eigenvalue analysis of the numerical model described in Section 5.3.2, some more *slave* equations between the geometric points of the ARTeMIS model were implemented, in order to obtain a better interpolation of the non-measured nodes. For example a higher deformability of the south-western walls of the transept was observed, both in the eigenvalue analysis and in the observations of the company that performed the tests and preliminarily processed

the data. This is due to the low geometrical stiffness of the south-western wall in the transversal direction, composed by a slender *iron-Baraccato* wall connected with the last row of columns of the gallery. Since no accelerometers were placed along the north and south façades of the transept, their geometrical points in ARTeMIS were manually interpolated with the measured DOFs of the church terraces. This *slave* interpolation operation was performed after a previous analysis of the data, discarding the measurements of the chancels of the church (measurement points nr. 1-8), which proved the consistency of the observed modal shapes of the corresponding façades between the numerical and the experimental models.

Figure 5.10 to Figure 5.12 show the resulting modal shapes of the three identified natural modes of vibration. In general, the identified modal shapes can be described as follows:

- *Mode I*: translational mode in the transversal direction of the church (y), characterized by major amplitudes of the transept and in-phase displacements between the central nave and the apse walls (Figure 5.10);
- *Mode II*: translational mode in the longitudinal direction of the church (x), characterized by major amplitudes in the central nave and in-phase displacements between the central nave and the apse walls (Figure 5.11);
- *Mode III*: mode characterized by the out-of-phase displacements of the longitudinal walls in the transversal direction (Figure 5.12).

The observed modal frequencies and modal shapes are consistent with the ones obtained by the S2X company (S2X Srl 2019).

Table 5.2 Dynamic identification results obtained from the OMA

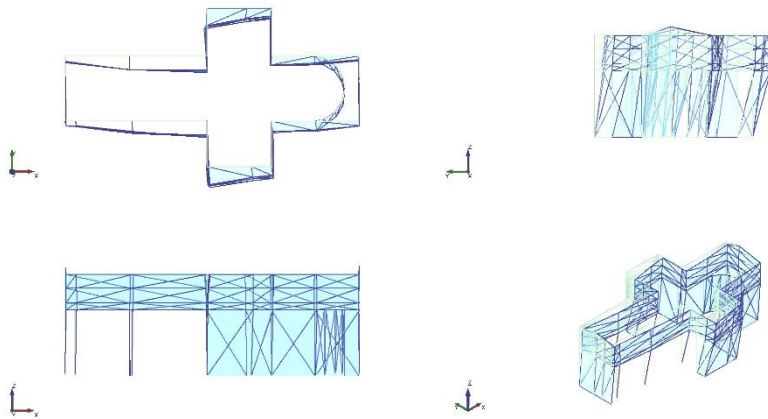| MODE NUMBER	FREQUENCY [Hz]	DAMPING RATIO [%]
#1	2.54	2.23
#2	3.75	1.43
#3	4.90	1.21

Figure 5.10 Modal shape of Mode 1, quad. view
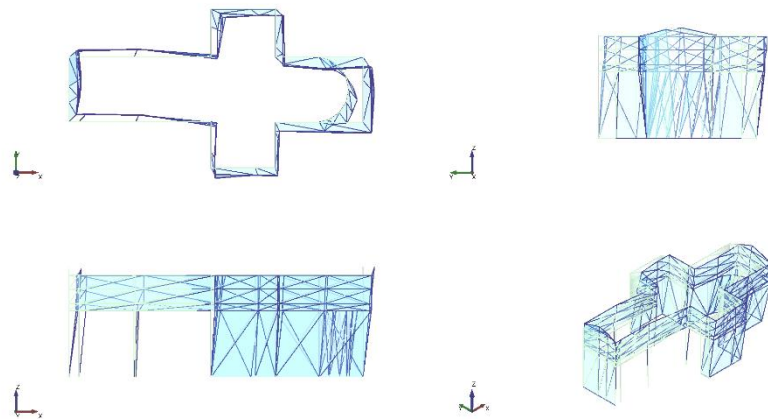

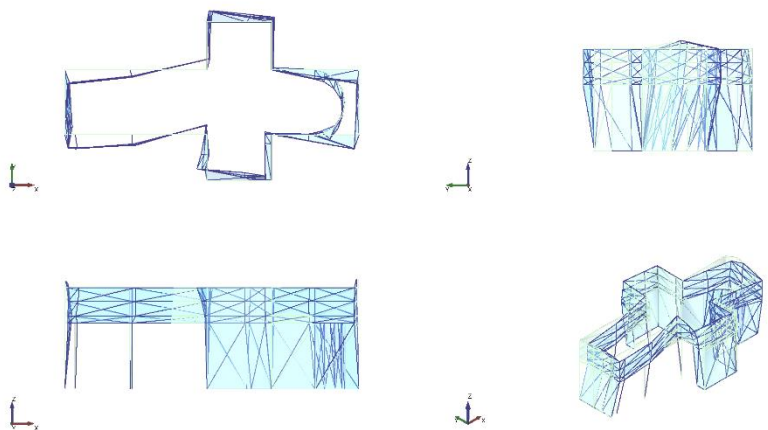**Figure 5.11 Modal shape of Mode 2, quad. view**

Figure 5.12 Modal shape of Mode 3, quad. view

5.3 Eigenvalue analysis and calibration of the numerical model

The results of the experimental campaign carried out for the dynamic identification of the structure through Operational Modal Analysis were used to validate the modelling strategies adopted and to calibrate the unknown mechanical properties of the materials used in the numerical model, which influence the dynamic response of the structure mainly in terms of stiffness.

Since, at the beginning of the calibration phase, unsatisfying results were obtained in terms of modal shapes of the numerical model, iterative procedures of calibration of the numerical modal shapes, and optimization of the geometrical representation of the experimental mode shapes, were implemented. In general, a matching of the first numerical and experimental modal shapes was performed in terms of global response. For this reason and for matters of space, in the following Section 5.3.1 representations of the only first global modes will be presented. In any case, it is worth mentioning that during the calibration of the modal shapes phase also the shapes of higher modes were taken into consideration. Once reached a reliable matching between the two models, the calibration of the modal frequencies was performed by calibrating the masonry Young's modulus and matching the first identified natural frequency of the structure.

5.3.1 Calibration of the modal shapes[12]

As mentioned, some of the modelling strategies of the initial versions of the numerical model had to be validated through the calibration of its first global modal shapes. The first results of the eigenvalue analysis on the complete model led to the observation of a first global modal shape of the numerical model. This shape mainly involved the transversal deformation of the western section of the transept and a relatively small deformation of the front and the back parts of the church (Figure 5.13). Firstly, a study on the two separate sections of the church – main body in *iron-Baraccato* structure and back part in *timber-Baraccato* structure – were performed in order to better understand their dynamic response in relation to the global structure.

---

[12] For reasons of space, unless needed, in the present Section just the top views of the modal shapes of the studied models are provided for comparison between the various models.

<div align="center">(a)   (b)</div>
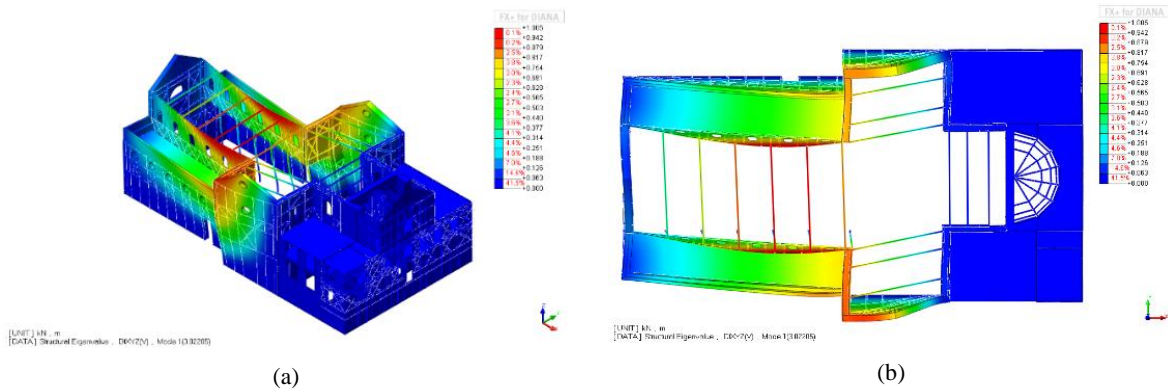
Figure 5.13 Results of the first attempt model of the church, 3D view (a) and top view (b)

5.3.1.1 Main body of the church model (Model_iron)

A model of the church that includes just the main body of the church (Model_iron) was created and analyzed (Figure 5.14) in terms of the first global modal shape. In particular, the relative deformability of the two sides of the transept, the longitudinal naves and the apsidal part of the church were inspected, in order to try to mobilize the back portion consistently with the modal displacements of the main body of the church This goal was reached by removing the possible stiffness sources located in the back portion of the apse constituted by the arch supporting the apsidal dome, whose materials and constructive system are unknown (Model_iron_a, Figure 5.15a), and the two extremities of the apsidal walls that were modelled with increased thickness to provide a geometrical connection with the back part of the church (Model_iron_b, Figure 5.15b). As observed from the following figures, the influence of the apsidal arch on the global stiffness is scarce, in terms of modal shape, since the high stiffness of the back part is provided by the two L-shaped walls constituted by the eastern walls of the transept and the lateral walls of the nave confining with the canonical house. By the way, it is worth mentioning that the removal of both the above-mentioned elements provides a better approximation of the numerical shape to the experimental one. However, in the global model of the church they cannot be removed. Moreover, the higher deformability of the western walls of the transept is, as already mentioned, provided by its geometrical configuration.

| (a) | (b) |
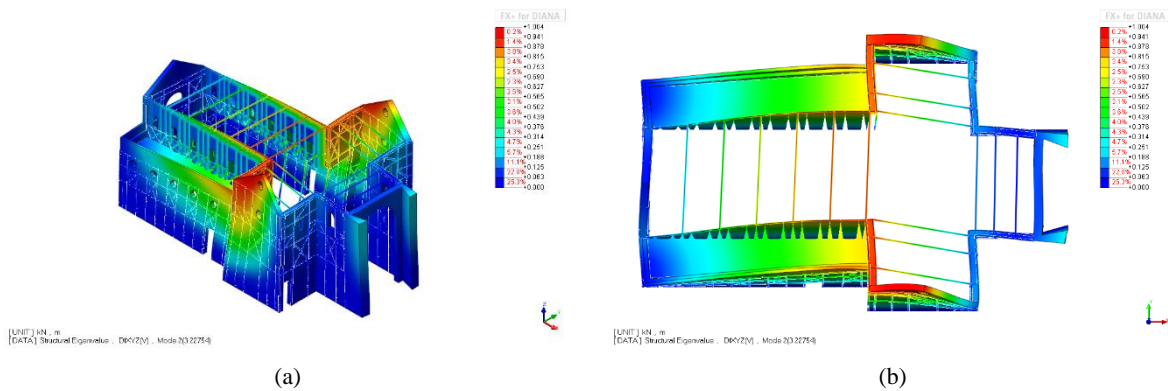
Figure 5.14 First global mode of the Model_iron, 3D view (a) ad top view (b)

| (a) | (b) |
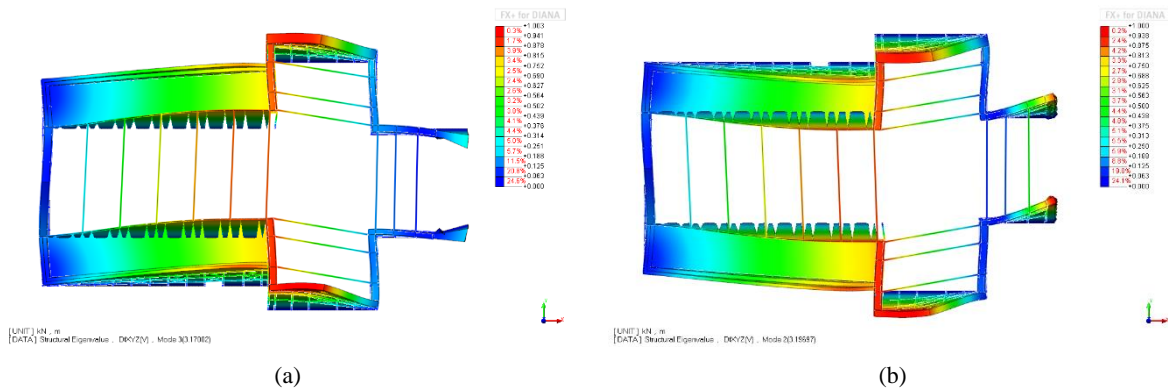
Figure 5.15 Top view of the first modal shapes of the two versions of the Model_iron model, Model_iron_a (a) and Model_iron_b (b)

5.3.1.2 Back part of the church model (Model_timber)

The analysis of a model representing just the back part of the building (Model_timber) evidenced that this portion of the church is characterized by a high stiffness. In fact, as observed from Figure 5.16, the model mainly exhibited local modes at low frequencies with low global participation. This is obviously due to the model geometry that presents unrestrained walls, whose behavior has no relevance in the reality since, for the sake of simplicity, this version of the model was just extracted from the global one. However, the lack of global modes for frequencies of the order of 10 Hz demonstrates the high stiffness of the structure.

ADVANCED MASTERS IN STRUCTURAL ANALYSIS OF MONUMENTS AND HISTORICAL CONSTRUCTIONS

#1 (f = 4.07 Hz)   #2 (f = 5.32 Hz)   #3 (f = 5.36 Hz)   #4 (f = 5.99 Hz)

#5 (f = 7.16 Hz)   #6 (f = 8.55 Hz)   #7 (f = 9.93 Hz)   #8 (f = 10.31 Hz)
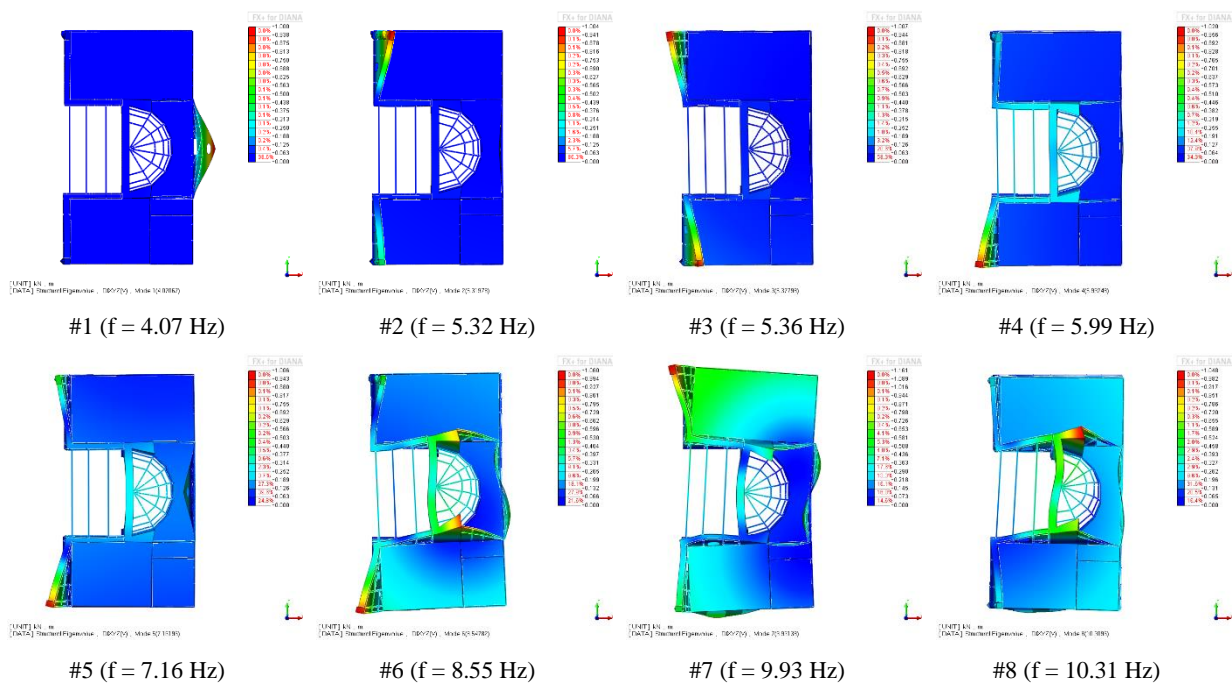
Figure 5.16 First eight modal shapes of the Model_timber model

Moreover, the influence of the presence of the floors (Model_timber_01) and the influence of the layout of the timber frames (Model_timber_02) were also inspected. As observed from Figure 5.17, the floor presence, and stiffness, has a relevant influence in the response of the church sub-structure since the floors contribute to decrease significantly the frequencies of the global modes. However, it is noticed that the modal shape of the church portion is mainly governed by L-shaped walls of the transept which do not allow the development of proper translational modal shapes (Figure 5.17). On the other hand, as expected, the layout of the timber frames scarcely influences the modal shapes of the sub-structures, as evidenced in the analysis of a model with the complete absence of timber elements (Model_timber_02), while having relevance in the modal frequencies (Table 5.3).

#4 (f = 3.90 Hz)   #8 (f = 5.97 Hz)   #9 (f = 6.52 Hz)
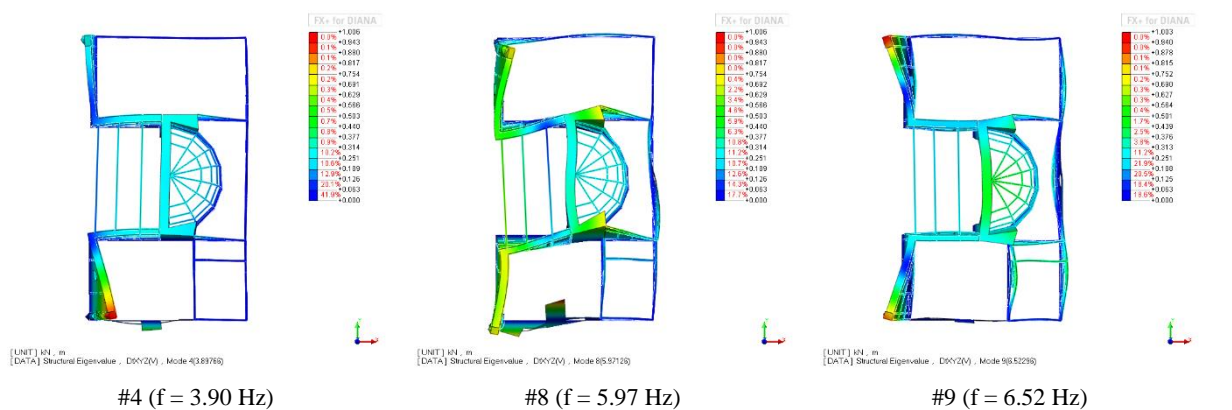
Figure 5.17 Global model of the model Model_timber_01

Table 5.3 Frequency comparison of the models Model_Timber and Model_timber_02

MODE	FREQUENCY [Hz]		DECREASE [%]
	Model_timber	Model_timber_02	
1	4.071	3.294	19.1
2	5.320	4.926	7.4
3	5.378	5.039	6.3
4	5.993	5.401	9.9
5	7.162	6.689	6.6
6	8.548	7.630	10.7
7	9.931	7.968	19.8
8	10.310	9.118	11.6

5.3.1.3 Complete model (Model_iron+timber)

All the observations carried out on the partial models led to the conclusion to inspect different modelling strategies applied globally to the numerical model, since they evidenced consistent responses with the global model and with the expected behavior of the church. In general, three different aspects of the modelling strategies application were taken into consideration, in the scope of obtaining at least a global translational mode in the transversal direction of the church:

- the influence of the geometrical stiffness of the back part;
- the influence of the modelling strategies to apply to the foundation system;
- the influence of the modelling strategies to apply to simulate the roofing system presence.

Geometrical stiffness influence

The geometrical stiffness influence of the back portion of the building was inspected taking into consideration firstly the stiffness contribution provided by the geometry of the back wall of the canonical house, which has a total length of about 21 m. In fact, the contribution of stiffness of such long wall to the global behavior is only assured if the wall in consideration does not present any joint or discontinuity. A version of the total model was then produced in which the central section of the back wall, the connected floors and the apsidal semicircular wall were suppressed (Model_iron+timber_G_a). Additionally, the other stiffness contributions were also inspected by removing the arch above the apse (Model_iron+timber_G_b), as already studied for the Model_iron models. Lastly, the combination of the two models was studied (Model_iron+timber_G_c). As observed from Figure 5.18, the geometrical stiffness contribution of the back wall of the church and of the apsidal arch is minimum with respect to the translational response of the structure, which is mainly governed by the high stiffness of the western branch of the transept (right side in the pictures) and by the higher deformability of the eastern branch (left side in the picture). For these reasons, since no evidences of discontinuities were found in the back wall of the canonical house and for consistency

with the geometrical survey, the arch, the back-wall section and the apse semicircular wall were inserted in the final model and further calibration strategies were adopted for the modal shapes.
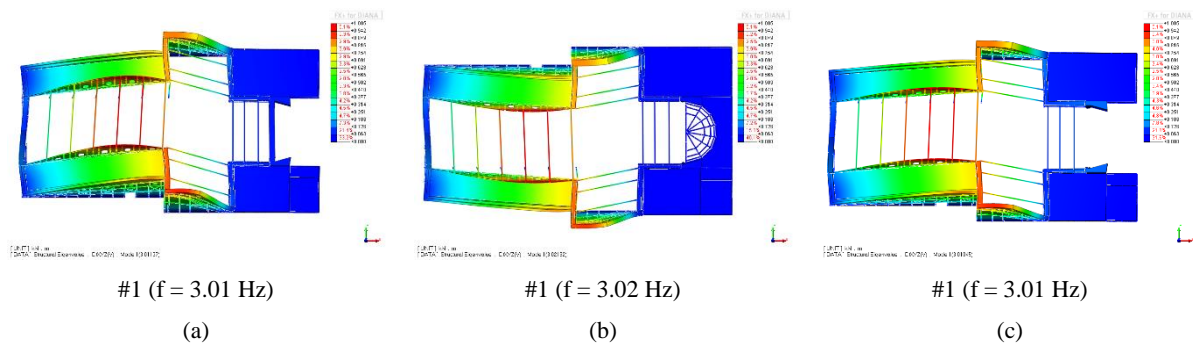

#1 (f = 3.01 Hz)	#1 (f = 3.02 Hz)	#1 (f = 3.01 Hz)
(a)	(b)	(c)

Figure 5.18 First global modal shapes of the models G: Model_iron+timber_G_a (a), Model_iron+timber_G_b (b), Model_iron+timber_G_c (c)

Foundation stiffness influence[13]

As mentioned in Section 4.3.3, the modelling strategy adopted for the foundations was the adoption of perfectly rigid boundary conditions to limit all the degrees of freedom of the nodes at the base. It is well known that in a realistic representation of the soil-structure interaction some movements, e.g. in terms of vertical settlements and rotations, are expected. For this reason, some analyses were performed in an updated model (Model_iron+timber_F_a), where soil-structure interaction was modelled through *interface elements* with assigned limited stiffness in the vertical direction. The adopted modelling strategy consists of a more refined approach to the modelling of the foundations. With this approach the yielding foundations of the church resulted to be modelled according to the Winkler's theory of the elastic soil representing the foundation as a spring bed with constant stiffness. The Winkler's constant (k) can be determined as a function of the oedometric modulus (M) of the interacting soil and the foundation thickness (b), following the equation(5.1):

$$k = \frac{M}{b} \qquad (5.1)$$

In this case, M is considered approximately equal to $1.15 \cdot E$, where E is the elastic modulus of the soil. However, it is worth remembering that such a refined model of the foundations is not supported by an appropriate level of knowledge about the soil-structure interaction characteristics. In fact, it was adopted only in the scope of inspecting the sensitivity of the dynamic response of the structure to these parameters and the need of deepening their knowledge. For this reason, literature values were used for the elastic modulus of the soil ($E = 100 - 120 \, MPa$).

---

[13] The figures in this section are presented using a three-dimensional view to visualize the foundation modelling strategy.

Moreover, since the eigenvalue analyses described so far never involved the translational response of the back portion of the church, an attempt of mobilizing it was carried out by decreasing significantly the mechanical stiffness of the material representing the masonry walls of the canonical house and the stiffness constant of the *interface* elements, representing the yielding foundations of the canonical house (Model_iron+timber_F_b), considering also optimal characteristics of these two parameters in the main body portion of the church (Model_iron+timber_F_c). As observed in Figure 5.19, the influence of these strategies with respect to the dynamic behavior of the church has relevance more in the natural frequencies of the structure rather than in the modal shapes. For this reason, and for the scarce knowledge of the soil-structure interaction characteristics of the church obtained, the *interface* modelling of the foundations was discarded and the same Young's Modulus for the main body walls and the back-part walls was adopted.
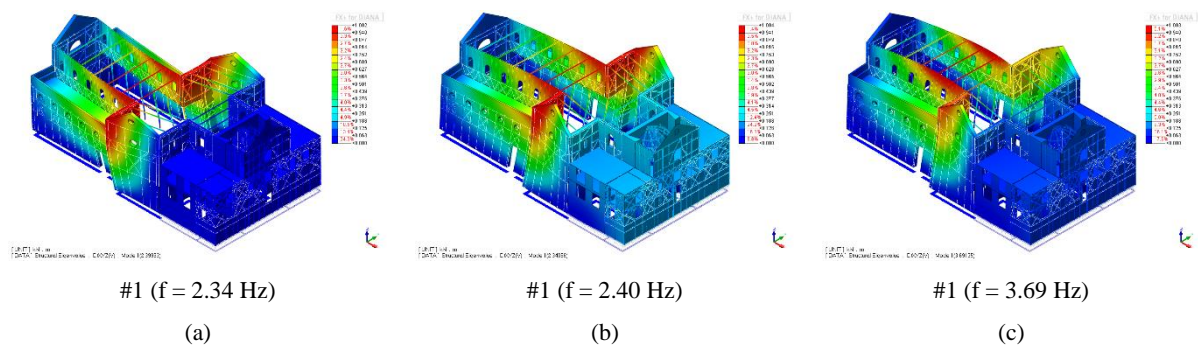

#1 (f = 2.34 Hz)	#1 (f = 2.40 Hz)	#1 (f = 3.69 Hz)
(a)	(b)	(c)

Figure 5.19 First global modal shapes of the models F: Model_iron+timber_F_a (a), Model_iron+timber_F_b (b) and Model_iron+timber_F_c (c)

Roof stiffness and mass influence

Finally, a crucial point in the modal shapes calibration was found by inspecting the different modelling strategies that can be adopted to simulate the influence of the roofing system at the top of the building, both in terms of mass participation and in terms of stiffness contribution of the roof structures. In fact, with the aim of reducing the model complexity and size, it was decided not to include the geometrical representation of the roofing system in the numerical model, as a first strategy, and to consider its presence just from the gravitational point of view by adding an equivalent load distributed along the roof perimeter. This approach included two different simplifications which, as will be explained, have great impact in the dynamic response of the structure: (a) the suppression of the participating mass of the roof located at the top of the construction; (b) the suppression of the stiffness contribution provided at the attic level by the attic floor slab and the roof trusses which, in particular, enable the redistribution of the horizontal loads at the top of the church walls in case of earthquake. In any case, the adopted modelling strategy was initially considered suitable for the case, seen the relatively small mass of the timber roof and the relatively high deformability of the attic floor slab.

Given the previous observations and since the previously mentioned analyses did not consist of relevant changes in the purpose of the first modal shape calibration, an additional model, in which the roof mass was applied at the top of the structure as a distributed mass (Section 4.2.2.3) along the perimeter of the church, was created and analyzed. As seen from Figure 5.20, the influence of the application of the roof mass has a great influence in the definition of the first modal shape of the model, since the response changed drastically from a shape governed by the deformability of the eastern wall of the transept (Figure 5.13) to a more consistent transversal oscillation of the whole church.
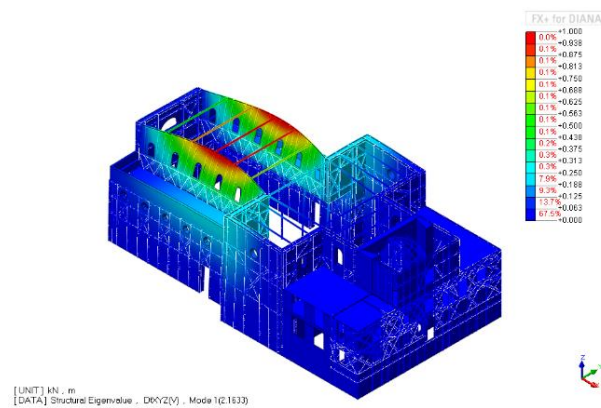

Figure 5.20 First global mode of the model with the distributed mass of the roof (#1, f = 2.16 Hz)

Moreover, some more changes and modelling strategies were inspected with this updated configuration of the model:

- implementation of a rigid link to provide consistent rotational stiffness of the wall corners of the *iron-Baraccato* wall, as explained in Section 4.2.2.1;
- influence on the stiffness at the roof level of the cross-shaft three-dimensional truss;
- influence of the attic floor slab stiffness by the implementation of *beam* elements instead of the *truss* elements that simulate the roof trusses ties.

The first strategy was adopted in order to correct an initial modelling error. In fact, in the previous configuration, the mutual rotation of the *iron-Baraccato* walls modelled as shells and the ones modelled as solids was allowed, which is not consistent with the reality.

Moreover, the additional studies were always performed always with the purpose of the mobilization of the back portion of the church. In particular, once proved the efficacy of inserting diagonal bracing elements to reduce the deformability of the cross-shaft space, a sensitivity analysis was performed on the roof bracings by modelling them as beams and by increasing their stiffness, both in the full model version and in the main body partial model version.

The following pictures present the various attempts carried out with the last presented modelling strategies. It can be observed that the implementation of the rigid links (Figure 5.21b and c, Figure 5.22b and c), provides more consistent deformed shapes of the second-story level of the central nave wall, as well as the insertion of diagonal bracings in the cross-shaft (Figure 5.21c). Instead, the adoption of regular size *beam* elements does not provide relevant changes in the modal shapes (Figure 5.22a and b). It is also noted that increasing the beams sections (Figure 5.22c) provides a notable global effect in the building.

(a)   (b)   (c)
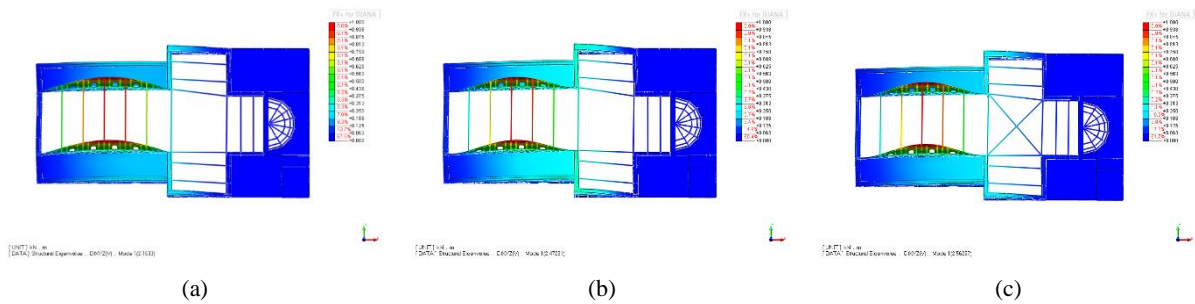
Figure 5.21 Roof ties modelled as *truss* elements: original model (a), model with rigid link of the walls (b) and model with rigid links and cross-shaft diagonal ties (c)

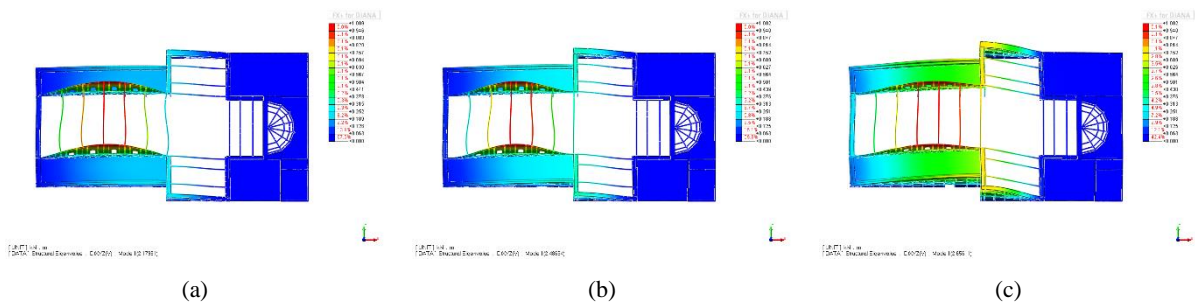(a)   (b)   (c)

Figure 5.22 Roof ties modelled as *beam* elements: original model (a), model with rigid links of the walls (b) and model with beams sections equal to an INP600 (c)

As mentioned, the previous observations led to the definition of an additional study of the beam stiffness influence at the roof level. Firstly, a partial model representing just the main body of the church portion was analyzed (Figure 5.23). In this last set of analyses the capability of the beams stiffness to mobilize the two western longitudinal branches of the church was studied (Figure 5.23a and b). In addition, the longitudinal walls of the central naves were also given additional stiffness to contribute to the purpose and to limit their local out-of-plane observed response (Figure 5.23c). Lastly, the study of the full model of the church with the same strategies to increase the attic level stiffness evidenced modal shapes close to the ones observed experimentally (Figure 5.24). In particular, for the case of increased cross-section of the roof beams and increased thickness of the longitudinal walls (Figure 5.25) the best qualitative accuracy was observed.

(a)   (b)   (c)
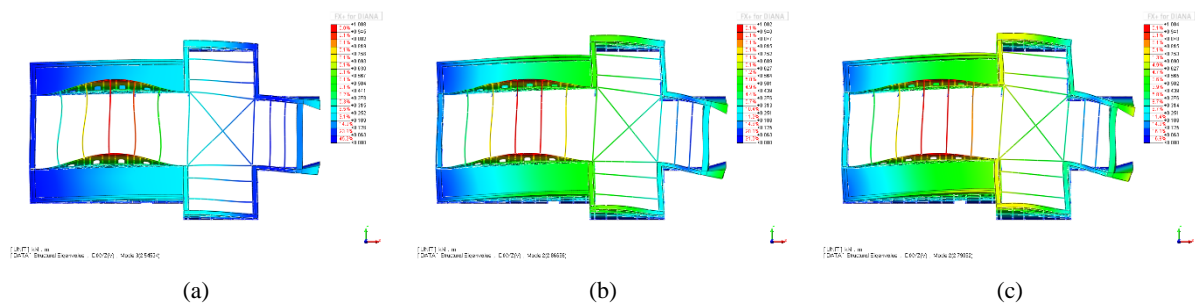
Figure 5.23 Main body of the church model with roof ties and rigid links: with diagonal bracings in the cross-shaft (a), INP600 section of the beams (b) and INP600 sections and 1 m thickness of the longitudinal nave wall (c)
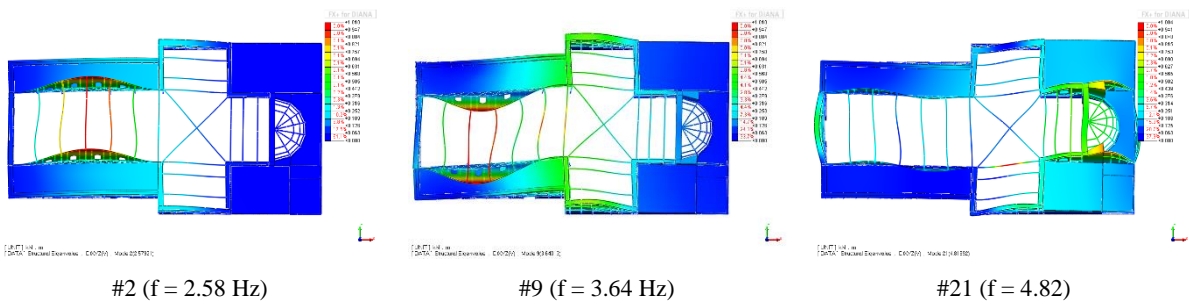

#2 (f = 2.58 Hz)   #9 (f = 3.64 Hz)   #21 (f = 4.82)

Figure 5.24 First global modal shapes of the full model with regular size roof beams

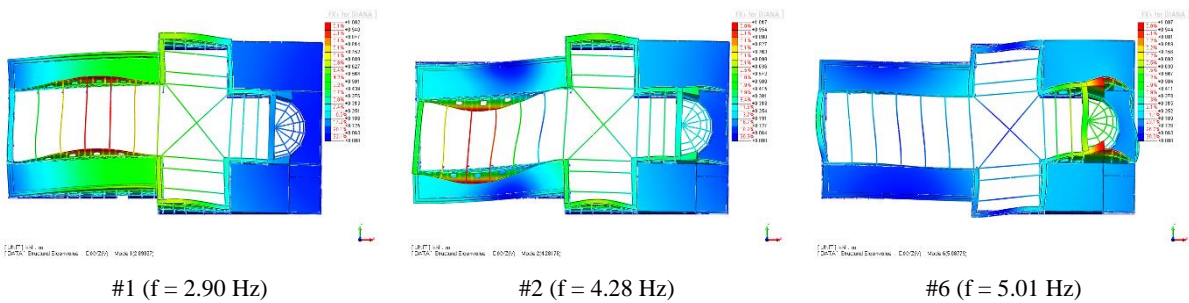#1 (f = 2.90 Hz)   #2 (f = 4.28 Hz)   #6 (f = 5.01 Hz)

Figure 5.25 First global modal shapes of the full model with INP600 roof beams and increased thickness of the longitudinal wall of the central nave

It must be pointed out that such an increase of the roof beams cross-section can only be justified by the observation of the constructive details of the structure. In fact, the roof timber trusses are laid on the top of the iron beams connecting the iron frames embracing the vertical masonry walls. These overlapped elements constitute a sort of composite section which has an increased stiffness with respect to the single iron beams, depending on the connection of the elements and the friction coefficient between them. Obviously, the approximation of such behavior with the equivalent behavior of an INP600 iron beam consists of an overestimation that is also found in the increased thickness of the longitudinal walls. In fact, attempts of calibrating the frequencies of the last modes recorded in Figure 5.25 would lead to a Young's modulus of about 450 MPa, representing a non-realistic simulation of the masonry material. Moreover, the adoption of un-restrained *beam* elements in the model also causes the development of local modes of vibration of the beams at lower frequencies.

In conclusion, it was observed that, disregarding the back-portion mobilization contribution of the *truss* and *beam* models, whose difference is minimum when regular size beams are adopted, the only improvement provided by the *beam* model is the partial limitation of the local out-of-plane mode of the longitudinal walls of the central nave. The local mode was detected in all the lastly described analysis and it is believed to have a relevance with the effective behavior of the structure. However, this response was not caught during the ambient vibration tests since the accelerometers layout did not enable its record. In fact, only a specific layout, set up for the purpose of placing accelerometers at the top-middle location of the second-story walls of the central nave, would catch their out-of-plane modal response. The comparison with the actual results of the experimental tests is only possible by removing from the visualization of the modal shapes of the numerical models the upper walls of the central nave. For these reasons a *truss* model was adopted for the roof stiffness contribution.

The final and best fitting modelling strategies can be summarized as follow:

- complete representation of the geometry of the church (main body and back portion);
- implementation of perfectly rigid boundary conditions at the foundation level of the model;
- adoption of the same mechanical characteristics for the masonry walls in the *iron-Baraccato* and *timber-Baraccato* systems;
- implementation of a rigid link connection between the interacting *solid* and *shell* elements of the central nave of the church;
- application of the roof mass as a distributed mass along the perimeter of the roof according to the tributary areas of the roof surfaces;
- insertion of diagonal ties to retain the cross-shaft space deformability at the roof level;
- implementation of *truss* elements to provide an equivalent attic floor slab stiffness.

 In sum, the several attempts explored to find a better agreement between the numerical and experimental models well testify the challenging complexity of the structural typology of the Santa Maria Maddalena church.

5.3.2 Eigenvalue analysis and calibration of the modal frequencies

Once identified the proper modelling strategies to adopt in the numerical model, a calibration of the modal frequency is possible. The calibration was carried out through the adaptation of the first numerical global frequency, corresponding to a global model, to the first experimental one, by iteratively updating the Young's modulus of the masonry walls, while all the other material properties were kept constant.

The iterative minimization procedure of error on the first frequency led to the estimation of a Young's modulus of the masonry material of 890 MPa, from a first tentative value of 920 MPa (Section 4.3.1.1). Subsequently, the Modal Assurance Criterion (MAC) was calculated to evaluate the modal shapes. The MAC is a statistical indicator relating the degree of consistency between the estimates of the mode shape vectors. It is capable of evaluating couples of selected modes (numerical and experimental), comparing their modal shapes, through the selection of appropriate nodal displacements, and expressing their perfect match (MAC value equal to 1.0) or total difference (MAC value equal to 0). The comparison is carried out in terms of modal displacements through the following equation:

$$MAC_{u,d} = \frac{\left|\sum_{i=1}^{n} \varphi_i^u \varphi_i^d\right|^2}{\sum_{i=1}^{n}(\varphi_i^u)^2 \sum_{i=1}^{n}(\varphi_i^d)^2} \qquad (5.2)$$

where:

- n is the number of the measured DOFs;
- φ^u is the nodal displacement of the current building condition (experimental) in the considered mode;
- φ^d is the nodal displacement of the model condition (numerical) in the considered mode.

The eigenvectors of the modal shapes were normalized to the maximum recorded modal displacements, so that the maximum modal displacement of the normalized eigenvector is equal to 1 (Mendes 2012). The normalization of the eigenvector assures the MAC values to assume values belonging to the $[0 - 1.0]$ range, where optimum correlations are represented by MAC≥0.9, good correlations by 0.8≤MAC<0.9 and acceptable correlations by 0.7≤MAC<0.8. MAC values lower than 0.7 are not considered acceptable for matched modes (Mendes 2012).

Table 5.4 presents the calculated MAC matrix for the three experimental modes identified during the Operational Modal Analysis phase with the first three global modes of vibration of the numerical model, updated following the modal shape calibration procedures. As observed, the matrix is characterized by low MAC values, where the best correlation is given by the first mode with a MAC of 0.74 (acceptable). Moreover, the highest values are not located along the diagonal of the matrix, indicator of non-biunivocal correspondence of coupled modes. The results presented were expected since many issues were encountered during the OMA and the calibration of the modal shape. As already mentioned, in the light of the eigenvalues analyses previously described, a refinement of the *in-situ* measurements is recommended. In particular, the numerical analyses performed here allowed to obtain vibrational responses of the model that the performed measurements were not able to catch in the real case structure, mainly for an incomplete setup definition. It is suggested to carry out additional

measurement setups in order to validate or discard the hypotheses drawn in the previous Section 5.3.1. The MAC values allow the effective matching only of the first mode of vibration as graphically presented in Figure 5.26.

Table 5.4 MAC matrix of the coupled modes of vibration of the church

		EXPERIMENTAL RESULTS		
		Mode #1. *f = 2.54 Hz*	Mode #2 *f = 3.75 Hz*	Mode #3. *f = 4.90 Hz5.12*
NUMERICAL RESULTS	**Mode #1** *f = 2.54 Hz*	0.743	0.058	0.006
	Mode #2 *f = 3.58 Hz*	0.392	0.168	0.255
	Mode #6 *f = 5.12 Hz*	0.208	0.266	0.264

3D VIEW

3D VIEW

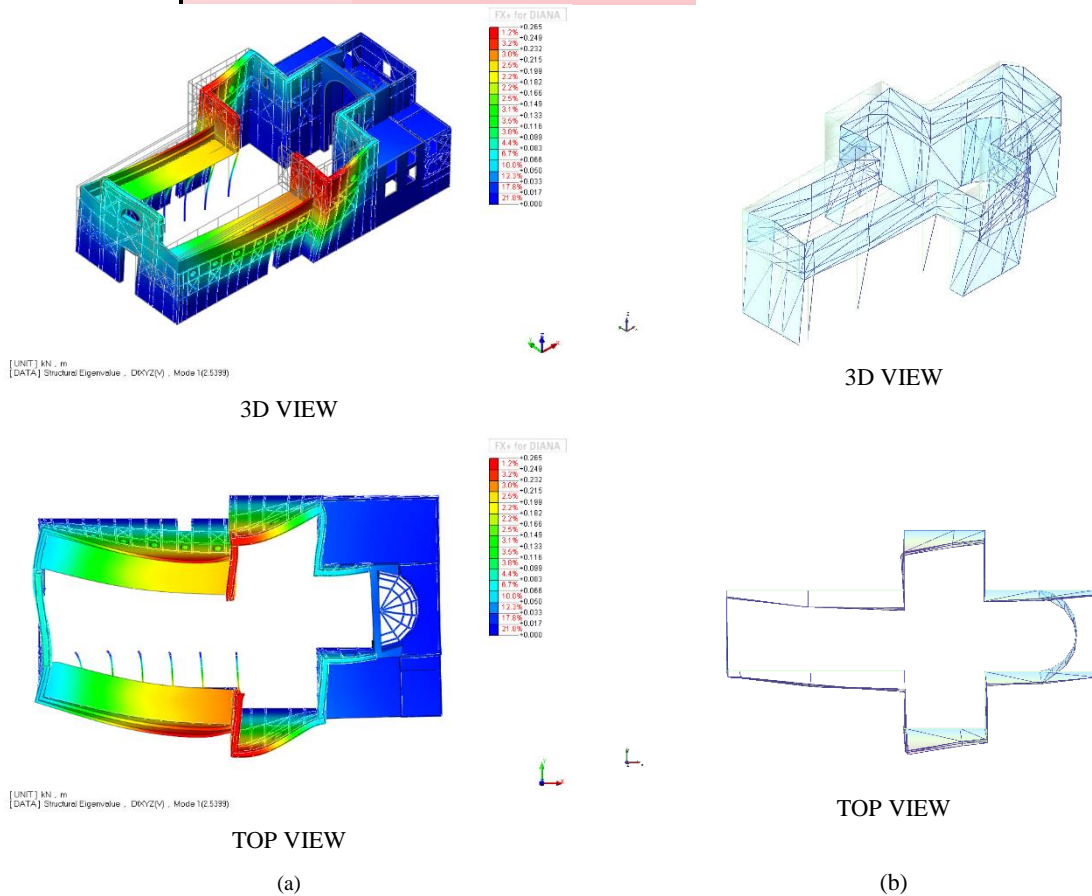

TOP VIEW

TOP VIEW

(a)

(b)

Figure 5.26 Calibrated modal shapes of the numerical model (a) and reference experimental modal shape (b) of the first mode (f = 2.54 Hz)

5.4 Open issues

As explained in the previous sections, the dynamic identification process of the structure set forth different issues. Firstly, the level of knowledge reached for the structural details of the church highly influenced the definition of the modeling strategies adopted for the numerical model and had to be inspected and validated through multiple structural analyses. These were carried out in the scope of inspecting the relevance of the selected modelling approaches in the dynamic response of the numerical model, with respect to the one of the real structure. In this sense, it was observed that simplifications adopted at the beginning of the modelling phase, e. g. the suppression of the roof modelling, highly influenced the response. Therefore, the modelling strategy and simplifications in the modelling of such a complex structure should be taken with great care.

Secondly, it was observed that the results of the performed ambient vibration tests revealed to be in some cases incomplete in the description of the complex dynamic response of the church. In fact, the adopted measurement layouts seemed to highly influence the outcome of the experimental campaign. When dealing with heritage structures with articulated shapes, materials and construction phases, etc., an appropriate planning of the experimental campaign is fundamental and should be carried out with the support of preliminary numerical models, to help the understanding of the expected dynamic response of the structure. In the present case, the layout configuration, which was mainly characterized by setups of accelerometers almost aligned along a single level of the church with some more accelerometers placed at a higher level but not aligned along the vertical direction, did not allow the description of the out-of-plane dynamic response of the walls. In addition, no accelerometers were placed in the church main façade and corresponding back façade and transept façades, which could have been useful for the description of the behavior of the connection between the church structural units and orthogonal walls.

In conclusion, the execution of more ambient vibration tests is suggested by planning accelerometer setups in which the sensors are placed along the height of the church in the aligned planes of the various transversal cross-sections of the church (longitudinal naves, transept, back portion, etc.), in a sufficient number to be placed at least at the bottom and at the top of each vertical wall. These setup definitions would allow the collection of more complete data regarding the dynamic response of the church and would be able to validate or discard some of the observations, hypotheses and conclusions drawn during the calibration phases, in the scope of the definition of the global behavior of the church as a basis for advanced structural analysis.

6 PRELIMINARY SAFETY ASSESSMENT

The present work aimed, as one of the main objectives, at the seismic assessment of the church when subjected to seismic loads. Seen the earthquake proneness of the area and the response of the structure to the last seismic event of 2017, a non-linear dynamic analysis seems to be the most suitable tool for addressing the objective. Moreover, since instrumental records of the last earthquake are available, a properly defined and calibrated numerical model of the structure could be tested by defining the recorded earthquake signal input, in the scope of the comparison between the numerical response of the adopted model and the effective observed damage in the structure. However, considering the various uncertainties that still characterize some of the structural details of the geometrical survey, the almost null knowledge of the experimental mechanical characteristics of the existing materials of the structural elements of the church, the still relevant issues regarding the dynamic identification of the structure and the relative calibration, such refined and high precision analysis is not yet applicable to the numerical model developed so far because the mentioned issues do not assure enough reliability of the results.

Nonetheless, a relevant step forward in the modelling progress of the church was achieved since its full implementation was accomplished, based on the data available at the moment. For these reasons, it was decided to perform a less time-consuming non-linear static analysis instead, with the scope of defining a range of response of the structure when submitted to horizontal loads. To this end, two different versions of the finalized model as described in Section 5.3.1.3 were prepared and analyzed:

(a) *Reinforced model*: in which all the geometries and elements were implemented as described in Chapter 4 and Section 5.3.1.3, under the assumption that the non-linear response of the structure is entirely defined by the masonry, for which non-linear constitutive laws are adopted (Section 4.3.1.1), while considering a linear behavior for the other materials;

(b) *Un-reinforced model*: in which the same geometry is implemented but the elements representing the iron and the timber frames are discarded.

The definition of the described models allows the pushover analysis results to show what are expected to be an upper-bound response and a lower-bound response of the structure. The former is represented by the model (a) response that defines an ideal condition where the reinforcing elements never get to failure and contribute to idealize the box-behavior of the masonry walls. The latter is represented by the model (b) response where the structural capacity is completely provided by the masonry walls.

The following sections will provide the results of the mentioned non-linear analyses performed on the two models, in the view of identifying a possible range for failure mechanisms and of defining the

influence of the reinforcing elements, seen the particular structural system of the church, instead of an understanding of the real case expected damage.

The pushover analyses were performed by applying an equivalent horizontal distribution of forces to the numerical model of the church, increased monotonically until the partial or global collapse of the building is detected. The codes and the engineering practice suggest that the considered horizontal forces applied throughout the height of the building should be defined at least according to two different distributions, per direction of application and per verso. Seen the scope of the performed analyses, for simplicity and for matters of computational time, in the present work just one distribution was applied, chosen among the second group of distributions indicated by the Italian code (NTC 2018). This consists of a constant distribution of accelerations through the height, commonly identified as a pushover analysis mass-proportional. Additionally, given the geometry of the church, which is symmetric along its longitudinal axis (x) in the model, only three different directions were considered (Figure 6.1):

(i) XX+ direction, application of a horizontal acceleration equivalent to the gravity constant (g) in the x-axis positive direction;

(ii) XX− direction, application of a horizontal acceleration equivalent to the gravity constant (g) in the x-axis negative direction;

(iii) YY+ direction, application of a horizontal acceleration equivalent to the gravity constant (g) in the y-axis positive direction.

The response of the model is, then, evaluated in terms of maximum displacement of a control point located at the top of the building. The Italian code (NTC 2018) suggests that the position of the control point is to be chosen as the one corresponding to the center of masses of the studied building. Nevertheless, in the present case different control points were chosen and plotted since, as already discussed, a complex building like the present church is characterized by a response not consistent in all of its parts, due to different stiffness of the various structural elements composing them and, most importantly, the possibility of local failure modes. Figure 6.1 illustrates the location of the control points, chosen specifically to describe the response of the following parts of the church:

(a) front façade;

(b) back façade;

(c) north façade of the transept;

(d) south façade of the transept;

(e) average response of the north lateral wall – average of points (c), (1) and (3);

(f) average response of the south lateral walls – average of points (d), (2) and (4);

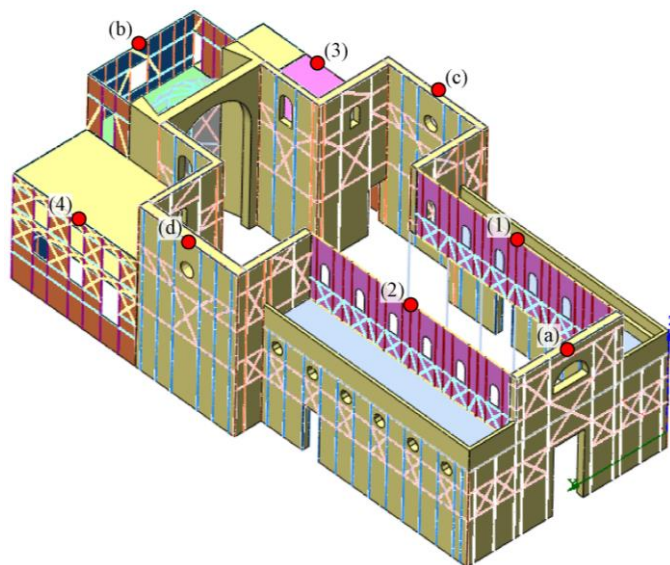(g) average response of the central nave longitudinal walls, - average of points (1) and (2).

Figure 6.1 Analysis directions and location of the control points (example for the reinforced model)

The pushover analyses were performed in the DIANA environment (DIANA FEA BV 2019), after the application of the self-weight of the structure. A load protocol was defined for each analysis, which implied consecutive load steps representing the percentages of the total load applied to the numerical model that, since the load is applied as an equivalent acceleration, is expressed in fractions of the total weight of the structure. The load step progression is equal, then, to the ratio (α) between the total weight and the horizontal base shear in the considered direction. Different load step sizes were used during the analyses execution to reach the convergence of the equilibrium equation system, which was defined through the definition of a convergence criterion based on the relative energy tolerance of 10^{-3}. The analyses were performed mainly with the regular Newton integration method, based on the definition of a stiffness matrix of the DOF system which is updated at each iteration. Even if requiring more computational effort with respect to other integration methods, this method was adopted since the updating of the stiffness matrix at each iteration assures a lower number of steps. In any case, it was observed that the complexity of the numerical model, especially in the strengthened condition that involves different material models and, more relevantly, different element types, required the setting of a relevant number of iterations – up to 200 – to reach the mentioned tolerance criterion. Finally, also the secant method (also known as quasi-Newton) was adopted.

6.1 Un-reinforced model – Longitudinal direction (XX+, XX-)

6.1.1 Positive direction (XX+)

The results of the pushover analysis performed on the unreinforced model in the longitudinal positive direction (east to west) are presented through the capacity curves of Figure 6.2. As observed, the non-linear response of the model is governed by the back-façade wall (orange curve) which suffers a first decrement of stiffness for a load factor equal to 0.18 and subsequently collapses for the rotation of the last level section. In this section, ultimate displacements of the order of 4.0 cm are observed for an ultimate load of 0.35g, while in the other selected control points the displacements are measured one order of magnitude lower. It was not possible for this case to define a post peak behavior of the structure since the observed damage, expressed in terms of principal strains, do not allow the equilibrium of the solution after the development of the collapse mechanism of the façade wall.

The observed damage is expressed in terms of principal strains, which are presented in Figure 6.3 in correspondence of two load steps: at the appearance of the first relevant damage (Figure 6.3a) represented by the diagonal crack starting from the upper-corner of the north wall third story opening, and at the failure of the system (Figure 6.3b), where the complete out-of-plane rotation of the last level of the back wall is observed. (Figure 6.4).
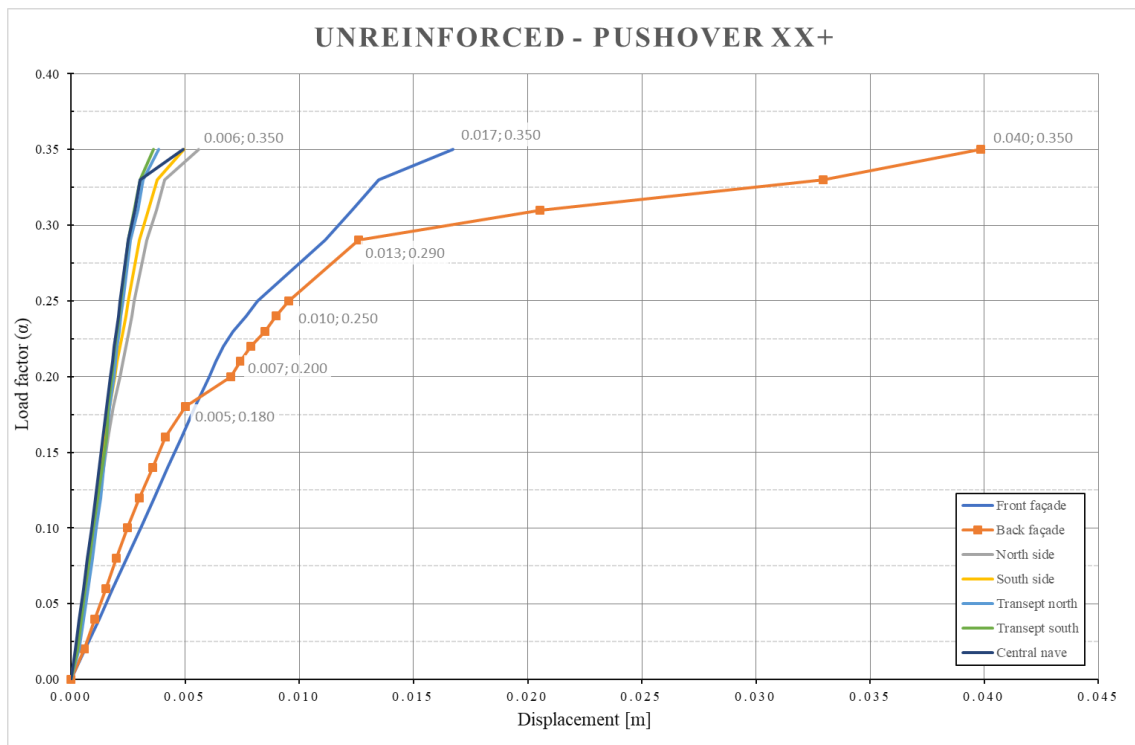

Figure 6.2 Pushover curves for the unreinforced model in the longitudinal direction (XX+)
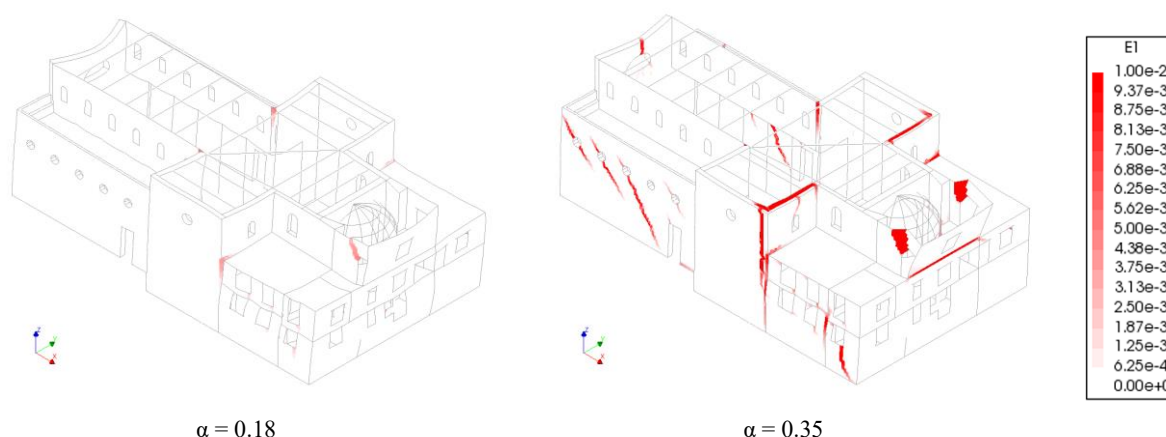
ADVANCED MASTERS IN STRUCTURAL ANALYSIS OF MONUMENTS AND HISTORICAL CONSTRUCTIONS

α = 0.18   α = 0.35

Figure 6.3 Principal strain distribution in the masonry walls at the development of the first damage (α = 0.18) and at the collapse (α = 0.35)
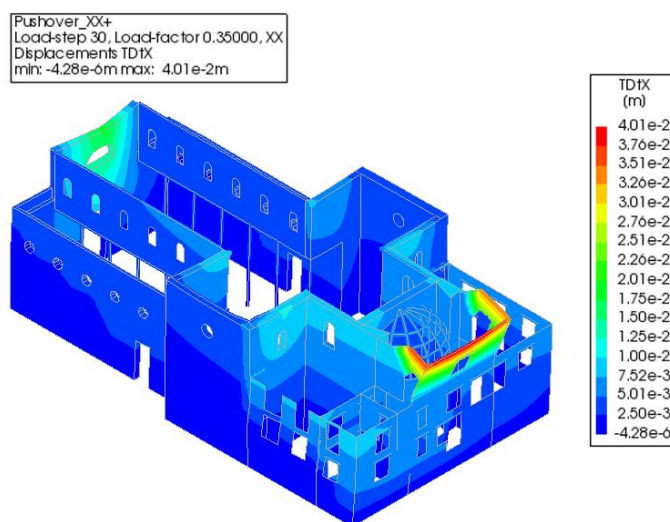

Figure 6.4 Total displacement in the *x*-direction plot of the unreinforced model (XX+) at the last load step (α = 0.35)

6.1.2 Negative direction (XX-)

The pushover analysis, performed along the reversed direction west to east oriented, evidenced a similar response with respect to the one previously described. In fact, also in this case, as shown in Figure 6.5, after an initial curve branch with constant stiffness, observed for all the control points, the main façade of the church governs the failure of the analysis and the expected end of the analysis. The load factor for such a failure is lower than the one previously observed, leading the model to fail for an equivalent acceleration of 0.22g (decrement of 36% with respect to the XX+ direction). The relative associated displacement in the main façade is calculated as 4.4 cm, while the displacements in the other sections of the church remains below 0.1 cm.

It can be observed that the presented curve of the front façade is characterized by a small number of equilibrium points. For the sake of clarity, it must be pointed out that the loading protocol was set to

ADVANCED MASTERS IN STRUCTURAL ANALYSIS OF MONUMENTS AND HISTORICAL CONSTRUCTIONS

relatively small step sizes (0.01) as well as bigger step sizes (0.1), but, seen the fragile connotation of the failure mechanism observed, the last equilibrium points are characterized by the defined small load increments associated to very large deformations.

Figure 6.6 presents the strain distributions for the two limit conditions highlighted by the curve: the start of the damage development in the connections of the façade with the orthogonal walls at the first story (Figure 6.6a), corresponding to a displacement of 0.6 cm in the front façade for a load factor of 0.17 with no relevant tensile principal strains, and the collapse of the system (Figure 6.6b) for the formation of a vertical damage in correspondence of the openings of the wall, combined with the failure of the orthogonal connections, i.e. for a combination of the out-of-plane rotation of the wall central portion and of its horizontal bending failure.(Figure 6.7).
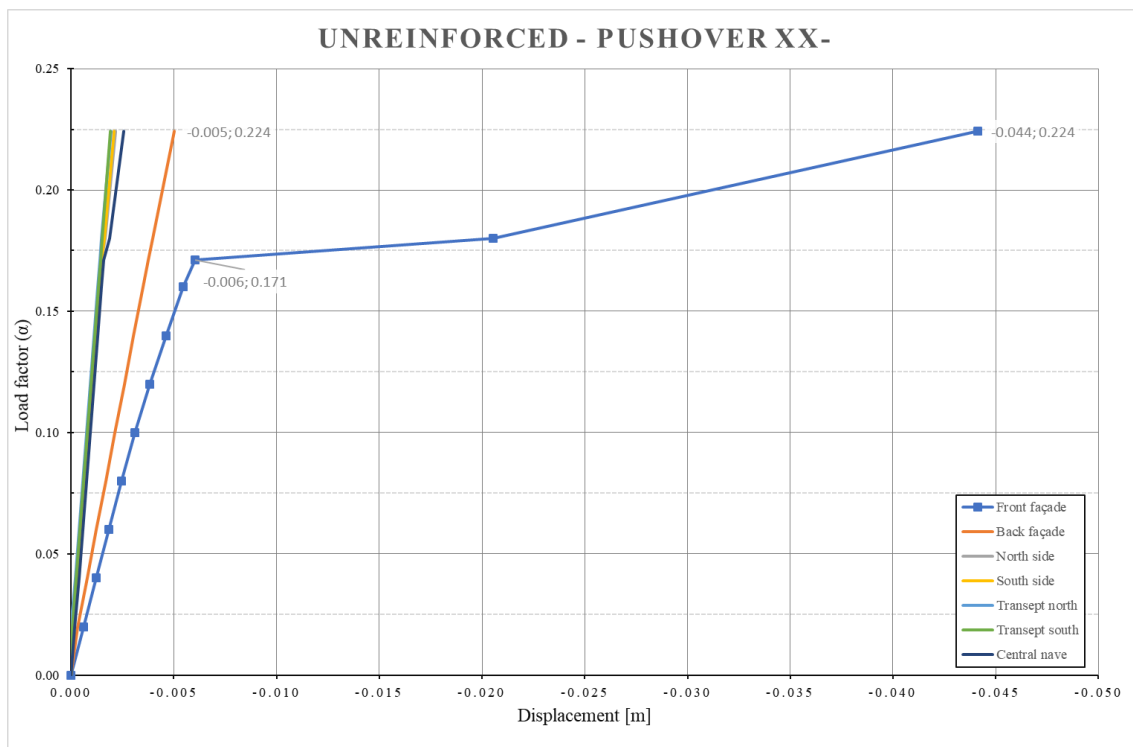
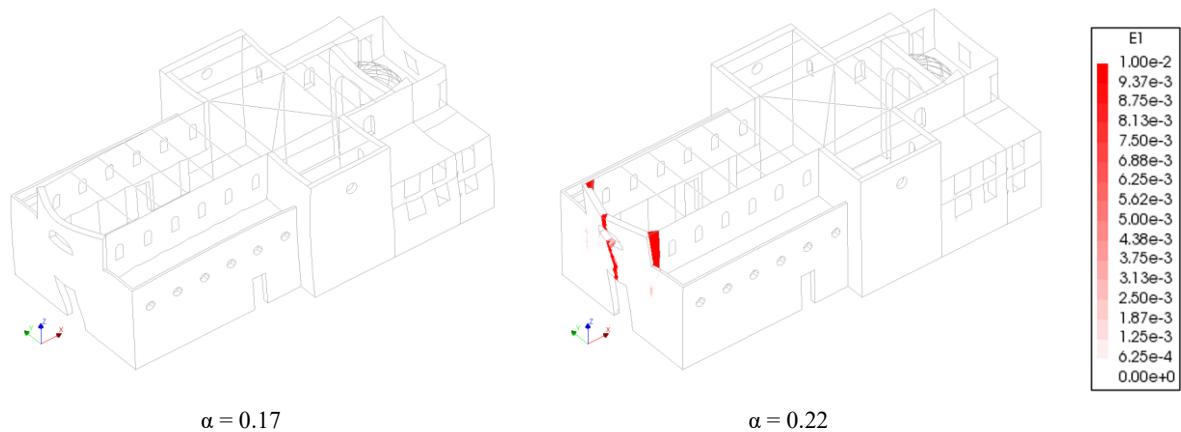**Figure 6.5 Pushover curves for the unreinforced model in the longitudinal direction (XX-)**

α = 0.17   α = 0.22

Figure 6.6 Principal strain distribution in the masonry walls at the development of the first damage (α = 0.17) and at the collapse (α = 0.22)
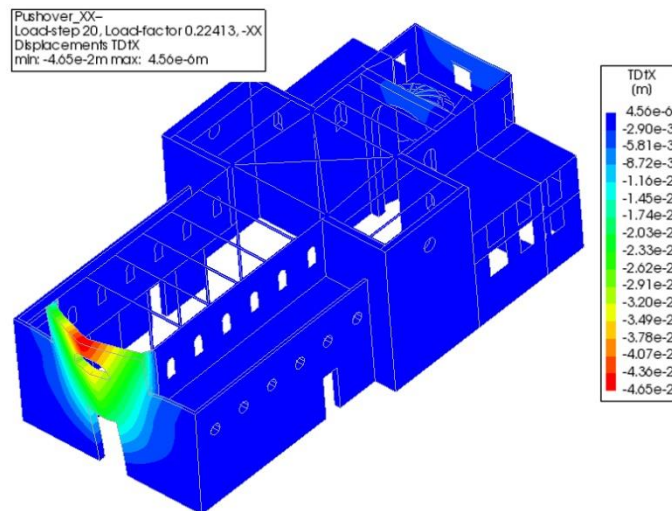

Figure 6.7 Total displacement in the *x*-direction plot of the unreinforced model (XX-) at the last load step (α = 0.22)

6.2 Un-reinforced model – Transversal direction (YY+)

The analysis carried out in the orthogonal direction evidenced the worst performance in terms of force-displacement response. In fact, during the defining of the loading protocol for the analysis, convergence issues were encountered when reaching the load factor α = 0.14. The relative applied horizontal load is very small when compared to the results obtained in the *x*-direction, representing the 57% decrement with respect to the XX+ analysis and the 38% with respect to XX-. Additionally, from Figure 6.8 it can be observed that the curves representing the horizontal response of the other control points defined a response still in the linear-elastic field with displacements of the order of 0.5 cm for maximum load factor.
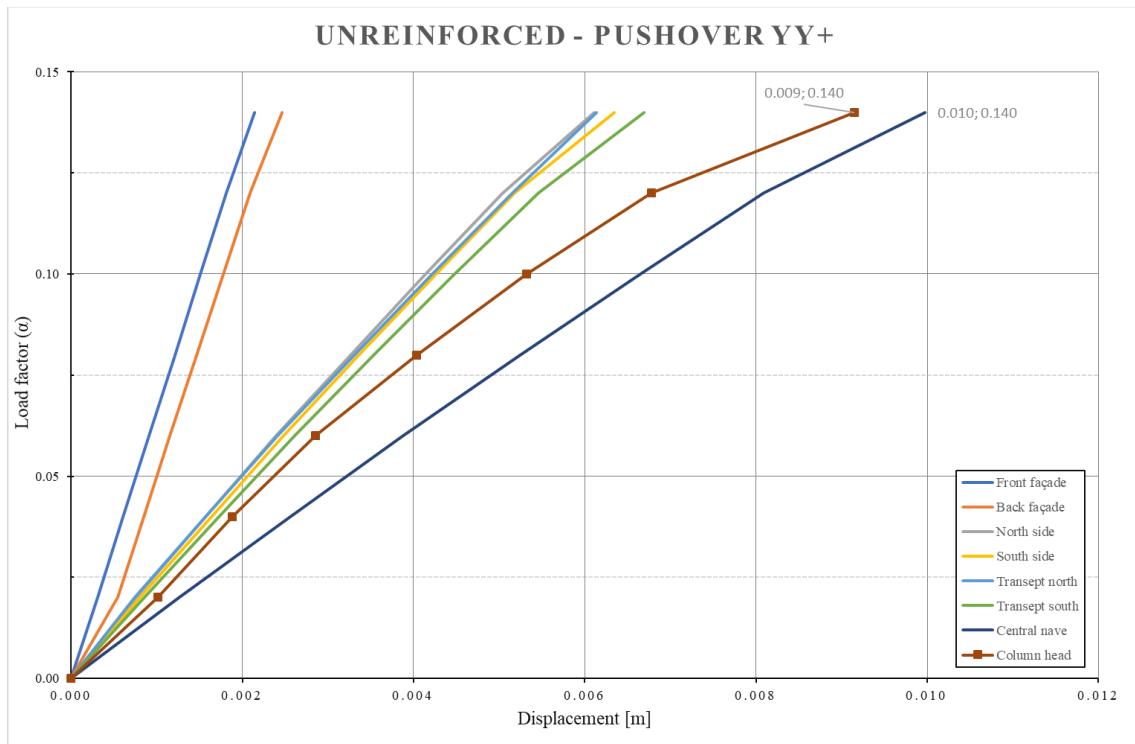
Figure 6.8 Pushover curves for the unreinforced model in the transversal direction (YY-)

It is just with the adopted damage indicator observation (E1) that is possible to understand the source of the numerical instability of the solution. As seen in Figure 6.9, where the principal strains are presented, the north-eastern wall of the transept experiences the development of a vertical crack dividing the wall into two sections in correspondence of the intersection of the transept wall with the northern nave lateral wall and connected terrace. Geometrically and from the mesh point of view, it is a singular point which sees the convergence of various elements of various types, e. g. solid elements for the walls, orthotropic shells for the floors, isotropic shells for other walls and beams for the columns of the gallery. Figure 6.10 shows the incremental displacement of the model at the last converged step witnessing the mobilization of this isolated portion of the transept.

A reading of the displacement of the top point of the corresponding last column of the gallery is also provided in Figure 6.8, where the brown curve evidences the displacements detected in the node. Moreover, it is observed that the load factor-displacement diagram of the node evidences an almost linear response until the presumed rupture.

An attempt to refine the model simplifications and try to correct the numerical response was carried out by inserting embedded beam elements at the lower corner of the solid wall superimposed to the gallery and prolongated through the length of the transept wall. The correction aimed at limiting the crack opening in the observed location, but also in this case the analysis evidenced similar behavior.

In the scope of a better understanding of the transversal response of the building, aiming at comparing it with the one representing the reinforced scenario, a refinement of the present analysis should be carried out in order to detect and eliminate possible sources of instability of the solution, to overcome the faced convergence problems or, eventually, validate the present observed behavior.
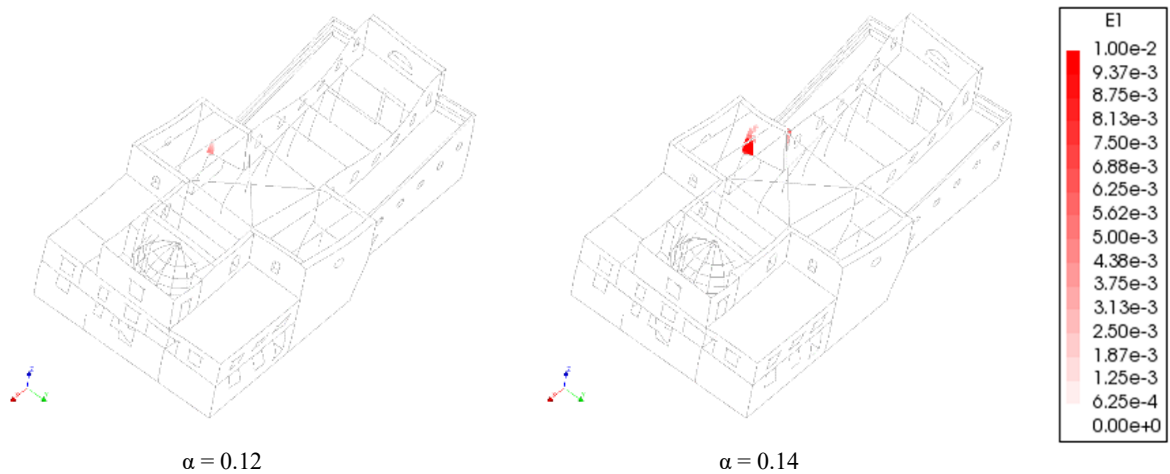

$\alpha = 0.12$ $\alpha = 0.14$

Figure 6.9 E1 plot evidencing the development of a vertical crack dividing the north-eastern wall of the transept
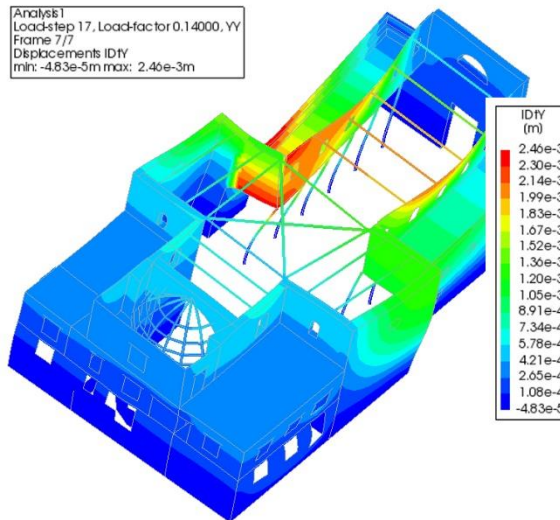
Figure 6.10 Incremental displacement in the *x*-direction plot of the unreinforced model (YY+) at the last load step (α = 0.14)

6.3 Reinforced model – Longitudinal direction (XX+, XX-)

6.3.1 Positive direction (XX+)

The pushover analysis performed in the reinforced version of the model developed more evident responses in the non-linear field. As observed from Figure 6.11, which represents the response of the structure when subjected to horizontal forces oriented along its longitudinal direction in the east to west direction, the maximum displacements are reached by the front and back façades of the structure. In fact, as can also be observed in Figure 6.12, the presence of the iron and timber frames in these walls allows the horizontal bending behavior of the two façades without damage, since the tensile stresses can be partially absorbed by the horizontal frames.

The pushover curve presents a first almost linear behavior ending for a load factor equal to 0.45, corresponding to about 0.8 cm of displacements at the top of the transversal façades; after this point the structure suffers a first decrement of stiffness, which is also evidenced by the appearance of a first damage in the north wall of the apse at the first floor (Figure 6.13a, damage indicator E1). The structure enters then in a non-linear phase that ends for an α = 1.17, which defines a small plateau before the post peak of the structure. Figure 6.13 shows the damage indicator distribution for the last found point of the solution.
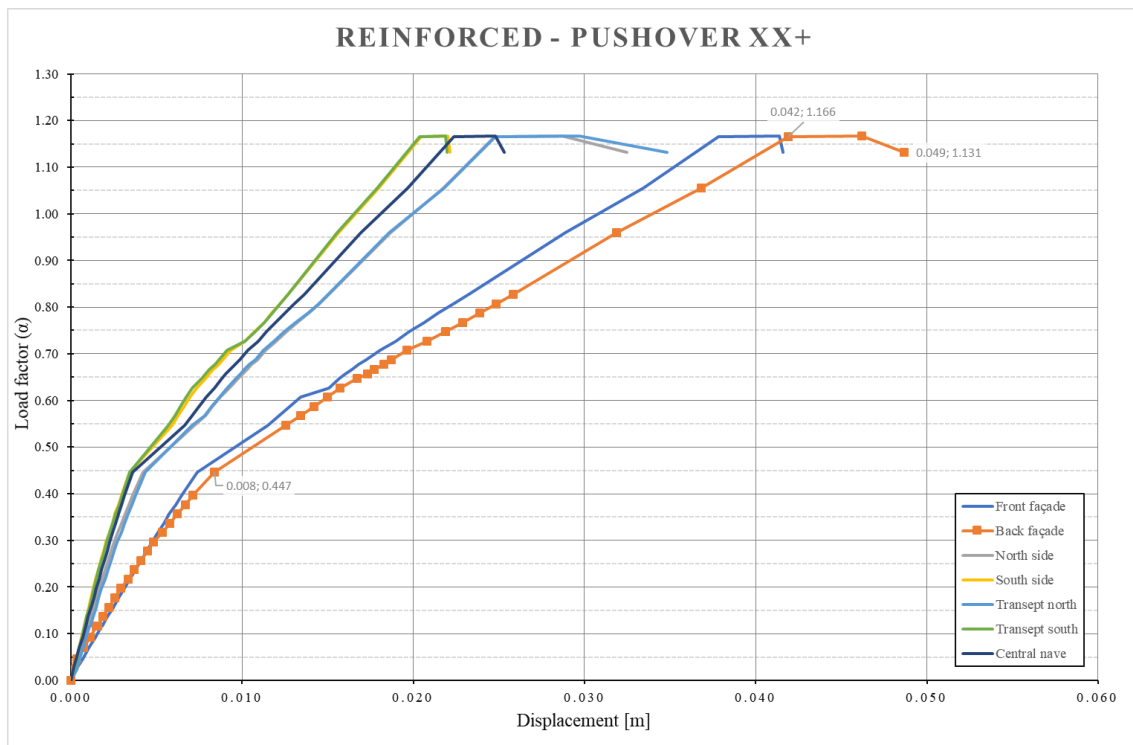

Figure 6.11 Pushover curves for the reinforced model in the longitudinal direction (XX+)

Analysis1
Load-step 63, Load-factor 1.1315, XX
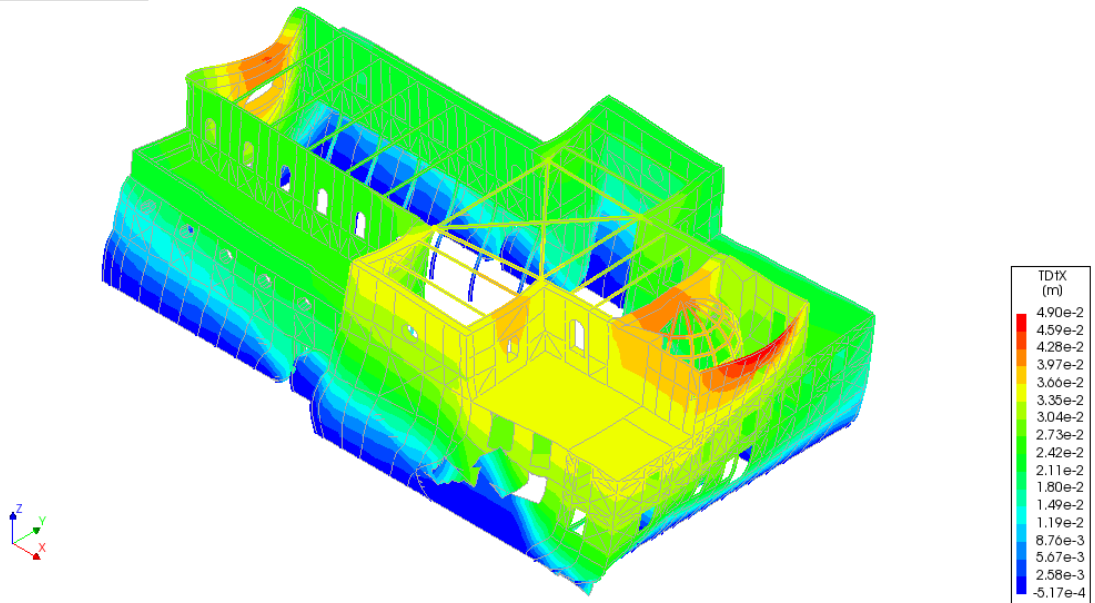Displacements TDtX
min: -5.17e-4m max: 4.90e-2m

TDtX
(m)
4.90e-2
4.59e-2
4.28e-2
3.97e-2
3.66e-2
3.35e-2
3.04e-2
2.73e-2
2.42e-2
2.11e-2
1.80e-2
1.49e-2
1.19e-2
8.76e-3
5.67e-3
2.58e-3
-5.17e-4

Figure 6.12 Total horizontal displacement (positive *x*-direction) at the last load step (α = 1.13)

E1
1.00e-2
9.37e-3
8.75e-3
8.13e-3
7.50e-3
6.88e-3
6.25e-3
5.62e-3
5.00e-3
4.38e-3
3.75e-3
3.13e-3
2.50e-3
1.87e-3
1.25e-3
6.25e-4
0.00e+0

α = 0.45 (bottom view)   α = 1.13
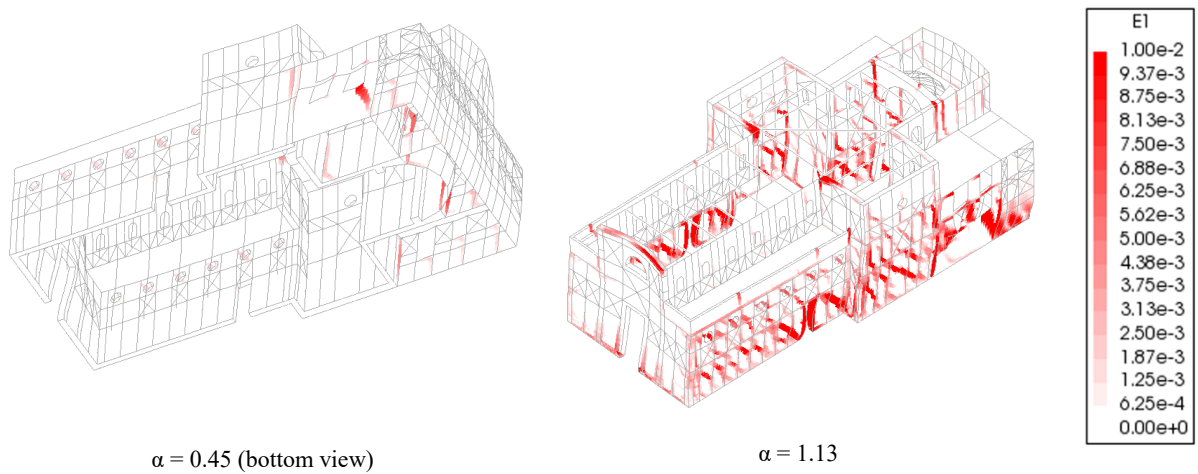
Figure 6.13 E1 plots showing the developing of damage indicators distributions

6.3.2 Negative direction (XX-)

When coming to the pushover in the corresponding negative direction, a similar behavior is expected and also observed. The elastic phase of the structure allows the development of load factors up to 0.48, which is a considerably high value when evaluating a masonry structure.

Thanks to the presence of the *Baraccato* system the structure reaches a maximum value of 1.49 load factor, after which a slightly descending branch is observed. The maximum displacement measured for

the front façade in this case allow the movement of the structure of about 7.1 cm, corresponding to 5.9 ‰ of drift with respect to the total height of the structure.

The damage observed (E1 indicator) shows that, in correspondence of the point where the initial stiffness of the structure is changed to a more non-linear behavior, diagonal damages appear on the north façade of the transept (Figure 6.15a). It must be pointed out that, as seen for the YY+ direction in the unreinforced condition, the response of the structure is not symmetrical. Although in this case (XX-) the source of this a-symmetric response is detected in the geometrical definition and in the modelling strategies adopted. In fact, in the north wall of the back part, already characterized by quite big openings, a section of the wall was modelled in its unreinforced condition (Section 3.2.2.3). This section presents damaged condition also for very small step loads. The progression of the crack below the lower corner of the last opening close to the transept wall, its combination with the appearing of the first damages also in the transept façade and the smaller thickness of the transept façade wall in this orientation with respect to the facing one, define the observed a-symmetrical behavior and the decrement of stiffness detected by the curve. The other plots (Figure 6.15b to d) show the widespread tensile strains distributed throughout the longitudinal masonry walls defining diagonal shear cracks.
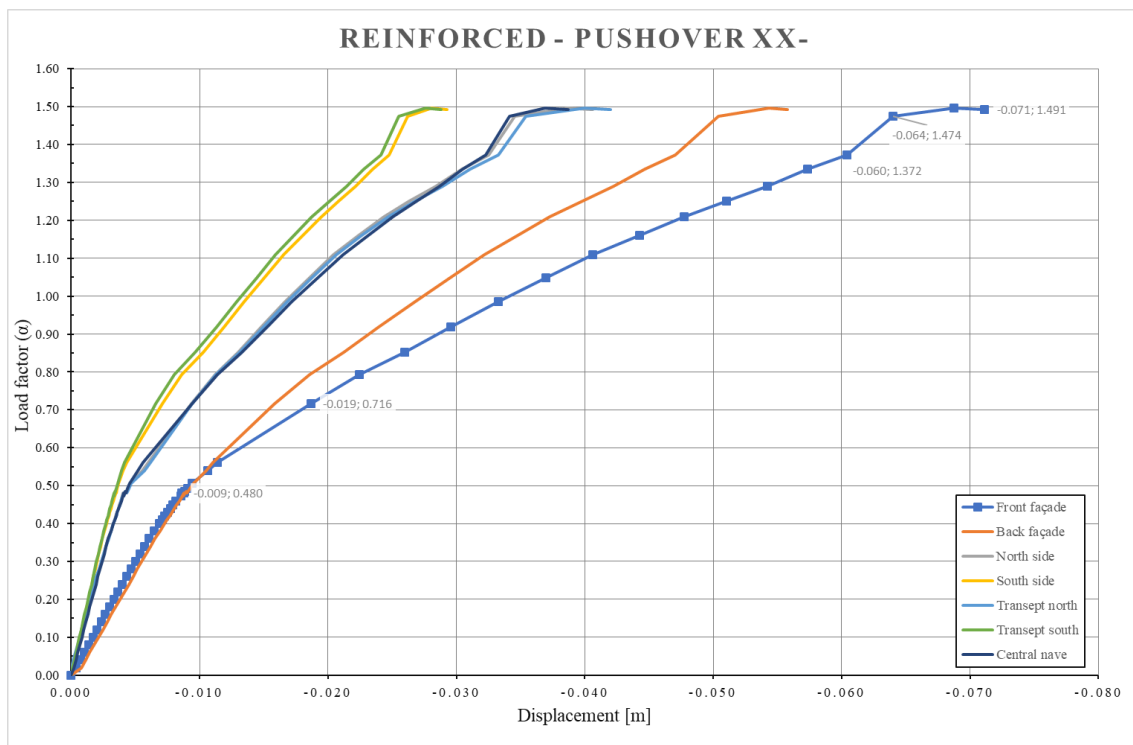

Figure 6.14 Pushover curves for the reinforced model in the longitudinal direction (XX-)

α = 0.48	α = 1.37

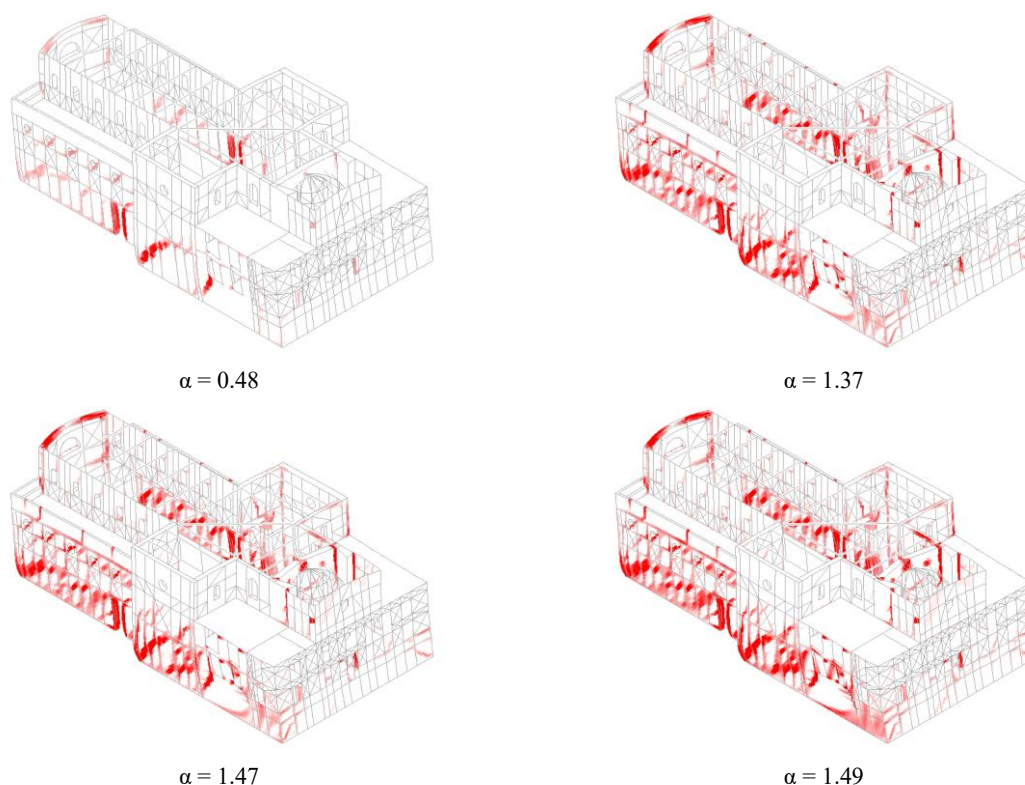|	
α = 1.47	α = 1.49

Figure 6.15 E1 distributions showing the expected damage development throug the reinforced model (XX+)

Moreover, it can be observed that, for the two pushover curves just presented (XX+ and XX-) the last calculated points may not necessarily be the ending points of the corresponding analyses since no clear failure mechanisms were observed in the presented plots, in spite of a quite widespread damage. For matters of time the results are here presented to the extent that the time at a disposal allowed, but the analyses should be carried on until reaching a clear failure mechanism, leading the structure to brittle collapse, or to a clearly identified post-peak behavior evidencing eventually a softening branch.

6.4 Reinforced model – Transversal direction (YY+)

The capacity curves of the measured structural elements managed to describe the complete non-linear behavior of the model in the reinforced condition while subjected to constantly distributed horizontal loads in the transversal direction of the church (north to south). In fact, as can be observed from Figure 6.18, the response presents a first slightly linear behavior, ending at around 0.22 of the load factor with a maximum displacement measured for the central nave walls of about 1.2 cm. After this point the pushover curve starts the development of the non-linear behavior of masonry by evidencing a constant decrement of the stiffness up to a limit point corresponding to the peak of the structure ($\alpha = 1.14$, $d_{max} = 13.8$ cm). In the post-peak phase of the analysis a maximum displacement is observed for a decreased load factor corresponding to 18.8 cm.

Bearing in mind that in this discussion the damage observed is always presented in terms of limited tensile principal strains up to a representative value of the 1.0%, few last comments can be carried out.

Firstly, the observed exit from the linear elastic behavior in the capacity curve is also witnessed by the appearance of damage indicators at the immediately subsequent load step (Figure 6.18a). These are representative of diagonal cracks appearing on the slenderest sections of the eastern wall of the transept at both sides of the church. The damage evolves throughout the transversal walls spreading also in the western wall of the transept until reaching a load factor that enables the development of failure in tension of some elements of the front façade wall ($\alpha= 0.39$), aligned along diagonal directions corresponding to in-plane shear cracks of the façade (Figure 6.18b). As already mentioned, the peak load of the structure is reached for $\alpha= 1.14$ (Figure 6.18c) and after the peak one more point is observed defining the softening of the model.

As just mentioned, the maximum displacement appears in the central nave. This result was expected since an already relevant deformability of the longitudinal walls of the nave was observed in the eigenvalues of the model. The application of the load in the weak direction of the walls allows the development of high deformations which consist of a 0.9% drift with respect to the total height of the church. Moreover, a relevant post peak deformation was also observed in the main façade of the church (Figure 6.18, medium blue curve). The great deformation, in this case is justified by the presence of largely widespread cracked elements diagonally aligned, representing in-plane shear cracks of the wall panel (Figure 6.20 and Figure 6.15).
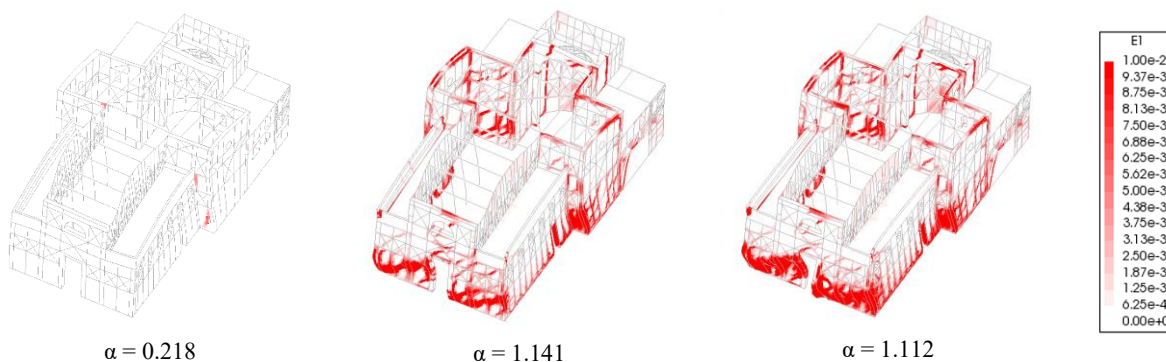

$\alpha = 0.218$ $\alpha = 1.141$ $\alpha = 1.112$

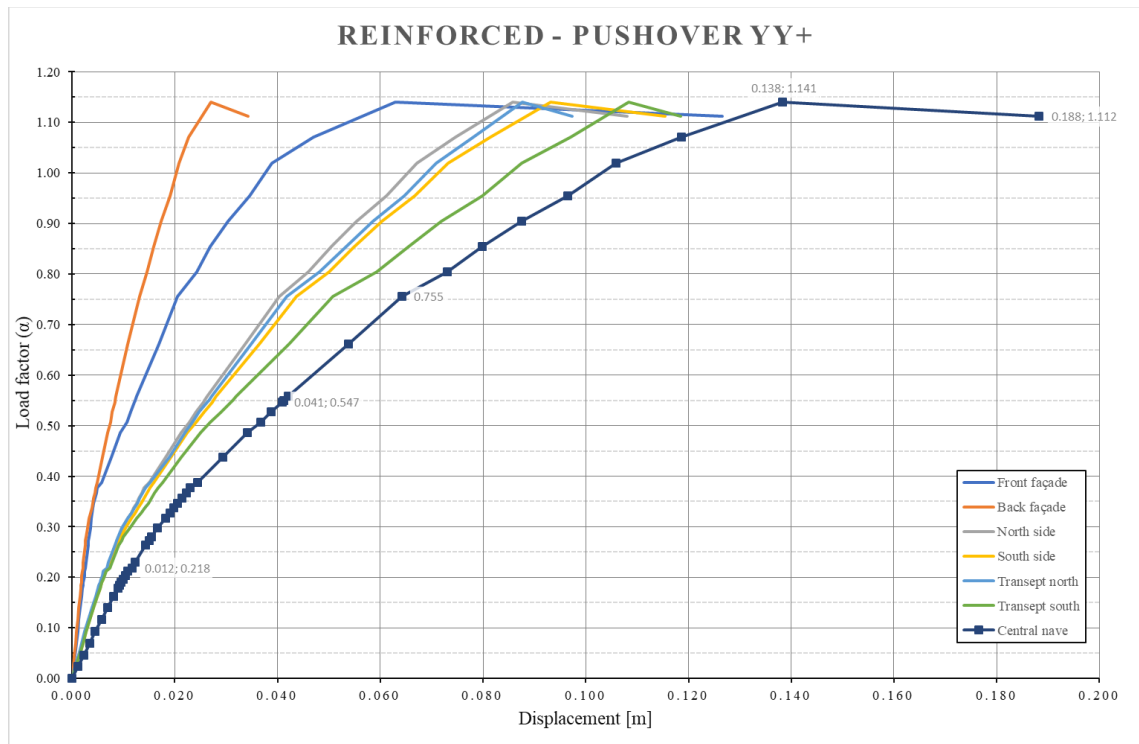**Figure 6.16 E1 plot of the highlighted steps of the pushover curve (R_YY+)**

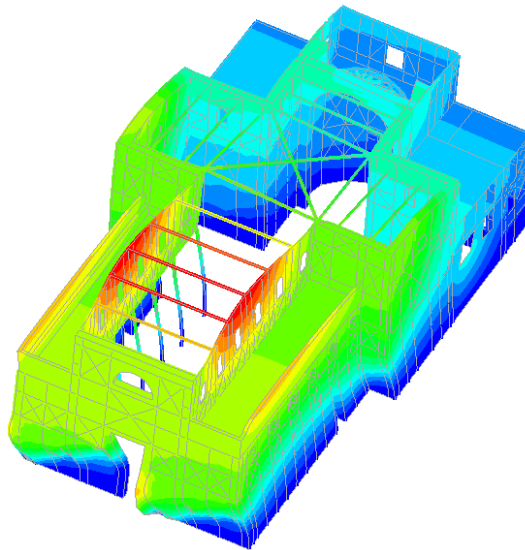**Figure 6.17 Pushover curves for the reinforced model in the transversal direction (YY+)**

Figure 6.18 YY displacements of the structure for α = 1.112

6.5 Comments and comparisons

The reading of the just described results of the performed non-linear analyses becomes more interesting when considered all together with the scope of a comparison. The presented Table 6.1 summarizes the ending criteria for the pushover curves plotted in the previous sections and performed on the two versions of the model in three different directions. The table is constructed with reference

to the structural element curve that, for each analysis, presented the worst performance. The selected curves can be easily visualized since they are represented with the dotted plot from Figure 6.2 to Figure 6.17.

Table 6.1 Summary of the observed failure in the models analyzed

DIRECTION	MODEL	MAX. LOAD FACTOR α	MAX. DISPL.[14] [cm]	LOCATION	FAILURE MECHANISM
XX+ (east to west)	Unreinforced	0.350	4.0	Back façade	Out-of-plane rotation of the façade
	Reinforced	1.166	4.9	Back façade	-
XX- (west to east)	Unreinforced	0.224	4.4	Front façade	Vertical bending failure of the façade
	Reinforced	1.491	7.1	Front façade	-
YY+ (north to south)	Unreinforced	0.140	10	North transept wall	Tensile vertical cracking of the wall
	Reinforced	1.112	18.8	Central nave	-

Thanks to the just presented table and the comparison graphs shown in Figure 6.19 and Figure 6.20 few observations are possible.

The analyses performed on XX direction, positive and negative, it is possible to observe that, firstly the two directions are characterized by similar stiffness in the reinforced condition (solid lines) while they have different slopes of the elastic branches of the curves when considering the unreinforced scenario (dashed lines). Even in the non-linear sections of the reinforced curves they present similar developments in terms of slopes of the curves. Thus, it can be observed that the presence of the iron frames contributes to homogenize the stiffness characteristics in the whole structure. This observation is also supported by the fact that the iron frames enable a box-behavior of the structure witnessed by the failure mechanisms observed in the previous sections.

Obviously, the reinforced condition presents a longer development of the curves, reaching the ending points of the curves for displacements which present on average a 28% of difference between the reinforced and the unreinforced conditions, even if in the XX+ cases the ultimate displacements differ just of 0.9 cm.

In terms of behavior the reinforced curves present still inclined developments for very high load factors, order of 0.9-1.1, while both the unreinforced curves already develop a plateau for load factors that are 5-7 less the ones registered for the reinforced condition.

---

[14] Considered as the maximum displacement recorded for the selected control points.

Conversely, by looking at Figure 6.20 the two compared curves, corresponding to the response of the central portion of the church (north-western wall of the transept – unreinforced condition, central nave – reinforced condition), present overlapping development for the elastic branch. Although, in the figure the bigger graph plots the curves with respect to two vertical axes, since the reinforced curve presents such a better performance that comparing both on the same graph tends to hide it. An attempt of visualizing the curves together is given in the figure in the right-handed lower corner where it is possible to observe, also in this case, overlapping curves. It must be remembered that the unreinforced curve was found to have great numerical instability and its implementation should be revised in the scope of understanding and overcoming its numerical instability or confirming the insurgence of the observed failure mechanism for such low load values.
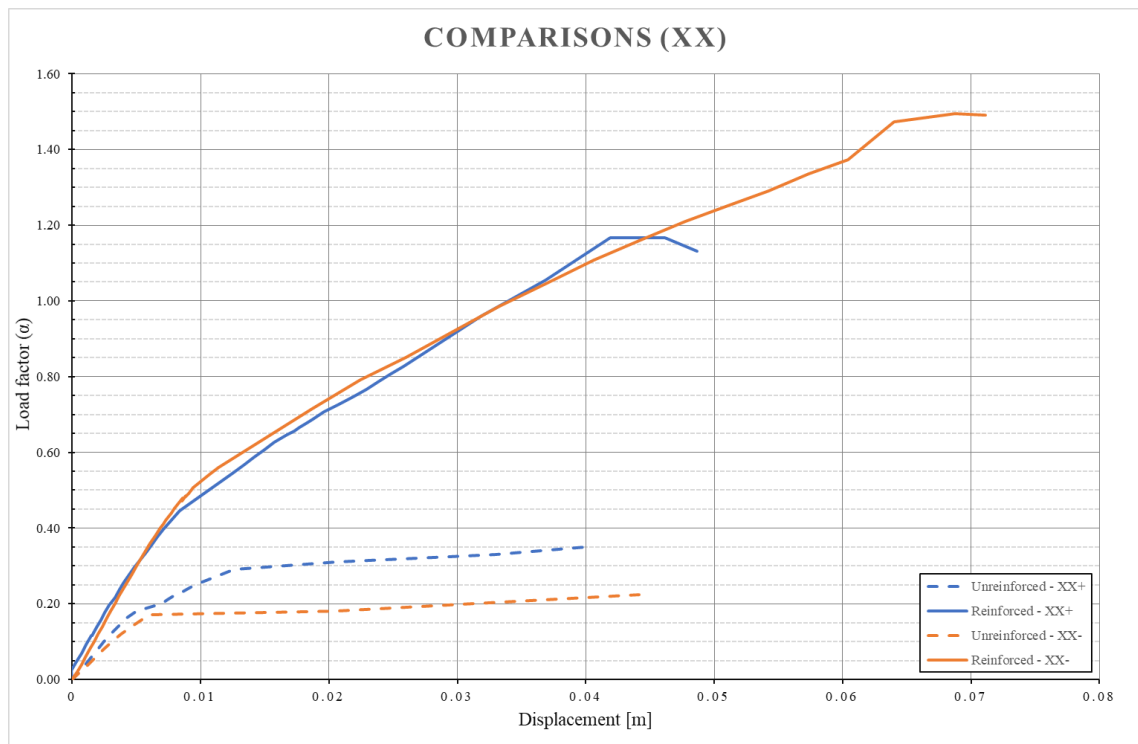
Figure 6.19 Comparison of the capacity curves in the XX direction

ADVANCED MASTERS IN STRUCTURAL ANALYSIS OF MONUMENTS AND HISTORICAL CONSTRUCTIONS
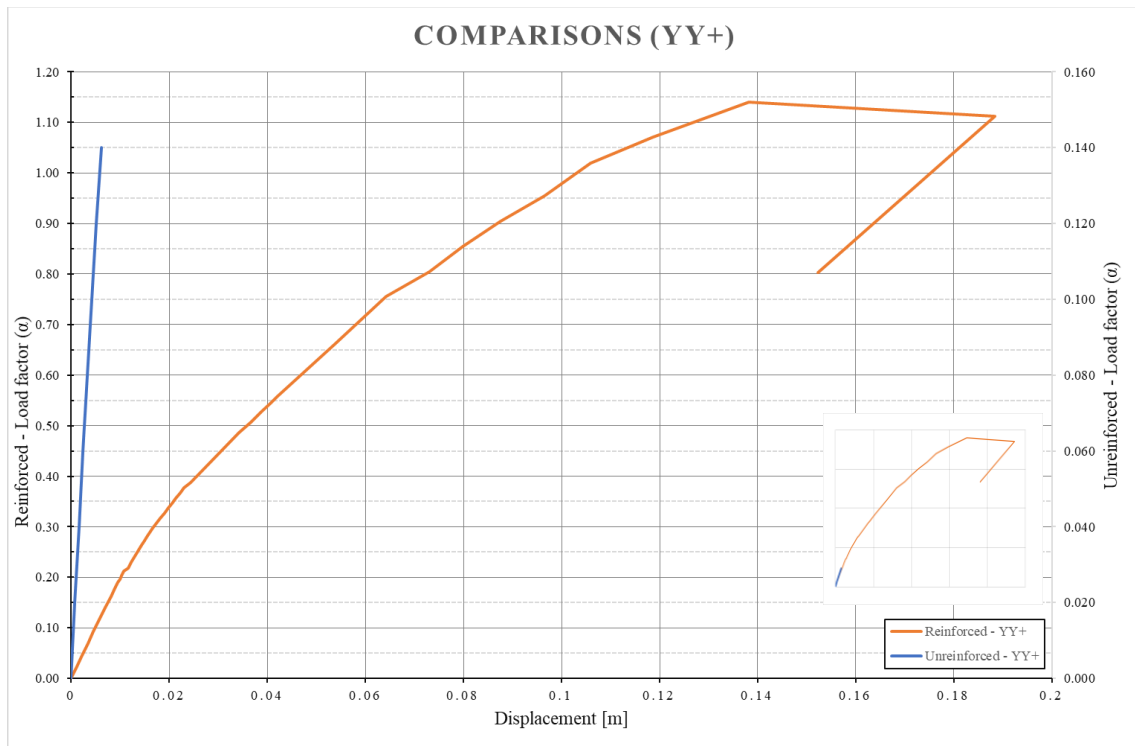
Figure 6.20 Capacity curves comparison in the YY+ direction (in the big plot different *y*-axis scales are used to visualize the curves

7 CONCLUSIONS

In conclusion the aim of the present work was to perform the seismic vulnerability assessment of the church of Santa Maria Maddalena in Ischia Island, Italy, through the implementation of a numerical model, representative of the complexity of the structure and capable of assuring reliable results when performing advanced structural analyses. The accomplishment of this ambitious tasks was addressed through various phases.

Firstly, a general understanding of the territorial and historical context interacting with the building was necessary, along with the geometrical and architectonical understanding of the church. Since, a site visit was not possible during the development of the present work, an effort was put in this latter task and in the technological definition and understanding of the structural details. In this sense, the data available were organized and studied in order to maximize their outcomes and gather the required information to construct a numerical model of the building as close to the real structural concept as possible.

Secondly, the data collected during the previously performed ambient vibration tests were post-processed with the scope of determining the natural modes of vibration of the real structure, and, in particular, of identifying and properly visualizing its modal shapes. The results of this phase were used later, after the implementation of the numerical model as a meter of comparison for the dynamic identification and calibration of the model.

The proper modelling phase focused on the already mentioned objectives. In this sense, firstly, a geometrical model of the entire church was prepared, taking into consideration the relevant details to be expressed in the numerical model and, at the same time, making the required geometrical simplification of the un-relevant elements of the geometry. In a finite element software environment, the geometry was then prepared for the meshing procedures. Lastly an appropriate size mesh was created. The different modelling issues and uncertainties, i.e. the modelling strategy to adopt for the simulation of the response of the *iron-Baraccato* and *timber-Baraccato* walls, modelling of the roofing system, etc., were addressed in this phase through the definition of best fitting solutions, compromising between the structural detail and the simplifications required from the reached level of knowledge and/or the need to limit the size of the already complex model. Since no direct *in-situ* tests on the materials constituting the church were available, the definition of the material properties was carried out according to codes and literature values, relying on the calibration phase to adjust their stiffness contribution to the dynamic behavior through the updating of their moduli of elasticity.

Moreover, some assumptions were carried out in consideration of the soil-structure interaction, in the lack of more precise information about its characteristics.

In the modal identification and calibration phases, since the resulting level of knowledge about the church structural details and the initially adopted modelling strategies did not allow a satisfying matching of the numerical and experimental modal shapes, the study was also focused on the sensitivity of the dynamic behavior of the structure to some of the mentioned strategies and uncertainties. Additionally, the complete description of the complex dynamic response of the church to natural vibrations was not always possible, since the adopted test setup layouts were not able to extensively catch them, due to the lack of some crucial measurement points. However, the calibration phase allowed to succeed in the definition of the optimum modelling approaches to match the measured structural behavior, and in the masonry Young's modulus updating to tune the measured real natural frequencies of the building.

Lastly a preliminary assessment of the structural safety of the church was performed through the execution of non-linear static analyses applied to two different versions of the model defined in the previous steps. The model versions were properly defined so that the corresponding results would represent an upper bound and a lower bound limit of the effective behavior of the structure.

The initial goal of achieving the complete implementation of a full numerical model, which includes all the structural aspects observed in the church, was satisfied. In fact, some preliminary numerical analyses were carried out and their results described a possible range of responses of the structure when subjected to horizontal loads. Moreover, the delineated numerical model is properly defined to implement further changes to be carried out in the light of the required updates and removal of the uncertainties, in the scope of performing more advanced numerical analyses and obtaining more reliable results, once an appropriate level of knowledge is reached for the still open issues highlighted in this work.

7.1 Open issues

Namely, the issues that the thesis work encountered and evidenced during its development can be grouped into three main categories dealing with: the geometry of the church, the experimental campaigns that are required in order to increase the level of knowledge, and the adoption of the appropriate modelling strategies. Moreover, the previous Chapter **Errore. L'origine riferimento non è stata trovata.** attains the discussion of the performed analyses results and can be considered a work-in-progress section.

Regarding the remaining issues about the church geometry and technological description, it is remarked the need to perform deeper inspections in order to confirm, refine or describe from scratch some of the element technologies and geometries still unknown. This is the case, for example, of the appropriate description of the floor slabs layers and main dimensions. In particular, the layout of the timber frames constituting the constructive system of the walls of the canonical house must be properly surveyed, in order to reach at least an acceptable level of knowledge of the geometry of the back portion of the church. Moreover, some aspects of the church should be investigated for the understanding of their effective structural concept and performance. In the specific, the geometrical and structural details of the second-story wall of the central nave are still unknown in the definition of the structural performance related to its support above the gallery and should be better investigated to refine also the modelling of this particular node.

As for the *in-situ* tests that should be performed on the church, the execution of some non-destructive and minor destructive tests of the church structural materials is recommended, along with the execution of some more ambient vibration tests with setup layouts capable of catching the still un-measured dynamic responses of the building, as suggested in Chapter 5. Lastly, a full description of the characteristics of the soil interacting with the church foundation system and some tests to inspect the effective correspondence of the existing foundations geometry with the historical drawings is desirable.

The modelling strategies that still need to be validated and further inspected mainly regards the modelling of the church roofing system, the modelling and the calibration of the connections between the two constructive systems detected in the church, and the modelling strategies to apply to the *Baraccato* walls. In particular, the last open issue regarding the modelling of the *Baraccato* walls can also be considered an interesting point for broader developments that do not regard the solely structural analysis of the Church of Santa Maria Maddalena.

7.2 Future developments

The appropriate modelling strategy to adopt for the *Baraccato* system is still an open issue in the numerical modelling of the present church, since it influences the outcomes of its eventual safety assessment other than the computational effort invested in the analysis. On the other hand, its definition has a relevance in the scope of the structural analysis of the several *Baraccato* buildings that can be found in Southern Italy and the other mixed timber-masonry, and more rarely iron-masonry, structures widespread all over the world. In particular, it would be interesting to investigate the

adoption of the appropriate modelling strategy in relation to the computational effort, the level of detail of the obtained numerical model, and the desired accuracy of the results.

Additionally, the execution of a complete safety assessment of the church in the light of the seismic hazard of the area in which the church is built is considered the natural development of the present work. In this sense, the thesis can be considered the first preliminary step essential for the formulation of a safety judgment of the church. Once reached satisfactory level of knowledge of the structural details and material characteristics, more advanced analyses would be possible, such as non-linear dynamic analyses with the seismic signals of the instrumental earthquake of the last seismic event, in the scope of a damage identification and comparison between the observed crack patterns and the ones expected in the numerical simulations.

Lastly, the damage observed in the structural elements church in consequence of the 21st August, 2017 earthquake of Casamicciola Terme is low when compared to the effective damage suffered from its decorative elements and *stucco* decorations. In this sense, the previously mentioned analyses can also help in the definition of a damage limit state for the church, e.g. in the scope of interventions aimed at the mitigation of the risk of these damages to occur, seen the architectonical and historical value of the church for the island identity.

REFERENCES

Acocella, V., and Funiciello, R. (1999). "The interaction between regional and local tectonics during resurgent doming: the case of the island of Ischia, Italy." *Journal of Volcanology and Geothermal Research*, 88(1–2), 109–123.

Acocella, V., Funiciello, R., and Lombardi, S. (1997). "Active tectonics and resurgence at Ischia Island (southern Italy)." *Il Quaternario Italian Journal of Quaternary Sciences*, 10(2), 427–432.

Arcamone, P., and Argiento, L. U. (2018). *Indagine Storiografica Chiesa Santa Maria Maddalena, Casamicciola Terme, Ischia (NA)*.

"Archivio di Stato di Napoli, Corpo Reale Genio Civile, fascio 342, incart. 3." (n.d.). .

ARTeMIS Modal v3.5.1.1. (2018). "Ambient Response Testing and Modal Identification Software." Aalborg East.

Briseghella, B., Demartino, C., Fiore, A., Nuti, C., Sulpizio, C., Vanzi, I., Lavorato, D., and Fiorentino, G. (2019). *Preliminary data and field observations of the 21st August 2017 Ischia earthquake. Bulletin of Earthquake Engineering*, Springer Netherlands.

Bussell, M. N. (1997). *Appraisal of existing iron and steel structures*. Steel Construction Institute (Great Britain).

Calderoni, B. (1996). "Valutazione sperimentale delle caratteristiche meccaniche di muratura di tufo per modelli in scala intermedia." *La meccanica delle murature tra teoria e progetto*, Pitagora Editrice Bologna, Messina, 95–104.

Calderoni, B., Cecere, G., Cordasco, E. A., Guerriero, L., Lenza, P., and Manfredi, G. (2006). "Costruzione e comportamento meccanico di macromodelli di murature in tufo postmedievali." *Quale sicurezza per il patrimonio architettonico?*, Mantova, 396–407.

Calderoni, B., Cordasco, E. A., Guerriero, L., and Lenza, P. (2008). "Prove a compressione di murature storiche napoletane." *Atlante delle tecniche costruttive tradizionali*, Napoli, arte Tipografica, Napoli, 289–300.

Calderoni, B., Cordasco, E. A., Guerriero, L., Lenza, P., and Manfredi, G. (2009). "Mechanical Behaviour of Post-Medieval Tuff masonry of the Naples Area." *Journal of the Intenational Masonry Society*, 21(3), 85–96.

Carlino, S. (2012). "The process of resurgence for Ischia Island (southern Italy) since 55 ka : the laccolith model and implications for eruption forecasting."

Carlino, S., Cubellis, E., and Marturano, A. (2010). "The catastrophic 1883 earthquake at the island of Ischia (southern Italy): Macroseismic data and the role of geological conditions." *Natural Hazards*, 52(1), 231–247.

"casamìcciola." (n.d.). *Treccani*.

Casapulla, C., Ceroni, F., Rainieri, C., Argiento, L. U., Arcamone, P., Fabbrocino, G., and Carducci, V. (2019a). "Structural assessment of Santa Maria Maddalena church in Ischia (Italy) by experimental modal analysis under operational conditions." *COMPDYN 2019*, Crete, 24–26.

Casapulla, C., Ceroni, F., Rainieri, C., Fabbrocino, G., Argento, L. U., Celano, T., and Arcamone, P. (2019b). *First report Santa Maria Maddalena*. Napoli.

Cubellis, E., and Marturano, A. (2009). *Il terremoto del 5 aprile 2008 nell'isola d'Ischia: studio macrosismico*. Napoli.

DIANA FEA BV. (2019). "DIANA Finite Element Analysis User's Manual Release 10.3." DIANA FEA BV, Delft.

EC-Standards. (1990). *EN 1990:2002E - Basis of structural design - EC0*. Brussels, 1–87.

EC-Standards. (1998). *En 1998-1 EC8*. 1–229.

EC-Standards. (2003). *EN 338:2003 - Structural timber — Strength classes (updated 2009)*. European Commitee for Standardization, Brussels.

G. Vivenzio. (1788). *Istoria de' tremuoti avvenuti nella Provincia della Calabria ulteriore e nella città di Messina nell'anno 1783, e di quanto nella Calabria ulteriore fu fatto per lo suo risorgimento fino al 1787, preceduta da una Teoria e Istoria generale de' Tremuoti*. Stamperia Regale, Napoli.

Galassi, S., Ruggieri, N., and Calabria, U. (2014). "Stability and Stiffness Contribution of the masonry in the Borbone Anti-seismic System." *9th International Masonry Conference, Guimarães 2014*, 9.

Galassi, S., Ruggieri, N., and Tempesta, G. (2015). "Historical Earthquake-Resistant Timber Frames in the Mediterranean Area." *Historical Earthquake-Resistant Timber Frames in the Mediterranean Area*, (February).

GNDT. (2001). "Scheda per il rilievo dei beni culturali - Danno alle chiese." Gruppo di lavoro per la salvaguardia dei beni culturali dai richi naturali.

Herman, M. W., Hayes, G. P., Smoczyk, G. M., Turner, R., Turner, B., Jenkins, J., Davies, S., Parker, A., Sinclair, A., Benz, H. M., Furlong, K. P., and Villaseñor, A. (2015). *Seismicity of the Earth 1900-2016 - Mediterranean Sea and Vicinity*. U.S. Geological Survey Open-File Report.

INGV. (n.d.). *Ricerca di risorse geotermiche finalizzata alla sperimentazione di un impianto pilota nel Comune di Serrara Fontana (ISOLA D'ISCHIA-NA) - Geologia e Inquadramento geotermico*. Napoli.

INGV. (2015). "1915-2015 Cento anni dal Terremoto della Marsica." Milano.

Li, Y., and Barbič, J. (2014). "Stable orthotropic materials." *ACM/Eurographics Symposium on Computer Animation*, 41–46.

Lourenço, P. B. (2008). "Structural masonry analysis: recent developments and prospects." *Proceedings of the 14th international brick & block masonry conference*, (2004), 1341–1356.

Luongo, G., Carlino, S., Cubellis, E., Delizia, I., Iannuzzi, R., and Obrizzo, F. (2006). *Il terremoto di Casamicciola 1883: una ricostruzione mancata*. Napoli.

Mendes, N. (2012). "Seismic assessment of ancient masonry buildings : Shaking table tests and numerical analysis." *PhD Thesis*, 228.

MIBACT. (2010). *Linee Guida per la valutazione e riduzione del rischio si- smico del patrimonio culturale allineate alle nuove Norme tecniche per le costruzioni (d.m. 14 gennaio 2008)*. Ministero per i Beni e le Attività Culturali.

MIBACT. (2015). *Aggiornameto della direttiva 12 dicembre 2013, relativa alle "Procedure per la gestione delle attività di messa in sicurezza e salvaguardia del partimonio culturale in caso di*

emergenze derivanti da calamità naturali."

Molin, P., Acocella, V., and Funiciello, R. (2003). "Structural, seismic and hydrothermal features at the border of an active intermittent resurgent block: Ischia Island (Italy)." *Journal of Volcanology and Geothermal Research*, 121(1–2), 65–81.

Nappi, R., Alessio, G., Gaudiosi, G., Nave, R., Marotta, E., Siniscalchi, V., Civico, R., Pizzimenti, L., Peluso, R., Belviso, P., and Porfido, S. (2018). "The 21 August 2017 Md 4.0 Casamicciola Earthquake: First Evidence of Coseismic Normal Surface Faulting at the Ischia Volcanic Island." *Seismological Research Letters*, 89(4), 1323–1334.

NTC-Circolare. (2018). *Circolare 21 gennaio 2019 n. 7 C.S.LL.PP. Istruzioni per l'applicazione dell'aggiornamento delle "Norme Tecniche per le Costruzioni" di cui al D.M. 17/01/2018. Consiglio Superiore dei Lavori Pubblici.*

NTC. (2018). *Aggiornamento delle «Norme tecniche per le costruzioni».* Ministero delle Infrastrutture e dei Trasporti, Roma, 1–198.

Orsi, G., Gallo, G., and Zanchi, A. (1991). "Simple-shearing block resurgence in caldera depressions. A model from Pantelleria and Ischia." *Journal of Volcanology and Geothermal Research*, Elsevier, 47(1–2), 1–11.

Poletti, E. (2013). "Characterization of the seismic behaviour of traditional timber frame walls." Universidade do Minho.

Poletti, E., Vasconcelos, G., Lourenço, P. B., and Ciocci, M. P. (2015). "Numerical Approaches for the Analysis of Timber Frame Walls." *Historical Earthquake-Resistant Timber Frames in the Mediterranean Area*, H. Cruz, J. Saporiti Machado, A. Campos Costa, X. P. Candeias, N. Ruggieri, and M. J. Catarino, eds., Springer Netherlands, 183–192.

Polverino, F. (1998). *Ischia Architettura e terremoto.* CLEAN Edizioni, Napoli.

Rovida, A., Locati, M., Camassi, R., Lolli, B., and Gasperini, P. (eds). (2016). "CPTI15, the 2015 version of the Parametric Catalogue of Italian Earthquakes." INGV - Istituto Nazionale di Geofisica e Vulcanologia.

Ruggieri, N., Sandhaas, C., and Ceccotti, A. (2015). "Seismic Vulnerability of Borbone Masonry Reinforced with Timber Frames." *Historical Earthquake-Resistant Timber Frames in the Mediterranean Area*, H. Cruz, J. Saporiti Machado, A. Campos Costa, X. P. Candeias, N. Ruggieri, and M. J. Catarino, eds., Springer Netherlands, 193–204.

Ruggieri, N., and Tampone, G. (2015). "Historical Earthquake-Resistant Timber Frames in the Mediterranean Area." *Historical Earthquake-Resistant Timber Frames in the Mediterranean Area.*

S2X Srl. (2019). *Prove dinamiche in condizioni operative Rapporto di prova condizioni operative : Chiesa Santa Maria Maddalena - Casamicciola Terme (NA).* Campobasso.

Salerno, G., Geremia, F., Pagano, E., Zampilli, M., Ruggieri, N., and Stellacci, S. (2015). "The Masonry Timber Framed Load Bearing Structure of 'Baraccato' System: A Numerical Model." *Historical Earthquake-Resistant Timber Frames in the Mediterranean Area*, H. Cruz, J. Saporiti Machado, A. Campos Costa, X. P. Candeias, N. Ruggieri, and M. J. Catarino, eds., Springer Netherlands, 205–2013.

Serpe, E., Caliendo, G., Cineri, V., and D'Andrea, M. (2016). "Presidi antisismici in Campania : evoluzione teorica , normativa e tecnologica tra il XVIII e il XX secolo." *AISI*, Genova.

Sousa, H. S., Branco, J. M., and Lourenço, P. B. (2014). "Characterization of cross sections from old chestnut beams weakened by decay." (May).

USGS. (n.d.). "Earthquakes (1900 - 2016) - Mediterranean Region and Vicinity." <https://earthquake.usgs.gov/earthquakes/tectonic/images/mediterranean_tsum.pdf> (Jun. 30, 2019).

Vezzoli, L. (1988). "Island of Ischia." *Quaderni della Ricerca Scientifica*, L. Vezzoli, ed., CNR-DT Consiglio Nazionale delle Ricerche, Rome, 1–122.

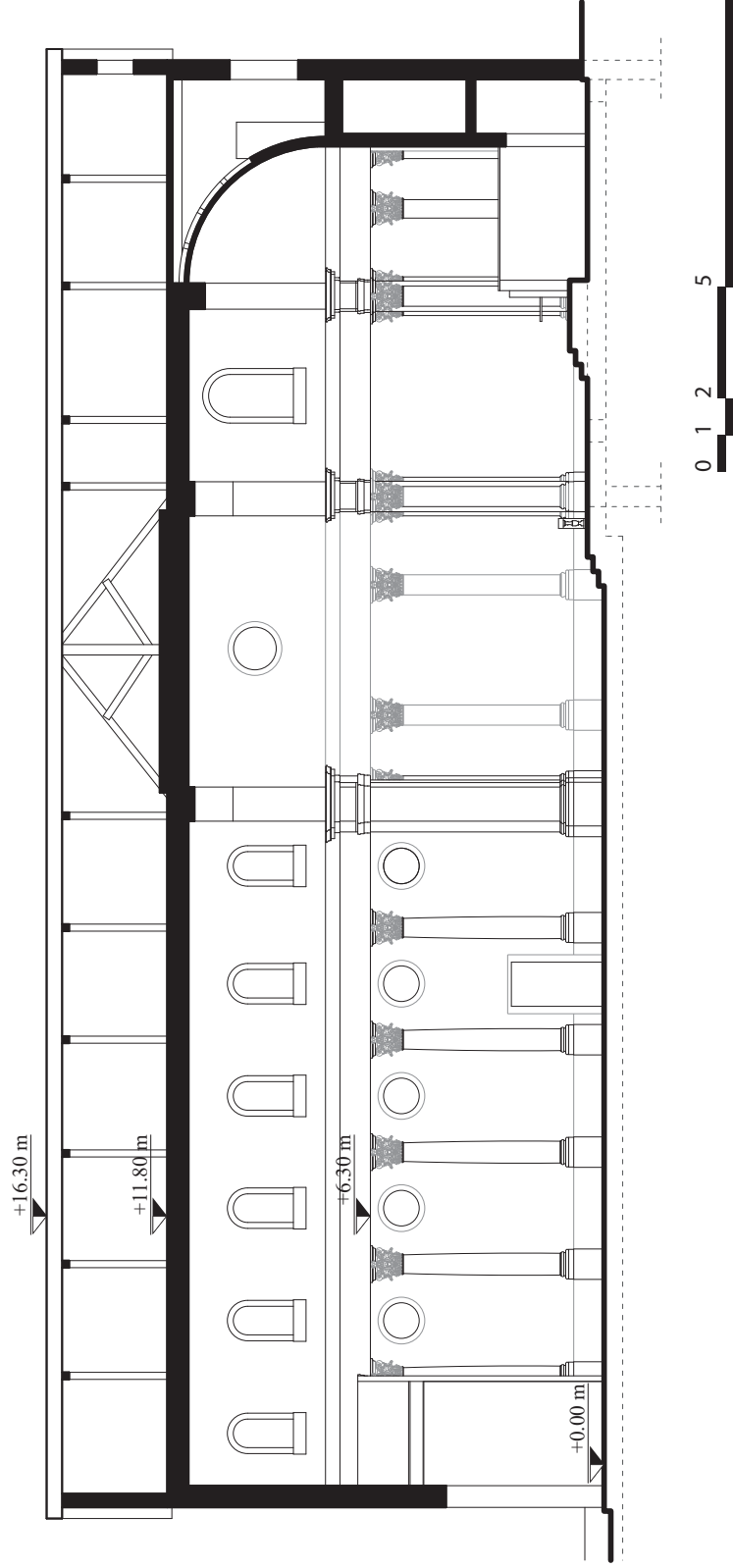"Website of the parish of Santa Maria Maddalena." (n.d.). <http://parrocchiacasamicciola.it/basilica-s-maria-maddalena/> (Apr. 17, 2019).

ADVANCED MASTERS IN STRUCTURAL ANALYSIS OF MONUMENTS AND HISTORICAL CONSTRUCTIONS

ANNEX 1   HISTORICAL DRAWINGS
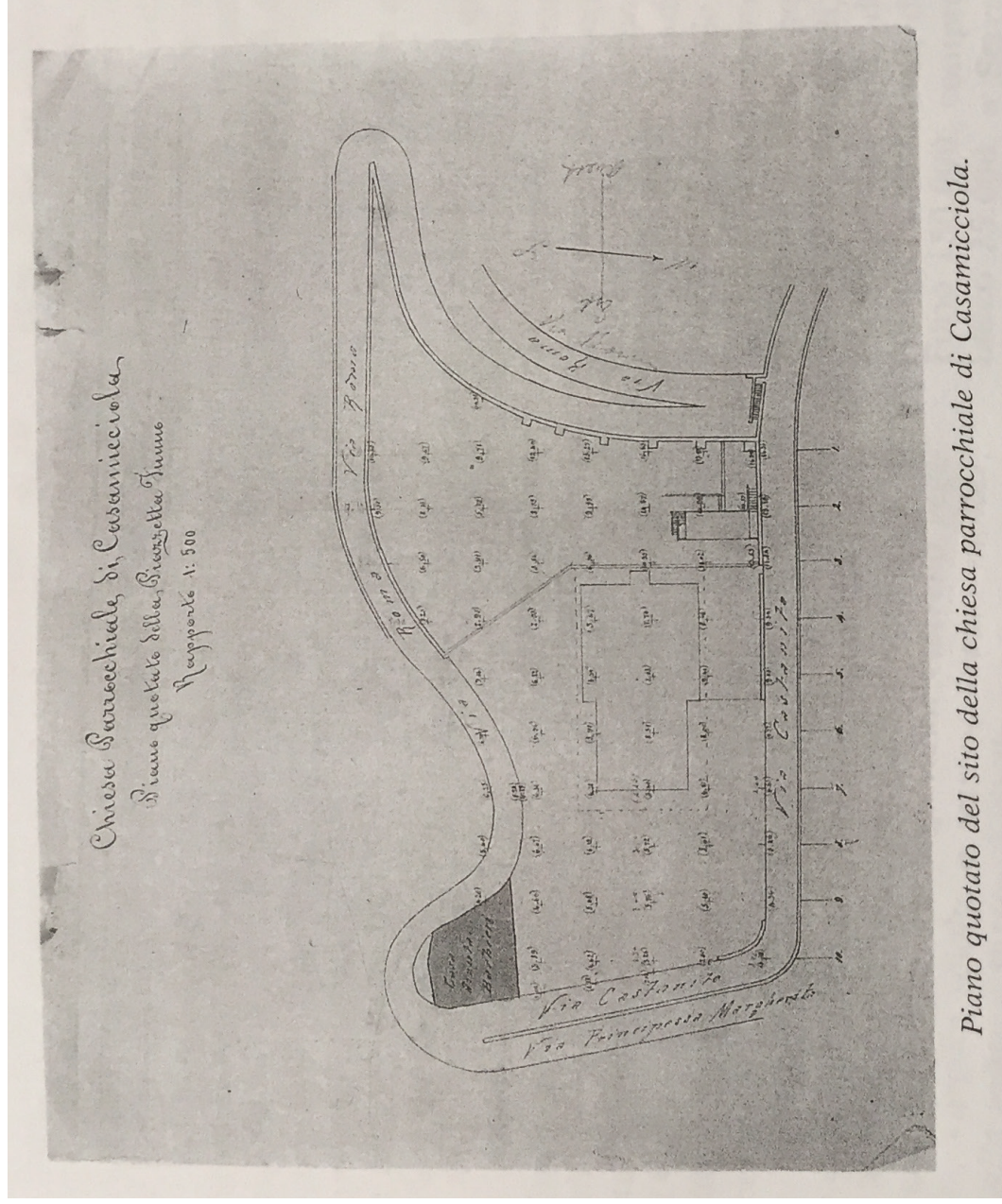
Piano quotato del sito della chiesa parrocchiale di Casamicciola.
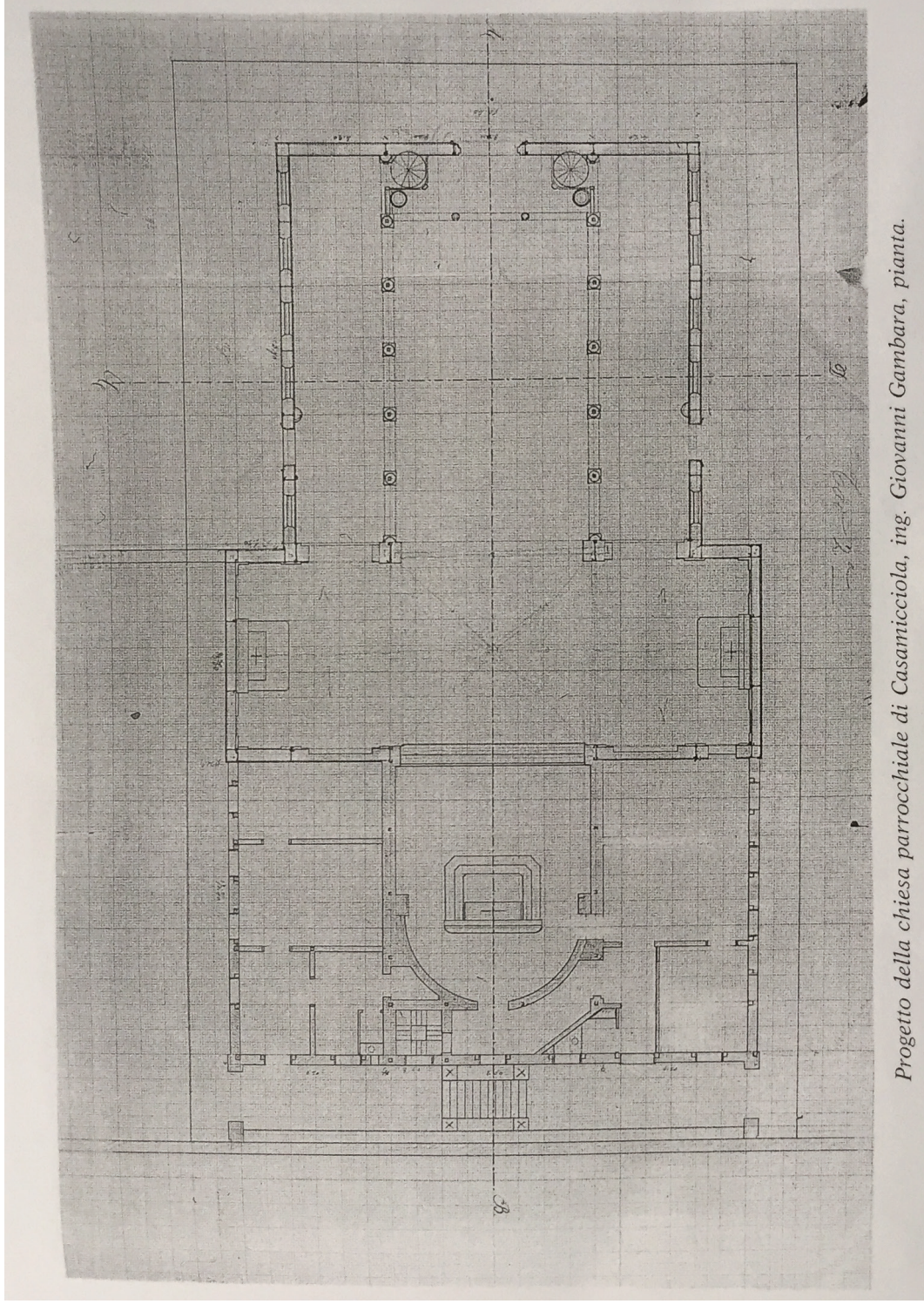
Progetto della chiesa parrocchiale di Casamicciola, ing. Giovanni Gambara, pianta.
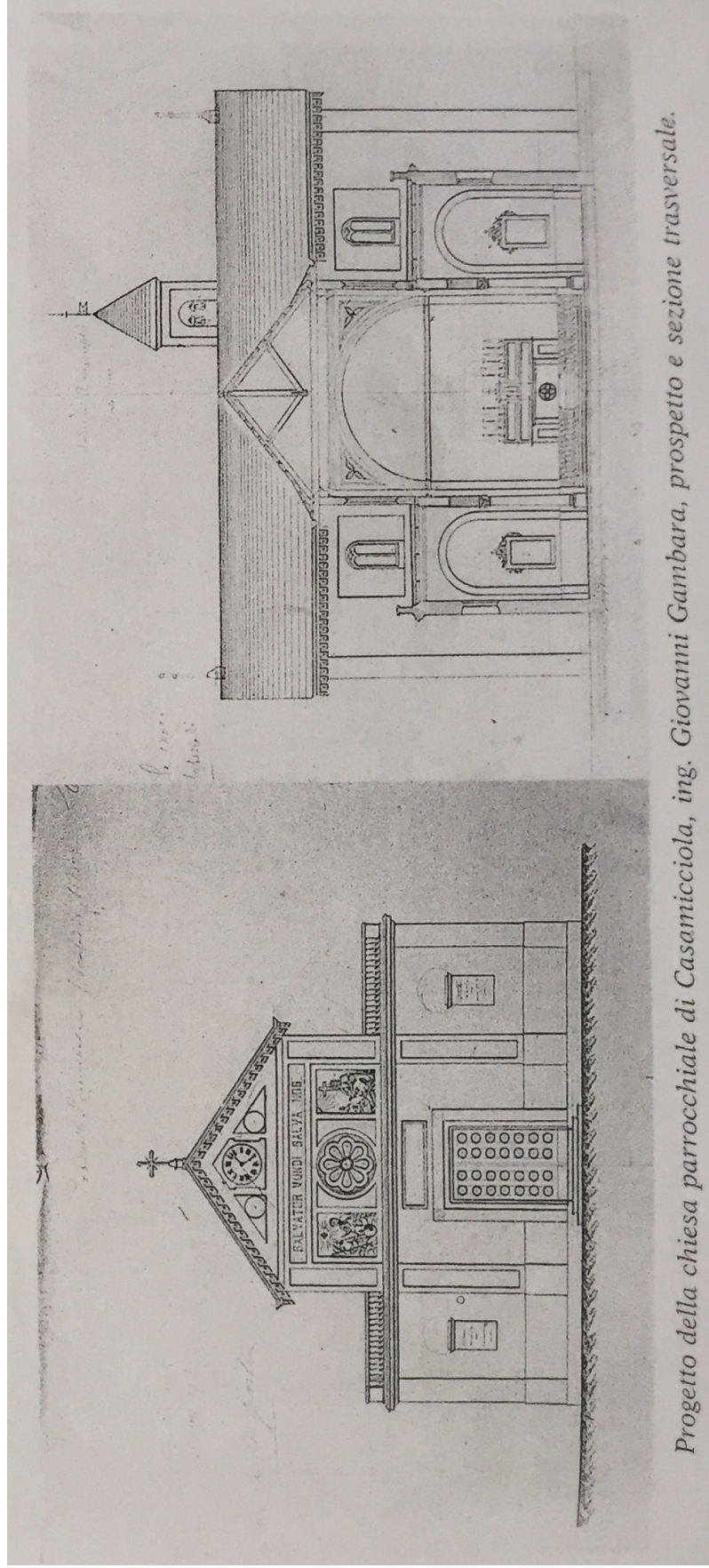
Progetto della chiesa parrocchiale di Casamicciola, ing. Giovanni Gambara, prospetto e sezione trasversale.
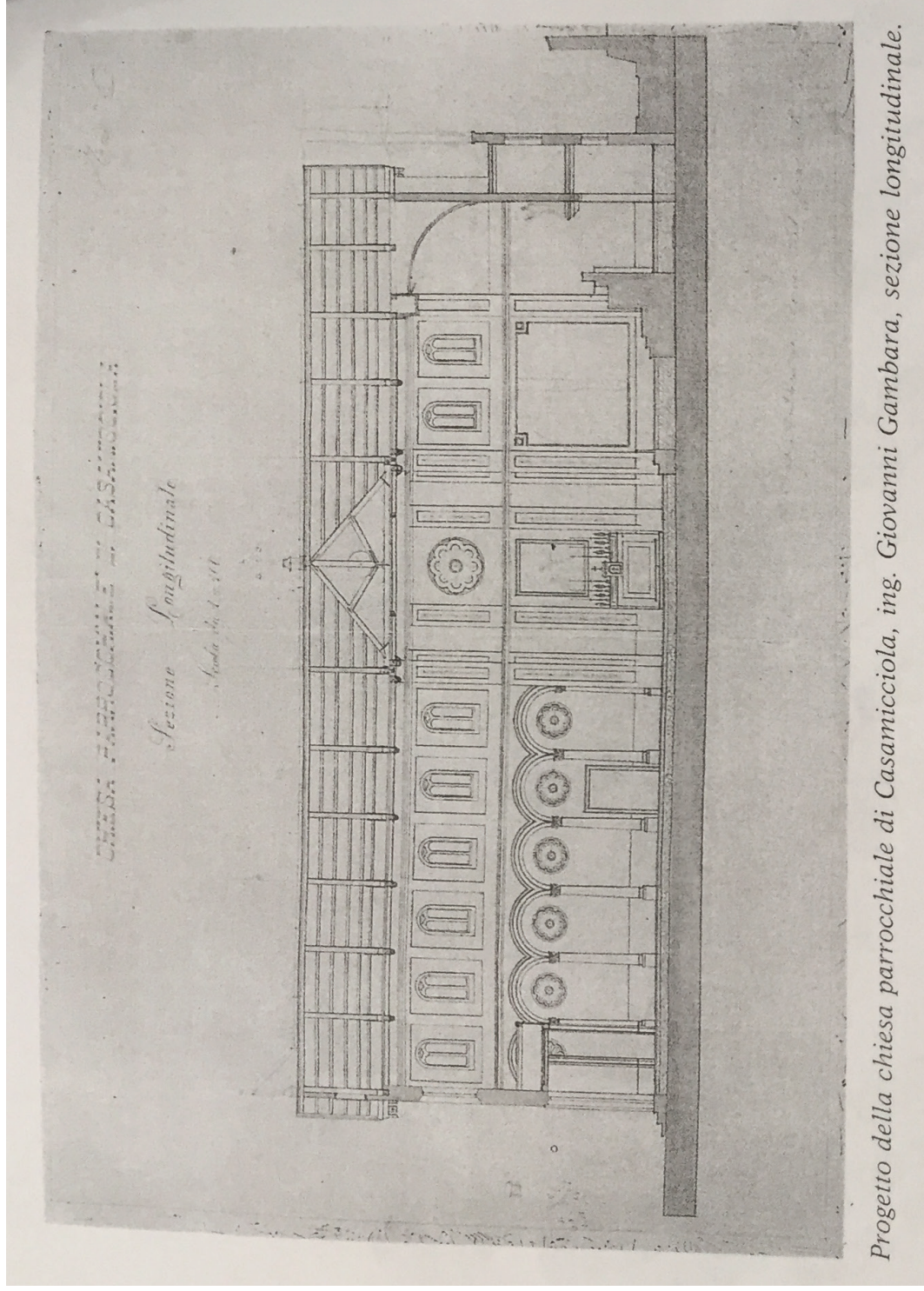
Progetto della chiesa parrocchiale di Casamicciola, ing. Giovanni Gambara, sezione longitudinale.
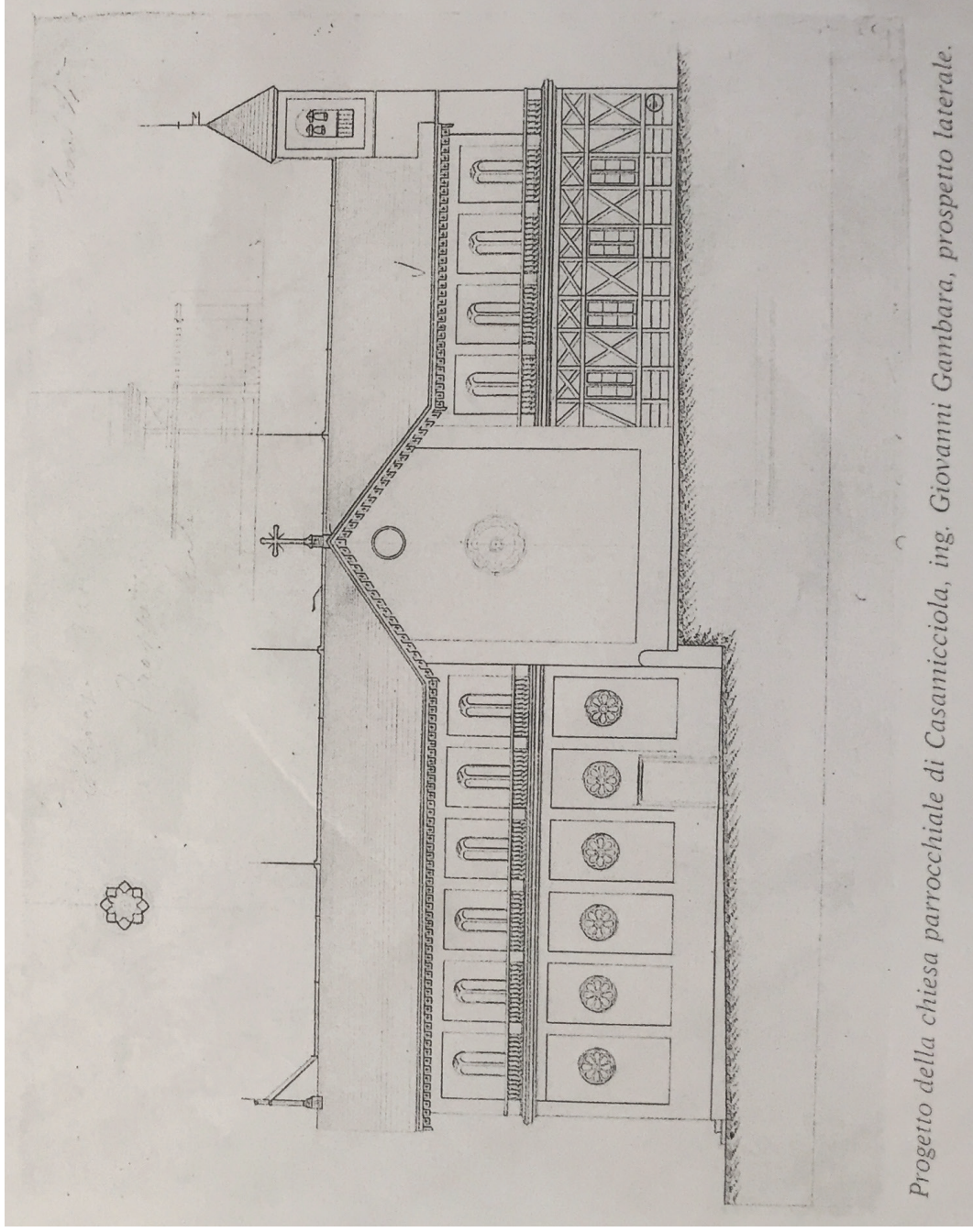
Progetto della chiesa parrocchiale di Casamicciola, ing. Giovanni Gambara, prospetto laterale.
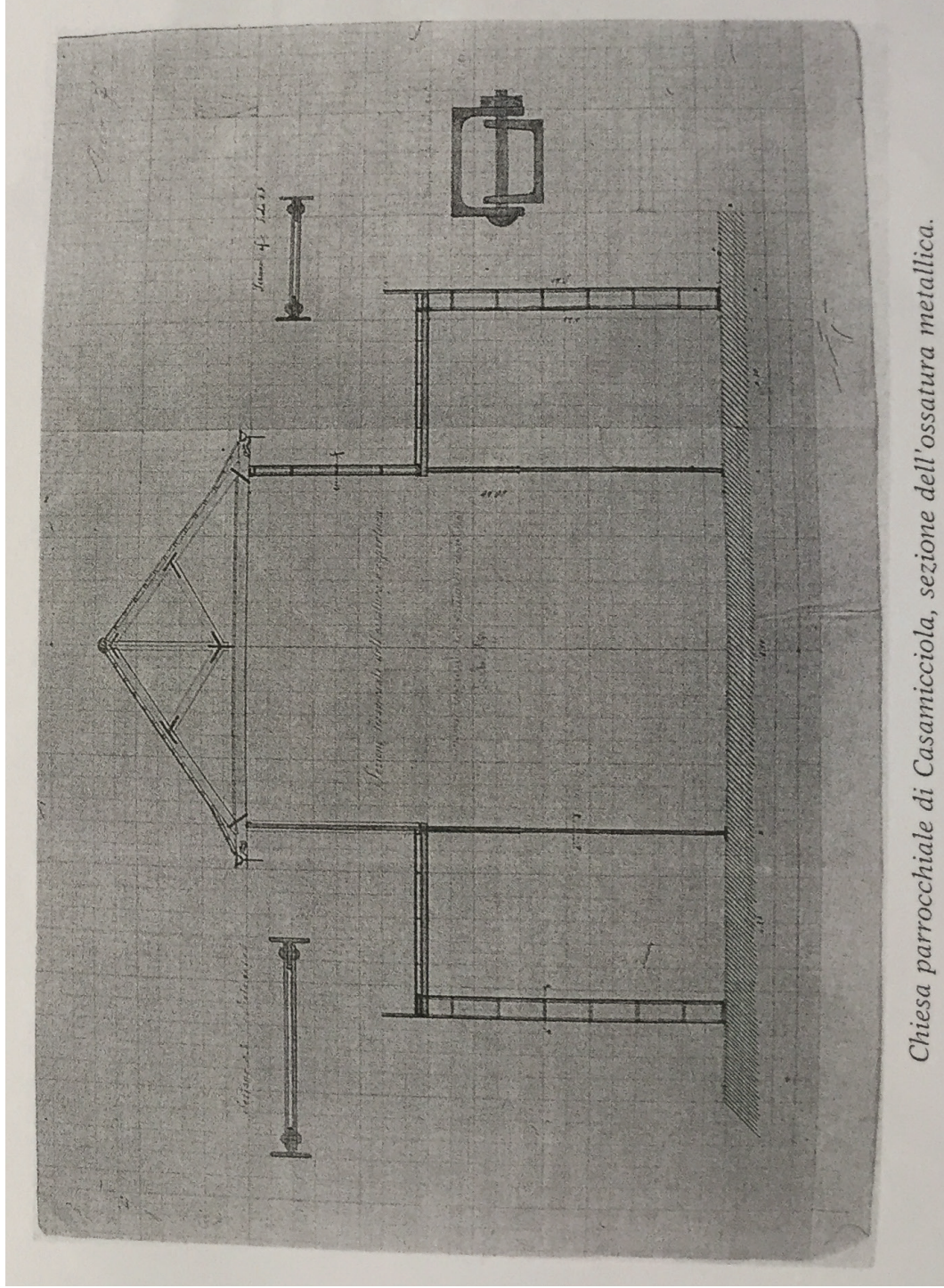
Chiesa parrocchiale di Casamicciola, sezione dell'ossatura metallica.
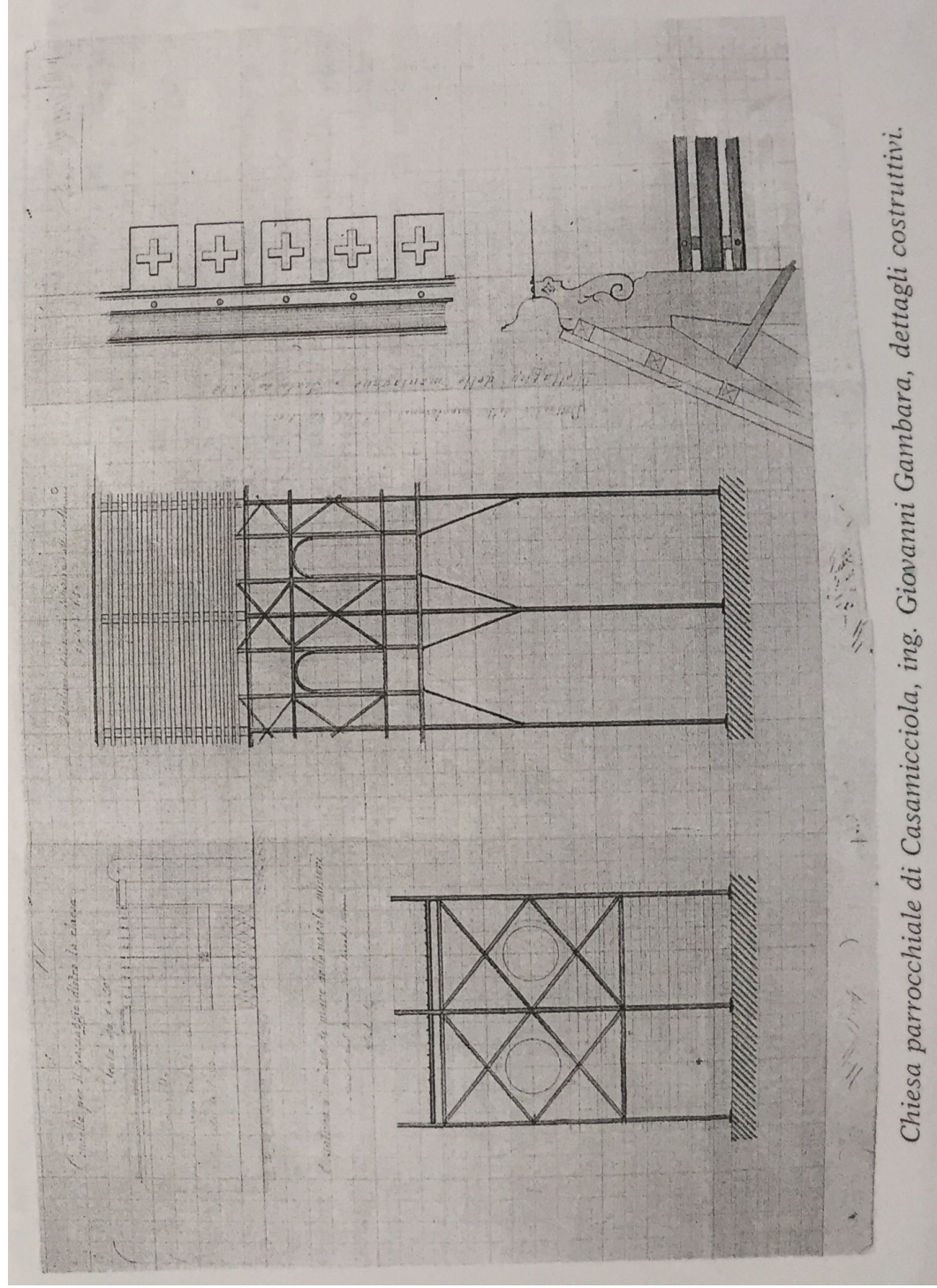
Chiesa parrocchiale di Casamicciola, ing. Giovanni Gambara, dettagli costruttivi.
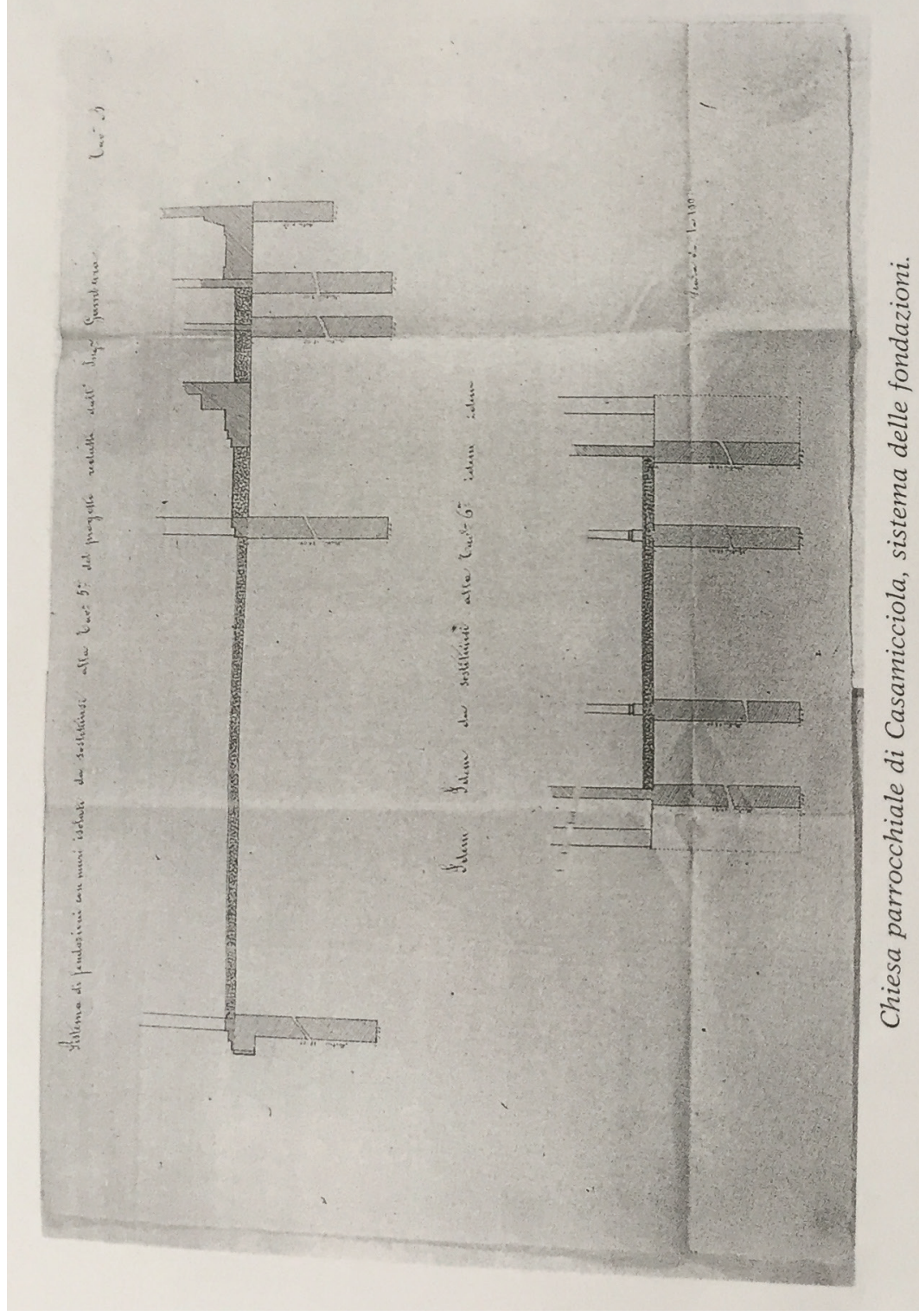
Chiesa parrocchiale di Casamicciola, sistema delle fondazioni.
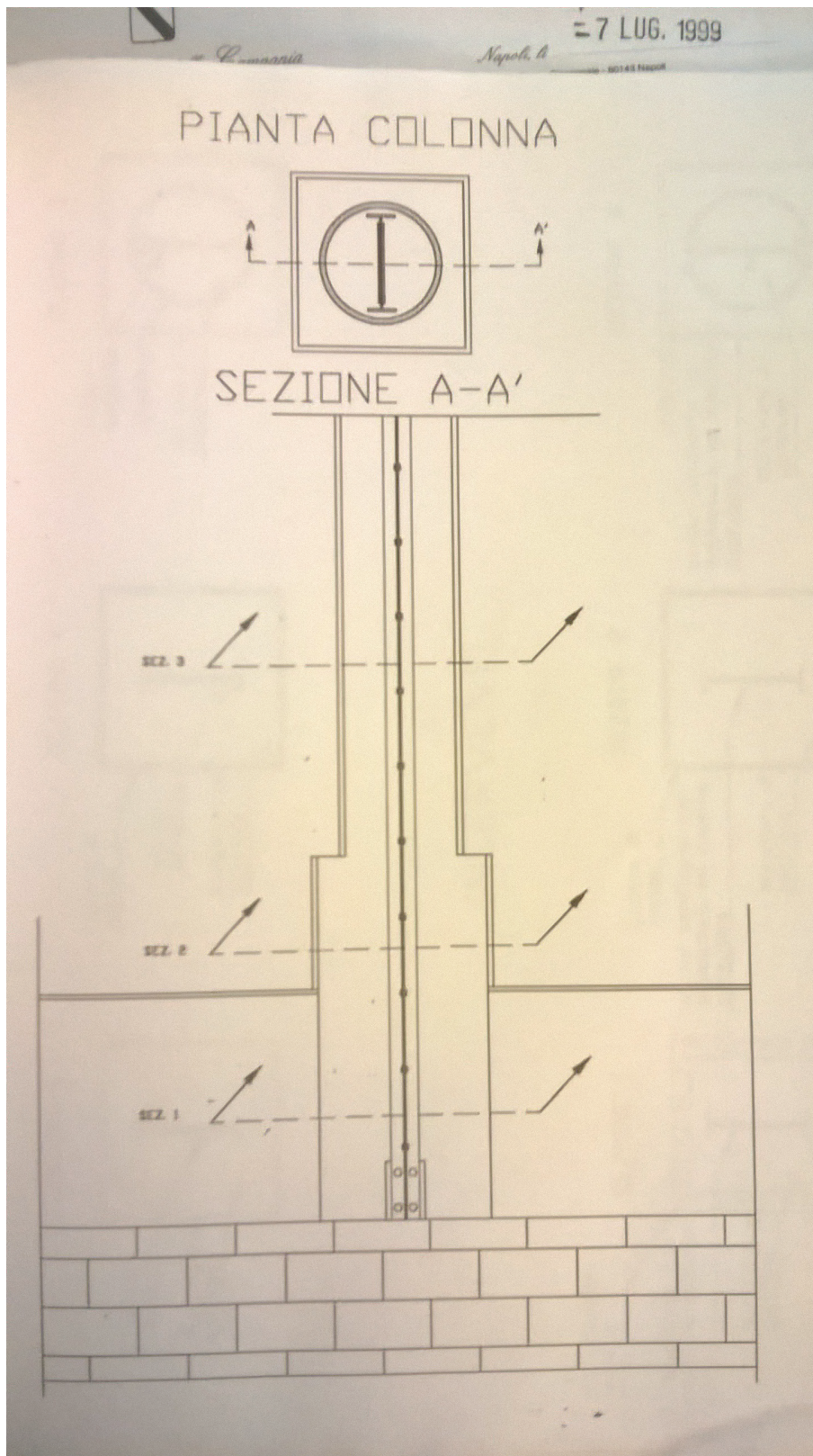
PIANTA COLONNA

SEZIONE A-A'

ANNEX 2   ARCHITECTRURAL   DRAWINGS

GROUND LEVEL (+0.00 m)

0 1 2   5   15

FIRST FLOOR LEVEL (+3.70 m)

0 1 2 5 15

CENTRAL NAVE LEVEL (+7.30 m)

0 1 2 5 15

| Annex 2 - Architectural drawings |

B7

ATTIC LEVEL (+13.08 m)

0 1 2   5   15

A A'

A A'

+16.30 m

+11.80 m

+6.30 m
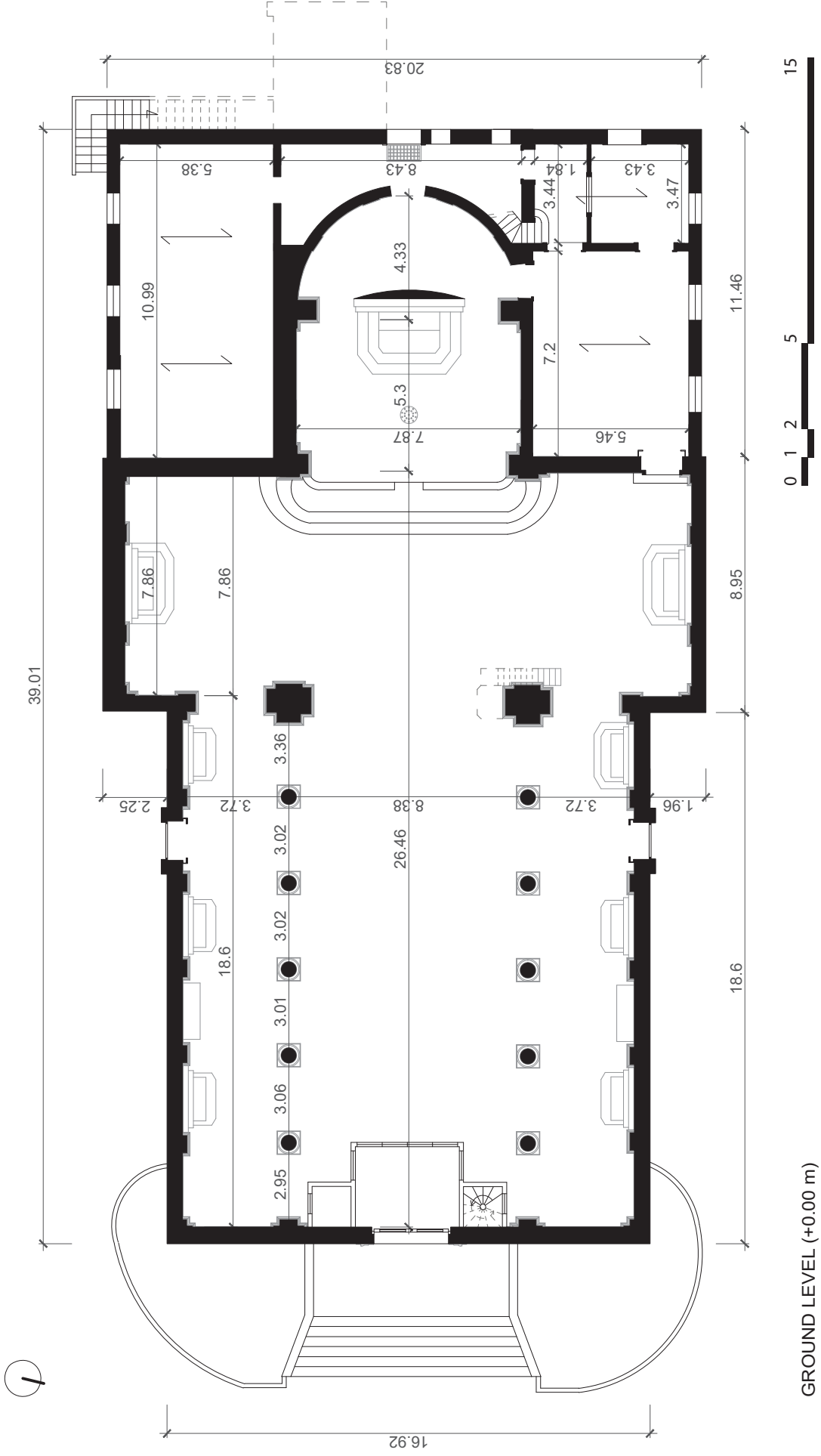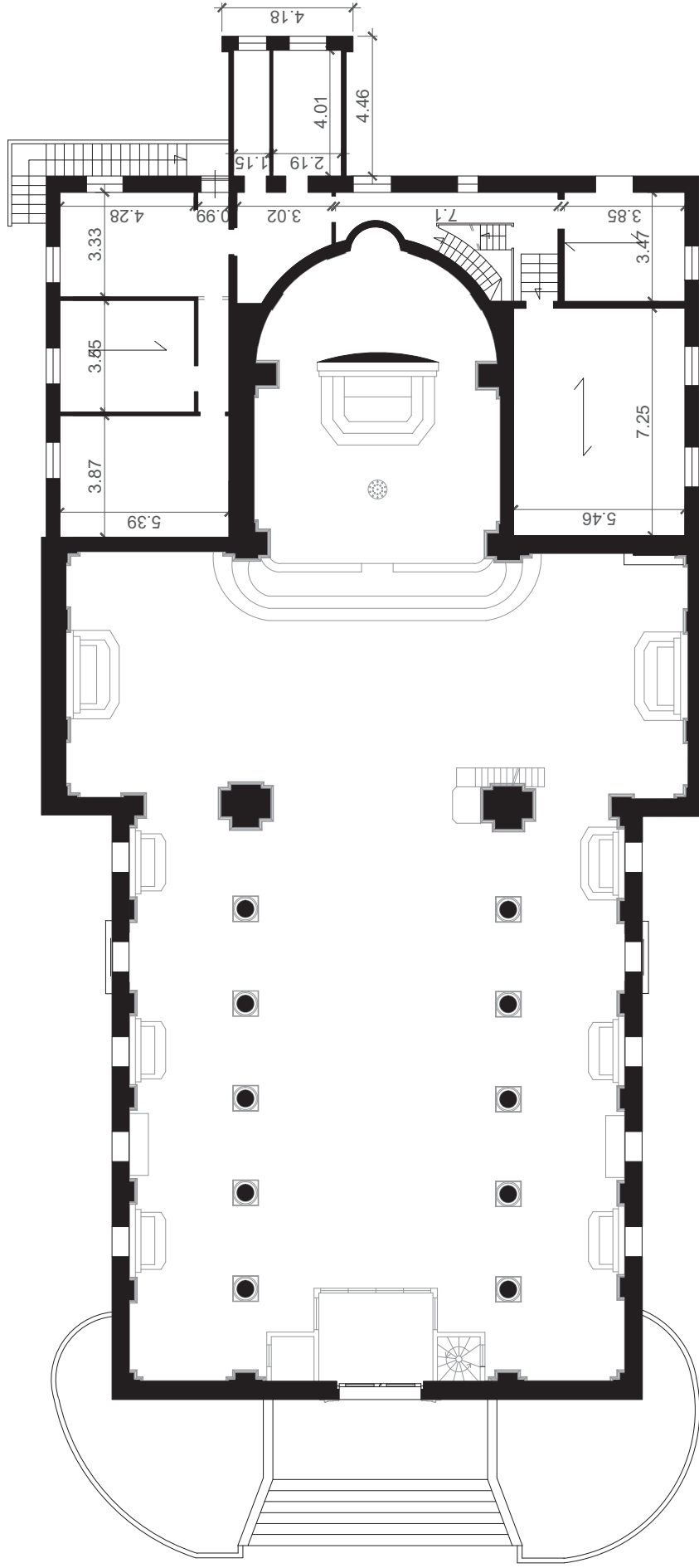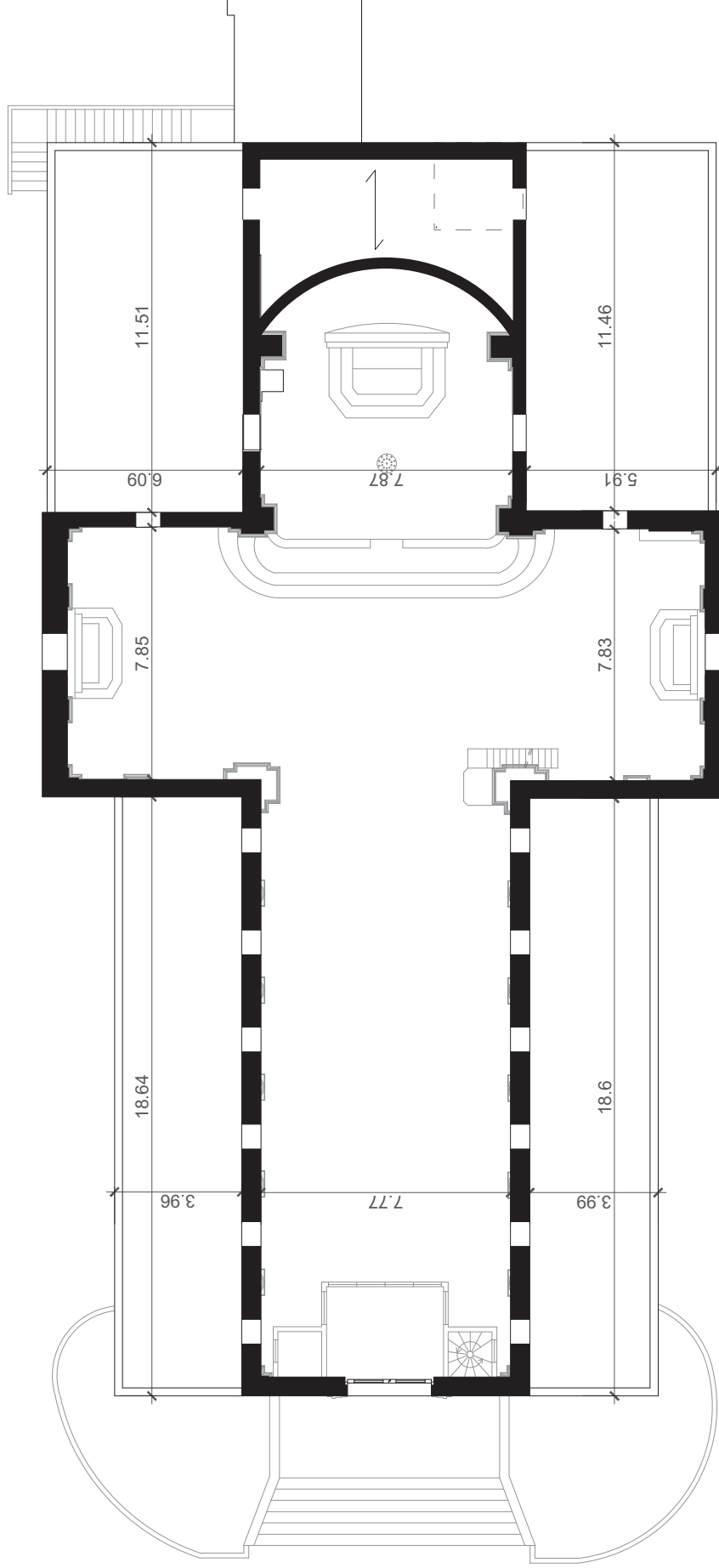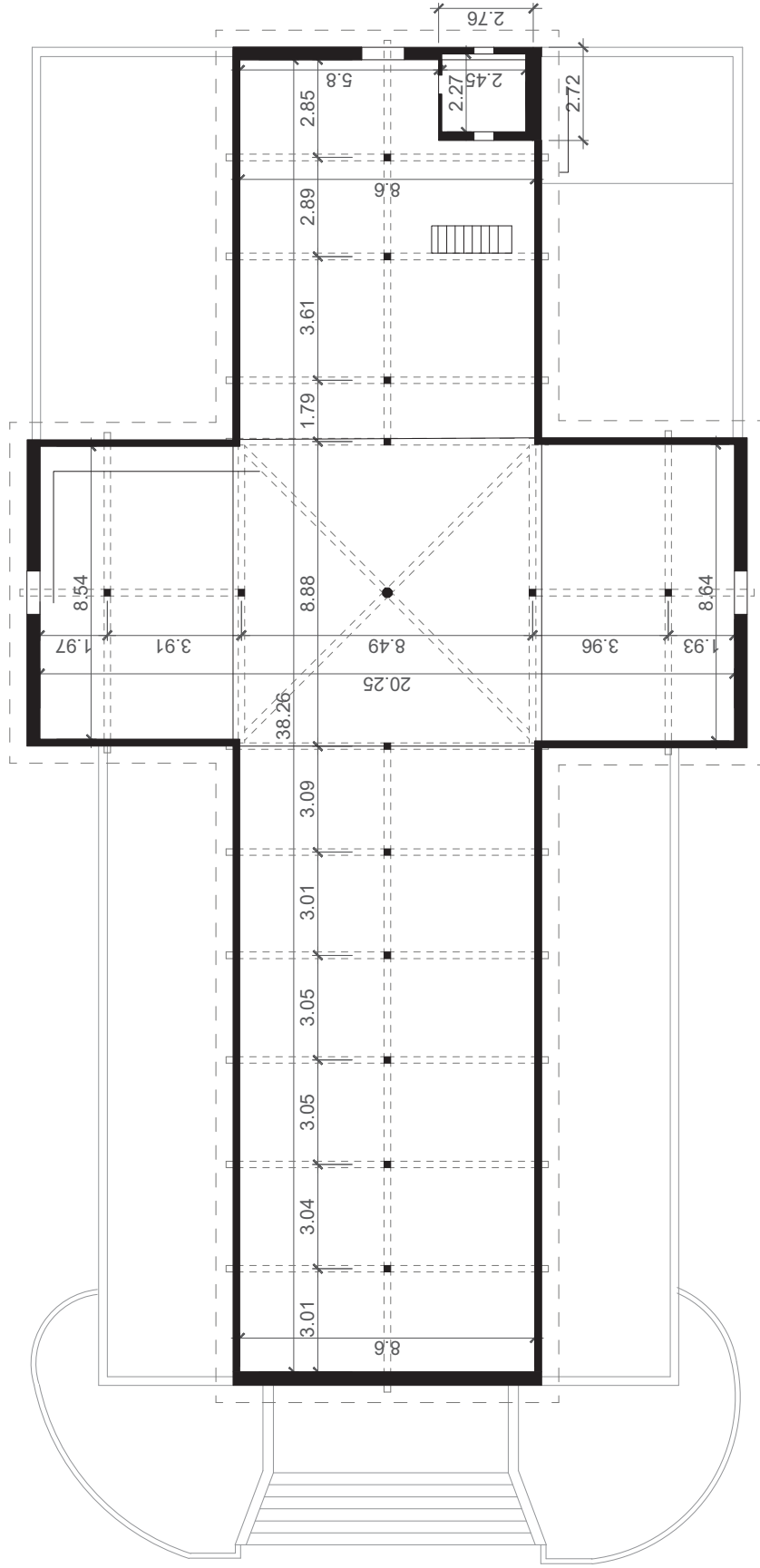
+0.00 m
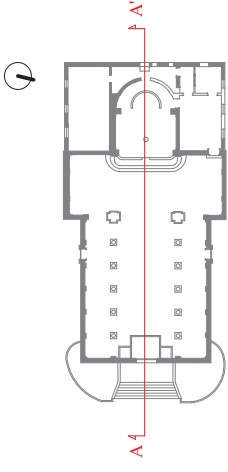
LONGITUDINAL SECTION (AA') - 1:200

0 1 2   5   15

| Annex 2 - Architectural drawings |

B11

Modelling and safety assessment of the Santa Maria Maddalena Church, Ischia, Italy

ADVANCED MASTERS IN STRUCTURAL ANALYSIS OF MONUMENTS AND HISTORICAL CONSTRUCTIONS

+22.30 m

+16.30 m

+11.80 m

+16.30 m

+11.80 m

+7.30 m

+0.00 m

+0.00 m

WEST FAÇADE (FRONT) AND TRANSVERSAL SECTION (BB') - 1:200

0 1 2   5   15

| Annex 2 - Architectural drawings |

B13

+22.30 m

+16.30 m

+11.80 m

+7.30 m

+0.00 m

NORTH FAÇADE - 1:200

0 1 2   5   15

Modelling and safety assessment of the Santa Maria Maddalena Church, Ischia, Italy

ADVANCED MASTERS IN STRUCTURAL ANALYSIS OF MONUMENTS AND HISTORICAL CONSTRUCTIONS

A A'

A A'
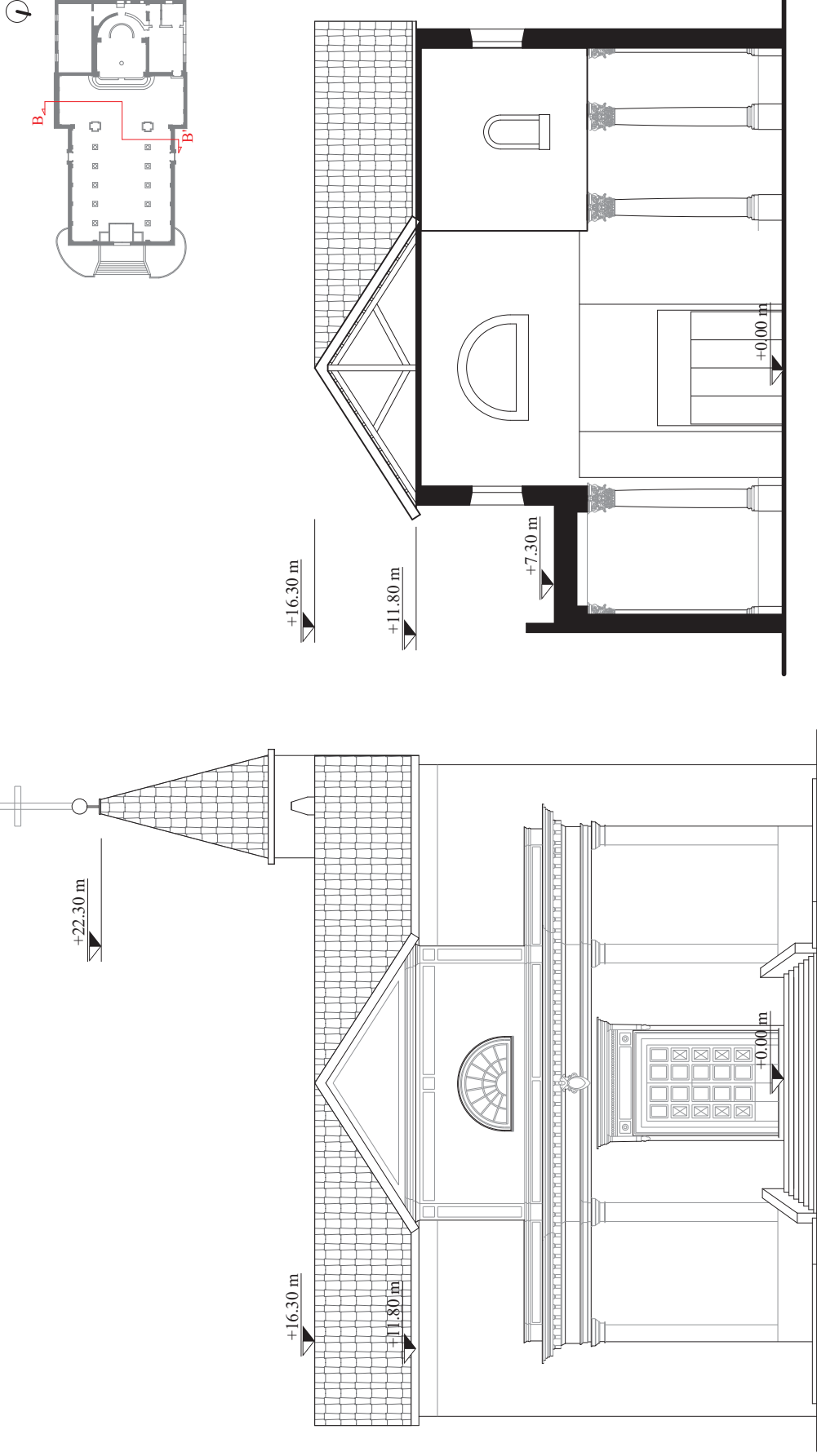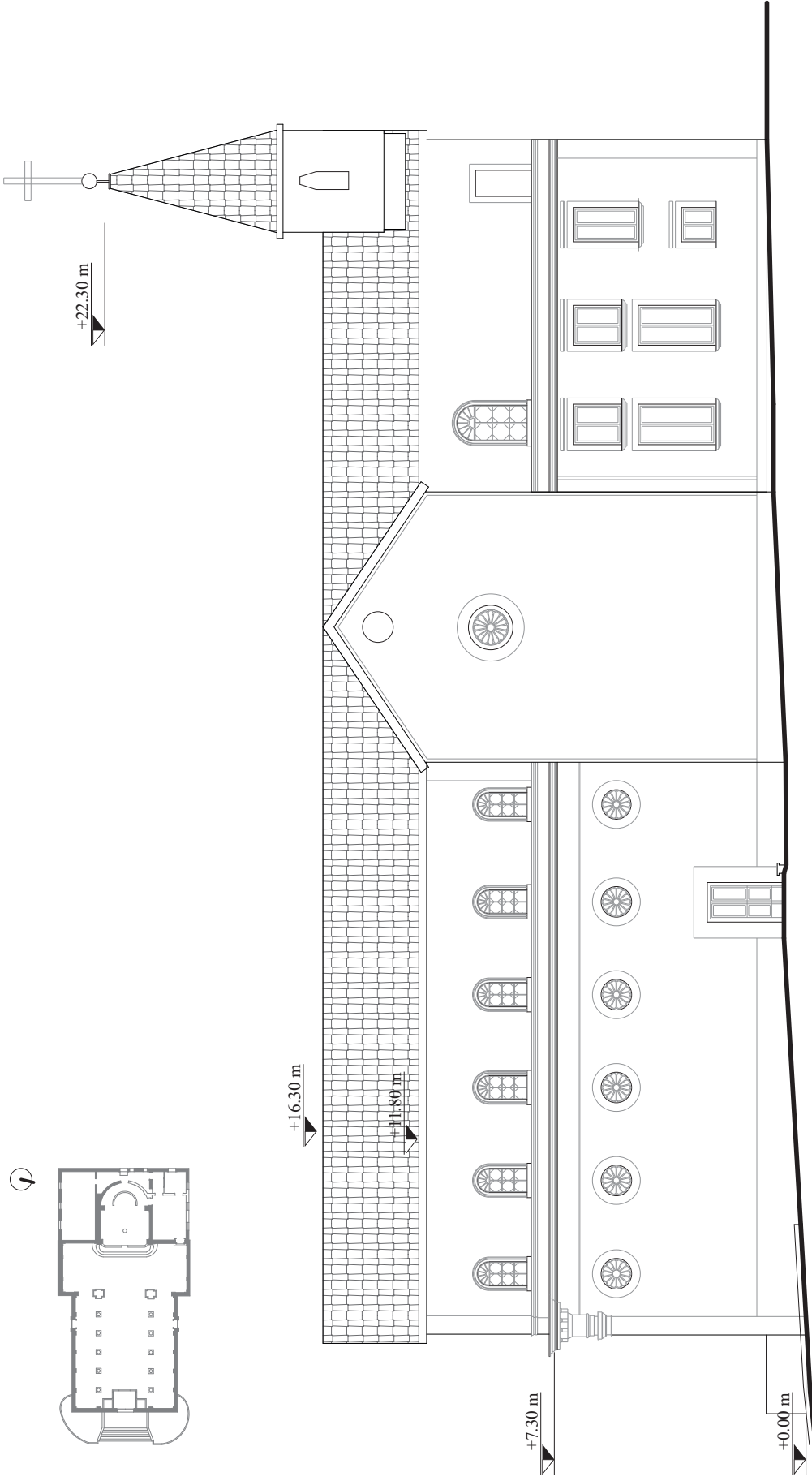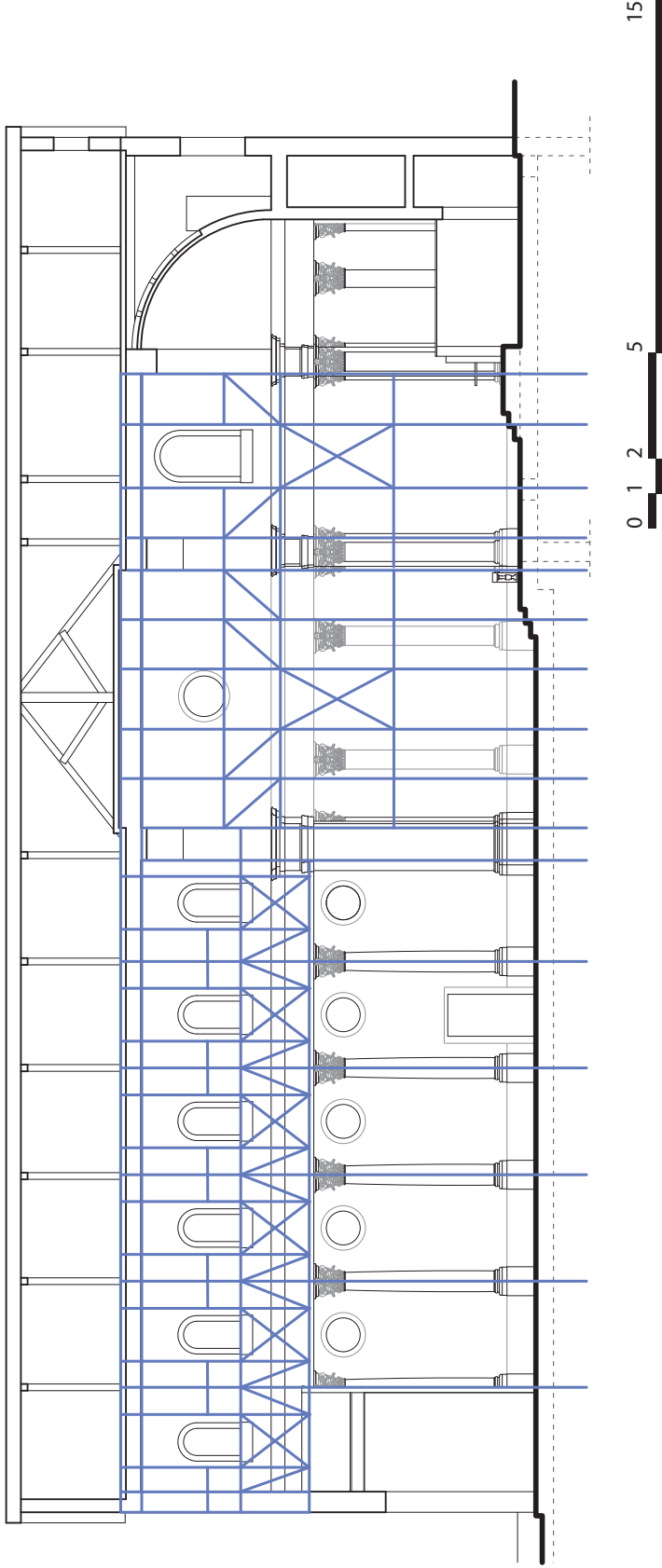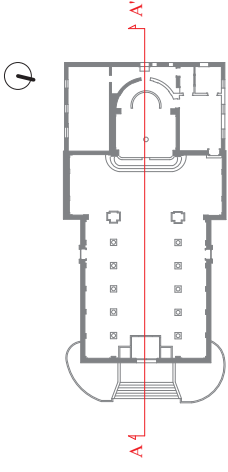
LONGITUDINAL SECTION - IRON FRAMES LAYOUT

0 1 2 5 15
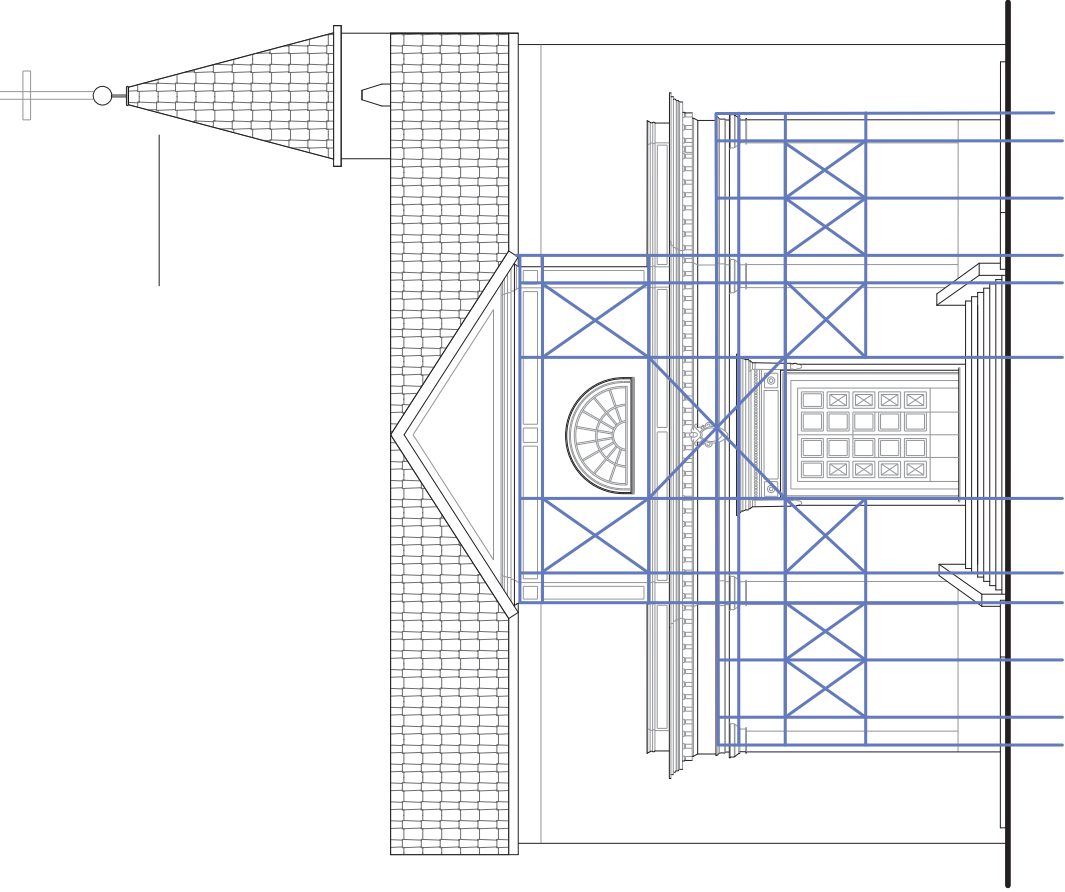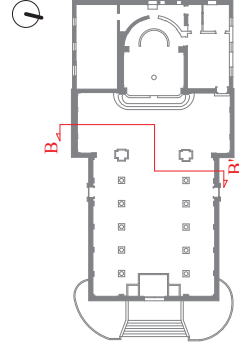
WEST FAÇADE (FRONT) AND TRANSVERSAL SECTION (BB') - IRON FRAMES LAYOUTS

| Annex 2 - Architectural drawings |

B19

0 1 2   5   15

NORTH FAÇADE - 1:200

0   1   2   5   15

ADVANCED MASTERS IN STRUCTURAL ANALYSIS OF MONUMENTS AND HISTORICAL CONSTRUCTIONS

ANNEX 3   ARCHITECTURAL SCHEMES

Modelling and safety assessment of the Santa Maria Maddalena Church, Ischia, Italy

ADVANCED MASTERS IN STRUCTURAL ANALYSIS OF MONUMENTS AND HISTORICAL CONSTRUCTIONS

LIBRARY/PARISH ROOM

SACRISTY

REP.

GROUND LEVEL (+0.00 m)

LR

BD

BD

WC

K

LIBR.

REPOSITORY

FIRST FLOOR LEVEL (+3.70 m)

CENTRAL NAVE LEVEL (+7.30 m)

ATTIC LEVEL (+13.08 m)

Central nave
Lateral naves
Transept

Apse
Deambulatory

Hallway/Services
Library
Sacristy/Living spaces

Bedrooms
Repository

Resulting space
Attic floor
Belltower

0 1 2   5   10

| Annex 3 - Architectural schemes |

A3

Modelling and safety assessment of the Santa Maria Maddalena Church, Ischia, Italy
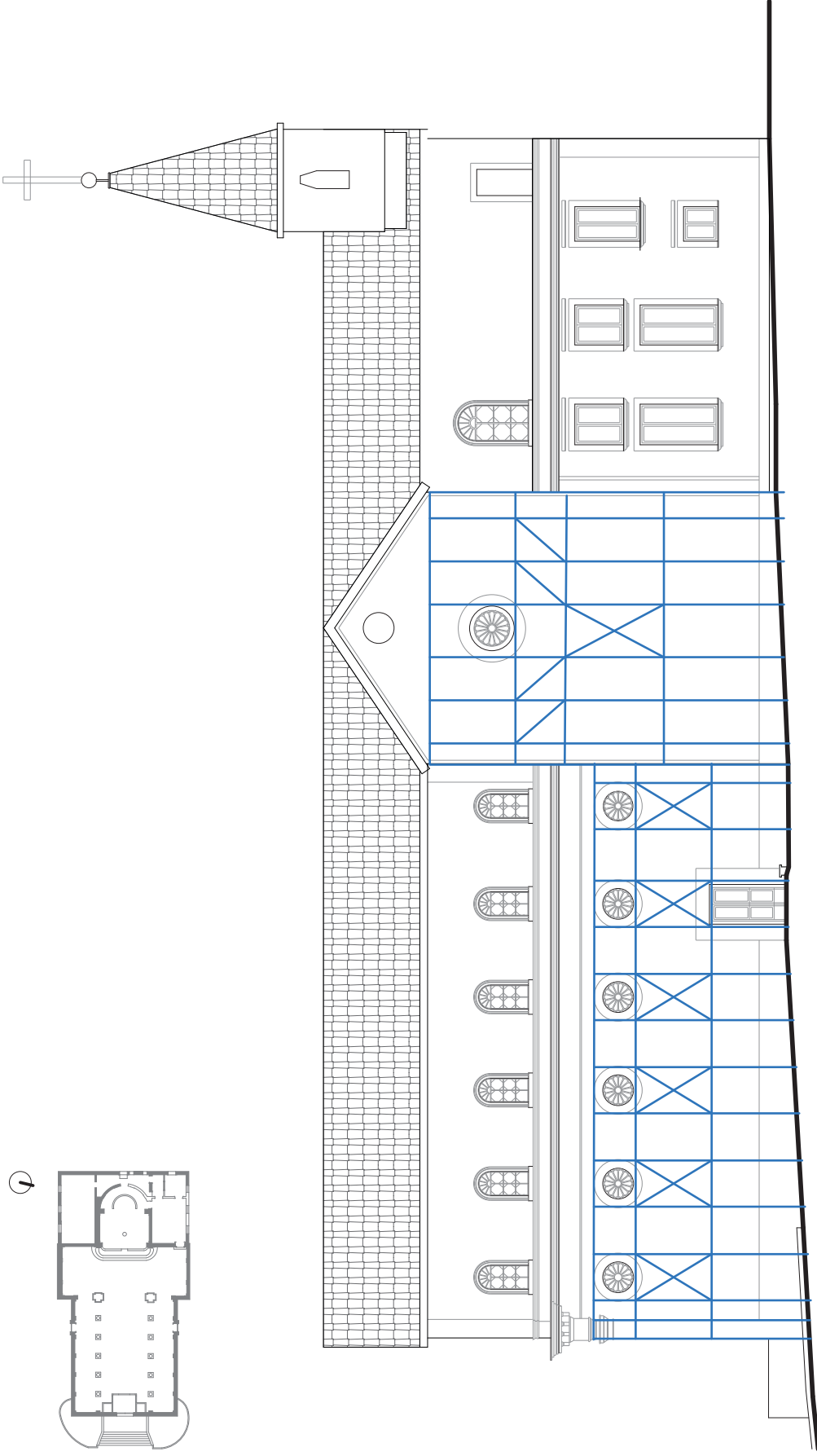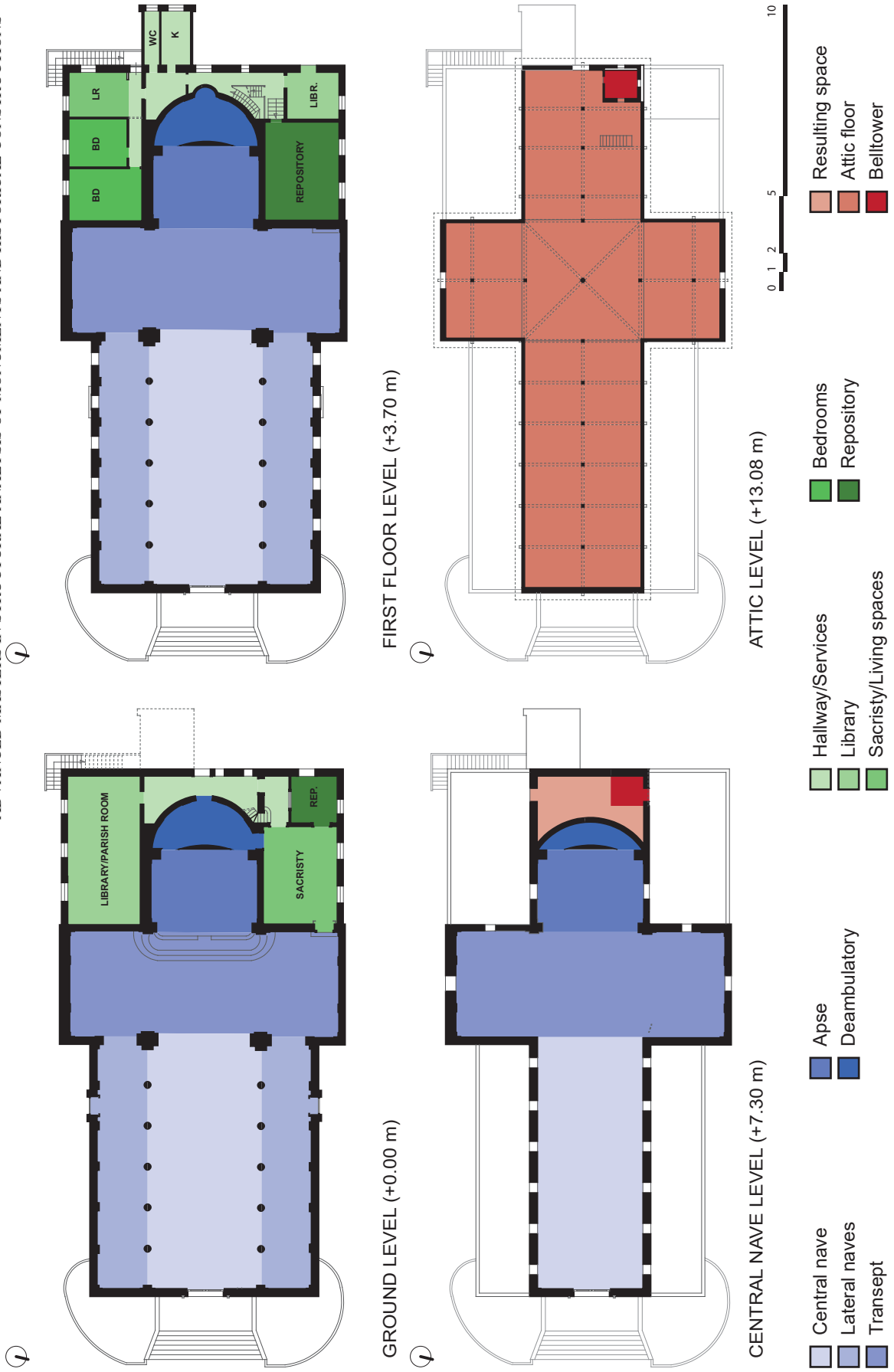
ADVANCED MASTERS IN STRUCTURAL ANALYSIS OF MONUMENTS AND HISTORICAL CONSTRUCTIONS
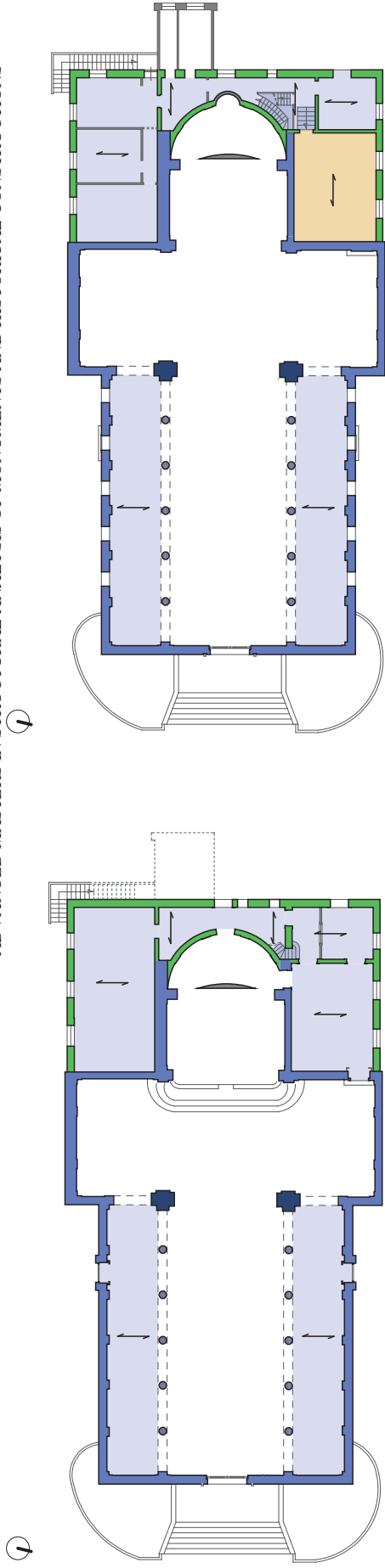
GROUND LEVEL (+0.00 m)

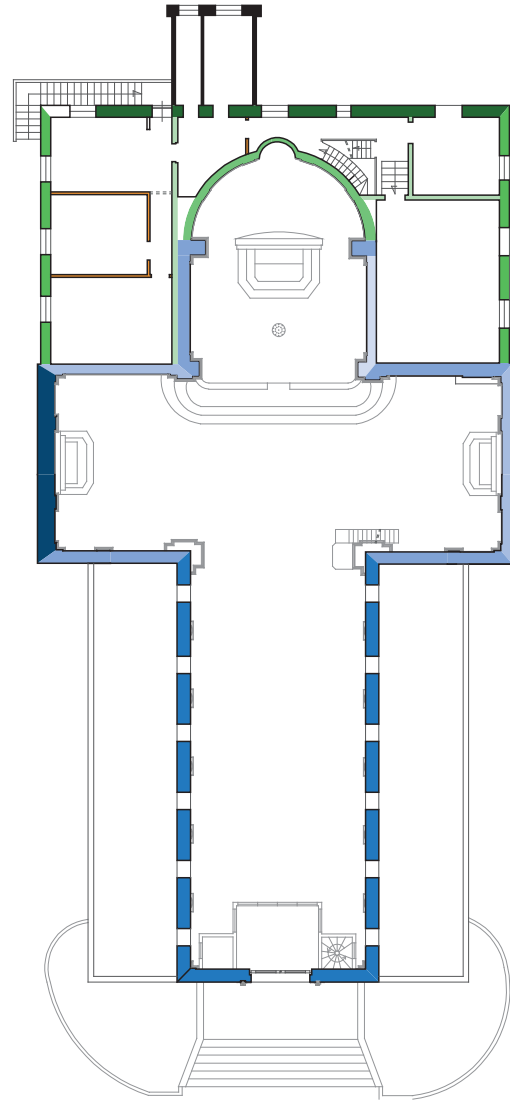FIRST FLOOR LEVEL (+3.70 m)
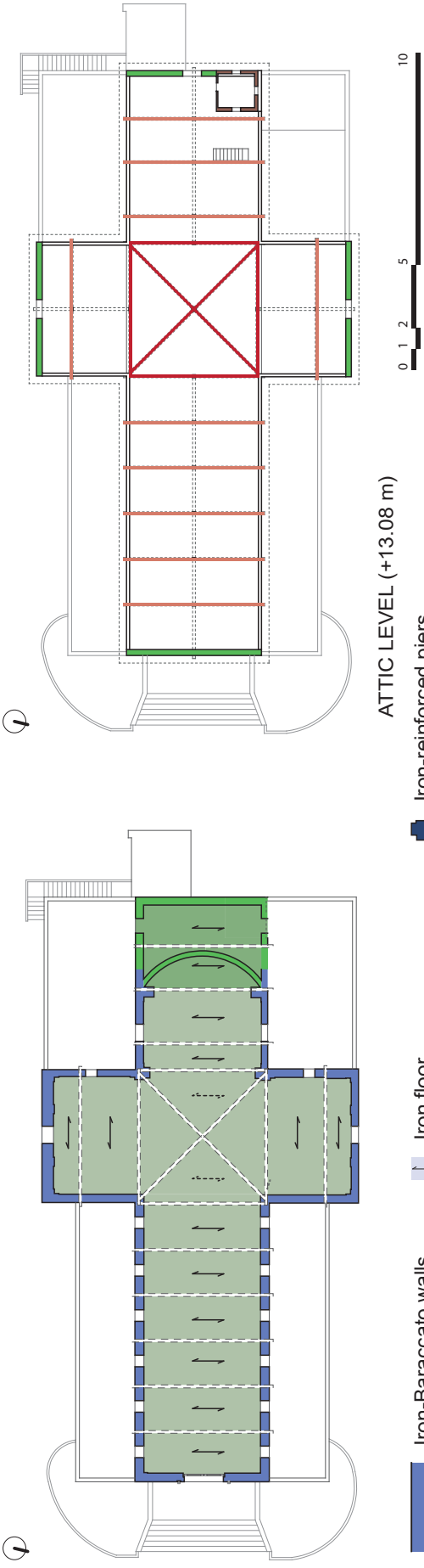
ATTIC LEVEL (+13.08 m)

Iron-reinforced piers
Iron-reinforced columns
Timber floor
Attic floor (truss supported)

Iron floor
Pre-stressed concrete slab
Timber floor
Attic floor (truss supported)

Iron-Baraccato walls
Timber-Baraccato walls
Iron-framed walls
Non-structural walls

0 1 2   5   10

| Annex 3 - Architectural schemes |

A5

ADVANCED MASTERS IN STRUCTURAL ANALYSIS OF MONUMENTS AND HISTORICAL CONSTRUCTIONS
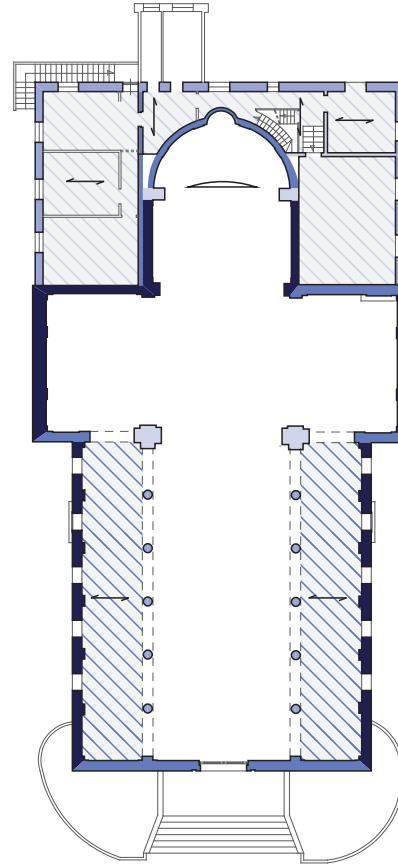

t = 0.775 m
t ≈ 0.600 m
t ≈ 0.550 m
t = 0.490 m
t ≈ 0.420 m
t = 0.520 m
t ≈ 0.450 m
t = 0.350 m
t ≈ 0.300 m
t ≈ 0.200 m
t ≈ 0.130 m

GROUND LEVEL

FIRST FLOORS LEVELS

Modelling and safety assessment of the Santa Maria Maddalena Church, Ischia, Italy

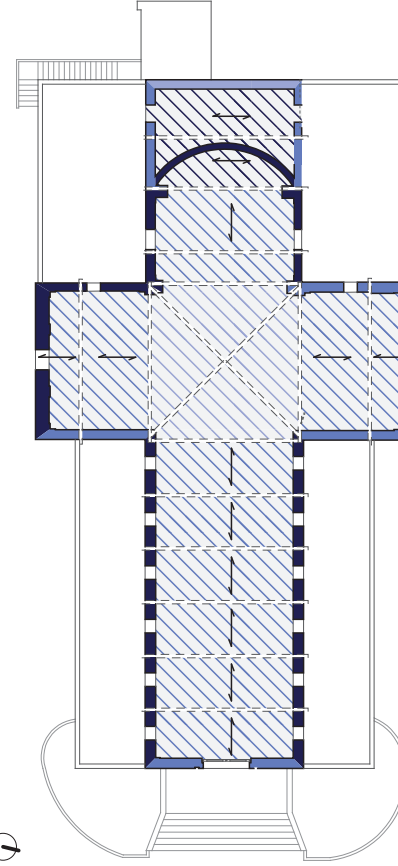ADVANCED MASTERS IN STRUCTURAL ANALYSIS OF MONUMENTS AND HISTORICAL CONSTRUCTIONS

GROUND LEVEL (+0.00 m)
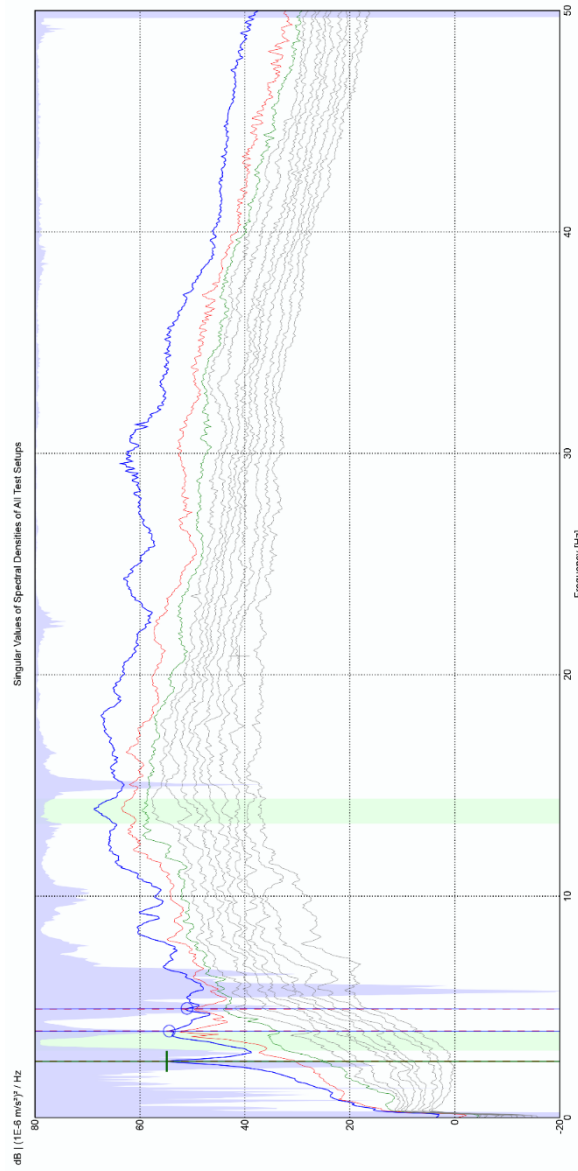
FIRST FLOOR LEVEL (+3.70 m)

CENTRAL NAVE LEVEL (+7.30 m)

ATTIC LEVEL (+13.08 m)

CL0 - Vertical el.	CL1 - Vertical el.	CL2 - Vertical el.	CL3 - Vertical el.
CL0 - Horizontal el.	CL1 - Horizontal el.	CL2 - Horizontal el.	CL3 - Horizontal el.

0 1 2   5   10

| Annex 3 - Architectural schemes |

A9
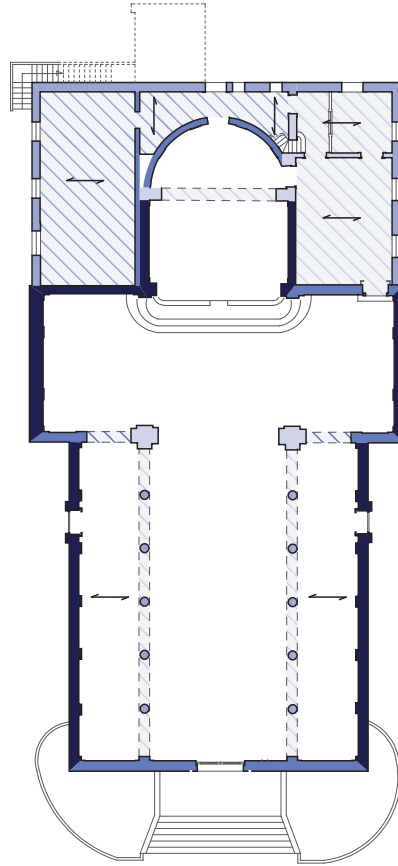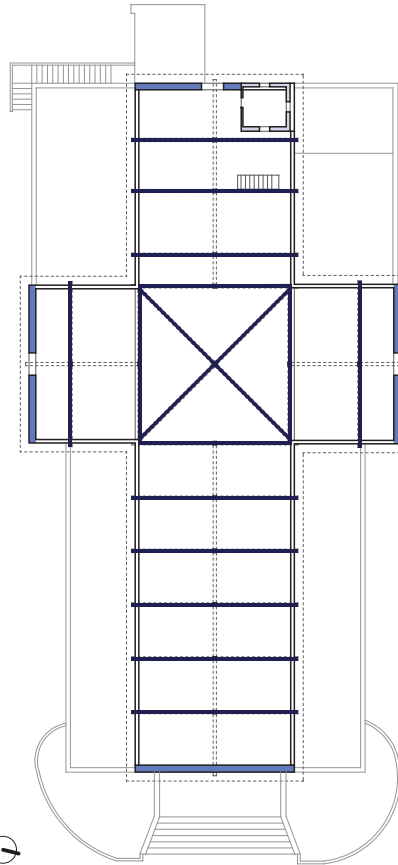
ANNEX 4   OPERATIONAL MODAL ANALYSIS RESULTS

ADVANCED MASTERS IN STRUCTURAL ANALYSIS OF MONUMENTS AND HISTORICAL CONSTRUCTIONS

Spectral density function diagram

ADVANCED MASTERS IN STRUCTURAL ANALYSIS OF MONUMENTS AND HISTORICAL CONSTRUCTIONS

SSI-UPCX Stabilization diagram – Setup_01

ADVANCED MASTERS IN STRUCTURAL ANALYSIS OF MONUMENTS AND HISTORICAL CONSTRUCTIONS

SSI-UPCX Stabilization diagram – Setup_02